Two Approaches to the Baryon Asymmetry of the Universe

Dissertation zur Erlangung des
naturwissenschaftlichen Doktorgrades
an der Fakultät für Physik und Astronomie
der Julius-Maximillians-Universität Würzburg

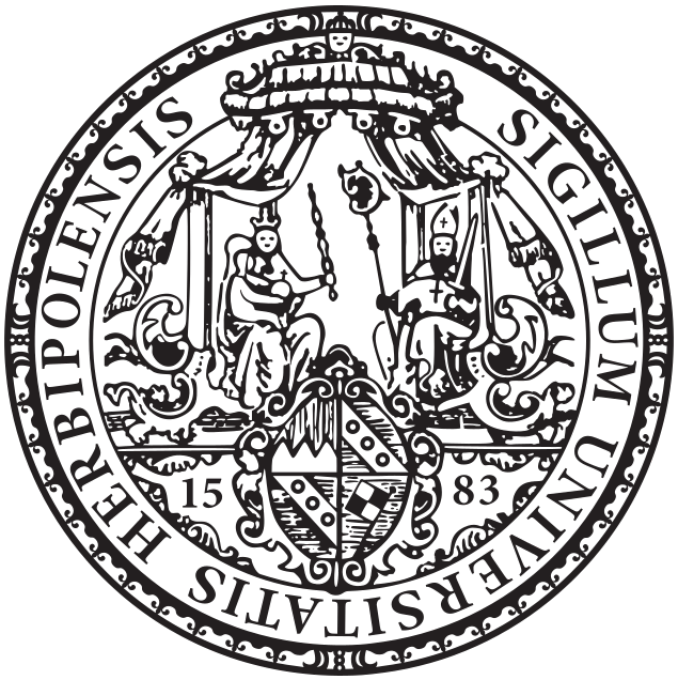

vorgelegt von
Amitayus Banik
aus Delhi, Indien

Würzburg, April 2023

Eingereicht bei der Fakultät für Physik und Astronomie am 28.04.2023

Gutachter der Dissertation:
1. Gutachter: Prof. Dr. Haye Hinrichsen
2. Gutachter: Prof. Dr. Werner Porod

Prüfer des öffentlichen Promotionskolloquiums:
1. Prüfer: Prof. Dr. Haye Hinrichsen
2. Prüfer: Prof. Dr. Werner Porod
3. Prüfer: Prof. Dr. Raimund Ströhmer

Tag des öffentlichen Promotionskolloquiums: 21.06.2023
Doktorurkunde ausgehändigt am: _____

Abstract

Explaining the baryon asymmetry of the Universe has been a long-standing problem of particle physics, with the consensus being that new physics is required as the Standard Model (SM) cannot resolve this issue. Beyond the Standard Model (BSM) scenarios would need to incorporate new sources of CP violation and either introduce new departures from thermal equilibrium or modify the existing electroweak phase transition. In this thesis, we explore two approaches to baryogenesis, i.e. the generation of this asymmetry.

In the first approach, we study the two-particle irreducible (2PI) formalism as a means to investigate non-equilibrium phenomena. After arriving at the renormalised equations of motions (EOMs) to describe the dynamics of a phase transition, we discuss the techniques required to obtain the various counterterms in an on-shell scheme. To this end, we consider three truncations up to two-loop order of the 2PI effective action: the Hartree approximation, the scalar sunset approximation and the fermionic sunset approximation. We then reconsider the renormalisation procedure in an $\overline{\text{MS}}$ scheme to evaluate the 2PI effective potential for the aforementioned truncations. In the Hartree and the scalar sunset approximations, we obtain analytic expressions for the various counterterms and subsequently calculate the effective potential by piecing together the finite contributions. For the fermionic sunset approximation, we obtain similar equations for the counterterms in terms of divergent parts of loop integrals. However, these integrals cannot be expressed in an analytic form, making it impossible to evaluate the 2PI effective potential with the fermionic contribution. Our main results are thus related to the renormalisation programme in the 2PI formalism: *(i)* the procedure to obtain the renormalised EOMs, now including fermions, which serve as the starting point for the transport equations for electroweak baryogenesis and *(ii)* the method to obtain the 2PI effective potential in a transparent manner.

In the second approach, we study baryogenesis via leptogenesis. Here, an asymmetry in the lepton sector is generated, which is then converted into the baryon asymmetry via the sphaleron process in the SM. We proceed to consider an extension of the SM along the lines of a scotogenic framework. The newly introduced particles are charged odd under a $\mathbb{Z}_2$ symmetry, and masses for the SM neutrinos are generated radiatively. The $\mathbb{Z}_2$ symmetry results in the lightest BSM particle being stable, allowing for a suitable dark matter (DM) candidate. Furthermore, the newly introduced heavy Majorana fermionic singlets provide the necessary sources of CP violation through their Yukawa interactions and their out-of-equilibrium decays produce a lepton asymmetry. This model is constrained from a wide

range of observables, such as consistency with neutrino oscillation data, limits on branching ratios of charged lepton flavour violating decays, electroweak observables and obtaining the observed DM relic density. We study leptogenesis in this model in light of the results of a Markov chain Monte Carlo scan, implemented in consideration of the aforementioned constraints. Successful leptogenesis in this model, to account for the baryon asymmetry, then severely constrains the available parameter space.

Kurzzusammenfassung

Die Erklärung der beobachteten Baryon-Asymmetrie im Universum ist ein seit langem ungelöstes Problem in der Hochenergiephysik. Ein weitgehender Konsens besteht darin, dass dafür "neue Physik" erforderlich ist, da dieses Problem nicht im Rahmen des Standardmodells gelöst werden kann. Dazu gehören CP-verletzende Erweiterungen des Standardmodells ebenso wie neue Aspekte des Nichtgleichgewichts und Modifikationen des elektroschwachen Phasenübergangs. In dieser Dissertation werden zwei Herangehensweisen untersucht, mit denen eine Baryon-Asymmetrie erzeugt werden könnte.

Die erste Herangehensweise besteht darin, den 2-Teilchen-irreduziblen (2PI) Formalismus anzuwenden, um auf diese Weise Nichtgleichgewichtsphänomene berücksichtigen zu können. Nach Ableitung der renormierten Bewegungsgleichungen, welche die Dynamik des Phasenübergangs beschreiben, werden Methoden diskutiert, mit denen die sogenannten Counterterme im "On-shell"-Schema berechnet werden können. Um dieses Ziel zu erreichen, betrachten wir drei verschiedene Näherungen der 2PI-Wirkung in zweiter Schleifenordnung, nämlich die Hartree- und die skalare 'sunset' Approximation sowie die fermionische 'sunset'-Approximation. Danach kehren wir zur Renormierungsprozedur in einem $\overline{\text{MS}}$-Schema zurück, um das effektive 2PI-Potential für die jeweiligen Abschneideverfahren zu berechnen. In den ersten beiden Fällen gelangen wir zu analytischen Ausdrücken für die verschiedenen Counterterme und berechnen anschließend durch Zusammenfügen aller Beiträge das effektive Potential. Im fermionischen Fall erhalten wir ähnliche Gleichungen für die Counterterme, deren Schleifenintegrale allerdings noch divergente Anteile enthalten. Weil diese Integrale nicht in analytisch geschlossener Form dargestellt werden können, ist es in diesem Fall nicht möglich, das effektive Potential zu berechnen. Die beiden wesentlichen Resultate beziehen sich also auf Renormierungsverfahren im 2PI-Formalismus: *(i)* eine Methode, um renormierte Bewegungsgleichungen, jetzt auch mit Fermionen, zu erhalten, die als Ausgangspunkt für Transportgleichungen in der elektroschwachen Baryogenese nutzbringend sein können, und *(ii)* eine Methode, um das effektive 2PI-Potential in einer transparenten Weise zu bestimmen.

Die zweite Herangehensweise befasst sich mit der Baryogenese durch Leptogenese. In diesem Fall wird zunächst eine Asymmetrie im leptonischen Sektor erzeugt, die dann vermittels eines Sphaleron-Prozesses in eine Baryonasymmetrie konvertiert wird. Wiederum betrachten wir eine Erweiterung des Standardmodells im Sinn eines skotogenen Ansatzes. Die zusätzlich eingeführten Teilchen sind ungerade geladen unter einer $\mathbb{Z}_2$-Symmetrie und die Massen für die Neutrinos im Standardmodell werden durch Strahlungskorrekturen

erzeugt. Wegen der $\mathbb{Z}_2$-Symmetrie sind die leichtesten Teilchen im erweiterten Standardmodell stabil und kommen damit als geeignete Kandidaten für dunkle Materie infrage. Darüber hinaus verursachen die zusätzlich eingeführten schweren Majorana-Singlet-Fermionen durch ihre Yukawa-Wechselwirkung die benötigte CP-Verletzung, wobei Zerfälle im Nichtgleichgewicht zu einer Leptonen-Asymmetrie führen. Dieses Model wird durch eine Vielzahl von Observablen eingeschränkt, wie z.B. Konsistenz mit den Daten zu Neutrino-Oszillationen, Schranken der Verzweigungsverhältnisse für leptonische Flavorverletzende Zerfälle, elektroschwache Präzisionsobservablen sowie die im Universum beobachtete Dichte dunkler Materie. Wir untersuchen die Leptogenese im Rahmen dieses Modells in einem Parameterraumbereich, der mithilfe einer Makovketten-Monte-Carlo-Simulation die unter Berücksichtigung der genannten Einschränkungen bestimmt wurde. Eine erfolgreiche Leptogenese in diesem Modell, welche auf die gewünschte Baryon-Asymmetrie führt, schränkt dann den Parameterraum erheblich weiter ein.

List of Publications

- [1] A. Alvarez, **A. Banik**, R. Cepedello, B. Herrmann, W. Porod, M. Sarazin and M. Schnelke. *Accommodating muon* $(g-2)$ *and leptogenesis in a scotogenic model.* JHEP **06** (2023) 163. doi: 10.1007/JHEP06(2023)163. arXiv: 2301.08485 [hep-ph].

Contents

List of Acronyms

The following acronyms will be made use of commonly throughout this thesis:

1PI One-Particle Irreducible

2PI Two-Particle Irreducible

***n*PI** n-Particle Irreducible

BBN Big Bang Nucleosynthesis

BE Boltzmann Equation

BPHZ Bogoliubov-Parasiuk-Hepp-Zimmermann

BSE Bethe-Salpeter Equation

BSM Beyond the Standard Model

CKM Cabbibo-Kobayashi-Maskawa

cLFV charged Lepton Flavour Violating

CMB Cosmic Microwave Background

COM Center of Mass

CW Colemann-Weinberg

DD Direct Detection

DM Dark Matter

EM Electromagnetic

EOM Equation of Motion

EW Electroweak

EWPT Electroweak Phase Transition

EWSB Electroweak Symmetry Breaking

FLRW Friedmann-Lemâitre-Robertson-Walker

GUT Grand Unified Theory

IR Infrared

LFV Lepton Flavour Violating

LHC Large Hadron Collider

MCMC Markov chain Monte Carlo

MS Minimal Subtraction

$\overline{\textbf{MS}}$ modified Minimal Subtraction

PMNS Pontecorvo-Maki-Nakagawa-Sakata

QFT Quantum Field Theory

RHN Right Handed Neutrino

SD Spin Dependent

SI Spin Independent

SM Standard Model

UV Ultraviolet

VEV Vacuum Expectation Value

Conventions

In this thesis, we will make use of natural units, where

$$c = \hbar = k_{\mathrm{B}} = 1\,,$$

where c is the speed of light in vacuum, $\hbar$ is the reduced Planck's constant and k_{B} is Boltzmann's constant. Accordingly, we define the Planck mass

$$M_{\mathrm{Pl}} = \frac{1}{\sqrt{G_{\mathrm{N}}}} = 1.22 \times 10^{19}\,\mathrm{GeV}\,,$$

where G_{N} is Newton's gravitational constant.

For the Minkowski metric, we will use the mostly minus convention, so that in four space-time dimensions

$$\eta_{\mu\nu} = \mathrm{diag}\,\{1, -1, -1, -1\}\ .$$

For the gamma matrices, we use the convention found in usual QFT textbooks such as Peskin and Schroeder [2] and Schwartz [3]. The corresponding Clifford algebra is then given as

$$\{\gamma^{\mu}, \gamma^{\nu}\} = 2\eta^{\mu\nu}\mathbb{I}_4\,,$$

where $\{...\}$ denotes the anti-commutator and $\mathbb{I}_4$ is the 4×4 identity matrix in spinor space.

Logarithms, referred to as log(...), are all taken with respect to the base e (natural logarithms), unless specified otherwise.

Chapter 1

Introduction

To the best of our knowledge, the observable structures in the Universe – stars, galaxies and clusters – consist mainly of matter, i.e. made up of baryons such as protons and neutrons with little to no anti-matter, otherwise they would annihilate. The Earth has been visited by galactic probes, such as comets and asteroids, and the fact that their remnants survive implies that they consist of matter. Studies of the composition of cosmic rays (see, for e.g. [4]) have found about 0.01% anti-protons and no heavy anti-nuclei. Thus, if there is a significant amount of anti-matter in the Universe, it must be segregated from matter on supercluster scales [5, 6], which is a scenario hard to envisage.

After the epoch of proton formation (see Fig. 1.1), matter and anti-matter remain in thermal equilibrium due to reactions such as $\gamma\gamma \to p\overline{p}$, until a temperature of about $T \approx 22\,\text{MeV}$. Assuming that there was no initial asymmetry between the two, this leads to equal number densities of baryons B and anti-baryons $\overline{B}$ in the present day t_0 [6]

$$\left.\frac{n_B^{\text{eq.}}}{n_\gamma}\right|_{t_0} = \left.\frac{n_{\overline{B}}^{\text{eq.}}}{n_\gamma}\right|_{t_0} \approx 6 \times 10^{-19}\,, \tag{1.1}$$

where we have normalised these to the photon number density. However, the observed abundances of light elements – deuterium, helium, tritium and lithium – from Big Bang Nucleosynthesis (BBN) [7, 8] and measurements of the Cosmic Microwave Background (CMB) [9–11] strongly constrain the value of the ratio of the number densities of baryons to photons to around

$$\left.\frac{n_B}{n_\gamma}\right|_{t_0} \approx 6.14 \times 10^{-10}\,, \tag{1.2}$$

meaning that the prediction (1.1) is off by 9 orders of magnitude. The only reasonable conclusion is that at early times in the Universe, an asymmetry between baryons and anti-baryons came into existence, which greatly reduced the number of anti-baryons present. To quantify this asymmetry, we define

$$\eta_B = \left.\frac{|n_B - n_{\overline{B}}|}{n_\gamma}\right|_{t_0} \approx \left.\frac{|n_B|}{n_\gamma}\right|_{t_0}\,, \tag{1.3}$$

where we have assumed that there is negligible anti-matter in the present day, so $n_B \gg n_{\overline{B}}$. The mechanism to produce this asymmetry is termed as **baryogenesis** and its goal is to

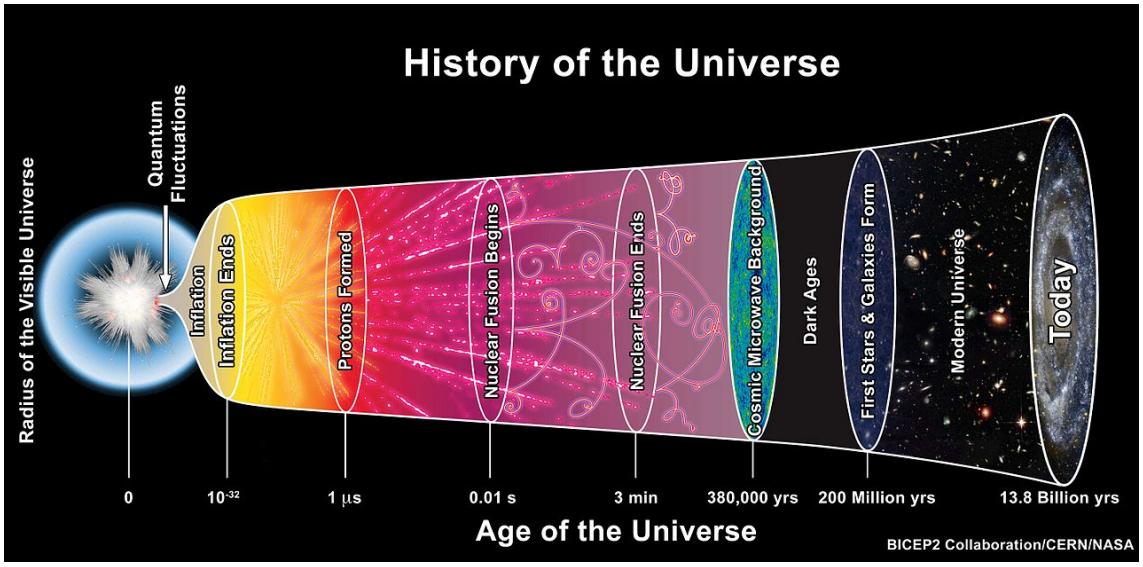

Figure 1.1: Illustration of the history of the Universe, from [13], starting from $t = 0$ till today at $t_0 = 13.8$ billion years, depicting various events in its thermal evolution. After the Big Bang at $t = 0$, observations of homogeneities of the CMB suggest a period of inflation. The small baryon asymmetry is believed to have been generated before the proton formation era and resulted in an elimination of anti-baryons. BBN takes place during the era where nuclear fusion begins. After nuclear fusion ends, electrons and atomic nuclei become bound to form neutral atoms (recombination) and photons start to go out of thermal equilibrium with matter. The photons of the CMB originate from this time.

successfully obtain the baryon asymmetry η_B close to the value in (1.2). Baryogenesis thus attempts to answer the question, *why is there more matter than anti-matter in the Universe?*

One might wonder whether it is possible to impose the baryon asymmetry as an initial condition at very early times. This is strongly disfavoured as it leads to a highly fine-tuned scenario: one would need about $30,000,001$ quarks, which constitute baryons, for every $30,000,000$ anti-quarks, which constitute anti-baryons, to ensure that η_B is close to the value in (1.2). A stronger reason favouring the dynamical generation of the baryon asymmetry is that observations of the CMB suggest an epoch of inflation took place during the history of the Universe, as shown in Fig. 1.1. Inflation is a period of exponential expansion of the Universe (c.f. [12] for a review) which would have washed away any primordial baryon asymmetry that might have been present. Thus, imposing the baryon asymmetry as an initial condition in an inflationary Universe would be useless.

The next question would be, knowing that this asymmetry is present, *how does one dynamically generate it?* The recipe for this was formulated by Sakharov, in the 1960s [14]. The three conditions for baryogenesis are:

- **Baryon number violating** interactions, in order to evolve an initial state with $\Delta B = 0$, to a final state with $\Delta B \neq 0$, where ΔB is the change in baryon number.

- C **and** CP **violation**, where C refers to charge conjugation symmetry and P refers to parity symmetry. This is required in order to have processes involving baryons proceeding at different rates than the C- or CP-conjugate processes involving anti-baryons. This then leads to a net baryon asymmetry.

- The baryon number violating processes must occur **out-of-equilibrium**, as no net baryon asymmetry can be produced in equilibrium. This is because processes generating and eliminating the asymmetry occur at the same rates in equilibrium by definition.

The Standard Model (SM) of particle physics, which has been successful in giving an accurate description of most observed data up to the TeV scale, technically contains, to an extent, all the aforementioned ingredients:

- Baryon number is violated in the SM through the *sphaleron process* [15], which are active during the early Universe due to the high temperature. As the Universe expanded and cooled, they started to become exponentially suppressed [16], and presently, are no longer active.
- The weak interactions of the SM violate C and CP via the phase in the Cabbibo-Kobayashi-Maskawa (CKM) matrix [17], which describes the mixing between quarks. The amount of CP violation [18], unfortunately, has been found to be too small [19, 20], and cannot generate the asymmetry to the order of (1.2).
- The electroweak phase transition (EWPT), whereby the $\mathrm{SU}(2)_L \times \mathrm{U}(1)_Y$ symmetry of the SM is broken after the Higgs acquires a vacuum expectation value (VEV), is an out-of-equilibrium process. However, it is not a strong first-order phase transition required for baryogenesis [21, 22], due to the observed Higgs mass of 125 GeV [23–25].

Thus, explaining the baryon asymmetry of the Universe underlines the call for physics beyond the Standard Model (BSM physics). This needs to be in the form of new sources of CP violation **and** (i) either a separate departure from thermal equilibrium besides the EWPT or (ii) a modification of the EWPT itself. In (i), this usually involves some newly introduced heavy particle(s) whose out-of-equilibrium decays produces a baryon asymmetry, whereas in (ii), termed as electroweak baryogenesis, the nature of the EWPT is altered by, for example, introducing new scalars in the SM Higgs potential.

So far, we have only discussed the generation of the observable, baryonic matter in the early Universe. However, this baryonic matter comprises only a small fraction of the total matter in the Universe. The rest of the total matter ($\sim 84\%$) is non-baryonic in nature and invisible as it does not have interactions with electromagnetic radiation. This dominant component is termed as **dark matter** (DM) for which there is well-established gravitational evidence, such as studies of galactic rotation curves (for e.g. [26–29]), the "Bullet Cluster" event [30, 31], gravitational lensing (see [32] for a review) and measurements of the power-spectrum of the CMB [9–11]. From what we know about dark matter [6, 33–37], particle physics candidates need to be non-relativistic ("cold"), at least till the onset of large structure formation (just before the period when the first stars and galaxies form, in Fig. 1.1), having little to no interactions with electromagnetic radiation and stable on cosmological time scales. The Standard Model does not contain such a candidate and one requires the advent of new physics to explain DM phenomena.

One might think that the Standard Model neutrinos would be good candidates for particle DM, as they do not interact with electromagnetic radiation. They, unfortunately, form the "wrong kind" of DM, as they would constitute hot dark matter which would, being relativistic during structure formation, wash out the small-scale structures of the Universe. However, neutrinos pose a further riddle, as they are massless in the SM, contrary to what has been established by neutrino oscillation experiments [38, 39].

This thesis thus intends to study methods aimed at the resolution of the baryon asymmetry of the Universe. To this end, we present two different approaches in two parts.

In Part I, we focus on non-equilibrium field theory, as a means to study phase transitions in a Quantum Field Theory (QFT), which forms the starting point to resolve the baryon asymmetry through electroweak baryogenesis. We introduce the two-particle irreducible (2PI) formalism in Chapter 2 by giving an overview of the features that make it ideal for studying non-equilibrium problems. We arrive at the quantum equations of motion that describe the dynamics of a phase transition, and stress the need to renormalise them. In Chapter 3, we explore the techniques to carry out renormalisation within the 2PI formalism and apply them to obtain expressions for the required counterterms that make the 2PI effective action finite. To this end, we describe an on-shell scheme and formulate the renormalisation procedure within the broken phase, i.e. at non-vanishing field expectation value. We also extend our techniques to include fermions in the 2PI formalism, which to our knowledge, has not been extensively described in the literature. Then, in Chapter 4, we apply an alternative approach to renormalise the 2PI effective action in the $\overline{\text{MS}}$ scheme, which makes it easier to calculate the 2PI effective potential. For the pure scalar cases, we obtain equations for the counterterms, in terms of divergent parts of loop integrals, which we solve analytically for explicit expressions. Subsequently, we are able to obtain the 2PI effective potential at zero temperature in a transparent manner by tracking finite quantities and using finite parts of these loop integrals, which, as far as we know, constitutes a novel result. With fermions, we are able to obtain similar equations for the various counterterms. The technical challenge lies that, although the divergent structures are known, we cannot evaluate the integrals analytically and extract the finite pieces needed to evaluate the 2PI effective potential. We close Part I with a future outlook of the methods we have presented.

Switching gears in Part II, we approach the baryon asymmetry problem from the perspective of BSM physics and the leptogenesis mechanism. In Chapter 5, we describe several key aspects of leptogenesis, namely the fulfilment of Sakharov's conditions. We demonstrate that the decays of newly introduced heavy neutrinos violate lepton number and generate CP violation. These decays, which source a lepton asymmetry, occur out-of-equilibrium and are tracked using Boltzmann equations. We then discuss how this lepton asymmetry is converted into the required baryon asymmetry through the sphaleron process. With this framework established, we investigate an extension of the SM allowing for radiative generation of neutrino masses in Chapter 6. We proceed to perform an analysis of this model in the context of DM phenomenology and leptogenesis, based on several considerations, such as generating SM neutrino masses compatible with neutrino oscillation data, constraints from branching ratios on charged lepton flavour violating processes, fitting the observed value of the anomalous magnetic moment of the muon, obtaining the correct DM relic density, etc. We show that this model is indeed capable of explaining the baryon asymmetry of the Universe, albeit within a severely constrained parameter space. We close by giving an outlook for the improvement of our analysis along the lines of leptogenesis.

We conclude this thesis in Chapter 7 by summarising our findings and giving an outlook for future directions along the lines of this work.

PART I

Chapter 2

The 2PI Formalism

In this chapter, we present and discuss formal aspects related to the two-particle irreducible (2PI) effective action [40]. Similar to the more familiar one-particle irreducible (1PI) effective action (see, for e.g. [2, 3]), the 2PI effective action involves a diagrammatic expansion in terms of closed loops. The main difference is that these diagrams are built from the resummed propagator in the 2PI formalism, instead of the bare one. A particular resummation is chosen by truncating the series of diagrams. Finally, a variational principle when applied to this truncated action leads to a set of self-consistent equations from which the independent quantities, the one- and two-point functions, are obtained. These equations are typically coupled, non-linear integro-differential equations which must be solved numerically.

Resummation schemes based on the 2PI effective action have been known to show many advantages compared to other methods. For example, in treating bosonic field theories at high temperature, "hard" thermal loops are resummed to resolve infrared (IR) singularities [41, 42]. This resulting resummed perturbation theory still shows poor convergence [43]. However, in the same context, improved convergence behaviour may be observed using systematic loop- or coupling-expansions of the 2PI effective action [44–46]. Furthermore, out-of-equilibrium properties of fields can also formally studied using 2PI techniques, whereby the resummation feature of the 2PI formalism allows one to obtain approximations uniform in time [47–50].

This chapter is intended to provide an introduction to the 2PI formalism by presenting various definitions and setting notation. Based on this framework, we will treat topics such as renormalisation and the evaluation of the 2PI effective potential in chapters 3 and 4. For comprehensive reviews on the 2PI formalism, we suggest [49, 50].

2.1 Properties of the 2PI and nPI Formalisms

To describe out-of-equilibrium phenomena, one needs the specification of an initial state and the Hamiltonian, which leads to an effective action Γ for the system and describes its time-evolution. Additional complications arise, however, which are *secularity* and *universality* [49, 50]. Secularity refers to the fact that the perturbative time evolution suffers from the presence of spurious terms growing with time and invalidating approximations,

meaning one needs to resort to non-perturbative methods for consistency. Universality is the insensitivity of the late-time behaviour to the initial conditions. This means that if one approaches thermal equilibrium, the late-time result is determined essentially by the specified energy density and other conserved quantities (charges).

The challenge of describing non-secular and universal behaviour can be fulfilled using functional integral techniques based on n-particle irreducible (nPI) effective actions $\Gamma_{n\mathrm{PI}}[\phi, G, ..., V_n]$. In this formalism, the mean field ϕ, the propagator G, and the $n-$point ($n > 2$) vertices V_n constitute dynamical degrees of freedom. The effective action then gives the **equations of motion** (EOMs) for these quantities, which are obtained by first-order functional differentiation

$$\frac{\delta\Gamma_{n\mathrm{PI}}[\phi, G, ..., V_n]}{\delta\phi} = \frac{\delta\Gamma_{n\mathrm{PI}}[\phi, G, ..., V_n]}{\delta G} = ... = \frac{\delta\Gamma_{n\mathrm{PI}}[\phi, G, ..., V_n]}{\delta V_n} = 0\,, \tag{2.1}$$

at some fixed values ($\phi = \overline{\phi}, G = \overline{G}, ..., V_n = \overline{V}_n$), which are termed as **stationarity conditions**.

For practical reasons, we need to understand that it is not necessary to calculate the general nPI effective action for arbitrarily large n, as there exists an equivalence hierarchy between nPI effective actions. For example, in terms of the loop expansion [51], we have in the absence of external sources

$$\Gamma^{\text{1-loop}}_{\text{1PI}} = \Gamma^{\text{1-loop}}_{\text{2PI}} = ... = \Gamma^{\text{1-loop}}_{n\text{PI}}\,,$$
$$\Gamma^{\text{2-loop}}_{\text{1PI}} \neq \Gamma^{\text{2-loop}}_{\text{2PI}} = ... = \Gamma^{\text{2-loop}}_{n\text{PI}}\,,$$
and so on.

Here $\Gamma^{k\text{-loop}}_{n\text{PI}}$ denotes the k^{th} loop order approximation of the respective nPI effective action. For instance, at two-loop order, the 1PI effective action differs from the 2PI effective action; $\Gamma_{2\mathrm{PI}}$ can be understood to resum an infinite series of contributions for $\Gamma_{1\mathrm{PI}}$ and provides a self-consistent description at this order. When employing nPI effective actions, we must then keep in mind the required (or typically, the computationally feasible) order of approximation that will capture a consistent picture. In this thesis, we will restrict ourselves to truncations at two-loop order, meaning that the 2PI effective action is sufficient for our purposes.

In particular, the 2PI formalism is known to provide a systematic method for resummations, as mentioned before. As we have hinted at, one can always improve the given approximation by truncating the 2PI effective action at higher order in some expansion parameter (like the coupling constant, etc.) [52, 53]. Approximations within the 2PI formalism have been shown to be consistent with (global) conservation laws stemming from Noether's theorem, implying that they guarantee charge and energy conservation [54, 55]. Furthermore, it has been shown that the 2PI effective action is consistent with Ward identities [46, 56–59]. Finally, the associated 2PI improved effective potential obtained from the 2PI effective action (see later in Sec. 2.4) has a tendency to give stronger transitions than the 1PI loop expanded effective potentials [60], which may be better in agreement with lattice results, when these are valid (see for e.g. [61], and [62] for a discussion on the validity of the lattice results).

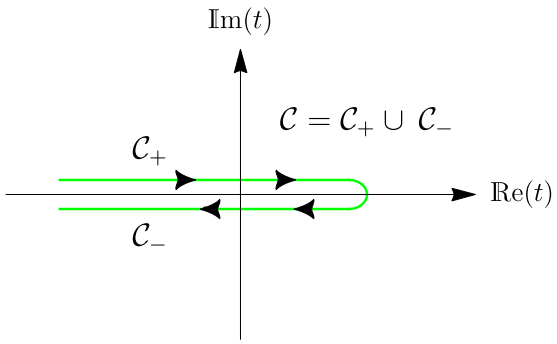

Figure 2.1: The Keldysh contour in the complex time plane, running from some initial time to an arbitrary future time and back again. The contour is shifted slightly away from the real axis for clarity.

2.2 Review of the 1PI Effective Action

We will briefly review the construction of the 1PI effective action, as the framework extends well to the 2PI effective action. Our starting point is the partition function or generating functional, given in a scalar field theory as

$$Z[J] = \int \mathcal{D}\varphi \exp\left[i\left(S[\varphi] + \int_x J(x)\varphi(x)\right)\right], \tag{2.2}$$

where

$$S[\varphi] = \int_x \mathcal{L}[\varphi(x)], \tag{2.3}$$

is the action and $\mathcal{L}$ is the Lagrangian for the scalar field $\varphi(x)$. $Z[J]$ is hence a functional integration over φ, with the addition of a source term $J(x)\varphi(x)$. As we are interested in the non-equilibrium evolution of the field theory, where a final state is not known, the integration in the exponential is defined as follows

$$\int_x \equiv \int_{\mathcal{C}} dx_0 \int d^{d-1}x\,, \tag{2.4}$$

whereby the temporal integration is carried out along the time-ordered Keldysh contour $\mathcal{C}$ [63] (see Fig. 2.1), which is a *closed time path*, and d refers to the spacetime dimension. Consequently, standard functional differentiation w.r.t. the source current J is modified to include time arguments on the Keldysh contour

$$\frac{\delta J(x)}{\delta J(y)} = \delta_{\mathcal{C}}(x-y) \equiv \delta_{\mathcal{C}}(x^0-y^0)\delta(\vec{x}-\vec{y})\,. \tag{2.5}$$

The temporal delta-function is defined on the time contour to be 0 everywhere except when $x^0 = y^0$, or if either x^0 and y^0 are both on the same branch $\mathcal{C}^+$ or $\mathcal{C}^-$, where it is infinite with

$$\int_{\mathcal{C}} dx^0 \delta_{\mathcal{C}}(x^0) = 1\,. \tag{2.6}$$

To define a generating functional of connected correlation functions, we introduce

$$W[J] = -i\log Z[J]\,. \tag{2.7}$$

The mean field ϕ, the propagator G, and n-point connected correlation functions $\Gamma^{(n)}$ can then be obtained by functional differentiations of $W[J]$ w.r.t. J, i.e.

$$i\frac{\delta W[J]}{i\delta J(x)} = \langle\varphi(x)\rangle_J \equiv \phi(x)\,, \tag{2.8}$$

$$i\frac{\delta^2 W[J]}{i\delta J(x)\, i\delta J(y)} = \langle \mathrm{T}_{\mathcal{C}}\varphi(x)\varphi(y)\rangle_J \equiv iG(x,y)\,, \tag{2.9}$$

$$i\frac{\delta^n W[J]}{i\delta J(x_1)\, i\delta J(x_2)\, ...\, i\delta J(x_n)} = \langle \mathrm{T}_{\mathcal{C}}\varphi(x_1)\varphi(x_2)\,....\,\varphi(x_n)\rangle_J \equiv i\Gamma^{(n)}(x_1,x_2,\,...\,,x_n)\,, \tag{2.10}$$

where we have denoted time ordering along the Keldysh contour through $\mathrm{T}_{\mathcal{C}}$. This is defined such that any point on $\mathcal{C}^-$ is later than any point on $\mathcal{C}^+$, alongside the usual time ordering used in vacuum QFT. The **1PI effective action** is given by the Legendre transform of $W[J]$ w.r.t. J,

$$\Gamma_{1\mathrm{PI}}[\phi] = W[J] - \int_x J(x)\frac{\delta W[J]}{\delta J(x)} = W[J] - \int_x J(x)\phi(x)\,, \tag{2.11}$$

and gets its name from the fact that it is the generating functional of one-particle-irreducible (1PI) diagrams (see, for e.g., [2, 3]), i.e. diagrams that cannot be disconnected by removing ("cutting") an internal propagator line.

Consider now the first derivative of the 1PI effective action w.r.t. the mean field

$$\begin{aligned}\frac{\delta\Gamma_{1\mathrm{PI}}[\phi]}{\delta\phi(x)} &= \frac{\delta W[J]}{\delta\phi(x)} - \int_y \frac{\delta J(y)}{\delta\phi(x)}\,\phi(y) - \int_y J(y)\,\frac{\delta\phi(y)}{\delta\phi(x)} \\ &= \int_y \frac{\delta J(y)}{\delta\phi(x)}\,\underbrace{\frac{\delta W[J]}{\delta J(y)}}_{=\phi(y)} - \int_y \frac{\delta J(y)}{\delta\phi(x)}\,\phi(y) - \int_y J(y)\,\delta_{\mathcal{C}}(y-x) = -J(x)\,.\end{aligned} \tag{2.12}$$

Notice that if we set $J = 0$ at some particular $\phi = \overline{\phi}$, we obtain the stationarity condition

$$\left.\frac{\delta\Gamma_{1\mathrm{PI}}[\phi]}{\delta\phi(x)}\right|_{\phi=\overline{\phi}} = 0\,, \tag{2.13}$$

which is, equivalently, the EOM for $\overline{\phi}$. The solutions to this are the vacuum states of the theory.

It is possible to explicitly evaluate $\Gamma_{1\mathrm{PI}}$ in the saddle-point approximation around the mean field ϕ [64]. To this end, consider

$$\begin{aligned}\exp\{i\,\Gamma_{1\mathrm{PI}}[\phi]\} &= \int \mathcal{D}\varphi \exp\left\{i\left[S[\varphi] + \int_x J(x)\,(\varphi(x)-\phi(x))\right]\right\} \\ &= \int \mathcal{D}\varphi \exp\left\{i\left[S[\varphi+\phi] + \int_x J(x)\varphi(x)\right]\right\} \\ &= \exp\{i\,S[\phi]\}\int \mathcal{D}\varphi \exp\left\{i\left[S[\varphi+\phi] - S[\phi] + \int_x J(x)\varphi(x)\right]\right\}\,,\end{aligned} \tag{2.14}$$

where in the second step, we have shifted the fluctuating field $\varphi \to \varphi + \phi$. Now, consider

$$S[\varphi+\phi] - S[\phi] = \int_x \left.\frac{\delta S[\varphi]}{\delta\varphi(x)}\right|_{\varphi=\phi}\varphi(x) + \frac{1}{2!}\int_x\int_y \varphi(x)\left.\frac{\delta^2 S[\varphi]}{\delta\varphi(x)\delta\varphi(y)}\right|_{\varphi=\phi}\varphi(y) + S_{\mathrm{int}}[\varphi,\phi]\,. \tag{2.15}$$

where we have Taylor expanded $S[\varphi+\phi]$ about the mean field ϕ. S_{int} contains in it cubic and quartic powers of the fluctuating field[1]. Substituting (2.15) into (2.14), we obtain

$$\exp\{i\,\Gamma_{1\text{PI}}[\phi]\} = \exp\{i\,S[\phi]\}\int\mathcal{D}\varphi\exp\left\{i\left[\frac{1}{2}\int_x\int_y\varphi(x)\,\left(i\tilde{G}^{-1}_\phi(x,y;\phi)\right)\,\varphi(y)\right.\right.$$
$$\left.\left.+\,S_{\text{int.}}[\varphi,\phi]+\int_x\frac{\delta S[\varphi]}{\delta\varphi(x)}\bigg|_{\varphi=\phi}\varphi(x)+\int_x\underbrace{J(x)}_{=-\frac{\delta\Gamma_{1\text{PI}}[\phi]}{\delta\phi(x)}}\varphi(x)\right]\right\} \tag{2.16}$$

where

$$\tilde{G}^{-1}_\phi(x,y;\phi)\equiv -i\frac{\delta S[\varphi]}{\delta\varphi(x)\delta\varphi(y)}\bigg|_{\varphi=\phi}. \tag{2.17}$$

We can evaluate the term which is quadratic in φ as a standard Gaussian integral (see [2, 3] for example),

$$\int\mathcal{D}\varphi\exp\left\{-\frac{1}{2}\int_x\int_y\varphi(x)\,\left(\tilde{G}^{-1}_\phi(x,y;\phi)\right)\,\varphi(y)\right\}=\left[\det\tilde{G}^{-1}_\phi(\phi)\right]^{-\frac{1}{2}} \tag{2.18}$$

The term $S_{\text{int.}}$ needs to be treated by expanding the exponential and is interpreted as an expansion in terms of connected diagrams. As a requirement, the linear term in φ is an example of a tadpole, which guarantees a vanishing field expectation value for φ when the shift $\varphi\to\varphi+\phi$ is performed. Thus, the final result can be expressed as [2, 3],

$$\Gamma_{1\text{PI}}[\phi]=S[\phi]+\underbrace{\frac{i}{2}\text{Tr}_{\mathcal{C}}\log\tilde{G}^{-1}_\phi(\phi)}_{\text{1-loop part}}-i\,[\text{connected diagrams}]\,+\,\text{const.} \tag{2.19}$$

where the "const." can be adjusted for proper normalisation and we have used $\log\det A=\text{Tr}\log A$ for the second term in (2.19). The $\text{Tr}_{\mathcal{C}}\,[...]$ refers to the integration over space-time coordinates on the Keldysh contour.

As it will become useful when we discuss fermions in the 2PI formalism, we briefly outline the technology required for fermionic fields. To this end, we introduce Grassmann variables, which are anti-commuting, complex numbers, making them suitable for describing fermionic fields. They have the property of differentiation and integration being treated on the same footing, i.e.

$$\int d\eta\,\eta=\frac{d}{d\eta}\,\eta=\int d\eta^*\,\eta^*=\frac{d}{d\eta^*}\,\eta^*=1\,,\quad\text{with}\quad\{\eta,\eta\}=\{\eta^*,\eta^*\}=0 \tag{2.20}$$

where $\{x,y\}=xy+yx$ denotes anti-commutation. The most relevant result is the equivalent of the Gaussian integral,

$$\int d\eta^*\,d\eta\,\exp[-b\eta^*\eta]=\int d\eta^*\,d\eta\,[1-b\eta^*\eta]$$
$$=-b\int d\eta^*\,d\eta\,\eta^*\eta=b \tag{2.21}$$

[1]Typically, in four space-time dimensions, one can write down up to a quartic interaction between scalars on account of renormalisability

where b is a complex number. In the last step, we have anti-commutated η^* in order to use (2.20). The analogue for the Gaussian functional integral for encountered for a fermionic field is hence

$$\int \mathcal{D}\overline{\psi}\mathcal{D}\psi \exp\left\{-\int_x\int_y \overline{\psi}(x)D(x,y)\,\psi(y)\right\} = \det D\,, \tag{2.22}$$

where $\overline{\psi}$ is the Dirac conjugate of ψ. Thus, on going through a similar evaluation as (2.19), one would obtain with fermions now,

$$\Gamma_{1\text{PI}}[\phi] = S[\phi,\psi] + \frac{i}{2}\text{Tr}_{\mathcal{C}}\log\tilde{G}^{-1}_{\phi}(\phi) - i\text{Tr}_{\mathcal{C}}\log\tilde{D}^{-1}_{\psi}(\phi) \;-\; i\,[\text{connected diagrams}] + \text{const.}\,, \tag{2.23}$$

where

$$\tilde{D}^{-1}_{\psi}(x,y;\phi) = -i\frac{\delta^2 S[\phi,\psi]}{\delta\overline{\psi}(y)\psi(x)}\bigg|_{\varphi=\phi,\,\psi=\bar{\psi}=0}\,. \tag{2.24}$$

Notice that we have not allowed fermionic field ψ to acquire a vacuum expectation value (VEV), on account of the fact that this would break Lorentz invariance. Essentially, the fermionic contributions come with a factor of -1 instead of the $1/2$ for scalars.

2.3 2PI Effective Action

We now introduce an additional bi-local source, $K(x,y) = K(y,x)$, in the partition function (2.2),

$$Z[J,K] = \int \mathcal{D}\varphi \exp\left[i\left(S[\varphi] + \int_x J(x)\varphi(x) + \frac{1}{2}\int_x\int_y \varphi(x)K(x,y)\varphi(y)\right)\right]\,, \tag{2.25}$$

for which we have the generating functional defined analogously as

$$W[J,K] = -i\log Z[J,K]\,. \tag{2.26}$$

The mean field and the connected two-point function (the propagator) are obtained by appropriate functional differentiation w.r.t. the sources J and K,

$$\begin{aligned}\frac{\delta W[J,K]}{\delta J(x)} &= \phi(x)\,,\\ \frac{\delta W[J,K]}{\delta K(x,y)} &= \frac{1}{2}\left[\phi(x)\phi(y) + G(x,y)\right]\,.\end{aligned} \tag{2.27}$$

The **2PI effective action** is formally defined as the Legendre transform of $W[J,K]$ w.r.t. the local and bi-local sources,

$$\Gamma_{2\text{PI}}[\phi,G] = W[J,K] - \int_x \frac{\delta W[J,K]}{\delta J(x)}J(x) - \int_x\int_y \frac{\delta W[J,K]}{\delta K(x,y)}K(x,y) \tag{2.28}$$

$$= W[J,K] - \int_x \phi(x)J(x) - \frac{1}{2}\int_x\int_y \left[\phi(x)\phi(y) + G(x,y)\right]K(y,x)\,. \tag{2.29}$$

The sources can then be re-expressed as

$$J(x) = -\frac{\delta\Gamma_{2\text{PI}}[\phi,G]}{\delta\phi(x)} - \int_y K(x,y)\phi(y)\,, \quad K(x,y) = -2\frac{\delta\Gamma_{2\text{PI}}[\phi,G]}{\delta G(x,y)}\,. \tag{2.30}$$

We mention that the use of both local and bi-local sources forms an appropriate setting for the study of non-equilibrium problems as these encode the initial conditions [49, 50].

2.3.1 Salient Features of the 2PI Effective Action

Along similar lines as we have obtained (2.19), we first notice that on performing a shift in the action,

$$S[\varphi] \to S[\varphi] + \frac{1}{2}\int_x \int_y \varphi(x) K(x,y) \varphi(y)$$

and replacing this in (2.14) and (2.15), a similar evaluation allows one to express $\Gamma_{2\text{PI}}$ in the following convenient form [40, 49, 50, 64, 65]

$$\Gamma_{2\text{PI}}[\phi, G] = S[\phi] + \underbrace{\frac{i}{2}\text{Tr}_{\mathcal{C}} \log G^{-1} + \frac{i}{2}\text{Tr}_{\mathcal{C}}\left[\tilde{G}_{\phi}^{-1}(\phi)\, G\right]}_{\text{1-loop}} + \underbrace{\Gamma_2[\phi, G]}_{\geq\text{2-loop}} + \text{const.} \tag{2.31}$$

where we collect all the contributions of two-loop and higher (multiplied by a factor of $-i$) into Γ_2. The second equation of (2.30) then gives

$$\begin{aligned} K(x,y) &= -2\left[-\frac{i}{2}G^{-1}(x,y) + \frac{i}{2}\tilde{G}_{\phi}^{-1}(x,y;\phi) + \frac{\delta\Gamma_2[\phi,G]}{\delta G(x,y)}\right] \\ \implies G^{-1}(x,y) &= \tilde{G}_{\phi}^{-1}(x,y;\phi) - iK(x,y) - \Pi(x,y;\phi,G) \end{aligned} \tag{2.32}$$

where we have introduced the **self-energy**

$$\Pi(x,y;\phi,G) = 2i\frac{\delta\Gamma_2[\phi,G]}{\delta G(x,y)} \tag{2.33}$$

to which only 1PI diagrams contribute [49, 50, 65]. The consequence of this is that Γ_2 contains only two-particle irreducible (2PI) contributions, i.e. it does not become disconnected upon removing two internal propagators. We can discern this by contradiction: suppose that Γ_2 had a two-particle reducible contribution of the form $\overline{\Gamma}\, G\, G\, \overline{\Gamma}'$, whereby removing two G's yields the separate contributions $\overline{\Gamma}$ and $\overline{\Gamma}'$. Calculating the self-energy using (2.33), we obtain $\Pi \sim \overline{\Gamma} G \overline{\Gamma}'$, which is one-particle reducible and cannot contribute to the self-energy.

In view of the renormalisation procedure, which we will study thoroughly in the next two chapters of this thesis, we split the classical action into a free and an interacting part $S[\phi] = S_0[\phi] + S_{\text{int}}[\phi]$ and to decompose $\tilde{G}_{\phi}^{-1} = \tilde{G}_0^{-1} + \tilde{G}_{\phi,\text{int}}^{-1}$ [65]. Correspondingly, one can split the 2PI effective action into $\Gamma_{2\text{PI}} = \Gamma_{2\text{PI},0} + \Gamma_{2\text{PI,int}}$, where

$$\Gamma_{2\text{PI},0}[\phi,G] = S_0[\phi] + \frac{i}{2}\text{Tr}_{\mathcal{C}}\left[\ln G^{-1}\right] + \frac{i}{2}\text{Tr}_{\mathcal{C}}[\tilde{G}_0^{-1}G]\,, \tag{2.34}$$

$$\Gamma_{2\text{PI,int}}[\phi,G] = S_{\text{int}}[\phi] + \frac{i}{2}\text{Tr}_{\mathcal{C}}[\tilde{G}_{\phi,\text{int}}^{-1}G] + \Gamma_2[\phi,G] + \text{const.} \tag{2.35}$$

and accordingly, we define the scalar self-energy as

$$\overline{\Pi}(x,y;\phi,G) = 2i\frac{\delta\Gamma_{2\text{PI,int}}[\phi,G]}{\delta G(x,y)}\bigg|_{\overline{\phi},\overline{G}}\,. \tag{2.36}$$

The stationary conditions are obtained from (2.30) by setting $J = K = 0$,

$$\frac{\delta\Gamma_{2\text{PI}}[\phi,G]}{\delta\phi(x)}\bigg|_{\overline{\phi},\overline{G}} = \frac{\delta S_0[\phi,G]}{\delta\phi(x)}\bigg|_{\overline{\phi}} + i\frac{\delta\Gamma_{2\text{PI,int}}[\phi,G]}{\delta\phi(x)}\bigg|_{\overline{\phi},\overline{G}} = 0\,, \tag{2.37}$$

$$\left.\frac{\delta\Gamma_{\rm 2PI}[\phi,G]}{\delta G(x,y)}\right|_{\overline{\phi},\overline{G}} = -\frac{i}{2}\overline{G}^{-1}(x,y) + \frac{i}{2}\tilde{G}_0^{-1}(x,y) + i\left.\frac{\delta\Gamma_{\rm 2PI,int}[\phi,G]}{\delta G(x,y)}\right|_{\overline{\phi},\overline{G}} = 0\,. \tag{2.38}$$

and then give the equations of motion (EOMs) to determine $\overline{\phi}$ and $\overline{G}$, with the specification of appropriate boundary conditions. For convenience, we will typically drop the bar symbol on ϕ and G from now onward, as we will assume that the sources are always switched off, unless specified otherwise.

2.3.2 A Pedagogical Example

Loop expansions of the 2PI effective action proceed in a similar manner as for the 1PI effective action, but one needs to keep in mind that contributions are parametrised using the resummed ("dressed") propagator G, obtained from the stationarity condition (2.38) instead of the classical propagator, and only 2PI contributions are to be kept. To illustrate this, we consider the following classical action

$$S[\varphi] = \int_x \left[\frac{1}{2}\partial_\mu\varphi(x)\partial^\mu\varphi(x) - \frac{m^2}{2}\varphi^2(x) - \frac{\lambda}{4!}\varphi^4(x)\right]. \tag{2.39}$$

For the example, we will work in the case of vanishing field expectation value. Up to three-loops, we then have the following contributions to Γ_2

$$\Gamma_{2,\rm ht} = (-i)\,(3)\left(-i\,\frac{\lambda}{4!}\right)\int_x G^2(x,x) = -\frac{\lambda}{8}$$

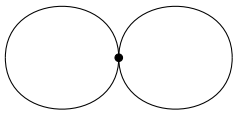

, (2.40)

$$\Gamma_{2,\rm bb} = (-i)\,(2)\,(4\times 3)\,\frac{1}{2}\left(-i\,\frac{\lambda}{4!}\right)^2\int_x\int_y G^4(x,y) = i\frac{\lambda^2}{48}$$

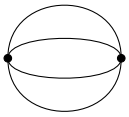

. (2.41)

Here, we keep the pre-factor of $-i$ in the definition of Γ_2 and have accounted for the various symmetry factors for the diagrams. The solid lines denote the full propagator G. We mention, for completeness, that the truncation till the two-loop diagram (2.40) is referred to as the "Hartree approximation" and the three-loop diagram (2.41) is called the "Basketball diagram" . The former of these will form a local term (depending on only one space-time coordinate) and the latter is a non-local term (depending on two space-time coordinates), which will lead to so-called *memory integrals* in the EOMs. We obtain the self-energies according to these diagrams in Γ_2 as

$$\Pi_{\rm ht}(x) = -i\,\frac{\lambda}{2}G(x,x) = -i\,\frac{\lambda}{2}$$

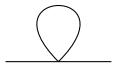 (2.42)

$$\Pi_{\rm bb}(x,y) = -\frac{\lambda^2}{6}G^3(x,y) = -\frac{\lambda^2}{6}$$

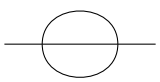 (2.43)

Thus, the mapping from obtaining the self-energy from Γ_2 is by "cutting" a single propagator line. This also illustrates the feature that the self-energy as defined in (2.33) is indeed one-particle irreducible.

Now, using

$$i\tilde{G}_{\phi}^{-1}(x,y) = \frac{\delta^2 S[\phi]}{\delta\phi(x)\delta\phi(y)} = \underbrace{-\left(\Box_x + m^2\right)\delta_{\mathcal{C}}(x-y)}_{i\tilde{G}_0^{-1}(x,y)} \underbrace{-\frac{\lambda}{2}\phi^2(x)\delta_{\mathcal{C}}(x-y)}_{i\tilde{G}_{\phi,\text{int}}^{-1}}, \tag{2.44}$$

we have the following interaction part of the 2PI effective action in this three-loop truncation

$$\Gamma_{\text{2PI, int}}[\phi, G] = -\frac{\lambda}{4!}\int_x \phi^4(x) - \frac{\lambda}{4}\int_x \phi^2(x)G(x,x) - \frac{\lambda}{8}\int_x G^2(x,x) + \frac{i\,\lambda^2}{48}\int_x\int_y G^4(x,y)\,. \tag{2.45}$$

This gives the EOMs according to (2.37) and (2.38) as

$$\left(\Box_x + m^2 + \frac{\lambda}{2}\phi^2(x) + \frac{\lambda}{2}G(x,x)\right)\phi(x) = 0\,, \tag{2.46}$$

$$\left[\Box_x + m^2 + \frac{\lambda}{2}\phi^2(x) + \frac{\lambda}{2}G(x,x)\right]G(x,z) - i\frac{\lambda^2}{6}\int_y G^3(x,y)G(y,z) = \delta_{\mathcal{C}}(x-z)\,, \tag{2.47}$$

where (2.47) was obtained by multiplying the stationarity condition (2.38) by $G(y,z)$ and integrating. As a result, the term outside of square parenthesis in this equation forms an example of the aforementioned memory integral as it integrates over the time history of the evolution [49, 50, 54]. One can then numerically solve these equations with a set of boundary conditions to obtain the profiles for ϕ and G. The memory integrals have been known to grow with time and tend to slow down the numerical evaluation [49, 50, 54].

2.3.3 Including Fermions

Analogously as in the 1PI effective action, the 2PI effective action is modified to include fermions as [40, 49, 50],

$$\begin{aligned}\Gamma_{\text{2PI}}[\phi, G, D] =& S[\phi,\psi] + \frac{i}{2}\text{Tr}_{\mathcal{C}}\log G^{-1} + \frac{i}{2}\text{Tr}_{\mathcal{C}}\left[\tilde{G}_{\phi}^{-1}(\phi)\,G\right] \\ &- \text{Tr}_{\mathcal{C}}\log D^{-1} - \text{Tr}_{\mathcal{C}}\left[\tilde{D}_{\psi}^{-1}\,D\right] + \Gamma_2[\phi, G, D] + \text{const.}\,,\end{aligned} \tag{2.48}$$

where D is the resummed fermionic propagator. One defines a self-energy corresponding to D [49, 50, 66] as

$$\Sigma(x,y) = i\frac{\delta\Gamma_2[\phi, G, D]}{\delta D(x,y)}\,. \tag{2.49}$$

We now give the stationarity condition for D as

$$\left.\frac{\delta\Gamma_{\text{2PI}}[\phi, G, D]}{\delta D(x,y)}\right|_{\overline{\phi},\overline{G},\overline{D}} = 0\,, \tag{2.50}$$

and do not write down one for the fermionic field ψ. The reason for this is one can interpret the stationarity condition for a field as it acquiring a vacuum expectation value (VEV). Assuming that Lorentz invariance is preserved, only scalar fields (like ϕ) can acquire VEVs.

Performing the similar splitting of the effective action as in (2.34) and (2.35) with the fermionic parts, we obtain the generic equation of motion for D as

$$(i\not{\partial}_x - M)D(x,z) + \int_y \overline{\Sigma}(x,y)D(y,z) = \delta_{\mathcal{C}}(x-z)\,, \tag{2.51}$$

where M is the free fermionic mass and we have defined

$$\overline{\Sigma}(x,y) = i\frac{\delta\Gamma_{\text{2PI, int}}[\phi,G,D]}{\delta D(x,y)}\bigg|_{\overline{\phi},\overline{G},\overline{D}}\,. \tag{2.52}$$

2.4 Effective Potential

We now describe how one obtains the effective potential from the effective action. Let us understand this from the more familiar 1PI formalism by referring to the stationarity condition (2.13)

$$\frac{\delta\Gamma_{\text{1PI}}[\phi]}{\delta\phi(x)}\bigg|_{\phi(x)=v(x)} = 0 \tag{2.53}$$

where v is the VEV. Equation (2.53) is alternately referred to as the *minimisation condition*.

The effective potential is an equilibrium quantity [60], so we can assume Poincaré invariance so that the vacuum states are independent of the space-time coordinate x. This reduces (2.53) to solving for the variable v. Now, the effective action, in analogy to thermodynamics, is an extensive quantity meaning that it is proportional to the volume of the space-time region, $\mathcal{V}$. With the aforementioned consideration of Poincaré invariance, we can express

$$\Gamma_{\text{1PI}}[\phi]\Big|_{\text{K.E.}\,=\,0} = \mathcal{V}\,\left(-V_{\text{1PI}}(\phi)\right)\,, \tag{2.54}$$

where K.E. $= 0$ refers to setting the kinetic terms of fields in the Lagrangian to 0. Hence, $V_{\text{1PI}}(\phi)$ is the *1PI effective potential* and this transforms the minimisation condition into

$$\frac{\partial V_{\text{1PI}}(\phi)}{\partial\phi}\bigg|_{\phi=v} = 0\,. \tag{2.55}$$

This analysis carries over to the 2PI formalism to similarly study the vacuum structure of a theory. One considers any ϕ and evaluates the corresponding propagators as a function of ϕ, i.e. $G \equiv G(\phi)$ and $D \equiv D(\phi)$. This leads to a 2PI effective action $\Gamma_{\text{2PI}}[\phi, G(\phi), D(\phi)] \equiv \Gamma_{\text{2PI}}[\phi]$ and gives rise to the 2PI effective potential in a similar manner to (2.54). As we will employ methods in momentum space in Chapters 3 and 4, it is more convenient to define the 2PI effective action normalised to the space-time volume, i.e.

$$\widehat{\Gamma}_{\text{2PI}}[\phi] = \frac{1}{\mathcal{V}}\,\Gamma_{\text{2PI}}[\phi]\,, \tag{2.56}$$

and accordingly, the 2PI improved effective potential is given by

$$V_{\text{2PI}}(\phi) = -\widehat{\Gamma}_{\text{2PI}}[\phi]\Big|_{\text{K.E.}\,=\,0}\,, \tag{2.57}$$

which then forms a convenient tool to study phase transitions in the 2PI formalism.

We mention here that, so far, we have considered the unrenormalised action. A crucial step to obtain self-consistent results and/or compare different approaches when solving the EOMs is to perform a consistent renormalisation of the 2PI effective action. This requires setting up appropriate renormalisation conditions and specific tools to resolve divergences and sub-divergences. Furthermore, the renormalisation of the 2PI effective action is a necessary step in the evaluation of the 2PI improved effective potential. Thus, the task of a consistent renormalisation programme in the 2PI formalism form the basis of Chapters 3 and 4.

Chapter 3

On-shell Renormalisation

In this chapter, which describes the results of [67], we carry out the renormalisation of the 2PI effective action. We restrict ourselves to all contributions up to two-loop order, which amounts to truncations till the Hartree approximation, the scalar sunset approximation and the fermionic sunset approximation. As novel aspects, we *(i)* carry out the renormalisation in the broken phase and *(ii)* will consistently treat the renormalisation of fermions in the 2PI formalism.

We take the following classical action as a starting point

$$\begin{aligned} S[\phi,\psi] &= S_0[\phi,\psi] + S_{\rm int}[\phi,\psi] \\ &= \int_x \left\{ \frac{1}{2}\partial_\mu\phi(x)\partial^\mu\phi(x) - \frac{m^2}{2}\phi^2(x) - \frac{\alpha}{3!}\phi^3(x) - \frac{\lambda}{4!}\phi^4(x) \right. \\ &\qquad \left. + \overline{\psi}(x)(i\partial\!\!\!/ - M)\psi(x) - g\overline{\psi}(x)\psi(x)\phi(x) \right\}. \end{aligned} \tag{3.1}$$

Accordingly (c.f. (2.34) and (2.35)), the 2PI action up to this order is given by

$$\begin{aligned} \Gamma_{\rm 2PI}[\phi,G,D] &= \int_x \left\{ \frac{1}{2}\partial_\mu\phi(x)\partial^\mu\phi(x) - \frac{m^2}{2}\phi^2(x) - \frac{\alpha}{3!}\phi^3(x) - \frac{\lambda}{4!}\phi^4(x) \right. \\ &- \frac{1}{2}\left(\Box_x + m^2\right) G(x,y)|_{x=y} - \frac{1}{2}\alpha\,\phi(x)\,G(x,x) - \frac{1}{8}\lambda G^2(x,x) - \frac{1}{4}\lambda\,\phi^2(x)\,G(x,x) \\ &\left. + \mathrm{tr}\left[\left(i\partial\!\!\!/_x - M\right) D(x,y)|_{x=y}\right] - g\,\phi(x)\ \mathrm{tr}[D(x,x)] \right\} \\ &+ \int_x\int_y \left\{ \frac{i}{12}(\alpha+\lambda\phi(x))(\alpha+\lambda\phi(y))\,G^3(x,y) - \frac{i}{2}g^2 G(x,y)\ \mathrm{tr}\left[D(x,y)D(y,x)\right] \right\}. \end{aligned} \tag{3.2}$$

Here, "tr[...]" indicates the trace taken over spinor indices. As mentioned in Chapter 2, we make the assumption that ψ does not acquire a VEV, allowing us to neglect terms linear in ψ.

In the 2PI formalism, the scalar and fermionic two-point functions, G and D, are propagators resummed to all orders in perturbation theory. Thus, terms in (3.2) involving only the one-point function ϕ and the propagators G and D as well as mixed terms involving G, D and ϕ, would constitute separate interactions, because we are essentially mixing orders in perturbation theory. Consequently, these vertices and the corresponding couplings need to be renormalised separately. To this end, we need to define different mass and coupling constant counterterms, depending on the combination of one- and two-point functions connecting to a 'vertex'. This becomes more clear as we define the renormalised fields from the bare ones, using their respective wave-function renormalisations,

$$\begin{aligned} \phi(x) &= Z_{\phi,2}^{\frac{1}{2}}\phi_R(x)\,, \qquad G(x,y) = Z_{\phi,0}\,G_R(x,y)\,, \\ \psi(x) &= Z_{\psi,2}^{\frac{1}{2}}\psi_R(x)\,, \qquad D(x,y) = Z_{\psi,0}\,D_R(x,y)\,. \end{aligned} \tag{3.3}$$

Then, the corresponding renormalised quantities would be given as

$$\begin{aligned} Z_{\phi,2}m^2 &= m_R^2 + \delta m_2^2\,, \quad Z_{\phi,2}^{\frac{i}{2}}Z_{\phi,0}^{\frac{3-i}{2}}\,\alpha = \alpha_R + \delta\alpha_i \quad (i=0,1,2,3)\,, \\ Z_{\phi,0}m^2 &= m_R^2 + \delta m_0^2\,, \quad Z_{\phi,2}^{\frac{j}{2}}Z_{\phi,0}^{\frac{(4-j)}{2}}\,\lambda = \lambda_R + \delta\lambda_j \quad (j=0,2,4)\,, \\ Z_{\psi,0}M &= M_R + \delta M_0\,, \quad Z_{\psi,0}Z_{\phi,2}^{\frac{k}{2}}Z_{\phi,0}^{\frac{1-k}{2}}\,g = g_R + \delta g_k \quad (k=0,1)\,, \end{aligned} \tag{3.4}$$

where we have indicated the number of fields $\phi\,(\psi)$ associated with a term by the index i in $Z_{\phi,i}\,(Z_{\psi,i})$ and adopted a similar notation for the coupling constants. Note that we have chosen to renormalise the masses for ϕ and G to the same value. We do the same for the trilinear, quartic and Yukawa couplings. Finally, one needs an additional counterterm in the action to cancel possible loop-induced divergences to the effective action linear in ϕ_R,

$$-\int_x \delta t_1\,\phi_R(x)\,. \tag{3.5}$$

With the renormalised quantities introduced, we can define the interacting part of the renormalised 2PI effective action

$$\begin{aligned} &\Gamma_{\text{2PI,int}}[\phi_R, G_R, D_R] \;= \\ &\int_x \Bigg\{ \frac{\delta Z_{\phi,2}}{2}\partial_\mu\phi_R(x)\partial^\mu\phi_R(x) - \frac{\delta m_2^2}{2}\phi_R^2(x) - \frac{(\alpha_R+\delta\alpha_3)}{3!}\phi_R^3(x) - \frac{(\lambda_R+\delta\lambda_4)}{4!}\phi_R^4(x) - \delta t_1\phi_R(x) \\ &- \frac{\delta Z_{\phi,0}}{2}\left(\Box_x + \delta m_0^2\right)G_R(x,y)|_{x=y} - \frac{(\alpha_R+\delta\alpha_1)}{2}\,\phi_R(x)\,G_R(x,x) - \frac{(\lambda_R+\delta\lambda_0)}{8}G_R^2(x,x) \\ &- \frac{(\lambda_R+\delta\lambda_2)}{4}\,\phi_R^2(x)\,G_R(x,x) \\ &+ \mathrm{tr}\left[\left(i\delta Z_{\psi,0}\partial\!\!\!/_x - \delta M_0\right)D_R(x,y)|_{x=y}\right] - (g_R+\delta g_1)\,\phi_R(x)\;\mathrm{tr}[D_R(x,x)]\Bigg\} \\ &+ \int_x\int_y \Bigg\{ \frac{i}{12}[(\alpha_R+\delta\alpha_0)+(\lambda_R+\delta\lambda_1)\phi_R(x)][(\alpha_R+\delta\alpha_0)+(\lambda_R+\delta\lambda_1)\phi_R(y)]\,G_R^3(x,y) \end{aligned}$$

$$- \frac{i}{2}(g_R + \delta g_0)^2 G_R(x,y)\ \mathrm{tr}\left[D_R(x,y)D_R(y,x)\right] \Bigg\} \,. \tag{3.6}$$

Correspondingly, we can write down now the renormalised equations of motion using (2.37), (2.38) and (2.51),

$$\left[(1+\delta Z_{\phi,2})\Box_x + \widehat{m}_2^2(x)\right]\phi_R(x) = -\delta t_1 - \frac{(\alpha_1+\delta\alpha_1)}{2}G_R(x,x) - (g_1+\delta g_1)\,\mathrm{tr}[D_R(x,x)] \\ - \frac{i}{6}\int_y \left[(\lambda_R+\delta\lambda_1)(\alpha_R+\delta\alpha_0+(\lambda_R+\delta\lambda_1)\phi_R(y)\right] G^3(x,y)\,, \tag{3.7}$$

$$\left[(1+\delta Z_{\phi,0})\Box_x + \widehat{m}_0^2(x)\right] G_R(x,y) = \delta_{\mathcal{C}}(x-y) - \int_z \Pi(x,z)G_R(z,y)\,, \tag{3.8}$$

$$\left[i\,(1+\delta Z_{\psi,0})\,\partial\!\!\!/_x - \widehat{M}_0(x)\right] D_R(x,y) = \delta_{\mathcal{C}}(x-y) - \int_z \Sigma(x,z)D_R(z,y)\,, \tag{3.9}$$

with

$$\widehat{m}_2^2(x) = m_R^2 + \delta m_2^2 + \frac{1}{2}(\alpha_3+\delta\alpha_3)\phi_R(x) + \frac{1}{6}(\lambda_4+\delta\lambda_4)\phi_R^2(x) + \frac{1}{2}(\lambda_2+\delta\lambda_2)G_R(x,x)\,, \tag{3.10}$$

$$\widehat{m}_0^2(x) = m_R^2 + \delta m_0^2 + \frac{1}{4}(\lambda_0+\delta\lambda_0)G_R(x,x) + \frac{1}{2}(\alpha_3+\delta\alpha_3)\phi_R(x) + \frac{1}{4}(\lambda_2+\delta\lambda_2)\phi_R^2(x)\,, \tag{3.11}$$

$$\widehat{M}_0(x) = (M_R+\delta M_0) + (g_1+\delta g_1)\phi_R(x)\,, \tag{3.12}$$

$$\Pi(x,z) = -\frac{i\left[(\alpha_0+\delta\alpha_0)+(\lambda_R+\delta\lambda_1)\phi_R(x)\right]\left[(\alpha_0+\delta\alpha_0)+(\lambda_R+\delta\lambda_1)\phi_R(z)\right]}{4} G_R^2(x,z) \\ + \frac{i(g_0+\delta g_0)^2}{2}\,\mathrm{tr}[D_R(x,z)D_R(z,x)]\,, \tag{3.13}$$

$$\Sigma(x,z) = \frac{i(g_0+\delta g_0)^2}{2}\,G_R(x,z)\left[D_R(x,z)+D_R(z,x)\right]\,. \tag{3.14}$$

Here, we have split the self-energies $\overline{\Pi}(x,z)$ and $\overline{\Sigma}(x,z)$ into non-local contributions $\Pi(x,z)$ and $\Sigma(x,z)$ and local ones which are absorbed in $\widehat{m}_0^2(x)$ and $\widehat{M}_0(x)$, respectively. The non-local contributions form the memory integrals that we have mentioned in the previous chapter.

The task now is to obtain the various counterterms. According to [65], renormalisation may be carried out in the vacuum at temperature $T = 0$. It is most convenient to proceed in momentum space, which allows us to employ the usual techniques to determine the various counterterms. In this chapter, we will employ an on-shell scheme, with appropriate renormalisation conditions to determine the various counterterms. This is useful in expressing various quantities in terms of measured masses and couplings. In line with this, we focus on obtaining the counterterms in the broken phase.

3.1 Tools for Renormalisation

We will now detail the various tools required to carry out the renormalisation in the 2PI formalism. We will then make use of these in further sections of this chapter, when we examine the various truncations.

3.1.1 2PI Kernels and Bethe-Salpeter Equations

The standard Bogoliubov-Parasiuk-Hepp-Zimmermann (BPHZ) analysis used in standard QFT to determine the structure of the divergences, does not suffice in case of the 2PI formalism (see, for e.g. [65] and references therein), due to the resummed nature of the propagator. The solution is to define auxiliary vertex functions which can be resummed such that a consistent renormalisation with only a finite number of counterterms is possible.

We first define the 2PI kernel [58, 65]

$$\overline{\Lambda}^{(4)}(x_1,x_2,x_3,x_4) \equiv 4\frac{\delta^2\Gamma_{\text{2PI,int}}}{\delta G(x_1,x_2)\delta G(x_3,x_4)}\bigg|_{\overline{\phi},\overline{G}}, \tag{3.15}$$

which is resummed by the following vertex function using a Bethe-Salpeter equation (BSE)

$$\begin{aligned}\overline{V}^{(4)}(x_1,x_2,x_3,x_4) &= \overline{\Lambda}^{(4)}(x_1,x_2,x_3,x_4)\\ &\quad+\frac{i}{2}\int_{y_1\ldots y_4}\overline{\Lambda}^{(4)}(x_1,x_2,y_1,y_2)\overline{G}(y_1,y_3)\overline{G}(y_2,y_4)\overline{V}^{(4)}(y_3,y_4,x_3,x_4)\,.\end{aligned} \tag{3.16}$$

In addition, we need an auxiliary vertex function

$$\begin{aligned}V^{(4)}(x_1,x_2,x_3,x_4) &= \Lambda^{(4)}(x_1,x_2,x_3,x_4)\\ &\quad+\frac{i}{2}\int_{y_1\ldots y_4}\Lambda^{(4)}(x_1,x_2,y_1,y_2)\overline{G}(y_1,y_3)\overline{G}(y_2,y_4)\overline{V}^{(4)}(y_3,y_4,x_3,x_4)\,,\end{aligned} \tag{3.17}$$

with

$$\Lambda^{(4)}(x_1,x_2,x_3,x_4) \equiv 4\frac{\delta^2\Gamma_{\text{2PI,int}}}{\delta G(x_1,x_2)\delta\phi(x_3)\delta\phi(x_4)}\bigg|_{\overline{\phi},\overline{G}}. \tag{3.18}$$

For fermions, we will introduce and describe the required machinery in Sec. 3.4, so for the moment, we give the framework for scalars.

The two-point functions in this case can be evaluated from the stationarity condition (2.38), leading to the **gap equation** for the scalars

$$\bar{G}^{-1}(x,y;\phi) = G_0^{-1}(x,y) - \overline{\Pi}(x,y;\phi)\,. \tag{3.19}$$

We will, in view of the renormalisation procedure, choose the point $\overline{G} = G_R$ and $\overline{\phi} = \phi_R \neq 0$. In the on-shell scheme that we will describe, ϕ_R is the VEV, and this is determined by the stationarity condition as

$$i\Gamma^{(1)}(x) = \frac{\delta\Gamma_{\text{2PI}}}{\delta\phi(x)}\bigg|_{\overline{\phi},\overline{G}} + \int_{y,z}\underbrace{\frac{\delta\Gamma_{\text{2PI}}}{\delta G(y,z)}\bigg|_{\overline{\phi},\overline{G}}}_{=0}\frac{\delta G(y,z)}{\delta\phi(x)} \stackrel{!}{=} 0 \tag{3.20}$$

where $\Gamma^{(1)}$ denotes the physical one-point function. Note that we have used the chain rule to obtain the second term, as G obtained from (3.19) depends on ϕ. This term vanishes due to the stationarity condition of the 2PI effective action, which we have marked. Now, in analogy to the 1PI formalism (see Sec. 2.2), it would be natural to consider further field derivatives of the 2PI effective action to obtain n-point functions ($n > 2$) pertaining to only the fields

$$i\Gamma^{(n)}(x_1,\ldots,x_n) \;=\; \frac{\delta^n\Gamma_{\text{2PI}}}{\delta\phi(x_1)\ldots\delta\phi(x_n)}\bigg|_{\overline{\phi},\overline{G}}\,. \tag{3.21}$$

As mentioned, one has to take care since G depends on ϕ. For example, consider the physical two-point function for the fields, obtained by taking another derivative of (3.20)

$$\begin{aligned}\frac{\delta^2\Gamma_{\text{2PI}}}{\delta\phi(x_1)\delta\phi(x_2)} = \frac{\delta^2\Gamma_{\text{2PI}}}{\delta\phi(x_1)\delta\phi(x_2)}\bigg|_{\overline{\phi},\overline{G}} + \int_{y_1,y_2}\frac{\delta\Gamma_{\text{2PI}}}{\delta\phi(x_1)\delta G(y_1,y_2)}\bigg|_{\overline{\phi},\overline{G}}\frac{\delta G(y_1,y_2)}{\delta\phi(x_2)}\\ + \int_{y_1,y_2}\underbrace{\frac{\delta\Gamma_{\text{2PI}}}{\delta G(y_1,y_2)}\bigg|_{\overline{\phi},\overline{G}}}_{=0}\frac{\delta^2 G(y_1,y_2)}{\delta\phi(x_1)\delta\phi(x_1)}\,.\end{aligned}$$

We take a field derivative of the propagator

$$\frac{\delta G(x,y)}{\delta\phi(z)} = -\int_{u,v} G(x,u)G(y,v)\frac{\delta G^{-1}(u,v)}{\delta\phi(z)} = \int_{u,v} G(x,u)G(y,v)\frac{\delta\overline{\Pi}(u,v)}{\delta\phi(z)}\,, \tag{3.22}$$

where, to obtain the second equality, we have used the gap equation (3.19). Substituting this into the equation for the physical two-point function for the fields,

$$\begin{aligned}i\Gamma^{(2)}(x_1,x_2) \equiv \frac{\delta^2\Gamma_{\text{2PI}}}{\delta\phi(x_1)\delta\phi(x_2)} = iG_0^{-1}(x_1,x_2) + \frac{\delta^2\Gamma_{\text{2PI,int}}}{\delta\phi(x_1)\delta\phi(x_2)}\bigg|_{\overline{\phi},\overline{G}}\\ + \int_{y_1\ldots y_4}\frac{\delta^2\Gamma_{\text{2PI,int}}}{\delta\phi(x_1)\delta G(y_1,y_2)}\bigg|_{\overline{\phi},\overline{G}}G(y_1,y_3)\frac{\delta\overline{\Pi}(y_3,y_4)}{\delta\phi(x_2)}G(y_4,y_2)\,.\end{aligned} \tag{3.23}$$

Thus, in general, for the n-point functions, a system of coupled integral equations emerges, which have the following form

$$\begin{aligned}i\frac{\delta^n\Gamma_{\text{2PI}}}{\delta\phi(x_1)\ldots\delta\phi(x_n)} \;&=\; \mathcal{A}^{(n)}(x_1,\ldots,x_n)\\ &+\int_{z_1\ldots z_4}\frac{\delta^2 i\Gamma_{\text{2PI,int}}}{\delta\phi(x_1)G(z_1,z_2)}\bigg|_{\overline{\phi},\overline{G}}\overline{G}(z_1,z_3)\frac{\delta^{n-1}\overline{\Pi}(z_3,z_4)}{\delta\phi(x_2)\ldots\delta\phi(x_n)}\overline{G}(z_4,z_2)\end{aligned} \tag{3.24}$$

$$\begin{aligned}\frac{\delta^n\overline{\Pi}(y_1,y_2)}{\delta\phi(x_1)\ldots\delta\phi(x_n)} \;&=\; \mathcal{B}^{(n)}(y_1,y_2,x_1,\ldots,x_n)\\ &+\int_{z_1\ldots z_4}\frac{\delta^2 2i\Gamma_{\text{2PI,int}}}{\delta G(y_1,y_2)\,\delta G(z_1,z_2)}\bigg|_{\overline{\phi},\overline{G}}\overline{G}(z_1,z_3)\frac{\delta^n\overline{\Pi}(z_3,z_4)}{\delta\phi(x_1)\ldots\delta\phi(x_n)}\overline{G}(z_4,z_2)\,.\end{aligned} \tag{3.25}$$

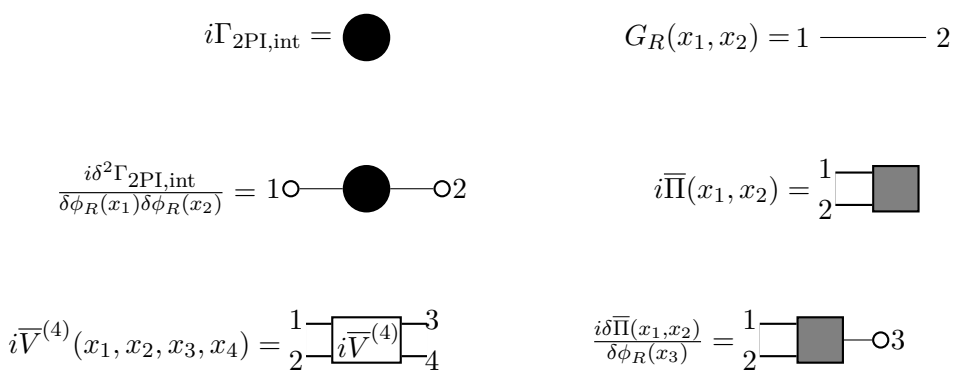

Figure 3.1: Graphical representation of basic building blocks

The functions $\mathcal{A}^{(n)}$ and $\mathcal{B}^{(n)}$ contain various derivatives of $\Gamma_{\text{2PI,int}}$ w.r.t. ϕ and G at the stationarity point [65], as well as field derivatives of $\overline{\Pi}$ of the form $\delta^k\overline{\Pi}/\delta\phi^k$ where $k < n$, as we have demonstrated from the simpler example of the two-point function for the fields. A formal solution [65] to the self-energy integral equation (3.25) can be given in terms of the vertex function $\overline{V}^{(4)}$, c.f. (3.16), as

$$\begin{aligned}\frac{\delta^n\overline{\Pi}(y_1, y_2)}{\delta\phi(x_1)\dots\delta\phi(x_n)} &= \mathcal{B}^{(n)}(y_1, y_2, x_1, \dots, x_n) \\ &\quad + \frac{1}{2}\int_{z_1\dots z_4} i\overline{V}^{(4)}(y_1, y_2, z_1, z_2)\overline{G}(z_1, z_3)\mathcal{B}^{(n)}(z_3, z_4, x_1, \dots, x_n)\overline{G}(z_4, z_2)\,,\end{aligned} \tag{3.26}$$

and from this, one also obtains the solution to (3.24).

3.1.2 Diagrammatic Treatment of Integral Equations

To treat the various integral equations encountered in the course of determining the n-point functions, it is useful to consider a diagrammatic representation, as described in [65]. The basic building blocks are given in Fig. 3.1.

Consider the physical two-point function in (3.23). Using the diagrams defined in Fig. 3.1, this reads in graphical form

$$\frac{\delta^2\Gamma_{\text{2PI}}}{\delta\phi_R(x_1)\delta\phi_R(x_2)} = iG^{-1}_{0,R}(x_1, x_2) + \quad 1 \quad 2 \quad + \frac{1}{2} \quad 1 \quad 2 \tag{3.27}$$

We can then replace the derivative of the self-energy w.r.t. a field expectation value, i.e. $\delta\overline{\Pi}/\delta\phi_R$ which is the third term of (3.27), using the following graphical representation, c.f. (3.26),

$$1\ 2\ 3 \ = \ 1\ 2\ 3 \ + \frac{1}{2} \ 1\ 2\ \overline{V}^{(4)}\ 3 \tag{3.28}$$

which are all known quantities.

One can then examine the three-point function for the fields. Another differentiation w.r.t. ϕ_R of (3.27) gives the following topologies

$\Gamma^{(3)} =$ 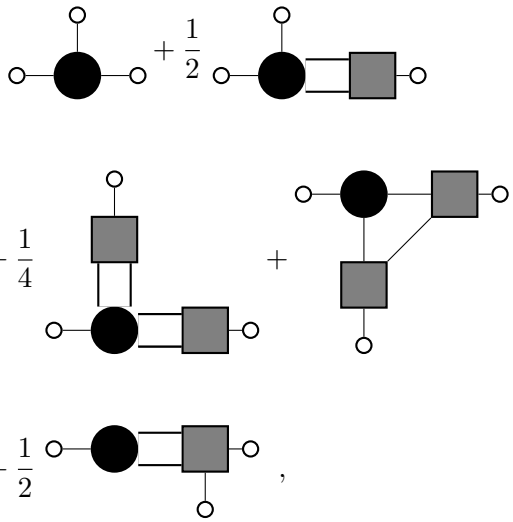 (3.29)

Taking now the four-point function, we have the possible contributing diagrams ,

$\Gamma^{(4)} =$ 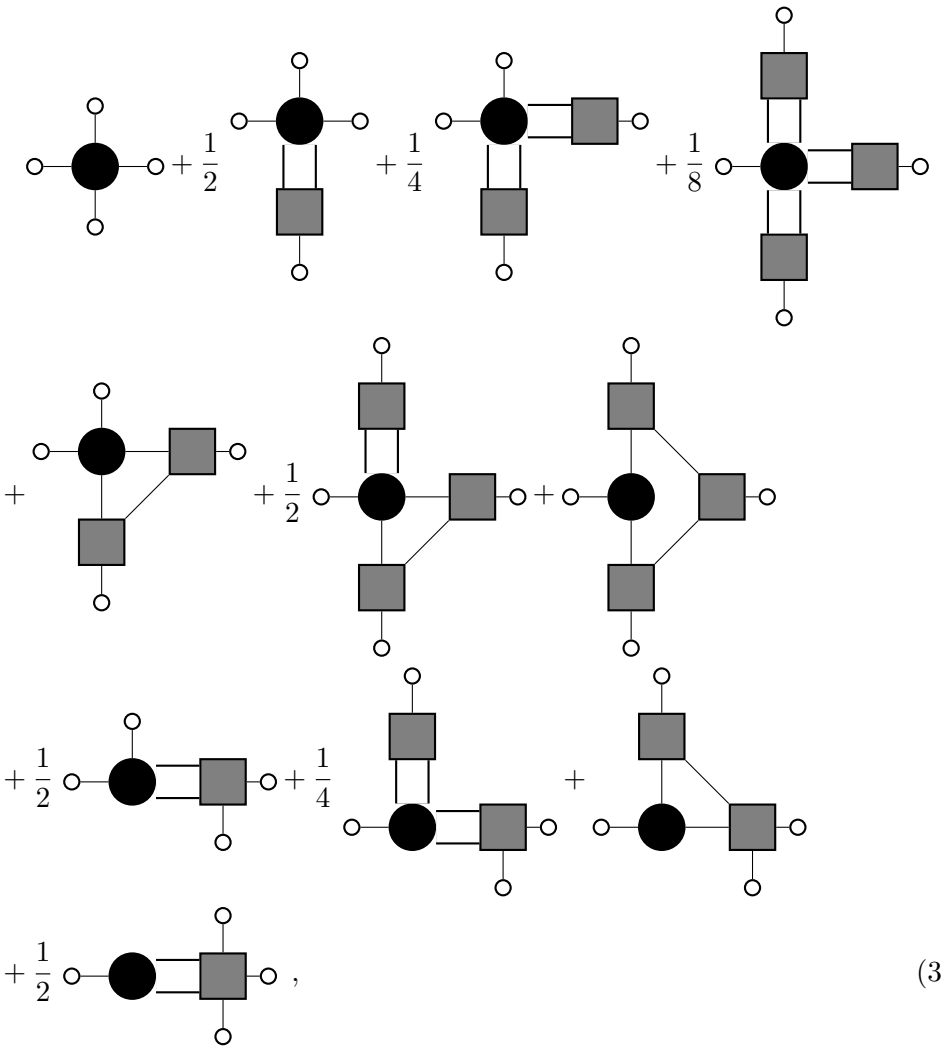 (3.30)

where in (3.29) and (3.30), the new quantities, $\delta^2\overline{\Pi}/\delta\phi_R^2$ and $\delta^3\overline{\Pi}/\delta\phi_R^3$ appear. For the sake of brevity, the "legs" representing the external space-time points, previously denoted in the diagrams with numbered indices, are now suppressed and it is understood that all permutations of x_2, x_3 (and x_4 for the four-point function) contribute, as long as the resulting diagrams are not equivalent. An example of such a diagram where permutations must be considered, is

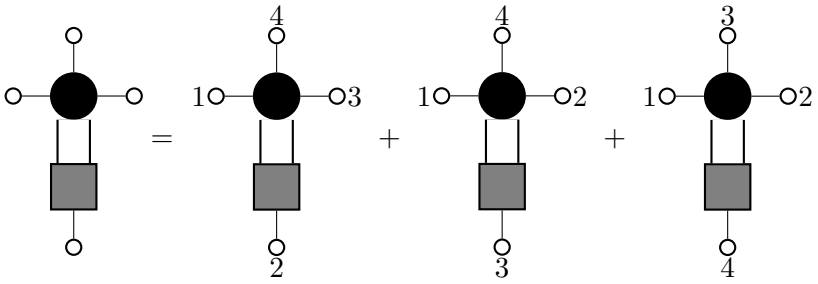

(3.31)

It is important to note that the index 1 is not part of the permutation. This happens because the diagrams are obtained by a subsequent differentiation with respect to the four fields $\phi_R(x_1)$, …, $\phi_R(x_4)$. The first self-energy box only appears in the second differentiation and thus the 1-index is always attached to the $\Gamma_{\text{2PI,int}}$ blob. In the subsequent discussion, the leg to the left side is always considered to correspond to the 1-index. At first glance, this might seem to not be in line with the symmetry properties of the 4-point function, such as $\Gamma^{(4)}(x_1, x_2, x_3, x_4) = \Gamma^{(4)}(x_2, x_1, x_3, x_4)$ and so on. However, these properties are only hidden in the above case and become apparent once the identities of the self-energy boxes are inserted.

The single derivative is given in (3.28). The other two can be expressed using diagrams that contain only the first derivative of the self-energy. Permutations of field indices are implied wherever they lead to non-equivalent topologies.

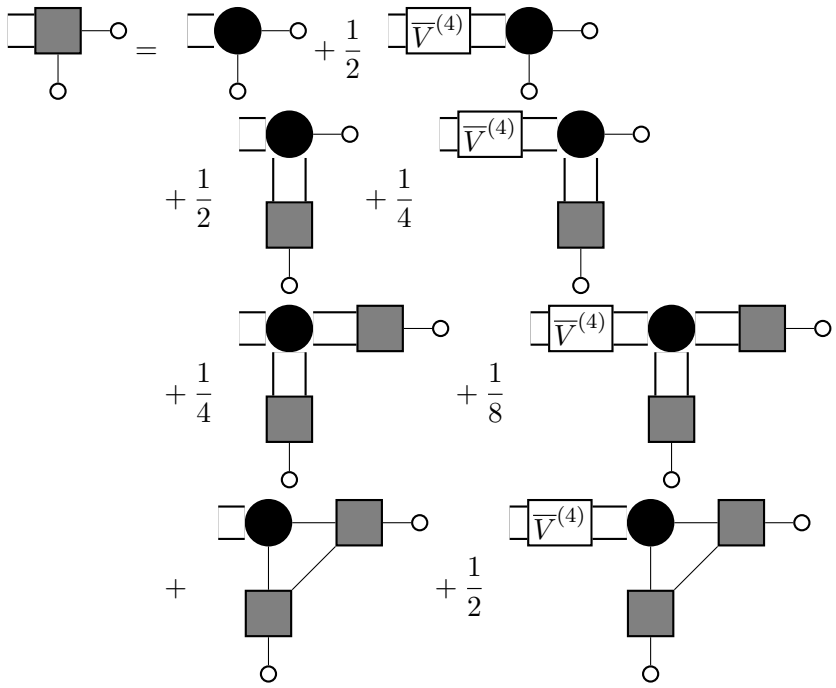

(3.32)

For the triple derivative $d^3\overline{\Pi}/d\phi_R^3$, it is more convenient to not insert instances of the double derivative $d^3\overline{\Pi}/d\phi_R^2$ as the expressions get too lengthy otherwise. One simply needs to substitute the corresponding diagrams from (3.32) at places where boxes with two field derivatives appear. Thus, we find

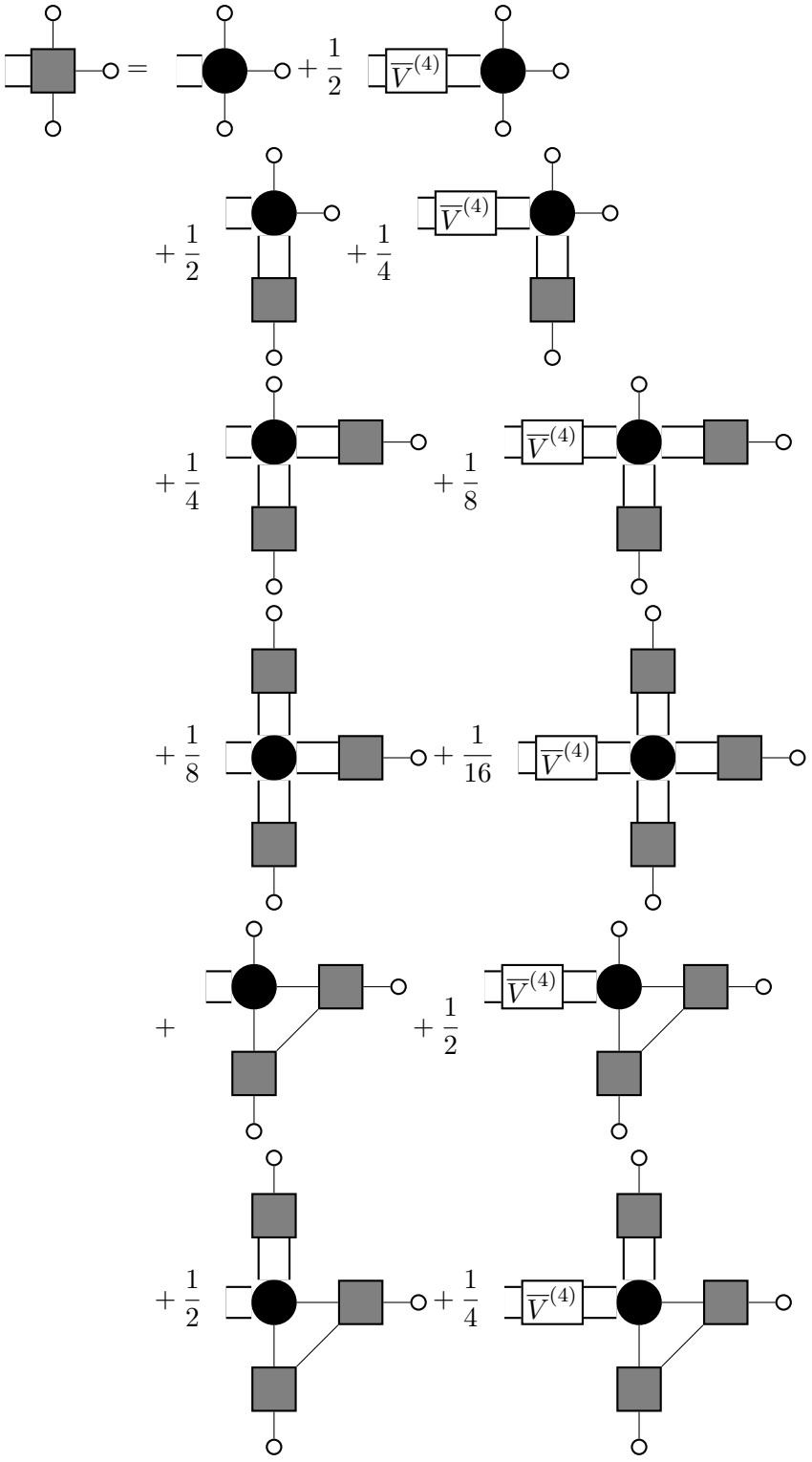

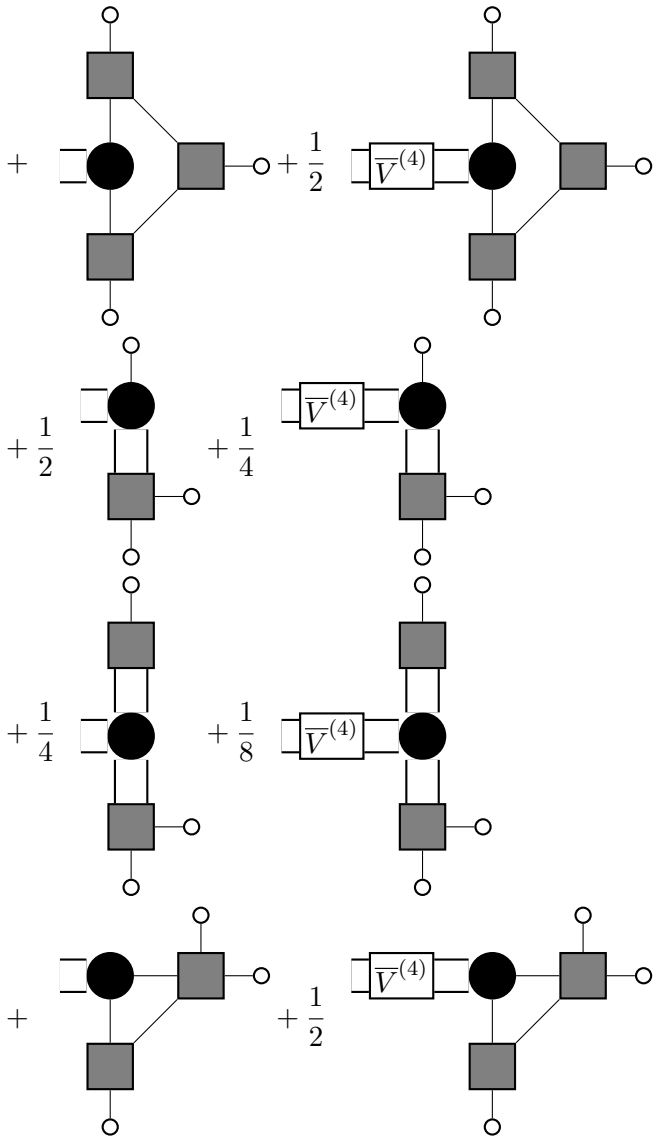

(3.33)

3.2 Hartree Approximation

Although the Hartree approximation has been treated in literature already several times [68–70], we will reconsider it in order to exemplify some of the details involved. As mentioned before, we will focus mainly on results in the broken phase. Consider now the interacting part of the 2PI effective action, in momentum space, normalised to the space-time volume (as discussed in Sec. 2.4)

$$\widehat{\Gamma}_{\text{2PI,int}}[\phi_R, G_R] = \frac{(\delta Z_{\phi,2}\, p^2 - \delta m_2^2)}{2}\phi_R^2 - \frac{(\lambda_R + \delta\lambda_4)}{4!}\phi_R^4 + \frac{\delta Z_{\phi,0}}{2}\int_p p^2 G_R(p)$$
$$- \frac{1}{2}\left[\delta m_0^2 + \frac{(\lambda_R + \delta\lambda_2)}{2}\phi_R^2\right]\int_p G_R(p) - \frac{(\lambda_R + \delta\lambda_0)}{8}\left(\int_p G_R(p)\right)^2 . \tag{3.34}$$

Note that here we have made the assumption that we are close to the minimum of the potential and taken ϕ_R to be constant, which we will continue to do so for the other truncations of the 2PI effective action we will discuss.

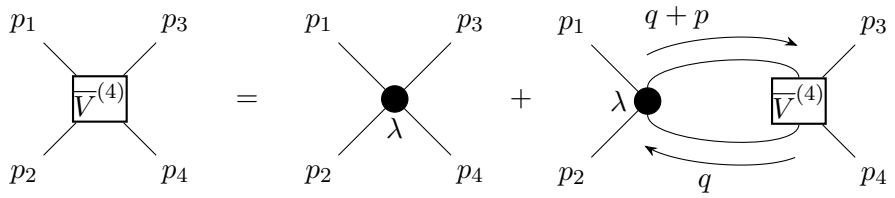

Figure 3.2: Illustration of the BSE in the Hartree approximation. Here, the convention is $p_{1,2}$ are incoming four-momenta and $p_{3,4}$ are outgoing, with $p = p_1 + p_2$.

We first obtain the four-point kernel

$$\overline{\Lambda}^{(4)} = 4\,\frac{\delta^2\widehat{\Gamma}_{\text{2PI,int}}}{\delta G_R(k)\delta G_R(q)} = -(\lambda_R + \delta\lambda_0)\,, \tag{3.35}$$

which is evidently independent of the (external) momentum. Thus, the Bethe-Salpeter equation (3.16) can be considerably simplified within the Hartree approximation. As the vertex function is an infinite resummation of iterations of this kernel, stitched together by loops with two propagators (see Fig. 3.2), the only origin of a momentum dependence in $\overline{V}^{(4)}$ is from the loop function depending on the sum of external momenta $p = p_1 + p_2$. Hence, we arrive at

$$\overline{V}^{(4)}(p) = -(\lambda_R + \delta\lambda_0) \;-\; \frac{i}{2}(\lambda_R + \delta\lambda_0)\,\overline{V}^{(4)}(p)\int_q G_R(q)G_R(p+q)\,. \tag{3.36}$$

At this point, it is convenient to calculate p^2 in the center of mass (COM) system. This gives the familiar result

$$p^2 = p_1^2 + p_2^2 + 2p_1\cdot p_2 = 4E_*^2\,, \tag{3.37}$$

where E_* is the COM energy. In the COM system, there are two variables that play a role, the three-momentum in the COM frame[1], $\vec{p}$, and the scattering angle, θ. Fixing these quantities amounts to fixing the renormalisation condition. Let $p_*^2 = 4m_R^2$ be the renormalisation point corresponding to the COM three-momentum $|\vec{p_*}| = 0$ and the scattering angle $\theta_* = \pi$. At this renormalisation point, let

$$\overline{V}(p_*) = -\lambda_R\,. \tag{3.38}$$

This allows us to solve exactly for the counterterm

$$\delta\lambda_0 = -\lambda_R + \frac{\lambda_R}{1 - \frac{1}{2}\lambda_R\mathcal{I}(p_*^2)} \quad \text{with} \quad \mathcal{I}(p^2) = i\int_q G_R(q)G_R(p+q)\,, \tag{3.39}$$

which we can insert in (3.36) to obtain the vertex function

$$\overline{V}^{(4)}(p) = -\frac{\lambda_R}{1 - \frac{\lambda_R}{2}\left(\mathcal{I}(p_*^2) - \mathcal{I}(p^2)\right)}\,. \tag{3.40}$$

From this, we can immediately observe that $\overline{V}^{(4)}(p)$ is finite as any potential divergences present in the loop integral $\mathcal{I}(p^2)$ cancels in the difference $\mathcal{I}(p_*^2) - \mathcal{I}(p^2)$. Furthermore,

[1] We have identical particles in the initial and final state, so the modulus of the three-momentum in the initial and final state are equivalent.

the renormalisation of the auxiliary vertex $V(p)$ proceeds along similar lines as

$$\Lambda^{(4)} = 2\,\frac{\delta^3\Gamma_{\text{2PI,int}}}{\delta^2\phi_R\,\delta G_R(q)} = -(\lambda_R + \delta\lambda_2)\,. \tag{3.41}$$

Using this in (3.16) and the result (3.40), along with the renormalisation condition (3.38), we obtain

$$\delta\lambda_2 = \delta\lambda_0 \quad \text{and} \quad V^{(4)}(p) = \overline{V}^{(4)}(p)\,. \tag{3.42}$$

We have made a choice to implement the same renormalisation conditions for both vertex functions. We will later do the same for the propagator and the two-point function of the scalar field, as in [70, 71], as well for the physical n-point functions of the scalar fields corresponding to the vertex functions. One may also choose to renormalise these functions to different parameters, such as in [60], but these correspond to shifts in the various counterterms.

The determination of these counterterms via the BSEs allows us to treat the sub-divergences, which are not accounted for by the usual BHPZ procedure, that would appear in the renormalisation of the two-point function [65, 69], for which we now turn to the gap equation

$$\begin{aligned} iG_R^{-1}(p) &= (p^2 - m_R^2) - i\overline{\Pi}(p^2) \\ &= (p^2 - m_R^2) + (\delta Z_{\phi,0}\,p^2 - \delta m_0^2) - \frac{(\lambda_R + \delta\lambda_2)}{2}\phi_R^2 - \frac{(\lambda_R + \delta\lambda_0)}{2}\int_q G_R(q)\,, \end{aligned} \tag{3.43}$$

where p here is the external momentum. Having determined $\delta\lambda_0$ and $\delta\lambda_2$, we seek the counterterms $\delta Z_{\phi,0}$ and δm_0^2 which can be used to treat the divergences that can be accounted for by the BHPZ procedure. Enforcing the following on-shell renormalisation conditions, we have

$$iG_R^{-1}(p)\Big|_{p^2=m_R^2} = -i\overline{\Pi}(p^2)\Big|_{p^2=m_R^2} \stackrel{!}{=} 0\,, \tag{3.44}$$

$$i\frac{\partial}{\partial p^2}G_R^{-1}(p)|_{p^2=m_R^2} = 1 - i\frac{\partial}{\partial p^2}\overline{\Pi}(p^2)|_{p^2=m_R^2} \stackrel{!}{=} 1\,. \tag{3.45}$$

which defines m_R as a *physical mass* corresponding to the pole of the propagator, like in standard QFT [2, 3]. From (3.45), we have

$$\delta Z_{\phi,0} = 0 \tag{3.46}$$

and then (3.44) gives

$$\delta m_0^2 = -\frac{\lambda_R + \delta\lambda_2}{2}\phi_R^2 - \frac{\lambda_R + \delta\lambda_0}{2}\int_q G_R(q)\,. \tag{3.47}$$

If we substitute this back into (3.43), we obtain

$$iG_R^{-1}(p^2) = p^2 - m_R^2\,, \tag{3.48}$$

or, in other words, the full propagator is identically the bare one. Consequently, all integrals over propagators can be expressed in terms of the well-known Passarino-Veltman functions, which we review and document in Appendix A.

We now apply the known form of the propagator (3.48) to obtain the coupling constant counterterms first, as these will be needed to obtain the mass counterterm δm_0^2. Using (3.39), we can determine

$$\delta\lambda_0 = -\lambda_R + \frac{\lambda_R}{1-\frac{1}{2}\lambda_R \mathcal{I}(p_*^2)} = -\lambda_R + \frac{\lambda_R}{1-\frac{\lambda_R}{32\pi^2}B_0(p_*^2, m_R^2, m_R^2)} = -\lambda_R - 32\pi^2\epsilon + \mathcal{O}(\epsilon^2)\,, \tag{3.49}$$

where $2\epsilon = 4-d$, and we have identified

$$\mathcal{I}(p^2) \equiv i\int_q G_R(q)G_R(p+q) \equiv \frac{B_0(p^2, m_R^2, m_R^2)}{16\pi^2}\,.$$

These coupling constant counterterms are evidently finite. Now, we can determine the counterterm δm_0^2 explicitly,

$$\begin{aligned}\delta m_0^2 &= -\frac{\lambda_R+\delta\lambda_2}{2}\phi_R^2 - \frac{\lambda_R+\delta\lambda_0}{2}\int_q G_R(q) \\ &= (16\pi^2\epsilon)\,\phi_R^2 + (16\pi^2\epsilon)\,\frac{A_0(m_R^2)}{16\pi^2} + \mathcal{O}(\epsilon^2) = -m_R^2 + \mathcal{O}(\epsilon)\,,\end{aligned} \tag{3.50}$$

where we have used that $\delta\lambda_0 = \delta\lambda_2$ in the Hartree approximation, c.f. (3.42). Note that we have determined (3.50) for any ϕ_R, so this holds true in the unbroken and broken phases. This counterterm also turns out to be finite. Furthermore, in the unbroken phase, we can exploit the $\mathbb{Z}_2$ symmetry of the Hartree approximation and make use of the identity [65]

$$\frac{\delta^2\Gamma_{\text{2PI,int}}}{\delta\phi_R^2}\bigg|_{\phi_R=0} + (\delta Z_{\phi,2}\,p^2 - \delta m_2^2) = 2\frac{\delta\Gamma_{\text{2PI,int}}}{\delta G_R}\bigg|_{\phi_R=0} + (\delta Z_{\phi,0}\,p^2 - \delta m_0^2) \tag{3.51}$$

to relate the counterterms for the propagator and the field

$$\delta Z_{\phi,2} = \delta Z_{\phi,0} \quad \text{and} \quad \delta m_0^2 = \delta m_2^2\,. \tag{3.52}$$

We now demonstrate explicitly that these relations do not hold for $\phi_R \neq 0$. To this end, we will examine the two-point function pertaining to the fields. Going forward, we would require the vertex function which, from (3.40) and using (3.48), we can write down as

$$\overline{V}^{(4)}(p) = -\frac{\lambda_R}{1-\frac{\lambda_R}{32\pi^2}\left[B_0(p_*^2, m_R^2, m_R^2) - B_0(p^2, m_R^2, m_R^2)\right]}\,. \tag{3.53}$$

We use (3.23) to obtain in momentum space

$$\begin{aligned}\Gamma^{(2)}(p) &= (p^2 - m_R^2) + (\delta Z_{\phi,2}\,p^2 - \delta m_2^2) - \frac{1}{2}(\lambda_R+\delta\lambda_4)\phi_R^2 - \frac{1}{2}(\lambda_R+\delta\lambda_2)\int_q G_R(q) \\ &\quad - \frac{1}{8}(\lambda_R+\delta\lambda_2)^2\left[\mathcal{I}(p^2)\right]\phi_R^2 + \frac{1}{16}(\lambda_R+\delta\lambda_2)^2\left[\mathcal{I}(p^2)\right]^2\overline{V}^{(4)}(p)\,\phi_R^2 \\ &= \left[(1+\delta Z_{\phi,2})p^2 - 2m_R^2 - \delta m_2^2\right] - \frac{1}{2}(\lambda_R+\delta\lambda_4)\phi_R^2\end{aligned}$$

$$+\frac{\lambda_R\phi_R^2}{4}\left\{1-\frac{\lambda_R}{32\pi^2}\left[B_0(p_*^2,m_R^2,m_R^2)-B_0(p^2,m_R^2,m_R^2)\right]\right\}^{-1}+O(\epsilon)\,. \quad (3.54)$$

Imposing the same renormalisation conditions as for G_R, c.f. (3.44) and (3.45), this yields

$$\delta Z_{\phi,2}=\frac{\lambda_R^2\phi_R^2}{128\pi^2}\,\dot{B}_0(m_R^2,m_R^2,m_R^2)\left\{1-\frac{\lambda_R}{32\pi^2}\left[B_0(p_*^2,m_R^2,m_R^2)-B_0(m_R^2,m_R^2,m_R^2)\right]\right\}^{-1} \quad (3.55)$$

$$\delta m_2^2=-m_R^2+m_R^2\delta Z_{\phi,2}-\frac{(\lambda_R+\delta\lambda_4)\,\phi_R^2}{2} +\frac{\lambda_R\phi_R^2}{4}\left\{1-\frac{\lambda_R}{32\pi^2}\left[B_0(p_*^2,m_R^2,m_R^2)-B_0(m_R^2,m_R^2,m_R^2)\right]\right\}^{-1}, \quad (3.56)$$

where

$$\dot{B}_0(p^2,m_R^2,m_R^2)=\left.\frac{\partial B_0(q^2,m_R^2,m_R^2)}{\partial q^2}\right|_{q^2=p^2}.$$

One recovers the equality with the corresponding counterterms for G_R in (3.52) when $\phi_R=0$, as claimed in [65]. Note that we are still missing $\delta\lambda_4$ to fully determine δm_2^2. We thus need to examine the three- and four-point functions for the fields.

Let us first consider the three-point function. Based on the discussion in Sec. 3.1.2, we can write down the following diagrammatic expansion,

$\Gamma^{(3)}$ =

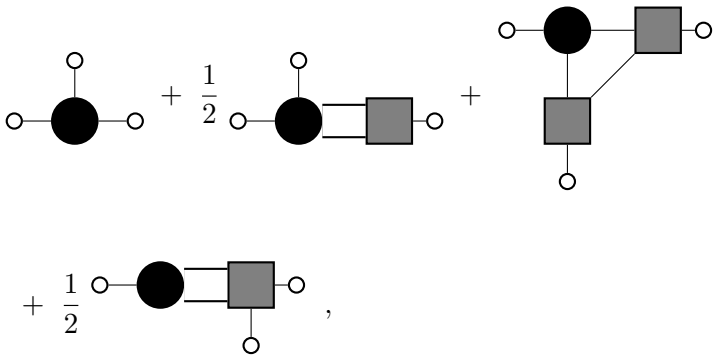

(3.57)

where we have retained those topologies that do not vanish after appropriate differentiation w.r.t. ϕ_R and G_R. We need to replace the second derivative of $\overline{\Pi}$,

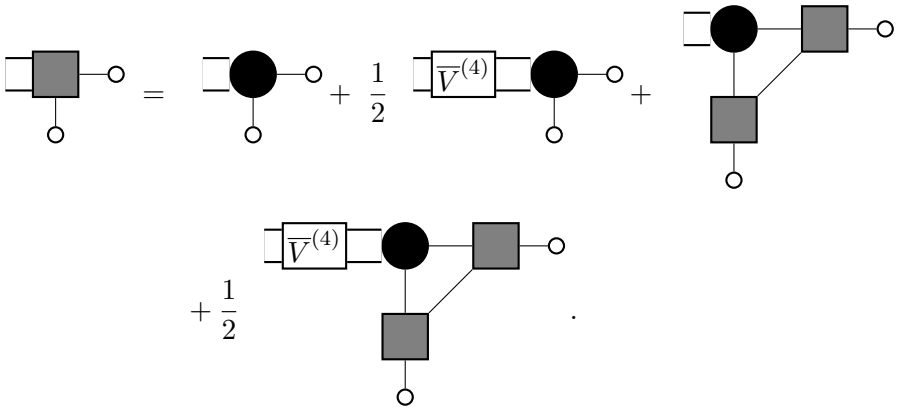

Even though many of the diagrams vanish in the Hartree approximation, there are still quite a few to evaluate, which we will become more apparent when we consider $\Gamma^{(4)}$.

However, before doing so explicitly, one can show that some of them only contribute at $O(\epsilon)$. This is because potential topologies that can contribute in any of the $\Gamma_{\text{2PI, int}}$ blobs that appear in loops and do not vanish are $\sim (\lambda_R + \delta\lambda_n)$, with $n = 0, 2$. These give a factor that is always $O(\epsilon)$, as discerned from (3.49) and observed in (3.50). The one- and two-point loop integrals are $O(\epsilon^{-1})$, but the three- and four-point ones are $O(1)$, being finite. Finally, the vertex function $\overline{V}^{(4)}$ is finite and hence $O(1)$. Thus, one can count the powers of ϵ for each diagram and it turns out that many diagrams only contribute at $O(\epsilon)$ to the total four-point function. We apply this same analysis to (3.58) and then find that only the second and fourth topologies are finite contributions.

Working with the convention that p_1 is the incoming four-momentum and p_2 and p_3 are outgoing, one obtains the final expression

$$\begin{aligned}\Gamma^{(3)}(p_1,p_2,p_3) = &-(\lambda_R+\delta\lambda_4)\phi_R + \frac{1}{2}\lambda_R\,\phi_R\,[J(p_1)+J(p_2)+J(p_3)] \\ &- \frac{1}{2}\lambda_R^3\,\phi_R^3\,J(p_1)J(p_2)J(p_3)\frac{[C_0(p_1,p_2)+C_0(p_1,p_3)]}{16\pi^2} + \mathcal{O}(\epsilon)\,,\end{aligned} \tag{3.58}$$

where the three-point loop integral function C_0 is introduced in Appendix A, but adopt the notation here,

$$C_0(r,l) = (16\pi^2)\int_q G_R(q)G_R(q+r)G_R(q+l)\,. \tag{3.59}$$

We have also introduced

$$J(p) \equiv \left[1 - \frac{\lambda_R}{32\pi^2}\left(B_0(p_*^2, m_R^2, m_R^2) - B_0(p^2, m_R^2, m_R^2)\right)\right]^{-1} \tag{3.60}$$

which originates from the vertex function, c.f. (3.53). One can observe that the three-point function vanishes in the unbroken phase, i.e. $\phi_R = 0$, as expected due to the $\mathbb{Z}_2$ symmetry of the Hartree approximation. Furthermore, the renormalisation of $\Gamma^{(3)}$ is determined by $\delta\lambda_4$, for which we turn to $\Gamma^{(4)}$.

For $\Gamma^{(4)}$, the contributing topologies are

$\Gamma^{(4)}$ =

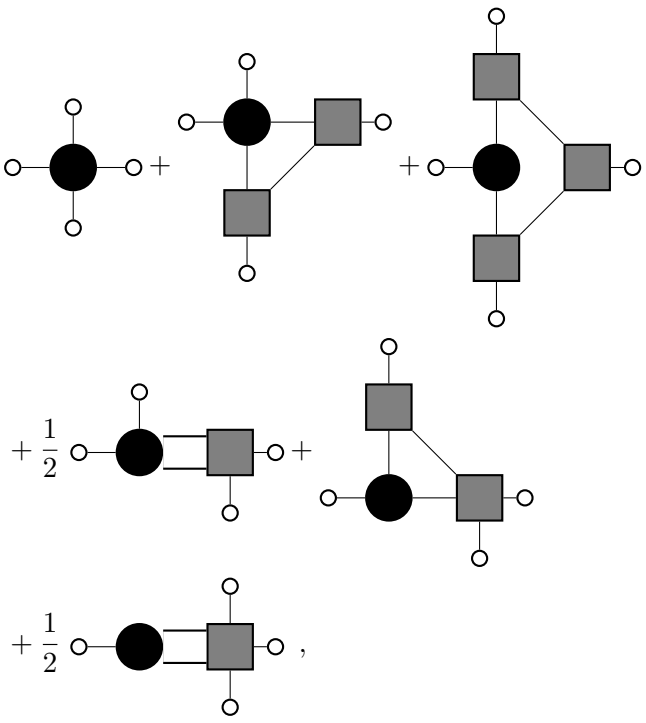

(3.61)

and then insert the required instances of (3.32) and (3.33), the former of which have been written and the latter of which we

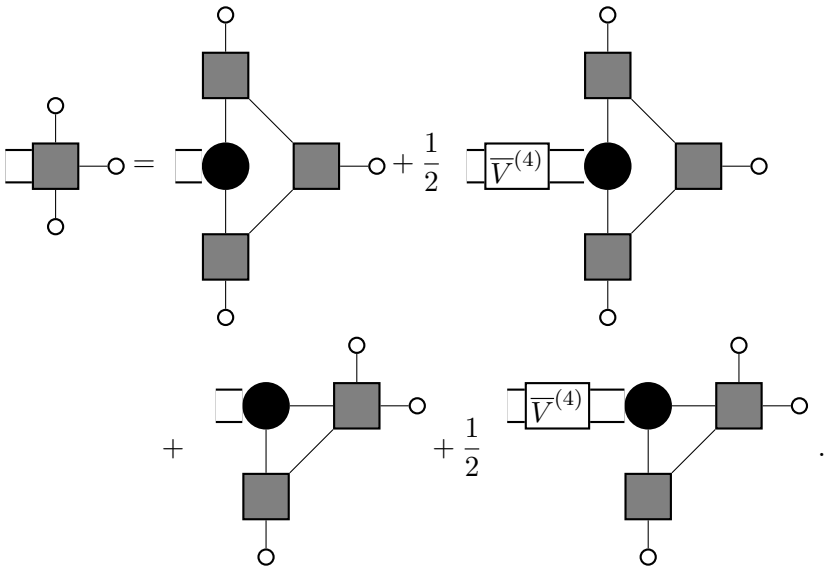

Performing the same analysis as in $\Gamma^{(3)}$ to identify the finite contributions, we assemble these to obtain

$$\begin{aligned}
\Gamma^{(4)}(p_1,p_2,p_3,p_4) &= -(\lambda_R+\delta\lambda_4)+\lambda_R\left[J(p_1+p_2)+J(p_1-p_3)+J(p_1-p_4)\right]\\
&+\frac{\lambda_R^3\phi_R^2}{16\pi^2}[J(p_1+p_2)J(p_3)J(p_4)C_0(p_1+p_2,p_4)+J(p_1-p_3)J(p_2)J(p_4)C_0(p_1-p_3,p_4)\\
&\qquad +J(p_1-p_4)J(p_2)J(p_3)C_0(p_1-p_4,p_3)+J(p_1)J(p_2)J(p_3+p_4)C_0(p_1,p_3+p_4)\\
&\qquad +J(p_1)J(p_3)J(p_2-p_4)C_0(p_1,p_2-p_4)+J(p_1)J(p_4)J(p_2-p_3)C_0(p_1,p_2-p_3)]\\
&-\frac{\lambda_R^4\phi_R^4}{16\pi^2}\,J(p_1)J(p_2)J(p_3)J(p_4)[D_0(p_2,p_1+p_2,p_3)+D_0(p_2,p_2-p_3,p_3)+D_0(p_2,p_2-p_4,p_4)]\\
&+\frac{\lambda_R^5\phi_R^4}{(16\pi^2)^2}\,J(p_1)J(p_2)J(p_3)J(p_4)[J(p_1+p_2)C_0(p_1,p_1+p_2)C_0(p_3+p_4,p_4)\\
&\quad +J(p_1-p_3)C_0(p_1,p_1-p_3)C_0(p_4-p_2,p_4)+J(p_1-p_4)C_0(p_1,p_1-p_4)C_0(p_3-p_2,p_3)]\,,
\end{aligned} \tag{3.62}$$

with the momentum assignments $p_{1,2}$ incoming and $p_{3,4}$ outgoing. Again, the four-point loop integral function D_0 is defined in Appendix A, and the notation here is

$$D_0(k,r,l) = (16\pi^2)i\int_q G_R(q)G_R(q+k)G_R(q+r)G_R(q+l)\,. \tag{3.63}$$

The counterterm, $\delta\lambda_4$ can then easily be obtained through an appropriate renormalisation condition,

$$\Gamma^{(4)}(p_{1*},p_{2*},p_{3*},p_{4*}) = -\lambda_R \tag{3.64}$$

where the p_{i*} are chosen to adhere to the renormalisation condition $p_*^2 = 4m_R^2$ for $|\vec{p_*}|=0$ and $\theta_*=0$. Note that $\delta\lambda_4$ would also be finite, as the quantities appearing in (3.62) are all finite. With this, we can then fully determine δm_2^2 from (3.56), which, on close examination, would also be finite. Evidently, in the Hartree approximation all counterterms turn out to be finite.

3.3 Scalar Sunset Approximation

In the broken phase, there exists a trilinear coupling $\sim \lambda_R \phi_R$, which thus naturally produces the scalar sunset diagram. Secondly, the inclusion of an additional trilinear coupling α can be thought of arising from integrating out heavy fermions. Thus, we write down the following 2PI functional,

$$\begin{aligned}
\widehat{\Gamma}_{\rm 2PI,int}[\phi_R, G_R] &= -\delta t_1\, \phi_R + \frac{(\delta Z_{\phi,2}\, p^2 - \delta m_2^2)}{2}\phi_R^2 - \frac{(\alpha_R + \delta\alpha_3)}{3!}\phi_R^3 - \frac{(\lambda_R + \delta\lambda_4)}{4!}\phi_R^4 \\
&+ \frac{\delta Z_{\phi,0}}{2}\int_p p^2 G_R(p) - \frac{1}{2}\left[\delta m_0^2 + (\alpha_R + \delta\alpha_1)\phi_R + \frac{(\lambda_R + \delta\lambda_2)}{2}\phi_R^2\right]\int_p G_R(p) \\
&- \frac{(\lambda_R + \delta\lambda_0)}{8}\left(\int_p G_R(p)\right)^2 \\
&+ \frac{i\,[(\alpha_R + \delta\alpha_0) + (\lambda_R + \delta\lambda_1)\phi_R]^2}{12}\int_p\int_q G_R(p) G_R(q) G_R(p+q)\,. \qquad (3.65)
\end{aligned}$$

We mention here that we cannot really speak of an "unbroken phase", as there is no corresponding symmetry that is broken; hence we proceed by carrying out our renormalisation at non-zero ϕ_R, assuming that it is a minima of the potential.

We may set the counterterms, $\delta\alpha_0 = \delta\lambda_1 = 0$, which is possible as they amount to finite renormalisations at this level of the 2PI truncation; more specifically, the first non-trivial contribution to these are obtained when one includes the basketball diagram [71–73]. We then obtain the following four-point kernels according to (3.15) and (3.18), which are now momentum dependent

$$\overline{\Lambda}^{(4)}(p_1, p_2, p_3, p_4) = -(\lambda_R + \delta\lambda_0) + 2i(\alpha_R + \lambda_R\phi_R)^2 G_R(p_3 - p_1)\,, \qquad (3.66)$$

$$\begin{aligned}
\Lambda^{(4)}(p_1, p_2, p_3, p_4) &= -(\lambda_R + \delta\lambda_2) + i\lambda_R^2\int_q G_R(q) G_R(p+q) \\
&\equiv -(\lambda_R + \delta\lambda_2) + \lambda_R^2\,\mathcal{I}(p)\,. \qquad (3.67)
\end{aligned}$$

where $p = p_1 + p_2$. In addition, we also define the following three-point kernel

$$\Lambda^{(3)}(p_1, p_2, p_3) = 2\frac{\delta^2\Gamma_{\rm 2PI,int}}{\delta\phi_R\,\delta G_R(p_1)} = -(\alpha_R + \delta\alpha_1) + \lambda_R(\alpha_R + \lambda_R\phi_R)\,\mathcal{I}(p_1)\,. \qquad (3.68)$$

The corresponding BSE for its resummation is

$$\begin{aligned}
V^{(3)}(p_1, p_2, p_3) &= \Lambda^{(3)}(p_1, p) \\
&+ \frac{i}{2}\int_q \Lambda^{(3)}(p_1, p_2, p_3) G_R(q) G_R(p_1 + q)\,\overline{V}^{(4)}(q + p_1, -q, p_2, p_3)\,. \qquad (3.69)
\end{aligned}$$

We now implement appropriate renormalisation conditions in order to determine the various coupling constant counterterms. For the four-point vertices, we continue to work with the convention that the we have $p_{1,2}$ as incoming and $p_{3,4}$ as outgoing momenta. We first have from (3.16),

$$\overline{V}^{(4)}(p_1,p_2,p_3,p_4) = \overline{\Lambda}^{(4)}(p_1,p_2,p_3,p_4) + \frac{i}{2}\int_q \overline{\Lambda}^{(4)}(p_1,p_2,q+p,-q)\,G_R(q)G_R(p+q)\,\overline{V}^{(4)}(q+p,-q,p_3,p_4)\,. \tag{3.70}$$

Let us set the renormalisation condition,

$$\overline{V}^{(4)}(p_{1*},p_{2*},p_{3*},p_{4*}) = -\lambda_R + 2i(\alpha_R+\lambda_R\phi_R)^2\,G_R(p_{3*}-p_{1*})\,, \tag{3.71}$$

which accounts for the fact that four scalars may scatter directly via the quartic coupling, or by a scalar exchange through two trilinear couplings. Like in the Hartree approximation, we work in the COM system, which is characterised by a COM momentum and scattering angle. In this case, as one might encounter infrared (IR) divergences on account of three- and four-point loop integrals generated from the kernel (3.66), we set $|\vec{p_*}|= m_R$ and $\theta_* = \pi$. Using (3.71) and solving for $\delta\lambda_0$, we obtain

$$\delta\lambda_0 = -\lambda_R + \frac{\lambda_R - (\alpha_R+\lambda_R\phi_R)^2\,I_2(p_*,p_{2*},p_{3*},p_{4*})}{1+\frac{1}{2}I_1(p_*,p_{3*},p_{4*})}\,, \tag{3.72}$$

where we have defined the following integrals over the vertex functions,

$$I_1(p,k,r) = i\int_q G_R(q)G_R(p+q)\overline{V}^{(4)}(q+p,-q,k,r)\,, \tag{3.73}$$

$$I_2(p,k,r,l) = \int_q G_R(q)G_R(q+p)G_R(q+k)G_R(q+r)\overline{V}^{(4)}(q+p,-q,r,l)\,. \tag{3.74}$$

Note that the functions I_1 and I_2 are at most logarithmically divergent and finite respectively, which we can ascertain by counting the number of propagators involved. The counterterm $\delta\lambda_0$ from (3.72) is hence discerned as finite. Plugging this back into (3.66) and (3.70), we obtain the following expression for the four-point function

$$\overline{V}^{(4)}(p_1,p_2,p_3,p_4) = -\lambda_R\left(\frac{1+\frac{1}{2}I_1(p,p_3,p_4)}{1+\frac{1}{2}I_1(p_*,p_{3*},p_{4*})}\right) + 2i(\alpha_R+\lambda_R\phi_R)^2G_R(p_3-p_1) + (\alpha_R+\lambda_R\phi_R)^2\left[I_2(p,p_2,p_3,p_4) - I_2(p_*,p_{3*},p_{4*})\left(\frac{1+\frac{1}{2}I_1(p,p_3,p_4)}{1+\frac{1}{2}I_1(p_*,p_{3*},p_{4*})}\right)\right]\,, \tag{3.75}$$

which is discerned to be finite from the arguments related to the loop integrals presented above.

As our model does not possess the $\mathbb{Z}_2$ symmetry in the Hartree case, our starting point to determine the counterterm $\delta\lambda_2$ is the following BSE

$$V(4)(p_1,p_2,p_3,p_4) = \Lambda^{(4)}(p_1,p_2,p_3,p_4) + \frac{i}{2}\int_q \Lambda^{(4)}(p_1,p_2,q+p,-q)G_R(q)G_R(q+p)\overline{V}^{(4)}(q+p,-q,p_3,p_4)\,. \tag{3.76}$$

From the definition (3.67), $\Lambda^{(4)}$ does not depend on the integrating loop momentum, which simplifies matters. We impose the renormalisation condition

$$V^{(4)}(p_{1*},p_{2*},p_{3*},p_{4*}) = -\lambda_R \tag{3.77}$$

and this leads to the following result

$$\delta\lambda_2 = -\lambda_R + \lambda_R^2 \mathcal{I}(p_*) + \frac{\lambda_R}{1 + \frac{1}{2} I_1(p_*, p_{3*}, p_{4*})} \,. \tag{3.78}$$

Firstly, we notice that, $\delta\lambda_2 \neq \delta\lambda_0$ unlike in the Hartree approximation, even if we set $\alpha = 0$. This is because, in the scalar sunset approximation, the effective trilinear coupling $\sim \lambda_R \phi_R$ gives a contribution which is the second term of (3.78). The very same term introduces a divergence in $\delta\lambda_2$ due to the loop integral $\mathcal{I}(p) = i \int_q G_R(q) G_R(q+p)$.

We now examine the three-point function (3.69), which has a similar structure to $V^{(4)}$. Firstly let us describe the kinematics: we take two of the scalars with p_2 and p_3 to be on-shell. By the conservation of four-momentum, we can calculate p_1 as

$$p_1^2 = (p_2 + p_3)^2 = 4(|\vec{p}|^2 + m_R^2) \,, \tag{3.79}$$

where we work in the COM frame for p_2 and p_3 so that these scalars are produced back-to-back. We then set $|\vec{p_*}| = m_R$ to fix the renormalisation condition as

$$V^{(3)}(p_{1*}, p_{2*}, p_{3*}) = -\alpha_R \,. \tag{3.80}$$

This gives us the following relation

$$\delta\alpha_1 = -\alpha_R + \lambda_R(\alpha_R + \lambda_R \phi_R)\, \mathcal{I}(p_{1*}^2) + \frac{\alpha_R}{1 + \frac{1}{2} I_1(p_{1*}, p_{2*}, p_{3*})} \,. \tag{3.81}$$

This counterterm is also divergent for the same reason as $\delta\lambda_2$.

We note here that, for the moment, we have given explicit expressions to calculate the counterterms via a numeric implementation (which we will shortly discuss in the context of the gap equation), and discussed their possible divergent structures. We will, in Chapter 4, determine analytic expressions in terms of expansions of ϵ for these counterterms, when we consider our $\overline{\text{MS}}$ scheme.

Turning now to the gap equation, with p being the external momentum, this reads

$$\begin{aligned} iG_R^{-1}(p) = (p^2 - m_R^2) + (\delta Z_{\phi,0}\, p^2 - \delta m_0^2) - (\alpha_R + \delta\alpha_1)\phi_R - \frac{(\lambda_R + \delta\lambda_2)}{2}\phi_R^2 \\ - \frac{(\lambda_R + \delta\lambda_0)}{2}\,\mathcal{T} + \frac{(\alpha_R + \lambda_R\phi_R)^2}{2}\,\mathcal{I}(p) \,, \end{aligned} \tag{3.82}$$

where we have the one-point integral

$$\mathcal{T} = \int_q G_R(q) \,. \tag{3.83}$$

Using the same on-shell renormalisation conditions in the Hartree approximation, as defined in (3.44) and (3.45), we first pick up a finite contribution to the wave function renormalisation given by

$$\delta Z_{\phi,0} = -\frac{(\alpha_R + \lambda_R\phi_R)^2}{2} \left.\frac{\partial \mathcal{I}(p)}{\partial p^2}\right|_{p^2 = m_R^2} \,. \tag{3.84}$$

The derivative eliminates any divergence present and therefore, $\delta Z_{\phi,0}$ is finite in the scalar sunset approximation. We can then determine the mass counterterm

$$\delta m_0^2 = \delta Z_{\phi,0} m_R^2 - (\alpha_R + \delta\alpha_1)\phi_R - \frac{(\lambda_R + \delta\lambda_2)}{2}\phi_R^2 - \frac{(\lambda_R + \delta\lambda_0)}{2}\mathcal{T} + \frac{(\alpha_R + \lambda_R\phi_R)^2}{2}\mathcal{I}(p)|_{p^2=m_R^2} . \tag{3.85}$$

This counterterm is no longer finite like in the Hartree approximation: the reason for this is that we have noted that the counterterms $\delta\lambda_2$ and $\delta\alpha_1$ are divergent. We plug back δm_0^2 and $\delta Z_{\phi,0}$ into (3.82) to obtain the following integral equation to ascertain the propagator

$$iG_R^{-1}(p) = (p^2 - m_R^2)\left[1 - \frac{(\alpha_R + \lambda_R\phi_R)^2}{2}\frac{\partial\mathcal{I}(q)}{\partial q^2}\bigg|_{q^2=m_R^2}\right] + \frac{(\alpha_R + \lambda_R\phi_R)^2}{2}\left[\mathcal{I}(p) - \mathcal{I}(q)|_{q^2=m_R^2}\right] . \tag{3.86}$$

In this form, the propagator is manifestly finite, due to potential divergences dropping out in the difference of the loop integral $\mathcal{I}$ or in its differentiation. However, G_R cannot be given in an explicit form but needs to be determined by solving (3.86), for which we use an iterative approach, described as follows:

1. Initialising with the free propagator, we evaluate the loop integrals in (3.86) to yield the first iteration of the propagator in terms of Passarino-Veltman functions

$$i(G_R^{-1}(p))^{(0)} = (p^2 - m_R^2)\left[1 - \frac{(\alpha_R + \lambda_R\phi_R)^2}{32\pi^2}\dot{B}_0(m_R^2, m_R^2, m_R^2)\right] + \frac{(\alpha_R + \lambda_R\phi_R)^2}{32\pi^2}\left[B_0(p^2, m_R^2, m_R^2) - B_0(m_R^2, m_R^2, m_R^2)\right] . \tag{3.87}$$

2. For the next iteration, convert (3.87) to Euclidean space, most easily done by $p^2 = -p_E^2$. Then, use a numerical implementation of the loop integral $\mathcal{I}(p)$ [2] which we have described at the end of Appendix A. In the course of the evaluation in Euclidean space, we set a UV cutoff that needs to be sufficiently large. We set this as $\Lambda = 10^5\,\text{GeV}$.

3. Generate a set of points for this iteration of the propagator and interpolate these to obtain the propagator at this iteration.

4. Repeat now from step (2) till convergence to desired accuracy. We define this as the relative difference between successive iterations getting smaller.

Our results in Fig. 3.3 show that there is indeed convergence for this iterative procedure as relative differences between successive iterations continue to get smaller for the very large couplings chosen. It would suffice, for smaller couplings hence, to use the first iteration of the propagator for practical purposes. We also observe a slight "kink" at $|p_E| = 200\,\text{GeV}$ in the same figure. In Minkowski space, we would interpret this as the on-shell production of two scalars ($m_R = 100\,\text{GeV}$), but as we are in Euclidean space, this might be the result of the loop contributions cancelling out, so that the various iterations match at this point.

[2] We have checked that the numeric implementation reproduces the correct values for the first iteration when compared to (3.87), in terms of Passarino-Veltman functions converted to Euclidean space.

Furthermore, we check the dependence on the UV cutoff, Λ in Fig. 3.4. We find the dependence to be rather small, with the relative difference being at most $\mathcal{O}(10^{-5})$, even when choosing a cutoff two orders of magnitude higher.

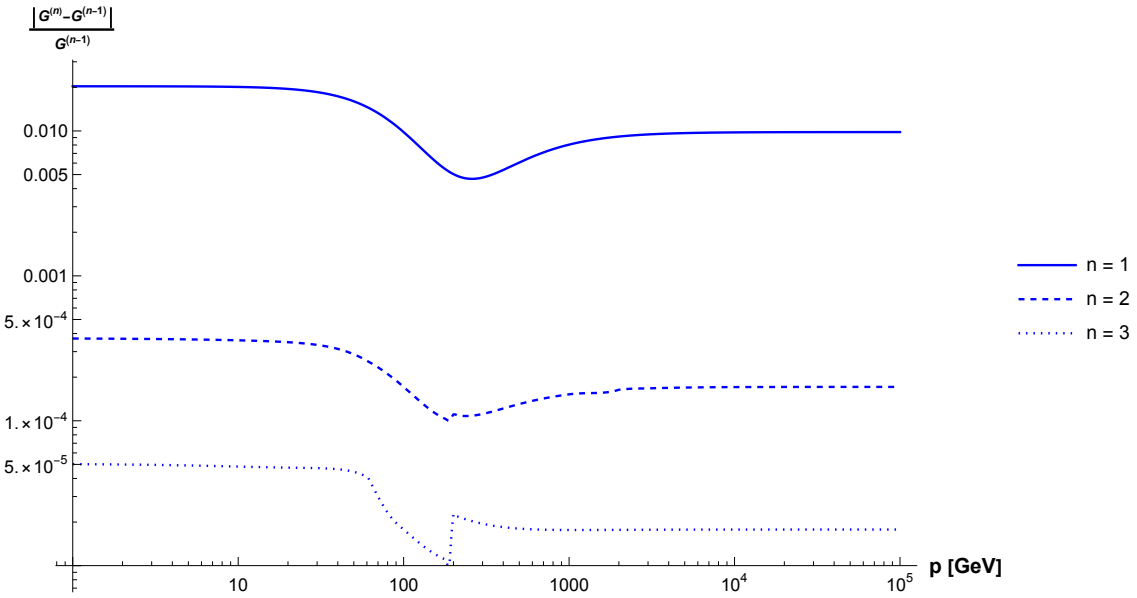

Figure 3.3: The relative difference between successive iterations of the scalar propagator for parameter choices of $m_R = 100\,\text{GeV}$, $\alpha_R = 200\,\text{GeV}$ and $\lambda_R = 4$, leading to $\phi_R \approx 70\,\text{GeV}$ for a range of the norm of the Euclidean four-momentum $\mathbf{p}$. We have the UV cutoff, $\Lambda = 10^5\,\text{GeV}$, required during the course of the numeric integration, as explained in the text.

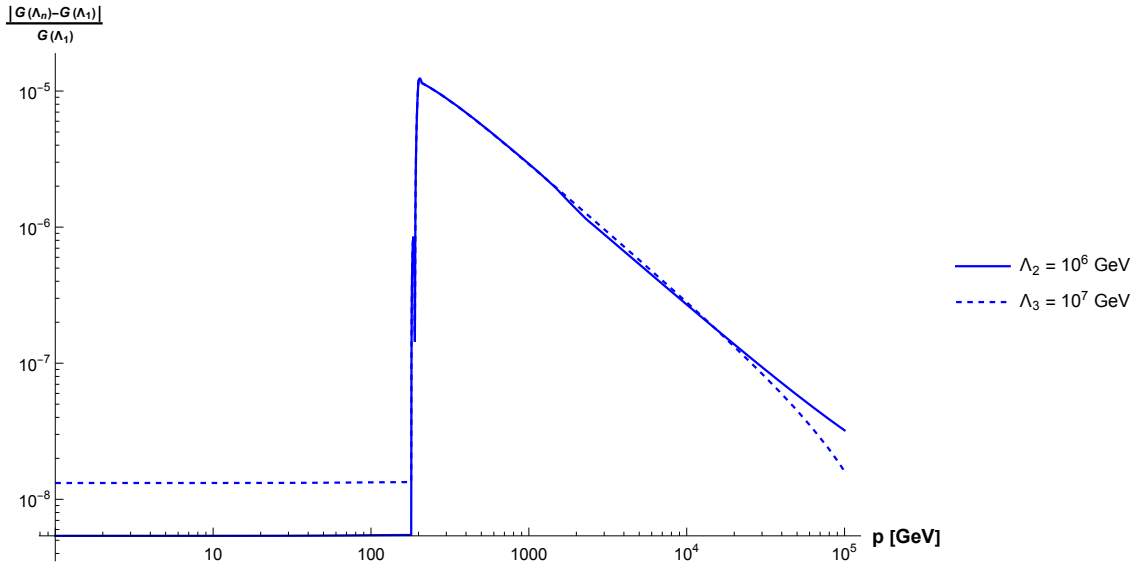

Figure 3.4: The relative difference between the second iteration of the scalar propagator evaluated with different cutoffs $\Lambda_2 = 10^6\,\text{GeV}$ and $\Lambda_3 = 10^7\,\text{GeV}$, and the one evaluated at $\Lambda_1 = 10^5\,\text{GeV}$ for a range of the norm of the Euclidean four-momentum $\mathbf{p}$. The parameters are taken to be $m_R = 100\,\text{GeV}$, $\alpha_R = 200\,\text{GeV}$ and $\lambda_R = 4$ which lead to $\phi_R \approx 70\,\text{GeV}$.

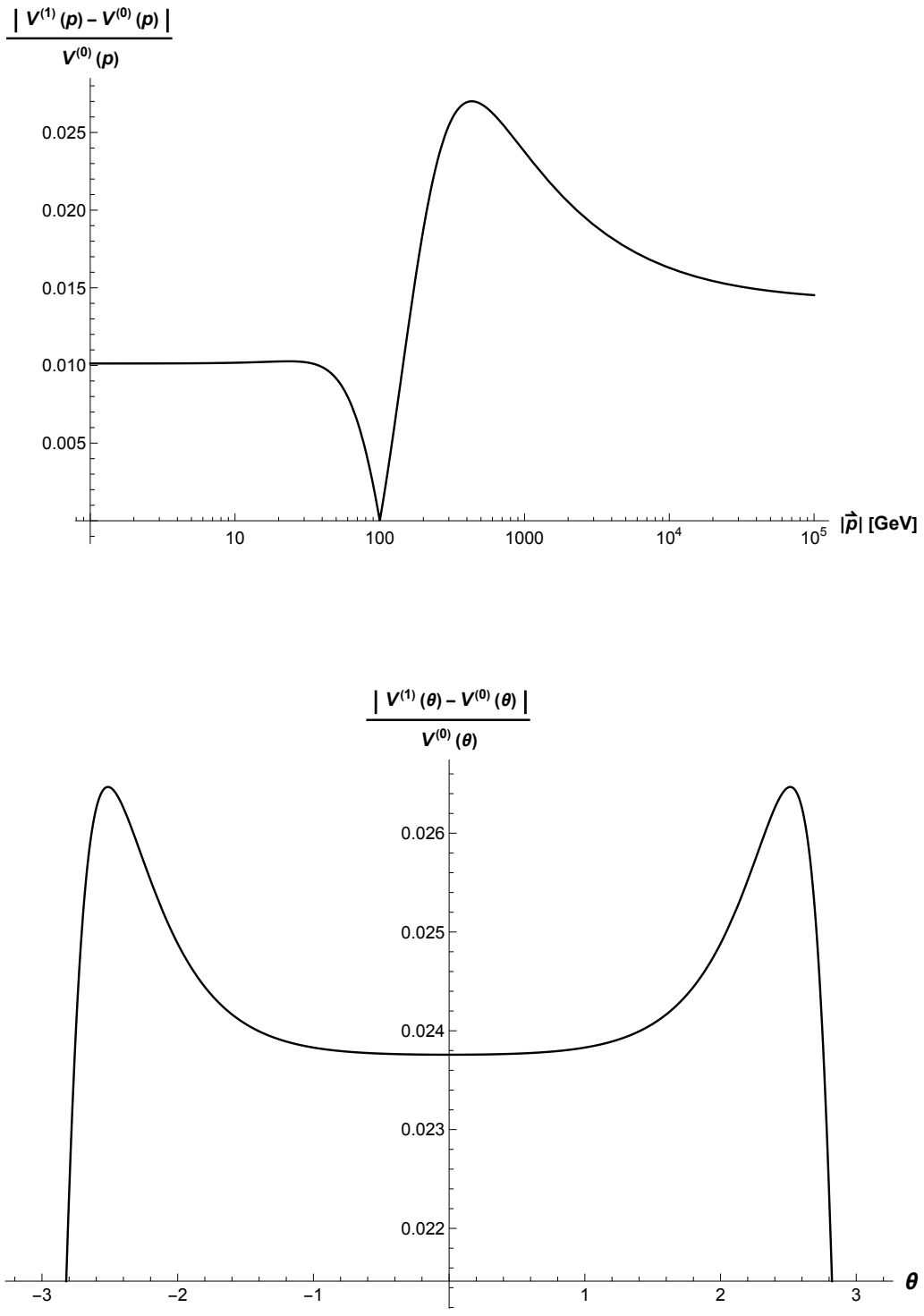

Figure 3.5: Top: The relative difference between the first and zeroth iteration of $\overline{V}^{(4)}$ as a function of the modulus of the COM three-momentum $|\vec{p}|$at fixed COM angle $\theta = 0$. Bottom: The relative difference between the first and zeroth iteration of $\overline{V}^{(4)}$ as a function of the COM angle for $|\vec{p}|= 1000\,\text{GeV}$. The parameters chosen are $m_R = 100\,\text{GeV}$, $\alpha_R = 75\,\text{GeV}$ and $\lambda_R = 0.8$, leading to $\phi_R \approx -450\,\text{GeV}$.

Having found the numerical solution to the gap equation, i.e. knowing the form of the propagator, one then proceeds to evaluate the loop integrals relevant to find the

counterterms $\delta\lambda_0$, $\delta\lambda_2$ and $\delta\alpha_1$, c.f. (3.73) and (3.74). As these involve convolution with the vertex function, one proceeds in a similar iterative manner for the vertex as we have outlined for the gap equation. Starting with the zeroth iteration of the vertex function $\overline{V}^{(4)}$, we have

$$\left(\overline{V}^{(4)}\right)^{(0)}(p_1,p_2,p_3,p_4) = -\lambda_R + 2i(\alpha_R+\lambda_R)^2 G_R^{(0)}(p_3-p_1)\,, \tag{3.88}$$

and calculate the first iteration

$$\begin{aligned}\left(\overline{V}^{(4)}\right)^{(1)}(p_1,p_2,p_3,p_4) &= -\lambda_R + 2i(\alpha_R+\lambda_R)^2 G_R^{(0)}(p_3-p_1)\\ &- \frac{(\alpha_R+\lambda_R)^2\,\lambda_R}{16\pi^2}\left[C_0(p_{1*},p_{3*}) - C_0(p_1,p_3)\right] + \frac{(\alpha_R+\lambda_R)^2}{8\pi^2}\left[D_0(p_{1*},p_{2*},p_{3*}) - D_0(p_1,p_2,p_3)\right]\,.\end{aligned} \tag{3.89}$$

In Fig. 3.5, we show the relative differences for a range of momentum and the angular variation.

For the determination of the remaining counterterms, we examine various derivatives of the 2PI effective potential. For example, the tadpole counterterm is straightforwardly obtained by taking a single derivative of the effective action w.r.t. ϕ_R. The stationarity condition then gives

$$\begin{aligned}\Gamma^{(1)} &= \left.\frac{\delta\widehat{\Gamma}_{\rm 2PI}}{\delta\phi_R}\right|_{p^2=0}\\ &= -\delta t_1 - (m_R^2+\delta m_2^2)\phi_R - \frac{(\alpha_R+\delta\alpha_3)}{2}\phi_R^2 - \frac{(\alpha_R+\delta\lambda_4)}{6}\phi_R^2\\ &\quad - \frac{1}{2}\left[(\alpha_R+\delta\alpha_1) + (\lambda_R+\delta\lambda_4)\phi_R\right]\mathcal{T} + \frac{\lambda_R\,(\alpha_R+\lambda_R\phi_R)}{6}\,\mathcal{S} \stackrel{!}{=} 0\,,\end{aligned} \tag{3.90}$$

where

$$\mathcal{S} = i\int_p\int_q G_R(p)G_R(q)G_R(p+q)\,. \tag{3.91}$$

The tadpole counterterm cannot be determined without first ascertaining the missing field counterterms. The easiest of this to find is δm_2^2, for which we look at $\Gamma^{(2)}$. Using equations (3.27) and (3.28) we obtain

$$\begin{aligned}\Gamma^{(2)} &= (p^2-m_R^2) + (\delta Z_{\phi,2}p^2 - \delta m_2^2) - (\alpha_R+\delta\alpha_3)\phi_R - \frac{1}{2}(\lambda_R+\delta\lambda_4)\phi_R^2\\ &- \frac{1}{2}(\lambda_R+\delta\lambda_2)\mathcal{T} + \frac{\lambda_R^2}{6}\,\mathcal{S}\\ &- \frac{1}{8}\left[(\alpha_R+\delta\alpha_1) + (\lambda_R+\delta\lambda_2)\phi_R - \frac{\lambda_R(\alpha_R+\lambda_R\phi_R)}{3}\mathcal{I}(p)\right]^2\mathcal{I}(p)\\ &+ \frac{1}{16}\Bigg\{\left[(\alpha_R+\delta\alpha_1) + (\lambda_R+\delta\lambda_2)\phi_R - \frac{\lambda_R(\alpha_R+\lambda_R\phi_R)}{3}\mathcal{I}(p)\right]^2\\ &\qquad \int_q\int_k G_R(p+q)G_R(q)\overline{V}^{(4)}(p+q,-q,p+k,-k)G_R(p+k)G_R(k)\Bigg\}\,,\end{aligned} \tag{3.92}$$

where the terms in parenthesis for the third and last lines appear from the replacement of the various building blocks in (3.27) and (3.28). The earlier analysis in the Hartree approximation does not carry over as $\delta\lambda_2 \neq \delta\lambda_0$, and moreover, $\delta\lambda_2$ is now contains a divergent part. We can determine the counterterms $\delta Z_{\phi,2}$ and δm_2^2 with the on-shell renormalisation conditions, to give

$$\begin{aligned}
\delta Z_{\phi,2} = \frac{1}{8}\Bigg[&(\alpha_R+\delta\alpha_1)+(\lambda_R+\delta\lambda_2)\phi_R-\frac{\lambda_R(\alpha_R+\lambda_R\phi_R)}{3}\mathcal{I}(p)\big|_{p^2=m_R^2}\Bigg]\\
&\Bigg\{\Bigg\{-\frac{\lambda_R(\alpha_R+\lambda_R\phi_R)}{3}\mathcal{I}(p)\big|_{p^2=m_R^2}\frac{\partial\mathcal{I}(p)}{\partial p^2}\Bigg|_{p^2=m_R^2}\\
&\quad+\Bigg[(\alpha_R+\delta\alpha_1)+(\lambda_R+\delta\lambda_2)\phi_R-\frac{\lambda_R(\alpha_R+\lambda_R\phi_R)}{3}\mathcal{I}(p)\big|_{p^2=m_R^2}\Bigg]\frac{\partial\mathcal{I}(p)}{\partial p^2}\Bigg|_{p^2=m_R^2}\Bigg\}\\
&+\frac{1}{2}\Bigg\{-\frac{\lambda_R(\alpha_R+\lambda_R\phi_R)}{3}\mathcal{I}(p)\big|_{p^2=m_R^2}\frac{\partial\mathcal{I}_V(p)}{\partial p^2}\Bigg|_{p^2=m_R^2}\\
&\quad+\Bigg[(\alpha_R+\delta\alpha_1)+(\lambda_R+\delta\lambda_2)\phi_R-\frac{\lambda_R(\alpha_R+\lambda_R\phi_R)}{3}\mathcal{I}(p)\big|_{p^2=m_R^2}\Bigg]\frac{\partial\mathcal{I}_V(p)}{\partial p^2}\Bigg|_{p^2=m_R^2}\Bigg\}\Bigg\},
\end{aligned} \tag{3.93}$$

$$\begin{aligned}
\delta m_2^2 = {}& m_R^2\,\delta Z_{\phi,2}-(\alpha_R+\delta\alpha_3)\phi_R-\frac{1}{2}(\lambda_R+\delta\lambda_4)\phi_R^2-\frac{1}{2}(\lambda_R+\delta\lambda_2)\mathcal{T}+\frac{\lambda_R^2}{6}\,\mathcal{S}\\
&-\frac{1}{8}\Bigg[(\alpha_R+\delta\alpha_1)+(\lambda_R+\delta\lambda_2)\phi_R-\frac{\lambda_R(\alpha_R+\lambda_R\phi_R)}{3}\mathcal{I}(p)\big|_{p^2=m_R^2}\Bigg]^2\mathcal{I}(p)\big|_{p^2=m_R^2}\\
&+\frac{1}{16}\Bigg[(\alpha_R+\delta\alpha_1)+(\lambda_R+\delta\lambda_2)\phi_R-\frac{\lambda_R(\alpha_R+\lambda_R\phi_R)}{3}\mathcal{I}(p)\big|_{p^2=m_R^2}\Bigg]^2\mathcal{I}_V(p)\big|_{p^2=m_R^2},
\end{aligned} \tag{3.94}$$

where

$$\mathcal{I}_V(p)=\int_q\int_k G_R(p+q)G_R(q)\overline{V}^{(4)}(p+q,-q,p+k,-k)G_R(p+k)G_R(k)\,. \tag{3.95}$$

On close inspection, we can discern that these counterterms would not be finite like in the Hartree approximation, due to the coupling constant counterterms being $\mathcal{O}(\epsilon^{-1})$. Furthermore, it is also obvious that the equalities $\delta Z_{\phi,2}=\delta Z_{\phi,0}$ and $\delta m_2^2=\delta m_0^2$ no longer hold true, as we had in the Hartree approximation.

Finally, the only undetermined counterterms are $\delta\alpha_3$ and $\delta\lambda_4$, which are needed to completely express δt_1 and δm_2^2. Based on our diagrammatic approach, the structures that do not vanish after successive differentiation w.r.t. ϕ_R and/or G_R are

$\Gamma^{(3)} \equiv \dfrac{\delta^3\Gamma}{\delta\phi^3} =$ 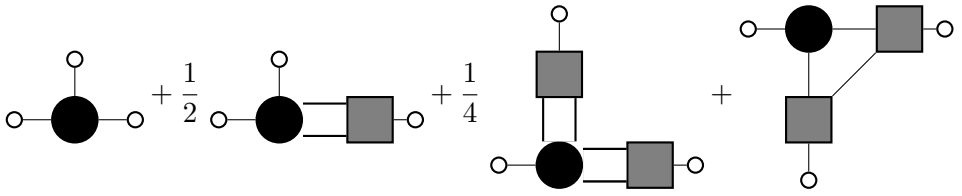 $+\frac{1}{2}$ $+\frac{1}{4}$ $+$

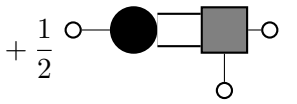

(3.96)

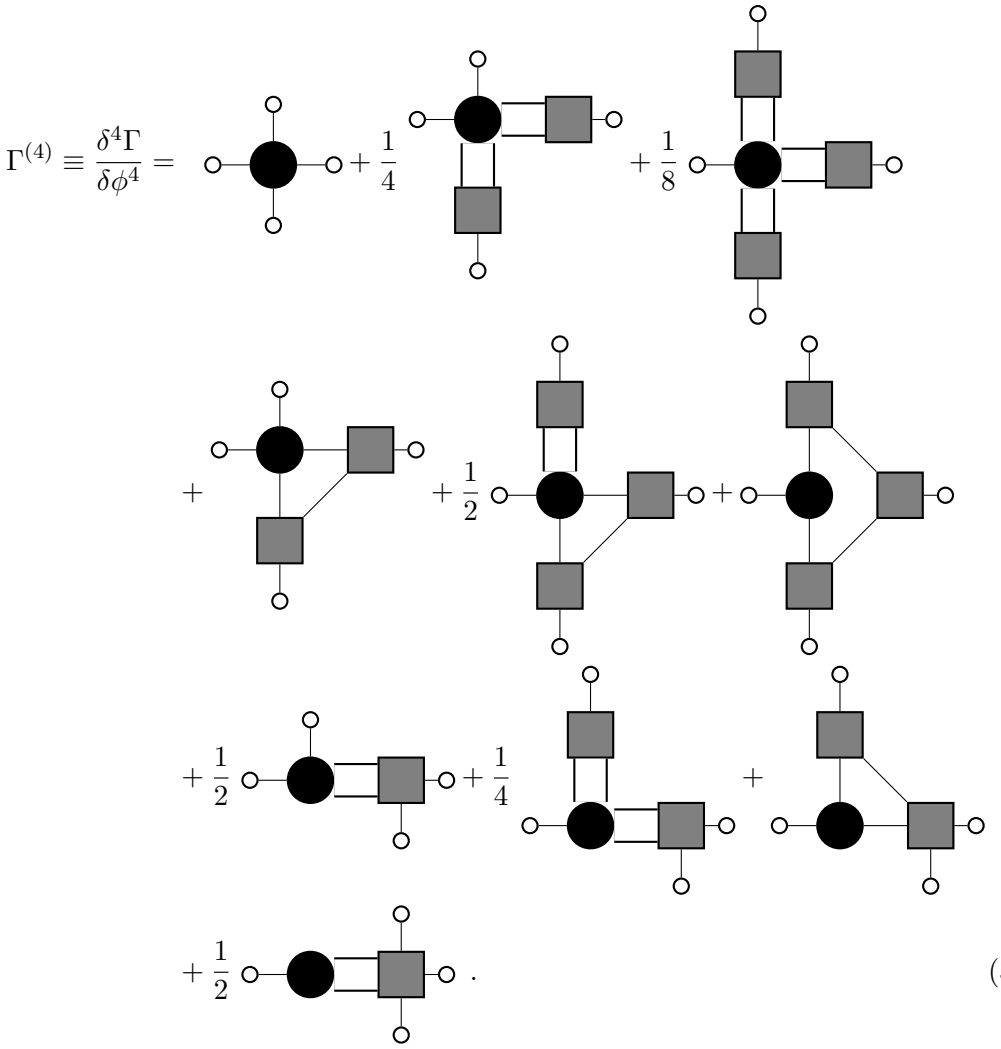

(3.97)

Referring now to (3.32) and (3.33), we first enlist the various non-vanishing contributions of the derivative of the self-energy w.r.t. ϕ_R that would be required.

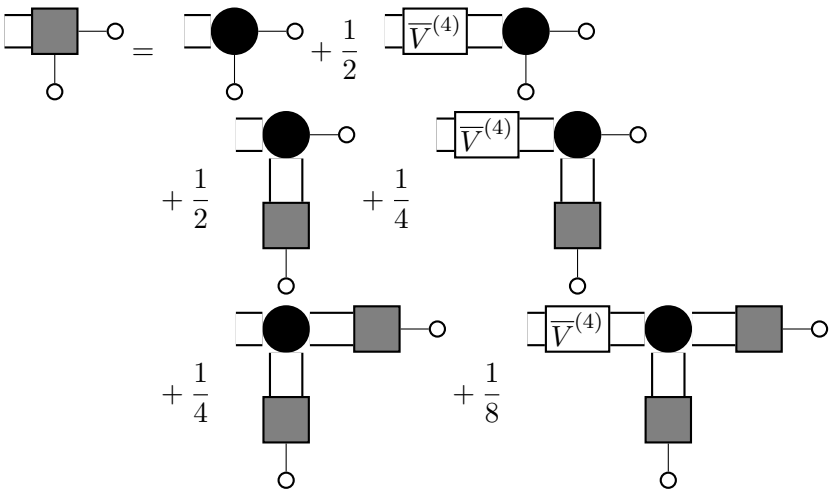

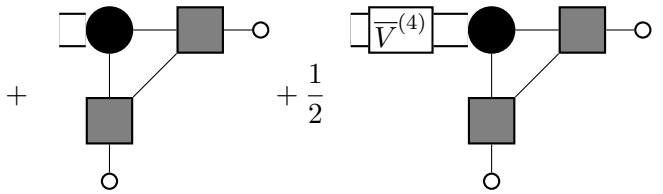
+
+ 1/2
$\overline{V}^{(4)}$

(3.98)

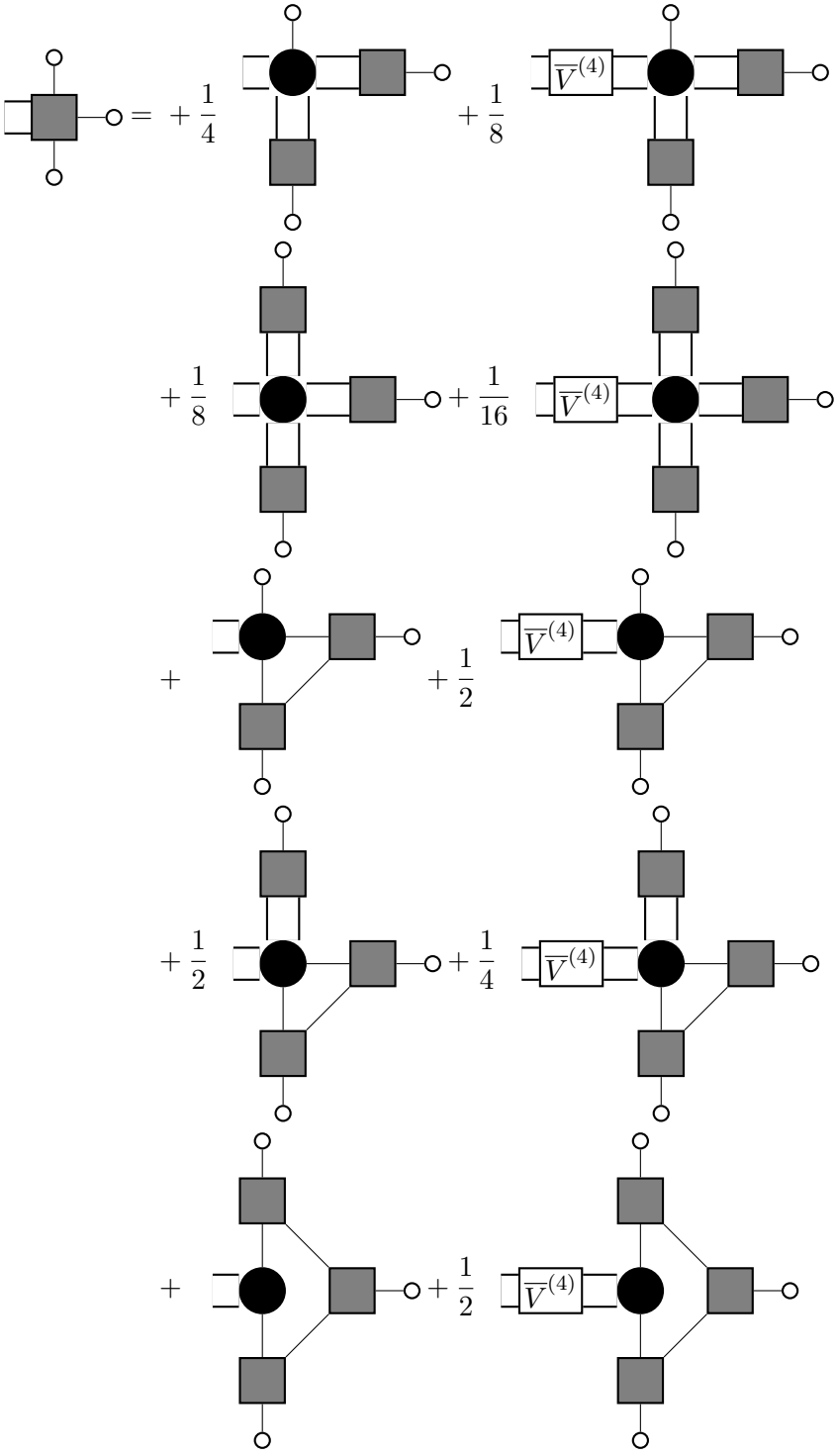
= + 1/4
+ 1/8
$\overline{V}^{(4)}$
+ 1/8
+ 1/16
$\overline{V}^{(4)}$
+
+ 1/2
$\overline{V}^{(4)}$
+ 1/2
+ 1/4
$\overline{V}^{(4)}$
+
+ 1/2
$\overline{V}^{(4)}$

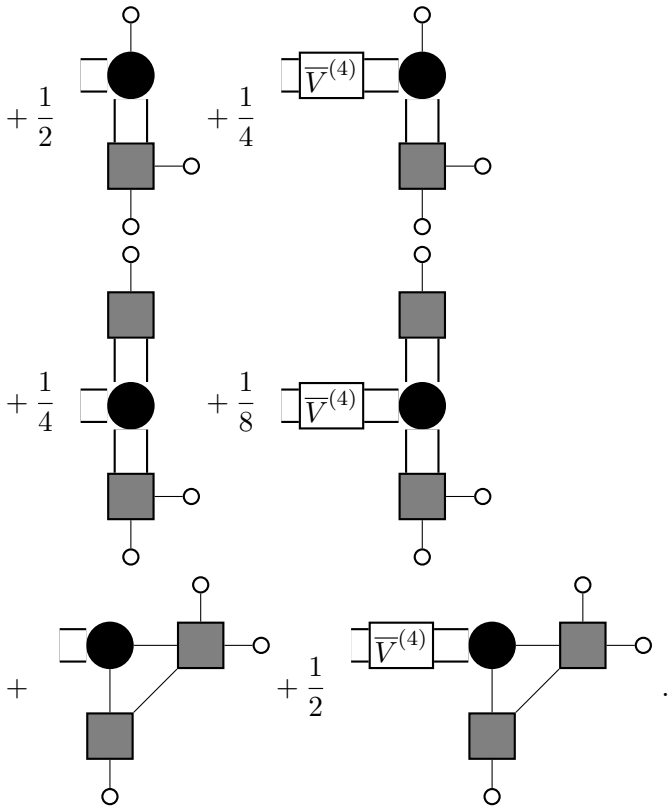

(3.99)

While performing the analysis of the diagrams, one may note the following: $\delta\lambda_0$ is still finite and differentiation w.r.t. to three propagators yields $\sim (\alpha_R + \lambda_R\phi_R)^2$ which is also finite. However, all other counterterms, besides $\delta\lambda_0$ are not finite, and hence one needs to be careful when such quantities multiply loop integrals, as they would introduce (sub-)divergences. The counterterms $\delta\alpha_3$ and $\delta\lambda_4$ are then obtained by placing the renormalisation conditions

$$\Gamma^{(3)}(p_{1*}, p_{2*}, p_{3*}) = -\alpha_R\,, \qquad \Gamma^{(4)}(p_{1*}, p_{2*}, p_{3*}, p_{4*}) = -\lambda_R\,. \tag{3.100}$$

The full determination of these counterterms in the on-shell scheme involve resolution of the various diagrams that we have presented. These lead to lengthy expressions which we do not list here; instead, in the next Chapter 4, we obtain analytic expressions for these in terms of expansions in ϵ, through an alternate approach. The presence of counterterms that are not finite after resummation in the 2PI formalism may seem strange, but we will show also in the next chapter of this thesis that this is not really an issue, as the 2PI effective potential remains finite.

3.4 Fermionic Sunset Approximation

Finally, introducing fermions into the theory, we can write down at two-loop order

$$\widehat{\Gamma}_{\text{2PI,int}}[\phi_R, G_R, D_R] = -\delta t_1\,\phi_R + \frac{(\delta Z_{\phi,2}\,p^2 - \delta m_2^2)}{2}\phi_R^2 - \frac{(\alpha_R + \delta\alpha_3)}{3!}\phi_R^3 - \frac{\lambda_R + \delta\lambda_4)}{4!}\phi_R^4$$
$$+ \int_p \frac{\delta Z_{\phi,0}}{2}\int_p p^2 G_R(p) - \frac{1}{2}\left[\delta m_0^2 + (\alpha_R + \delta\alpha_1)\phi_R + \frac{(\lambda_R + \delta\lambda_2)}{2}\phi_R^2\right]\int_p G_R(p)$$

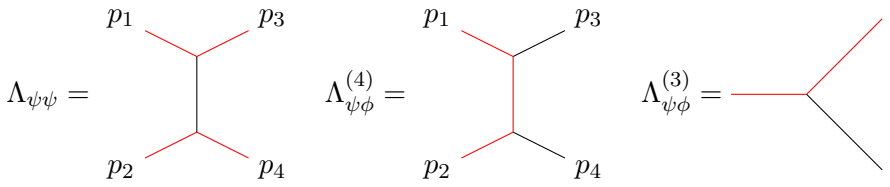

Figure 3.6: Illustration of the various kernels in the fermionic sunset approximation. Red lines indicate the fermionic propagator D_R.

$$
\begin{aligned}
&+ \int_p \mathrm{tr}\left[\left(\delta Z_{\psi,2}\not{p} - \delta M_0\right) D(p)\right] - (g_R + \delta g_1)\phi_R \int_p \mathrm{tr}[D_R(p)] \\
&- \frac{(\lambda_R + \delta\lambda_0)}{8}\left(\int_p G_R(p)\right)^2 + \frac{i\,(\alpha_R + \lambda_R\phi_R)^2}{2}\int_p\int_q G_R(p)G_R(q)G_R(p+q) \\
&- \frac{i(g_R+\delta g_0)^2}{2}\int_p\int_q G_R(p)\,\mathrm{tr}[D_R(q)D_R(p+q)]\,,
\end{aligned}
\tag{3.101}
$$

where we have already set the corresponding coupling counterterms for the scalar sunset contribution to 0. We retain the counterterm for the Yukawa coupling corresponding to the fermionic sunset diagram, δg_0, for the moment. Note that as long as the fermionic mass, $M_R \neq 0$, we require an additional trilinear coupling α_R, to account for potential divergences in scalar three-point functions with a fermionic loop. We can then obtain the following additional four-point kernels involving fermions and scalars

$$
\Lambda_{\psi\psi}(p_1,p_2,p_3,p_4)_{ab,cd} \equiv -\frac{\delta^2\Gamma_{\mathrm{2PI,int}}}{\delta D_R^{ba}(p)\,\delta D_R^{cd}(q)} = i(g_R+\delta g_0)^2\,\delta_{db}\,G_R(p_3-p_1)\,\delta_{ac}\,, \tag{3.102}
$$

$$
\Lambda^{(4)}_{\psi\phi}(p_1,p_2,p_3,p_4)_{ab} \equiv -2\frac{\delta^2\Gamma_{\mathrm{2PI,int}}}{\delta D_R^{ba}(p)\,\delta G_R(q)} = 2i(g_R+\delta g_0)^2\,D_R(p_1-p_3)_{ab}\,, \tag{3.103}
$$

$$
\left(\Lambda^{(3)}_{\psi\phi}\right)_{ab} \equiv -\frac{\delta^2\Gamma_{\mathrm{2PI,int}}}{\delta\phi_R\,\delta D_R^{ba}(p)} = -(g_R+\delta g_1)\delta_{ab}\,, \tag{3.104}
$$

alongside the scalar kernels that we had in the scalar sunset approximation, c.f. (3.66), (3.67) and (3.68). For now, we have indicated the spinor indices in lowercase Latin alphabets. The Kronecker deltas refer to the identity matrix in spinor space.

We proceed by defining first the governing BSE for the kernel $\Lambda_{\psi\psi}$ as

$$
\begin{aligned}
&V_{\psi\psi}(p_1,p_2,p_3,p_4)_{ab,cd} = \Lambda_{\psi\psi}(p_1,p_2,p_3,p_4)_{ab,cd} \\
&\quad + i\int_q \Lambda_{\psi\psi}(p_1,p_2,q+p,-q)_{ab,ef}D_R(q)_{eg}V_{\psi\psi}(q+p,-q,p_3,p_4)_{gh,cd}D_R(p+q)_{hf} \\
&= i(g_R+\delta g_0)^2\delta_{db}\,G_R(p_3-p_1)\,\delta_{ac} \\
&\quad - (g_R+\delta g_0)^2\int_q G_R(q+p_2)D_R(q)_{ae}V_{\psi\psi}(q+p,-q,p_3,p_4)_{ef,cd}D_R(p+q)_{fb}\,,
\end{aligned}
\tag{3.105}
$$

and $p = p_1 + p_2$. This vertex function is essentially a resummation of ladder diagrams contributing to t-channel $\psi\overline{\psi} \to \psi\overline{\psi}$ scattering via the exchange of a scalar propagator. On inspection, we can easily discern that $V_{\psi\psi}$ is finite by counting the number of propagators. The counterterm δg_0 hence accounts for a finite renormalisation which we determine using the condition

$$V_{\psi\psi}(p_{1*}, p_{2*}, p_{3*}, p_{4*})_{ab,cd} = i g_R^2 \, \delta_{db} \, G_R(p_{3*} - p_{1*}) \, \delta_{ac} \, . \tag{3.106}$$

where we continue to work in the COM frame to give the renormalisation conditions. Imposing this and appropriately contracting the spinor indices, with $\sum_a \delta_{aa} = 4$, we obtain the following expression for δg_0

$$\delta g_0 = -g_R + \frac{g_R}{\sqrt{1 - \frac{1}{4} G_R^{-1}(p_{3*} - p_{1*}) \, F_2}} \tag{3.107}$$

where

$$F_2 = i \int_q G_R(q + p_{2*}) D_R(q)_{ae} V_{\psi\psi}(q + p_*, -q, p_{3*}, p_{4*})_{ef,ab} D_R(p_* + q)_{fb} \, . \tag{3.108}$$

Note that δg_0 is a finite renormalisation, i.e. $\mathcal{O}(1)$ and therefore, does not modify divergent structures. Thus, for convenience, we choose to set $\delta g_0 = 0$ from this point onward.

Consider the BSE for the kernel $\Lambda^{(4)}_{\psi\phi}$,

$$\begin{aligned} V^{(4)}_{\psi\phi}(p_1, p_2, p_3, p_4)_{ab} &= \Lambda_{\psi\phi}(p_1, p_2, p_3, p_4)_{ab} \\ &+ i \int_q \Lambda^{(4)}_{\psi\phi}(p_1, p_2, q + p, -q)_{ae} D_R(q)_{ef} V^{(4)}_{\psi\phi}(q + p, -q, p_3, p_4)_{fb} G_R(p + q) \end{aligned} \tag{3.109}$$

This is again finite by power counting. We will use this now for the three-point kernel $\Lambda^{(3)}_{\psi\phi}$ to define a BSE of the form

$$V^{(3)}_{\psi\phi}(p_1, p_2, p_3)_{ab} = \left(\Lambda^{(3)}_{\psi\phi}\right)_{ab} + i \left(\Lambda^{(3)}_{\psi\phi}\right)_{ac} \int_q D_R(q)_{cd} V^{(4)}_{\psi\phi}(q + p_1, -q, p_2, p_3)_{db} G_R(p_1 + q) \, . \tag{3.110}$$

We will make use of this now to determine the counterterm δg_1. With the renormalisation condition,

$$V^{(3)}_{\psi\phi}(p_{1*})_{(\alpha\beta)} = -g_R \, \delta_{\alpha\beta} \, . \tag{3.111}$$

We then obtain

$$\delta g_1 = -g_R + \frac{g_R}{1 + \frac{1}{4} F_3} \, , \tag{3.112}$$

where

$$F_3 = i \int_q \mathrm{tr} \left[D_R(q) V^{(4)}_{\psi\phi}(q + p_{1*}, -q, p_{2*}, p_{3*}) \right] G_R(q + p_{1*}) \, , \tag{3.113}$$

where appropriate contraction of the spinor indices leads to the resultant trace.

In dealing with the scalar four-point vertex functions, we have to treat the possibility of divergences introduced by fermionic loops. To this end, with $\overline{\Lambda}^{(4)}$ as the base, we build the following "modified scalar kernel" using $\Lambda^{(4)}_{\psi\phi}$ and the four-point vertex $V_{\psi\psi}$ [66]

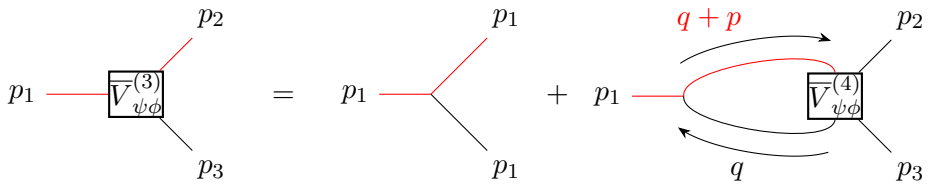

Figure 3.7: Illustration of BSE for the resummation of the three-point vertex $\overline{V}^{(3)}_{\psi\phi}$ using the four-point vertex $\overline{V}^{(4)}_{\psi\phi}$.

$$
\begin{aligned}
\tilde{\Lambda}_{\phi\phi}(p_1,p_2,p_3,p_4) &= \overline{\Lambda}^{(4)}(p_1,p_2,p_3,p_4) \\
&\quad - i\int_q D_R(p+q)_{db}\,\Lambda^{(4)}_{\psi\phi}(q+p,-q,p_3,p_4)_{ba}\,D_R(q)_{ac}\,\Lambda^{(4)}_{\psi\phi}(p_1,p_2,p+q-q)_{cd} \\
&\quad + i\int_q\int_r \Big\{ D_R(q+p)_{fb}\,\Lambda^{(4)}_{\psi\phi}(p_1,p_2,p+q,-q)_{ba}\,D_R(q)_{ae} \\
&\qquad V^{\psi\psi}(p+q,-q,r+p,-r)_{ef,gh} D_R(r)_{gc}\,\Lambda^{(4)}_{\psi\phi}(r+p,-r,p_3,p_4)_{cd}\,D_R(r+p)_{dh}\Big\} \\
&= \overline{\Lambda}^{(4)}(p_1,p_2,p_3,p_4) - 4ig_R^4\int_q \mathrm{tr}\left[D_R(q+p)D_R(q+p_1)D_R(q)D_R(q+p_3)\right] \\
&\quad + 4ig_R^4\int_q\int_r \mathrm{tr}\Big[D_R(q+p)D_R(q+p_1)D_R(q)V^{\psi\psi}(p+q,-q,r+p,-r) \\
&\qquad\qquad D_R(r)D_R(r+p_3)D_R(r)\Big]\,,
\end{aligned}
\tag{3.114}
$$

where in the second equality, we have contracted the spinor indices to obtain the trace. We can now iterate this four-point scalar kernel via its usual BSE

$$
\begin{aligned}
\overline{V}^{(4)}(p_1,p_2,p_3,p_4) &= \tilde{\Lambda}_{\phi\phi}(p_1,p_2,p_3,p_4) \\
&\quad + \frac{i}{2}\int_q \tilde{\Lambda}_{\phi\phi}(p_1,p_2,q+p,-q)\,G_R(q)G_R(p+q)\,\overline{V}^{(4)}(q+p,-q,p_3,p_4)\,.
\end{aligned}
\tag{3.115}
$$

The quartic scalar coupling divergences generated will then be absorbed into the counterterm $\delta\lambda_0$. Imposing the same renormalisation condition as in the scalar sunset approximation, c.f. (3.71), we solve for the counterterm to obtain

$$
\begin{aligned}
\delta\lambda_0 &= -\lambda_R + \frac{\lambda_R - (\alpha_R+\lambda_R\phi_R)^2\,I_2}{1+\frac{1}{2}I_1} \\
&\quad + 4g_R^4\left[\frac{F_4-\frac{1}{2}F_{4V}}{1+\frac{1}{2}I_1}\right] - 4g_R^4\left[\frac{F_V-\frac{1}{2}F_{VV}}{1+\frac{1}{2}I_1}\right]\,,
\end{aligned}
\tag{3.116}
$$

where $I_{1,2}$ are the same integrals in (3.73) and (3.74), defined at the renormalisation point, and the following notation has been introduced for the new loop integrals pertaining to

the fermions

$$F_4 = i\int_q \mathrm{tr}\left[D_R(q+p_*)D_R(q+p_{2*})D_R(q)D_R(q+p_{4*})\right], \tag{3.117}$$

$$F_{4V} = \int_q\int_r \mathrm{tr}\left[D_R(q+p_*)D_R(q+p_{2*})D_R(q)D_R(q-r)\right]G_R(r)G_R(p_*+r)\overline{V}^{(4)}(r+p_*,p_{3*}), \tag{3.118}$$

$$F_V = i\int_q\int_r \mathrm{tr}\Big[D_R(q+p_*)D_R(q+p_{2*})D_R(q)V_{\psi\psi}(p_*+q,r+p_*) D_R(r)D_R(r+p_{4*})D_R(r+p_*)\Big], \tag{3.119}$$

$$F_{VV} = \int_k\int_q\int_r \Big\{\mathrm{tr}\Big[D_R(q+p_*)D_R(q+p_{2*})D_R(q)V_{\psi\psi}(p_*+q,r+p_*) D_R(r)D_R(r-k)D_R(r+p_*)\Big]G_R(k)G_R(k+p_*)\overline{V}^{(4)}(k+p_*,p_{3*})\Big\}. \tag{3.120}$$

Note that F_V and F_{VV} are both finite, whereas F_4 and F_{4V} are logarithmically divergent. The remaining counterterms are $\delta\lambda_2$ and $\delta\alpha_1$ are obtained in the exact same manner as in the scalar sunset case, and the expressions are the same (3.78) and (3.81), with the vertex function function now being defined with the modified four-point scalar kernel to include the contributions from fermions.

We can now turn to the formulation of the gap equations to determine the form of the fermionic and scalar propagators. These are given by

$$\begin{aligned} iG_R^{-1}(p) &= p^2 - m_R^2 - i\overline{\Pi}(p) \\ &= (p^2-m_R^2) + (\delta Z_{\phi,0}\,p^2 - \delta m_0^2) - (\alpha_R+\delta\alpha_1)\phi_R - \frac{(\lambda_R+\delta\lambda_2)}{2}\phi_R^2 \\ &\quad - \frac{(\lambda_R+\delta\lambda_0)}{2}\mathcal{T} + \frac{(\alpha_R+\lambda_R\phi_R)^2}{2}\mathcal{I}(p) - ig_R^2\int_q \mathrm{tr}[D_R(q)D_R(p+q)] \\ &\equiv (p^2-m_R^2) + (\delta Z_{\phi,0}\,p^2 - \delta m_0^2) - (\alpha_R+\delta\alpha_1)\phi_R - \frac{(\lambda_R+\delta\lambda_2)}{2}\phi_R^2 \\ &\quad - \frac{(\lambda_R+\delta\lambda_0)}{2}\mathcal{T} + \frac{(\alpha_R+\lambda_R\phi_R)^2}{2}\mathcal{I}(p) - g_R^2\left[p^2\mathcal{F}_1(p)+\mathcal{F}_2(p)\right] \end{aligned} \tag{3.121}$$

$$\begin{aligned} iD_R^{-1}(p) &= \not{p} - M_R - i\overline{\Sigma}(\not{p}) \\ &= \not{p} - M_R + (\delta Z_{\psi,0}\not{p} - \delta M_0) - (g_R+\delta g_1)\phi_R - ig_R^2\int_q D_R(p+q)G_R(q) \\ &\equiv \not{p} - M_R + (\delta Z_{\psi,0}\not{p} - \delta M_0) - (g_R+\delta g_1)\phi_R - g_R^2\left[X(p)\not{p} + Y(p)\right], \end{aligned} \tag{3.122}$$

and are evidently coupled. For the loop integrals related to fermions, we have decomposed them into the forms based on possible Lorentz structures. We now impose the appropriate

on-shell renormalisation conditions to obtain the counterterms related to the propagators. For the scalar propagator, we have

$$\delta Z_{\phi,0} = -\frac{(\alpha_R+\lambda_R\phi_R)^2}{2}\,\frac{\partial\mathcal{I}(p)}{\partial p^2}\bigg|_{p^2=m_R^2} + g_R^2\left[\mathcal{F}_1(p) + m_R^2\frac{\partial\mathcal{F}_1(p)}{\partial p^2} + \frac{\partial\mathcal{F}_2(p)}{\partial p^2}\right]\bigg|_{p^2=m_R^2}, \tag{3.123}$$

$$\begin{aligned}\delta m_0^2 = {}& \delta Z_{\phi,0} m_R^2 - (\alpha_R+\delta\alpha_1)\phi_R - \frac{(\lambda_R+\delta\lambda_2)}{2}\phi_R^2 - \frac{(\lambda_R+\delta\lambda_0)}{2}\,\mathcal{T} \\ & + \frac{(\alpha_R+\lambda_R\phi_R)^2}{2}\,\mathcal{I}(p)|_{p^2=m_R^2} - g_R^2\left[m_R^2\mathcal{F}_1(p)+\mathcal{F}_2(p)\right]|_{p^2=m_R^2},\end{aligned} \tag{3.124}$$

and for the fermionic propagator

$$\delta Z_{\psi,0} = g_R^2 X(p)|_{p^2=M_R^2} + 2g_R^2\,M_R\left[M_R\frac{\partial X(p)}{\partial p^2} + \frac{\partial Y(p)}{\partial p^2}\right]\bigg|_{p^2=M_R^2}, \tag{3.125}$$

$$\delta M_0 = \delta Z_{\psi,0} M_R - (g_R+\delta g_1)\phi_R - g_R^2[M_R\,X(p)+Y(p)]|_{p^2=M_R^2}\,. \tag{3.126}$$

Note that the counterterms for the scalar and fermionic wave function renormalisations are not finite, due to the loop integrals not always being subtracted.

We proceed now in the same manner as in the scalar sunset approximation: we substitute these counterterms into the gap equations to obtain the following coupled integral equations to solve for the propagators

$$\begin{aligned}iG_R^{-1}(p) = {}& (p^2-m_R^2)\left[1 - \frac{(\alpha_R+\lambda_R\phi_R)^2}{2}\,\frac{\partial\mathcal{I}(q)}{\partial q^2} + g_R^2\left(m_R^2\frac{\partial\mathcal{F}_1(q)}{\partial q^2} + \frac{\partial\mathcal{F}_1(q)}{\partial q^2}\right)\right]\bigg|_{q^2=m_R^2} \\ & + \frac{(\alpha_R+\lambda_R\phi_R)^2}{2}\left[\mathcal{I}(p) - \mathcal{I}(q)|_{q^2=m_R^2}\right] \\ & - g_R^2\left[p^2\left(\mathcal{F}_1(p) - \mathcal{F}_1(q)|_{q^2=m_R^2}\right) + \left(\mathcal{F}_2(p) - \mathcal{F}_2(q)|_{q^2=m_R^2}\right)\right],\end{aligned} \tag{3.127}$$

$$\begin{aligned}iD_R^{-1}(p) = {}& (\not{p} - M_R)\left[1 + 2g_R^2 M_R\left(M_R\frac{\partial X(q)}{\partial q^2} + \frac{\partial Y(q)}{\partial q^2}\right)\right]\bigg|_{q^2=M_R^2} \\ & - g_R^2\left[\not{p}\left(X(p) - X(q)|_{q^2=M_R^2}\right) + \left(Y(p^2) - Y(q)|_{q^2=M_R^2}\right)\right] \\ \equiv {}& W(p)\not{p} - Z(p)\,.\end{aligned} \tag{3.128}$$

These are manifestly finite due to divergences dropping out due to the subtraction from a fixed point or differentiation of the divergent functions. In the last step for the fermionic propagator, we have defined the following quantities

$$W(p) = 1 - g_R^2\left(X(p) - X(q)|_{q^2=M_R^2}\right) + 2g_R^2 M_R\left(M_R\frac{\partial X(q)}{\partial q^2} + \frac{\partial Y(q)}{\partial q^2}\right)\bigg|_{q^2=M_R^2}, \tag{3.129}$$

$$Z(p) = M_R - g_R^2\left(Y(p) - Y(q)|_{q^2=M_R^2}\right) - 2g_R^2 M_R^2\left(M_R\frac{\partial X(q)}{\partial q^2} + \frac{\partial Y(q)}{\partial q^2}\right)\bigg|_{q^2=M_R^2}, \tag{3.130}$$

according to which we can explicitly write down the expressions for $X(p)$ and $Y(p)$,

$$X(p) = i\int_q W(p+q)G_R(q)\,, \qquad Y(p) = i\int_q Z(p+q)G_R(q)\,. \tag{3.131}$$

For the trace that appears in the scalar propagator, we resolve this as

$$\begin{aligned}
\mathrm{Tr}[D_R(q)D_R(p+q)] &= \mathrm{Tr}\left\{\frac{i}{W(q)\not{q} - Z(q)}\,\frac{i}{W(p+q)(\not{p}+\not{q}) - Z(p+q)}\right\} \\
&= \frac{\mathrm{Tr}\left\{[W(q)\not{q} + Z(q)][W(p+q)(\not{p}+\not{q}) + Z(p+q)]\right\}}{[W^2(q)q^2 - Z^2(q)]\,[W^2(p+q)(p+q)^2 - Z^2(p+q)]} \\
&= 4\,\frac{(p\cdot q + q^2)W(q)W(p+q) + Z(q)Z(p+q)}{[W^2(q)q^2 - Z^2(q)]\,[W^2(p+q)(p+q)^2 - Z^2(p+q)]} \\
&= p^2\left\{\frac{-2\,W(q)W(p+q)}{[W^2(q)q^2 - Z^2(q)][W^2(p+q)(p+q)^2 - Z^2(p+q)]}\right\} \\
&\quad + 2\left\{\frac{((p+q)^2 - q^2)W(q)W(p+q) + Z(q)Z(p+q)}{[W^2(q)q^2 - Z^2(q)][W^2(p+q)(p+q)^2 - Z^2(p+q)]}\right\}
\end{aligned} \tag{3.132}$$

where in the second last step we have used $2p\cdot q = (p+q)^2 - p^2 - q^2$. This finally gives the expressions for the functions $\mathcal{F}_1$ and $\mathcal{F}_2$

$$\mathcal{F}_1(p) = -2i\int_q \frac{W(q)W(p+q)}{[W^2(q)q^2 - Z^2(q)][W^2(p+q)(p+q)^2 - Z^2(p+q)]}\,, \tag{3.133}$$

$$\mathcal{F}_2(p) = 2i\int_q \frac{((p+q)^2 - q^2)W(q)W(p+q) + Z(q)Z(p+q)}{[W^2(q)q^2 - Z^2(q)][W^2(p+q)(p+q)^2 - Z^2(p+q)]}\,. \tag{3.134}$$

We know have the entire setup to solve the gap equations, which we approach in the same iterative manner outlined for the scalar sunset approximation, beginning with the free propagators. This yields,

$$X^{(1)}(p^2) = \frac{1}{16\pi^2}\left[B_1(p^2, m_R^2, M_R^2) + B_0(p^2, m_R^2, M_R^2)\right]\,, \tag{3.135}$$

$$Y^{(1)}(p^2) = \frac{1}{16\pi^2}\left[M_R\,B_0(p^2, m_R^2, M_R^2)\right]\,, \tag{3.136}$$

$$\begin{aligned}
i(G_R^{-1}(p))^{(0)} = p^2\Bigg\{1 &- \frac{g_R^2}{8\pi^2}\left[B_0(p^2, M_R^2, M_R^2) - B_0(m_R^2, M_R^2, M_R^2)\right] \\
&- \frac{g_R^2}{4\pi^2}\left(M_R^2 - \frac{m_R^2}{2}\right)\dot{B}_0(m_R^2, M_R^2, M_R^2) - \frac{(\alpha_R + \lambda_R\phi_R)^2}{32\pi^2}\,\dot{B}_0(m_R^2, m_R^2, m_R^2)\Bigg\} \\
- m_R^2\Bigg\{1 &- \frac{g_R^2}{8\pi^2}\frac{M_R^2}{m_R^2}\left[B_0(p^2, M_R^2, M_R^2) - B_0(m_R^2, M_R^2, M_R^2)\right] \\
&- \frac{g_R^2}{4\pi^2}\left(M_R^2 - \frac{m_R^2}{2}\right)\dot{B}_0(m_R^2, M_R^2, M_R^2) + \frac{(\alpha_R + \lambda_R\phi_R)^2}{32\pi^2}\,\dot{B}_0(m_R^2, m_R^2, m_R^2)\Bigg\} \\
&+ \frac{(\alpha_R + \lambda_R\phi_R)^2}{32\pi^2}\left[B_0(p^2, m_R^2, m_R^2) - B_0(m_R^2, m_R^2, m_R^2)\right]\,,
\end{aligned} \tag{3.137}$$

which are converted to Euclidean space for the next iteration. We focus on the case of a large Yukawa coupling, $g_R = 2$, and set smaller couplings pertaining to scalars. We again see that the relative difference between successive iterations drops by about two orders of magnitude for the scalar propagator (Fig. 3.8) and the functions $W(p)$ (Fig. 3.9) and $Z(p)$ (Fig. 3.10), showing that this iterative approach does appear to converge. We point out that certain spurious points where the relative difference between the second and first iterations appear to go to 0 in the various plots are not physical; these are purely numeric effects and these would smooth out when sets a higher accuracy for the integrations.

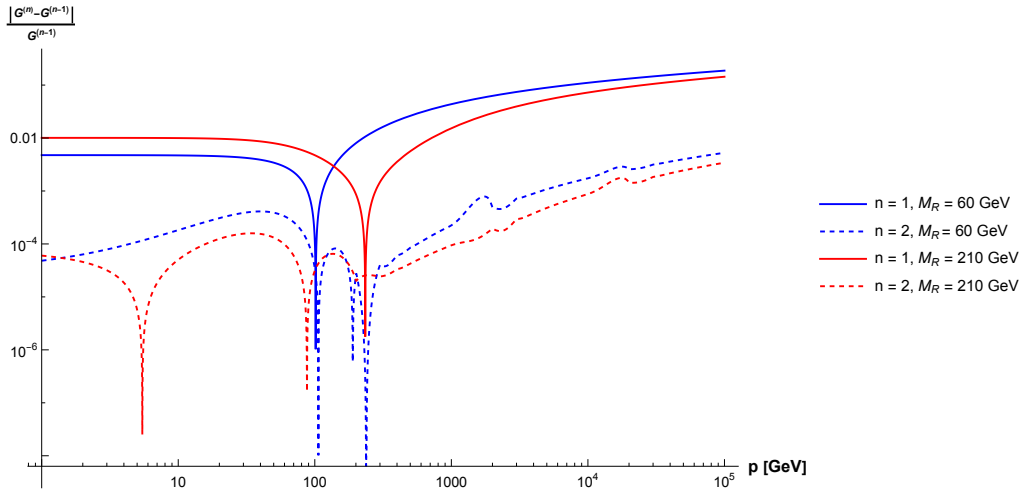

Figure 3.8: The relative difference between the two successive iterations of the scalar propagator for two choices of the renormalised fermionic mass, M_R. We have set $g_R = 2$, $\lambda_R = 0.5$, $\alpha_R = 50\,\text{GeV}$, $\phi_R \approx 227.5\,\text{GeV}$ and $m_R = 100\,\text{GeV}$ in all cases. The UV cutoff was taken to be $\Lambda = 10^5\,\text{GeV}$.

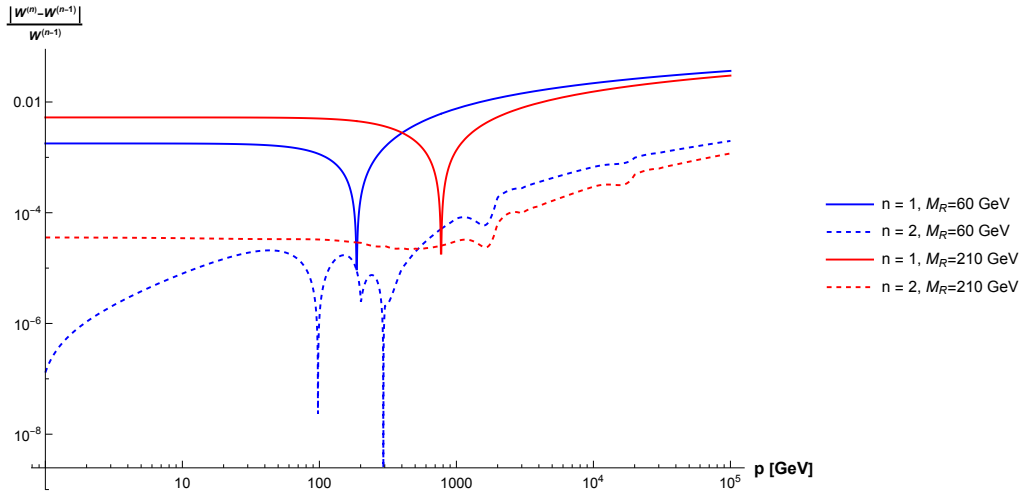

Figure 3.9: The relative difference between the two successive iterations of the function $W(p)$ for two choices of the renormalised fermionic mass, M_R. We have set $g_R = 2$, $\lambda_R = 0.5$, $\alpha_R = 50\,\text{GeV}$, $\phi_R \approx 227.5\,\text{GeV}$ and $m_R = 100\,\text{GeV}$ in all cases. The UV cutoff was taken to be $\Lambda = 10^5\,\text{GeV}$.

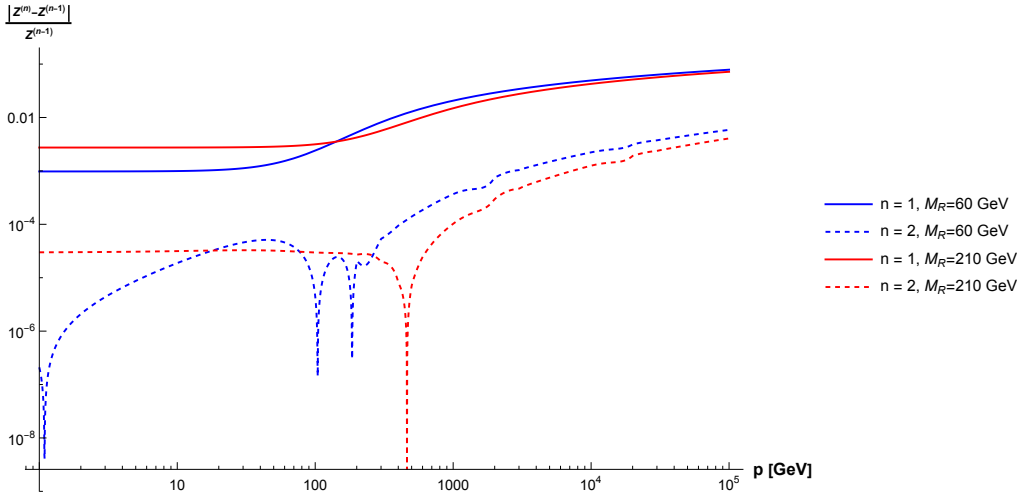

Figure 3.10: The relative difference between the two successive iterations of the function $Z(p)$ for two choices of the renormalised fermionic mass, M_R. We have set $g_R = 2$, $\lambda_R = 0.5$, $\alpha_R = 50\,\text{GeV}$, $\phi_R \approx 227.5\,\text{GeV}$ and $m_R = 100\,\text{GeV}$ in all cases. The UV cutoff was taken to be $\Lambda = 10^5\,\text{GeV}$.

We now outline the procedure to obtain the remaining counterterms, which pertain to the scalar field. We must start with the generic expression involving field derivatives of the effective action and include the relevant modifications due to the presence of fermions. However, simplifications occur if we treat the fermions are treated as background fields which cannot acquire VEVs, motivated by the fact that these break Lorentz invariance.

Starting with the scalar one-point function, we have

$$\frac{\delta\Gamma_{2\text{PI}}}{\delta\phi_R(x_1)} = \frac{\delta\Gamma_{2\text{PI}}}{\delta\phi_R(x_1)} + \int_{y_1,y_2} \frac{\delta\Gamma_{2\text{PI}}}{\delta G_R(y_1,y_2)} \frac{\delta G_R(y_1,y_2)}{\delta\phi_R(x_1)} + \int_{y_1,y_2} \text{tr}\left\{ \frac{\delta\Gamma_{2\text{PI}}}{\delta D_R(y_1,y_2)} \frac{\delta D_R(y_1,y_2)}{\delta\phi_R(x_1)} \right\}$$

where the second and third terms are obtained from the chain rule. The stationarity conditions of $\Gamma_{2\text{PI}}$,

$$\left.\frac{\delta\Gamma_{2\text{PI}}}{\delta G_R}\right|_{\phi_R,\,G_R,\,D_R} = \left.\frac{\delta\Gamma_{2\text{PI}}}{\delta D_R}\right|_{\phi_R,\,G_R,\,D_R} \stackrel{!}{=} 0\,, \tag{3.138}$$

cause these to drop out. We thus obtain, by converting to momentum space,

$$\Gamma^{(1)} = \left.\frac{\delta\widehat{\Gamma}_{2\text{PI}}}{\delta\phi_R}\right|_{p^2=0} = -\delta t_1 - (m_R^2 + \delta m_2^2)\phi_R - \frac{(\alpha_R + \delta\alpha_3)}{2}\phi_R^2 - \frac{(\lambda_R + \delta\lambda_4)}{6}\phi_R^3$$

$$- \frac{1}{2}\left[(\alpha_R + \delta\alpha_1) + (\lambda_R + \delta\lambda_2)\phi_R\right]\mathcal{T} + \frac{\lambda_R\,(\alpha_R + \lambda_R\phi_R)}{6}\,\mathcal{S} - (g_R + \delta g_1)\int_q \text{tr}\left[D_R(q)\right] \stackrel{!}{=} 0\,, \tag{3.139}$$

which is the same minimisation condition as in the scalar sunset, but with a new contribution from the fermionic tadpole, which is the last term in the second line.

Consider the physical two-point function of the scalar field,

$$\Gamma^{(2)}(x_1,x_2) \equiv \frac{\delta^2\Gamma_{2\text{PI}}}{\delta\phi(x_1)\delta\phi(x_2)}$$

$$= \left.\frac{\delta^2\Gamma_{2\text{PI}}}{\delta\phi_R(x_1)\delta\phi_R(x_2)}\right|_{\phi_R,\,G_R,\,D_R} + \int_{y_1,\ldots,y_4} \left.\frac{\delta^2\Gamma_{2\text{PI}}}{\delta\phi_R(x_1)\delta G_R(y_1,y_2)}\right|_{\phi_R,\,G_R,\,D_R} \frac{\delta G_R(y_1,y_2)}{\delta\phi_R(x_2)}$$

$$+\int_{y_1,\dots,y_4}\mathrm{Tr}\left\{\frac{\delta^2\Gamma_{\mathrm{2PI}}}{\delta\phi(x_1)\delta D_R(y_1,y_2)}\bigg|_{\phi_R,G_R,D_R}\frac{\delta D_R(y_1,y_2)}{\delta\phi_R(x_2)}\right\}$$

$$\begin{aligned}
&= iG^{-1}_{0,R} + \frac{\delta^2\Gamma_{\mathrm{2PI,int}}}{\delta\phi_R(x_1)\delta\phi_R(x_2)}\bigg|_{\phi_R,G_R,D_R} \\
&\quad + \int_{y_1,\dots,y_4}\frac{\delta^2\Gamma^R_{\mathrm{int}}}{\delta\phi_R(x_1)\delta G_R(y_1,y_2)}\bigg|_{\phi_R,G_R,D_R} G_R(y_1,y_3)\frac{\delta\overline{\Pi}(y_3,y_4)}{\delta\phi_R(x_2)}G_R(y_4,y_2) \\
&\quad + \int_{y_1,\dots,y_4}\mathrm{tr}\left\{\frac{\delta^2\Gamma_{\mathrm{2PI,int}}}{\delta\phi_R(x_1)\delta D_R(y_1,y_2)}\bigg|_{\phi_R,G_R,D_R} D_R(y_1,y_3)\frac{\delta\overline{\Sigma}(y_3,y_4)}{\delta\phi_R(x_2)}D_R(y_4,y_2)\right\}.
\end{aligned} \tag{3.140}$$

The last line gives explicit fermionic contributions by virtue of $\delta\overline{\Sigma}/\delta\phi_R$. In a similar manner to (3.28), it can be expanded out using the following diagrammatic equation

$\frac{\delta\overline{\Sigma}(x_1,x_2)}{\delta\phi_R(x_3)} \equiv$ 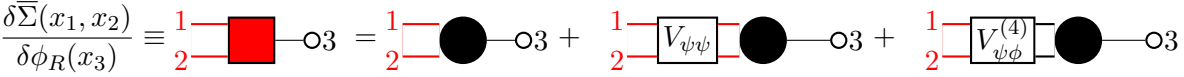

(3.141)

where we have the new building blocks involving fermions. Red lines indicate fermionic propagators. Note the appearance of the vertex functions $V_{\psi\psi}$ and $V_{\psi\phi}$ now, which appear as a solution to the self-energy equation of $\delta\overline{\Sigma}/\delta\phi_R$, in the similar manner that $\overline{V}^{(4)}$ appeared as solution to $\delta\overline{\Pi}/\delta\phi_R$. We stress that the $\overline{V}^{(4)}$ used is (3.115), with the modified four-point scalar kernel. Furthermore, note that correspondingly $\delta\overline{\Pi}/\delta\phi_R$ is modified from (3.28), and gains the additional part

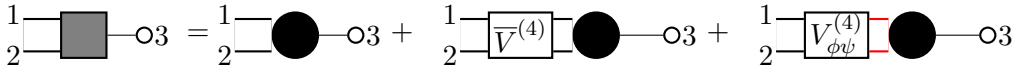

(3.142)

where $V^{(4)}_{\phi\psi}$ is the transpose of the vertex function $V^{(4)}_{\psi\phi}$. We continue now with the diagrammatic analysis and look at the 3-point and 4-point functions, required to obtain the counterterms $\delta\alpha_3$ and $\delta\lambda_4$. Besides the scalar contributions in (3.96) and (3.97), we have the following new topologies from the fermions

$\Gamma^{(3)}\big|_{\text{fermions}} =$ 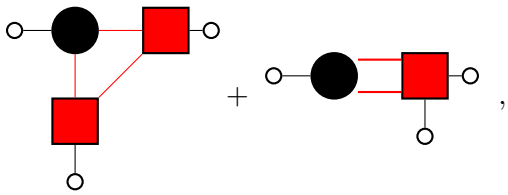

(3.143)

$\Gamma^{(4)}\big|_{\text{fermions}} =$ 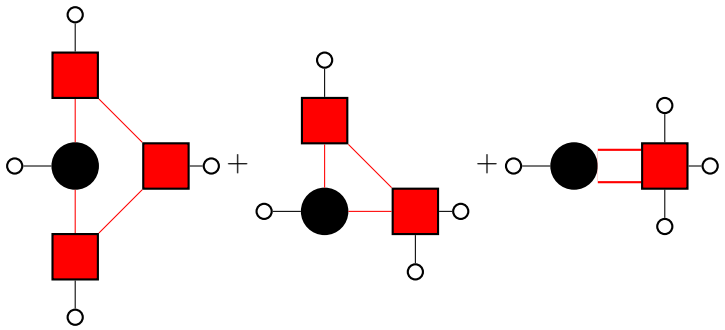

(3.144)

A factor of $\frac{1}{2}$ does not appear for the fermionic self-energy insertions as this quantity is not defined with a factor of 2 (compare (2.36) and (2.52)). Now, we list the non-vanishing fermionic contributions to the derivatives of the scalar self-energy which would be inserted in to the above equations

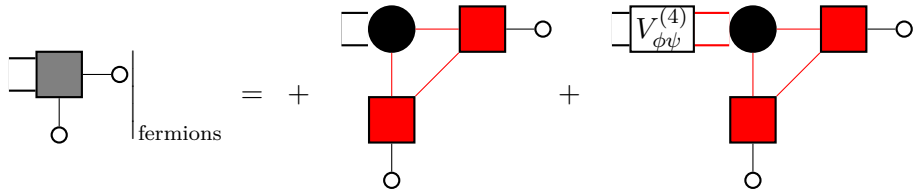

(3.145)

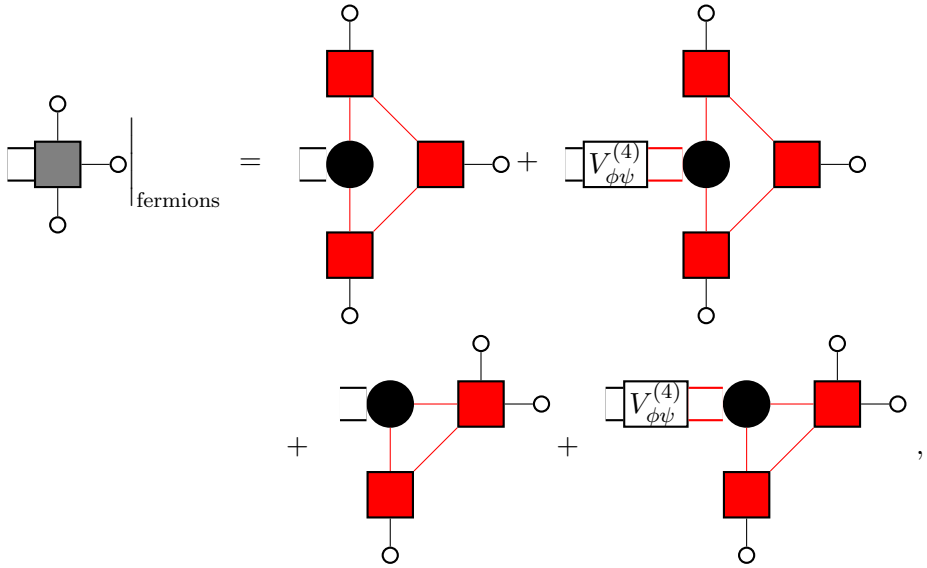

(3.146)

and finally, those of the fermionic self-energy

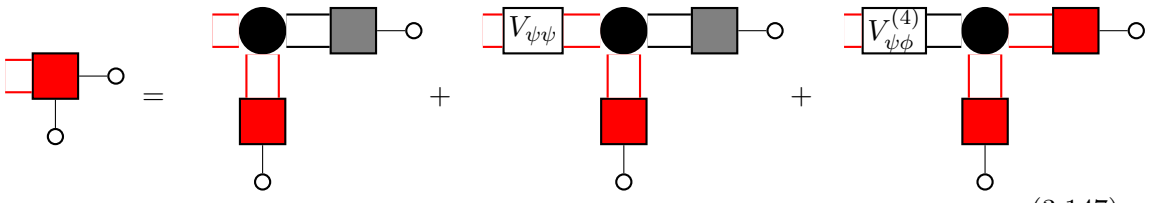

(3.147)

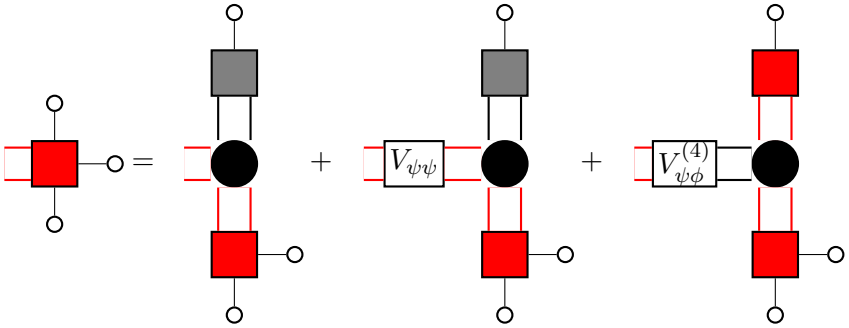

(3.148)

With these, one can analyse the scalar n-point functions with fermionic contributions and obtain the field counterterms. Moreover, we note that these diagrammatic tools extend to higher truncations of the 2PI effective action involving fermions.

3.5 Summary

In this chapter, we focused on the renormalisation of the 2PI effective action in the broken phase, $\phi_R \neq 0$. By first defining the renormalised effective action up to two-loop order and presenting the tools required, we proceeded to systematically analyse three different truncations of the 2PI effective action: the Hartree approximation, the scalar sunset approximation and the fermionic sunset approximation, the last of which involves a systematic treatment of fermions in the 2PI formalism. We used an on-shell scheme to obtain the various counterterms.

In the Hartree approximation, we saw that all results could be obtained analytically due to the fact that the renormalised propagator corresponded to the bare one. Furthermore, all counterterms were finite and relations existed between the various quartic coupling and vertex counterterms, as well as the mass ones. This was not the case, however, in the scalar sunset approximation, as many of the counterterms were not finite. The propagator could now only be determined via a numerical solution to the gap equation. To this end, we utilised an iterative approach which we showed converges rapidly, even with large couplings. We then extended our techniques to fermions, by defining an arsenal of additional kernels and vertex functions. To treat the system of coupled gap equations for the fermionic and scalar propagator, we reduced the system to a set of self-consistent equations for the scalar functions $W(p)$ and $Z(p)$, to which we applied our iterative procedure. We again saw that this converges. Lastly, we extended our diagrammatic analysis to include fermions and obtain the various scalar n-point functions with fermionic contributions.

The importance of determining these counterterms is that they appear in the renormalised equations of motion (EOMs) to describe the evolution of the scalar field and propagator, and fermionic propagators. The scalar EOMs can be used to study phenomena such as bubble evolution during phase transitions, where as the inclusion of fermions serves as the starting point for the transport equations to investigate electroweak baryogenesis (see for e.g. [74, 75]).

We have presented thus a consistent way to renormalise the 2PI effective action in our on-shell scheme, and our numeric approach can also be extended to obtain the effective potential. However, we note that going beyond Hartree implies a loss of analytic insights in the approach we have presented; for example, we could not write down explicit expressions for the counterterms. Thus, in the next chapter, we renormalise the 2PI effective action through an alternative method and obtain, where possible, useful expansions of the counterterms in terms of ϵ in dim. reg., and correspondingly the 2PI improved effective potential.

Chapter 4

$\overline{\text{MS}}$ Renormalisation and the 2PI Effective Potential

In this chapter, we reconsider the renormalisation of the 2PI effective potential in the $\overline{\text{MS}}$ scheme according to the various truncations of the 2PI effective action studied in the previous chapter. Closely following the approach in [72], we will obtain field-independent counterterms without reference to the various 2PI kernels and Bethe-Salpeter equations (BSEs) described in the previous chapter. Furthermore, as in [67], we express, when possible, the counterterms in expansions of ϵ in dimensional regularisation and subsequently determine the 2PI improved effective potential in a transparent manner. Both these points, to our knowledge, have not yet been reported in the literature. For comparison, we verify that the coupling constant counterterms obtained match in the Hartree and the scalar sunset approximations when one considers an $\overline{\text{MS}}$ scheme analysis of the 2PI BSEs in Appendix B. Finally, for the fermionic sunset approximation, we show that although one arrives at equations to solve for the counterterms, exact solutions cannot be found as the loop integrals cannot be evaluated analytically.

4.1 Hartree Approximation

As mentioned in the previous chapter, the Hartree approximation has been treated widely in the literature; specifically, the effective potential has been calculated in [76] and more recently in [60]. Hence, we will use the Hartree approximation as a stepping stone to outline the method involved in obtaining the counterterms and effective potential. Our starting point is the gap equation (3.43), obtained from the 2PI effective action in the Hartree approximation, c.f. (3.34),

$$\begin{aligned} iG_R^{-1}(p^2) &= p^2 - m_R^2 - i\overline{\Pi}(p^2) \\ &= p^2 - \left[m_R^2 + \delta m_0^2 + \frac{\lambda_R + \delta\lambda_2}{2}\phi^2 + \frac{\lambda_R + \delta\lambda_0}{2}\int_q G_R(q) - p^2\delta Z_0 \right], \end{aligned} \tag{4.1}$$

according to which, we may parameterise the renormalised propagator as

$$iG_R^{-1}(p^2) = p^2 - M^2(\phi; p^2)\,, \tag{4.2}$$

where we have the field- and momentum-dependent (squared) mass

$$M^2(\phi;p^2) = m_R^2 + \delta m_0^2 + \frac{\lambda_R + \delta\lambda_2}{2}\phi^2 + \frac{\lambda_R + \delta\lambda_0}{2}\int_q G_R(q) - p^2\delta Z_0\,. \tag{4.3}$$

We use the following condition to obtain the wave-function renormalisation,

$$i\frac{\partial G_R^{-1}(p^2)}{\partial p^2}\bigg|_{p^2=0,\,\phi=v_R} = 1\,, \qquad \implies \delta Z_0 = 0\,, \tag{4.4}$$

where v_R is the renormalised VEV and we choose the renormalisation point at $p^2 = 0$, as this is where the effective potential is evaluated. We thus have

$$M^2(\phi;p^2) \equiv m^2(\phi)\,,$$

and can evaluate all loop integrals in dimensional regularisation. Using the results in Appendix A, we have

$$\mathcal{T} = \int_q G_R(q) \equiv \frac{A_0(m^2(\phi))}{16\pi^2} = \underbrace{-\frac{m^2(\phi)}{16\pi^2\epsilon}}_{\mathcal{T}_{\text{div.}}} + \underbrace{\frac{m^2(\phi)}{16\pi^2}\left\{\overline{\log}\left[m^2(\phi)\right] - 1\right\}}_{\mathcal{T}_{\text{fin.}}[\phi]}\,, \tag{4.5}$$

where $\mathcal{T}_{\text{div.}}$ denotes the UV divergent piece, signified by the ϵ^{-1} pole, and $\mathcal{T}_{\text{fin.}}[\phi]$ refers to the remaining UV finite part. The $\overline{\log}[...]$ is as defined in Appendix A. Substituting (4.5) in (4.3)

$$m^2(\phi) = m_R^2 + \frac{\lambda_R}{2}\phi^2 + \frac{\lambda_R}{2}\mathcal{T}_{\text{fin.}}[\phi] + \delta m_0^2 + \frac{\delta\lambda_2}{2}\phi^2 + \frac{\lambda_R + \delta\lambda_0}{2}\mathcal{T}_{\text{div.}} + \frac{\delta\lambda_0}{2}\mathcal{T}_{\text{fin.}}[\phi]\,. \tag{4.6}$$

The first three terms are explicitly finite, and give the following renormalised quantity.

$$m^2(\phi) = m_R^2 + \frac{\lambda_R}{2}\phi^2 + \frac{\lambda_R}{2}\mathcal{T}_{\text{fin.}}[\phi]\,, \tag{4.7}$$

and the following **cancellation condition** to determine the counterterms

$$\delta m_0^2 + \frac{\delta\lambda_2}{2}\phi^2 + \frac{\lambda_R + \delta\lambda_0}{2}\mathcal{T}_{\text{div.}} + \frac{\delta\lambda_0}{2}\mathcal{T}_{\text{fin.}}[\phi] \stackrel{!}{=} 0\,. \tag{4.8}$$

We now use the definition of $\mathcal{T}_{\text{div.}}$ from (4.5), and substitute (4.7). This allows us to isolate the pieces proportional to ϕ^0, ϕ^2 and $\mathcal{T}_{\text{fin.}}[\phi]$ as follows

$$\left[\delta m_0^2 - \frac{(\lambda_R + \delta\lambda_0)\,m_R^2}{32\pi^2\epsilon}\right] + \left[\delta\lambda_2 - \frac{(\lambda_R + \delta\lambda_0)\,\lambda_R}{32\pi^2\epsilon}\right]\frac{\phi^2}{2} + \left[\delta\lambda_0 - \frac{(\lambda_R + \delta\lambda_0)\,\lambda_R}{32\pi^2\epsilon}\right]\frac{\mathcal{T}_{\text{fin.}}[\phi]}{2} \stackrel{!}{=} 0\,.$$

To fulfil this condition for any ϕ, it is required that each of these coefficients vanish individually. Thus, we obtain the counterterms as

$$\delta\lambda_0 = \frac{(\lambda_R + \delta\lambda_0)\,\lambda_R}{32\pi^2\epsilon}$$

$$\implies \delta\lambda_0 = \frac{\lambda_R}{32\pi^2\epsilon}\frac{\lambda_R}{\left(1 - \frac{\lambda_R}{32\pi^2\epsilon}\right)} = -\lambda_R - 32\pi^2\epsilon - \frac{(32\pi^2\epsilon)^2}{\lambda_R} - \mathcal{O}(\epsilon^3)\,, \tag{4.9}$$

$$\delta\lambda_2 = \frac{(\lambda_R + \delta\lambda_0)\,\lambda_R}{32\pi^2\epsilon} = \delta\lambda_0\,, \tag{4.10}$$

$$\delta m_0^2 = \frac{(\lambda_R + \delta\lambda_0)\,m_R^2}{32\pi^2\epsilon} = \frac{m_R^2}{\lambda_R}\delta\lambda_0 = -m_R^2 - \frac{m_R^2}{\lambda_R}(32\pi^2\epsilon) - \mathcal{O}(\epsilon^2)\,. \tag{4.11}$$

These counterterms match the ones we obtained in our on-shell scheme and also see again the peculiar feature of the Hartree approximation that $\delta\lambda_2 = \delta\lambda_0$.

The remaining counterterms required for the effective potential are δm_2^2 and $\delta\lambda_4$, for which we use the stationarity condition

$$\left.\frac{\delta\Gamma_{\text{2PI}}}{\delta\phi}\right|_{\phi=v_R\,,\,p^2=0} \stackrel{!}{=} 0\,. \tag{4.12}$$

This gives us the following equation

$$\begin{aligned} & m_R^2 + \delta m_2^2 + \frac{\lambda_R + \delta\lambda_4}{6}v_R^2 + \frac{\lambda_R + \delta\lambda_2}{2}\mathcal{T} = 0 \\ \implies\; & m_R^2 + \frac{\lambda_R}{6}v_R^2 + \frac{\lambda_R}{2}\mathcal{T}_{\text{fin.}}[v_R] + \underbrace{\delta m_2^2 + \frac{\delta\lambda_4}{6}v_R^2 + \frac{\lambda_R + \delta\lambda_2}{2}\mathcal{T}_{\text{div.}} + \frac{\delta\lambda_2}{2}\mathcal{T}_{\text{fin.}}[v_R]}_{=0} = 0\,, \end{aligned} \tag{4.13}$$

where we demand, as before, that the parts containing divergences and counterterms vanish. The remaining finite parts give, after a slight manipulation,

$$\begin{aligned} & m_R^2 + \frac{\lambda_R}{2}v_R^2 + \frac{\lambda_R}{2}\mathcal{T}_{\text{fin.}}[v_R] + \frac{\lambda_R}{6}v_R^2 - \frac{\lambda_R}{2}v_R^2 = 0 \\ \implies\; & m^2(v_R) = \frac{\lambda_R}{3}v_R^2 \end{aligned} \tag{4.14}$$

which is nothing but the tree-level relation between the quartic coupling, the VEV and a physical mass defined at the VEV. Returning to the cancellation condition obtained from the minimisation requirement, we substitute again the definition of $\mathcal{T}_{\text{div.}}$ and $m^2(v_R)$ and isolate the various pieces

$$\begin{aligned} & \left[\delta m_2^2 - \frac{(\lambda_R + \delta\lambda_2)\,m_R^2}{32\pi^2\epsilon}\right] + \left[\frac{\delta\lambda_4}{3} - \frac{(\lambda_R + \delta\lambda_2)\,\lambda_R}{32\pi^2\epsilon}\right]\frac{v_R^2}{2} \\ & \qquad + \left[\delta\lambda_2 - \frac{(\lambda_R + \delta\lambda_2)\,\lambda_R}{32\pi^2\epsilon}\right]\frac{\mathcal{T}_{\text{fin.}}[v_R]}{2} \stackrel{!}{=} 0\,. \end{aligned} \tag{4.15}$$

These are actually three equations to determine the two unknown ones; the equation arising from the requirement that the coefficient of $\mathcal{T}_{\text{fin.}}[v_R]$ vanishes actually serves as a consistency check for the counterterm $\delta\lambda_2$. Using the fact that $\delta\lambda_2 = \delta\lambda_0$, we now obtain the unknown counterterms

$$\delta m_2^2 = \delta m_0^2 \quad \text{and} \quad \delta\lambda_4 = 3\delta\lambda_2 = 3\delta\lambda_0\,. \tag{4.16}$$

Evidently, we again obtain the result $\delta m_0^2 = \delta m_2^2$, which we saw is valid in the unbroken phase in the previous chapter (see (3.52)).

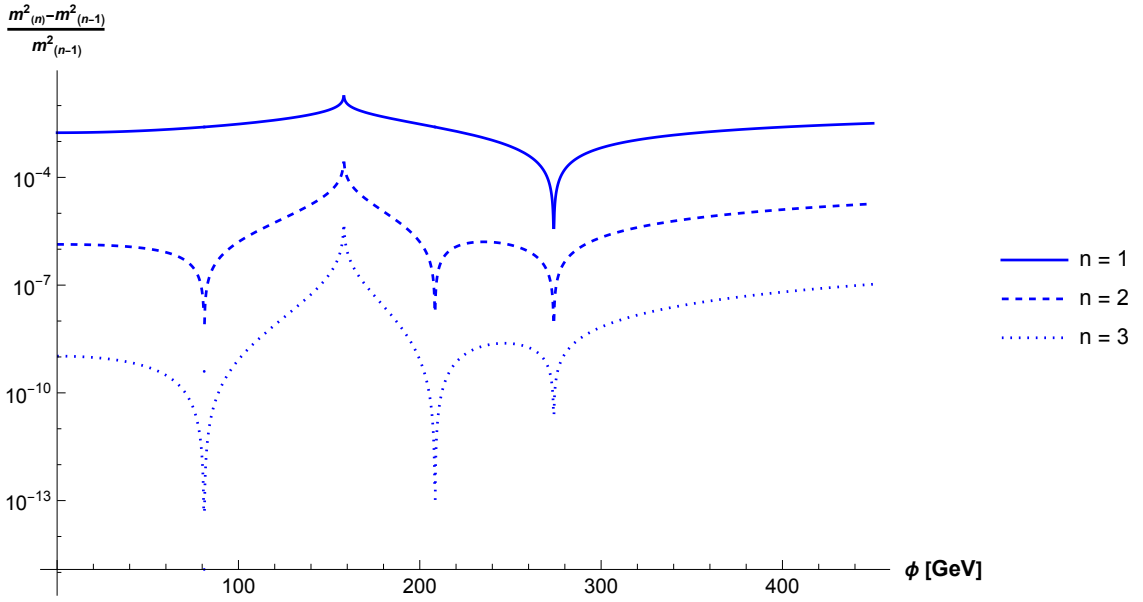

Figure 4.1: The relative difference between successive iterations of $m^2(\phi)$ versus the field value ϕ. The parameters are $\lambda_R = 0.8$ and $|m_R| = 100\,\text{GeV}$, leading to $v_R \approx 274\,\text{GeV}$.

Effective Potential

The 2PI effective potential is given by (see Sec. 2.4)

$$V_{2\text{PI}}(\phi) = -\widehat{\Gamma}_{2\text{PI}}[\phi]\Big|_{\text{K.E.}=0} = V_0(\phi) - \frac{i}{2\mathcal{V}}\text{Tr}\left[\log G_R^{-1}\right] - \frac{i}{2\mathcal{V}}\text{Tr}\left[\tilde{G}_\phi^{-1}\, G_R\right] - \frac{1}{\mathcal{V}}\Gamma_2\,, \quad (4.17)$$

where $\mathcal{V}$ is the space-time volume. Based on our earlier calculations, we know

$$G_R^{-1}(p) = p^2 - \underbrace{\left[m_R^2 + \frac{\lambda_R}{2}\phi^2 + \frac{\lambda_R}{2}\mathcal{T}_{\text{fin.}}[\phi]\right]}_{\equiv\, m^2(\phi)}\,, \quad \text{with} \quad \mathcal{T}_{\text{fin.}}[\phi] = \frac{m^2(\phi)}{16\pi^2}\left\{\overline{\log}\left[|m^2(\phi)|\right] - 1\right\}\,. \quad (4.18)$$

We use the absolute value of $m^2(\phi)$ to account for the region where the argument of the logarithm is negative. Note that $\mathcal{T}_{\text{fin.}}$ is defined implicitly by $m^2(\phi)$; therefore, we solve this iteratively, as we approached the gap equation in Chapter 4, beginning with

$$m^2_{(0)}(\phi) = m_R^2 + \frac{\lambda_R}{2}\phi^2$$

and then use this to obtain $\mathcal{T}_{\text{fin.}}$ and then the first iteration $m^2_{(1)}(\phi)$, and so on. Fig. 4.1 shows that this converges rather quickly, with the relative error between successive iterations decreasing by two orders of magnitude. We thus make use of the first iteration from now onward in the corresponding numerics.

For the first two parts of (4.17), we have

$$V_0(\phi) \equiv \frac{(m_R^2 + \delta m_2^2)}{2}\phi^2 + \frac{(\lambda_R + \delta\lambda_4)}{4!}\phi^4 = -\frac{\lambda_R}{12}\phi^4 + \mathcal{O}(\epsilon) \quad (4.19)$$

$$-\frac{i}{2}\text{Tr}\left[\log G_R^{-1}\right] \equiv \mathcal{V}\, i\int_p \log G_R^{-1}(p) = \mathcal{V}\left\{-\frac{m^4(\phi)}{64\pi^2\epsilon} + \frac{m^4(\phi)}{64\pi^2}\left\{\overline{\log}\left[|m^2(\phi)|\right] - \frac{3}{2}\right\} + \mathcal{O}(\epsilon)\right\} \quad (4.20)$$

where for the second part, we have used the formula described in Appendix A. For the third term of (4.17), we use

$$\tilde{G}_\phi^{-1}(p) = G_R^{-1}(p) + \Pi(p) \equiv G_R^{-1}(p) + 2i\frac{\delta\Gamma_2}{\delta G_R(p)}$$

$$\implies G_0^{-1}(p)G_R(p) = 1 + 2i\frac{\delta\Gamma_2}{\delta G_R(p)}G_R(p)\,,$$

and therefore, in the Hartree approximation, with

$$\Gamma_2 = -\frac{\mathcal{V}}{8}\left(\lambda_R + \delta\lambda_0\right)\left[\int_q G_R(q)\right]^2\,, \tag{4.21}$$

we have

$$\begin{aligned}\frac{i}{2}\mathrm{Tr}\left[\tilde{G}_\phi^{-1}\,G_R\right] &= -\mathcal{V}\int_p \frac{\delta\Gamma_2}{\delta G_R(p)}G_R(p) + \text{const.}\\ &= \frac{\mathcal{V}}{4}\left(\lambda_R + \delta\lambda_0\right)\left[\int_q G_R(q)\right]^2 + \text{const.}\,,\end{aligned} \tag{4.22}$$

where the "const." is a vacuum term, removed by appropriate subtraction. Adding (4.22) with the last term of (4.17), we have

$$\begin{aligned}-\frac{i}{2}\mathrm{Tr}\left[\tilde{G}_\phi^{-1}\,G_R\right] - \Gamma_2 &= -\frac{\mathcal{V}}{8}\left(\lambda_R + \delta\lambda_0\right)\left[\int_q G_R(q)\right]^2\\ &= \frac{\mathcal{V}}{8}\left[32\pi^2\epsilon + \frac{(32\pi^2\epsilon)^2}{\lambda_R} + \mathcal{O}(\epsilon^3)\right]\left[-\frac{m^2(\phi)}{16\pi^2\epsilon} + \frac{m^2(\phi)}{16\pi^2}\left\{\overline{\log}\left[|m^2(\phi)|\right] - 1\right\}\right]^2\\ &= \mathcal{V}\left\{\frac{m^4(\phi)}{64\pi^2\epsilon} + \frac{m^4(\phi)}{2\lambda_R} - \frac{m^4(\phi)}{64\pi^2}\left[\overline{\log}\left[|m^2(\phi)|\right] - 1\right]\right\}\,.\end{aligned} \tag{4.23}$$

We observe that the divergences from (4.20) and (4.23) cancel between each other. Thus, the effective potential in the Hartree approximation is given by

$$V_{2\mathrm{PI}}(\phi) = -\frac{\lambda_R}{12}\phi^4 + \frac{m^4(\phi)}{2\lambda_R} - \frac{m^4(\phi)}{64\pi^2}\left\{\overline{\log}\left[|m^2(\phi)|\right] - \frac{1}{2}\right\}\,. \tag{4.24}$$

In Fig. 4.2, we show the 2PI effective potential along with the tree-level potential,

$$V_{\mathrm{tree}}(\phi) = \frac{m_R^2}{2}\phi^2 + \frac{\lambda_R}{4!}\phi^4\,. \tag{4.25}$$

and the Coleman-Weinberg potential [2, 3] corresponding to this,

$$V_{\mathrm{CW}}(\phi) = V_{\mathrm{tree}}(\phi) + \frac{1}{64\pi^2}\left(\frac{\partial^2 V_{\mathrm{tree}}(\phi)}{\partial\phi^2}\right)^2\left\{\overline{\log}\left(\left|\frac{\partial^2 V_{\mathrm{tree}}(\phi)}{\partial\phi^2}\right|\right) - \frac{3}{2}\right\} \tag{4.26}$$

for comparison. To allow for a symmetry-breaking, bounded tree-level potential, we choose $m_R^2 < 0$ and $\lambda_R > 0$. For a fair comparison, we choose the renormalisation scale as the

physical (renormalised) mass at the VEV for $V_{2\text{PI}}$ and V_{CW}, and define all parameters at this scale. We see that for our choices $\lambda_R = 0.8$ and $|m_R| = 100\,\text{GeV}$, we obtain $v_R \approx 274\,\text{GeV}$, which is approximately the same for all three potentials. This leads to a physical mass of about 200 GeV at the VEV. The correction V_{CW} more or less coincides with the tree-level potential, i.e. the corrections are small, and $V_{2\text{PI}}$ provides a noticeable correction, more prevalent at field values beyond the VEV.

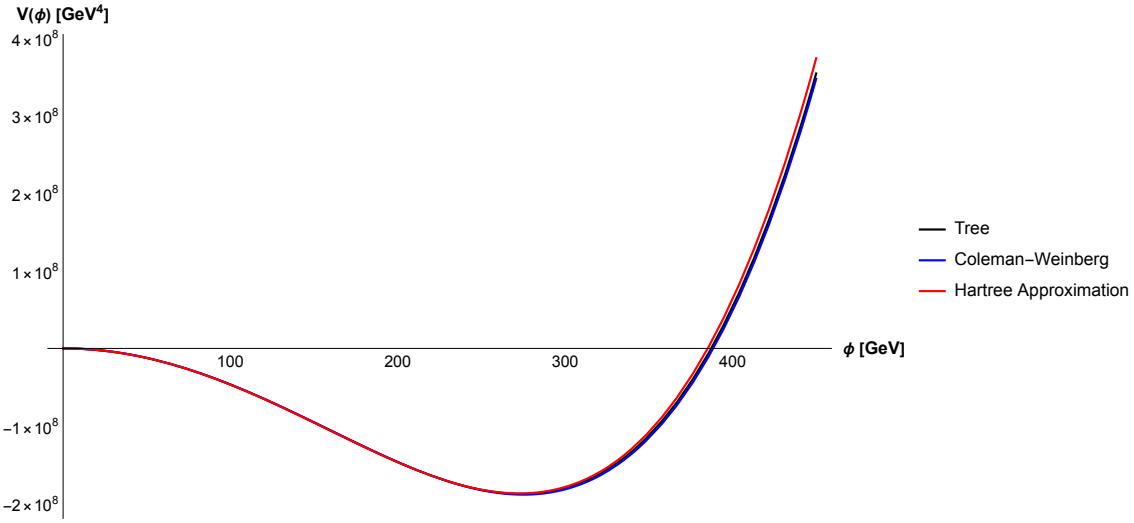

Figure 4.2: The 2PI improved effective potential in the Hartree approximation (red curve) against the field value, with the tree-level (black curve) and Coleman-Weinberg (blue curve) potentials for comparison. The parameters are $\lambda_R = 0.8$ and $|m_R| = 100\,\text{GeV}$, leading to $v_R \approx 274\,\text{GeV}$.

4.2 Scalar Sunset Approximation

From the 2PI functional (3.65), we obtain the following field and momentum dependent mass from the gap equation (3.82)

$$M^2(\phi;p^2) = m_R^2 + \delta m_0^2 + (\alpha_R + \delta\alpha_1)\phi + \frac{(\lambda_R + \delta\lambda_2)}{2}\phi^2 + \frac{\lambda_R + \delta\lambda_0}{2}\int_q G_R(q) \\ - \frac{i\left[(\lambda_R + \delta\lambda_1)\phi + (\alpha_R + \delta\alpha_0)\right]^2}{2}\int_q G_R(p+q)G_R(q) - p^2\delta Z_{\phi,0} \tag{4.27}$$

Based on our discussions in the previous chapter, we set $\delta\alpha_0 = \delta\lambda_1 = 0$. To extract the divergences in the various loop integrals that appear, it is convenient to define a Pauli-Villars-type auxiliary propagator

$$iG_a^{-1}(p) = p^2 - m_0^2 \tag{4.28}$$

where m_0 is an auxiliary mass parameter. In general, this corresponds to a renormalisation scale, but foreshadowing of what is to come, we have chosen it to be the physical mass at the VEV. Now, we parameterise G_R as

$$iG_R^{-1}(p) \equiv p^2 - M^2(\phi;p^2) \equiv p^2 - \left[m^2(\phi) + \Pi_2(p^2;\phi)\right] , \tag{4.29}$$

i.e. we split the self-energy into a manifestly momentum-independent part, akin to the field-dependent mass in the Hartree approximation, and an explicitly momentum-

dependent part, which behaves as

$$\lim_{p^2\to\infty} \frac{\Pi_2(p^2;\phi)}{p^2} \longrightarrow 0\,.$$

For brevity, we will suppress the field-dependence in the argument of Π_2 in the following equations. Let us now obtain the expansion for the renormalised propagator,

$$\begin{aligned} G_R(p) &= \frac{i}{p^2-[m^2(\phi)+\Pi(p^2)]} - \frac{i}{p^2-m_0^2} + \frac{i}{p^2-m_0^2} \\ &= \frac{i}{p^2-m_0^2} + i\left[\frac{m^2(\phi)-m_0^2+\Pi_2(p^2)}{(p^2-m_0^2)(p^2-M^2(\phi;p^2))}\right] \\ &= G_a(p) - iG_a(p)\left[m^2(\phi)-m_0^2+\Pi_2(p^2)\right]G_R(p) \\ &\equiv G_a(p) + \delta G(p)\,. \end{aligned} \tag{4.30}$$

In the third equality, we may iterate G_R as needed to extract divergences in loop integrals, according to power counting arguments. For the loop integral over two renormalised propagators, this amounts to

$$\mathcal{I} = i\int_q G_R(p+q)G_R(q) = i\int_q G_a^2(q)\Big|_{\text{div.}} + \mathcal{I}_{\text{fin.}}(p^2) \equiv T_d^{(0)} + \mathcal{I}_{\text{fin.}}(p^2) \tag{4.31}$$

With this, we can determine the wave function renormalisation,

$$\begin{aligned} \delta Z_{\phi,0} &= \left\{\left[\frac{(\alpha_R+\lambda_R\phi)^2}{2}\frac{\partial}{\partial p^2}(T_d^{(0)} + \mathcal{I}_{\text{fin.}}(p^2))\right]\Big|_{p^2=0,\phi=v_R}\right\}\Big|_{\text{div.}} \\ &= \left\{\left[\frac{(\alpha_R+\lambda_R\phi)^2}{2}\frac{\partial\mathcal{I}_{\text{fin.}}(p^2)}{\partial p^2}\right]\Big|_{p^2=0,\phi=v_R}\right\}\Big|_{\text{div.}} = 0\,, \end{aligned} \tag{4.32}$$

due to the fact that the divergent part has no momentum dependence.

Next, we have the integral over a single propagator

$$\begin{aligned} \mathcal{T} &= \int_q G_R(q) \\ &= \int_q G_a(q)\Big|_{\text{div.}} - \left[m^2(\phi)-m_0^2\right]\, i\int_q G_a^2(q)\Big|_{\text{div.}} - i\int_q G_a^2(q)\Pi_2(p^2)\Big|_{\text{div.}} \\ &\quad + \mathcal{T}_{\text{fin.}} \end{aligned} \tag{4.33}$$

where the $\mathcal{T}_{\text{fin.}}$ encompasses the finite parts of the marked divergent loop integrals and the remaining finite integrals due to simple power counting (three or more propagators are involved). Inserting these expressions into (4.27),

$$\begin{aligned} M^2(\phi;p^2) &= m_R^2 + \alpha_R\phi + \frac{\lambda_R}{2}\phi^2 + \frac{\lambda_R}{2}\mathcal{T}_{\text{fin.}} - \frac{(\alpha_R^2+2\alpha_R\lambda_R\phi+\lambda_R^2\phi^2)}{2}\mathcal{I}_{\text{fin.}}(p^2) \\ &+ \delta m_0^2 + \delta\alpha_1\phi + \frac{\delta\lambda_2}{2}\phi^2 + \frac{(\lambda_R+\delta\lambda_0)}{2}\mathcal{T}_{\text{div.}} + \frac{\delta\lambda_0}{2}\mathcal{T}_{\text{fin.}} - \frac{(\alpha_R^2+2\alpha_R\lambda_R\phi+\lambda_R^2\phi^2)}{2}T_d^{(0)} \end{aligned} \tag{4.34}$$

The first line of the above equation allows us to identify the manifestly finite quantities based on the parameterisation in (4.29)

$$m^2(\phi) = m_R^2 + \alpha_R\phi + \frac{\lambda_R}{2}\phi^2 + \frac{\lambda_R}{2}\mathcal{T}_{\text{fin.}}\,, \qquad \Pi_2(p^2) = -\frac{(\alpha_R + \lambda_R\phi)^2}{2}\,\mathcal{I}_{\text{fin.}}(p^2)\,. \tag{4.35}$$

Having determined Π_2, we can insert this into (4.33), and identify the divergent pieces

$$\mathcal{T} = \underbrace{T_d^{(2)} - \left[m^2(\phi) - m_0^2\right]\, T_d^{(0)} + \frac{(\alpha_R + \lambda_R\phi)^2}{2} T_d^{(I,0)}}_{\mathcal{T}_{\text{div.}}} + \mathcal{T}_{\text{fin.}}\,, \tag{4.36}$$

where we have defined the following quantities

$$T_d^{(2)} = \int_q G_a(q)\Big|_{\text{div.}} \tag{4.37}$$

$$\begin{aligned} T_d^{(I,0)} &= i\int_q G_a^2(q)\,\mathcal{I}_{\text{fin.}}(q^2)\Big|_{\text{div.}} = i\int_q G_a^2(q)\,\mathcal{I}_{a,\text{fin.}}(q^2)\Big|_{\text{div.}} \\ &= \left\{ i\int_q G_a^2(q)\,\left[i\int_k G_a(k+q)G_a(k) - G_a^2(k)\right]\right\}\Big|_{\text{div.}} \end{aligned} \tag{4.38}$$

where, for $T_d^{(I,0)}$, the replacement $\mathcal{I}_{\text{fin.}} \to \mathcal{I}_{a,\text{fin.}}$ involves replacing all renormalised propagators of (4.31) with auxiliary propagators. This suffices as we intend to extract the divergent part of the loop integral.

As in the Hartree approximation, the **cancellation condition** obtained from the last line of (4.34) yields the following equations to determine the unknown counterterms

$$\frac{\delta\lambda_0}{2} + \frac{\lambda_R + \delta\lambda_0}{2}\left(-\frac{\lambda_R}{2}\,T_d^{(0)}\right) = 0\,, \tag{4.39}$$

$$\delta\alpha_1 + \frac{\lambda_R + \delta\lambda_0}{2}\left(-\alpha_R\,T_d^{(0)} + \alpha_R\lambda_R\,T_d^{(I,0)}\right) - \alpha_R\lambda_R\,T_d^{(0)} = 0\,, \tag{4.40}$$

$$\frac{\delta\lambda_2}{2} + \frac{\lambda_R + \delta\lambda_0}{2}\left(-\frac{\lambda_R}{2}\,T_d^{(0)} + \frac{\lambda_R^2}{2}\,T_d^{(I,0)}\right) - \frac{\lambda_R^2}{2}\,T_d^{(0)} = 0\,, \tag{4.41}$$

$$\delta m_0^2 + \frac{\lambda_R + \delta\lambda_0}{2}\left[T_d^{(2)} - (m_R^2 - m_0^2)\,T_d^{(0)} + \frac{\alpha_R^2}{2}\,T_d^{(I,0)}\right] - \frac{\alpha_R^2}{2}T_d^{(0)} = 0\,. \tag{4.42}$$

Using the results from Appendix B, we obtain the counterterms as

$$\delta\lambda_0 = -\lambda_R - 32\pi^2\epsilon - \frac{(32\pi^2\epsilon)^2}{\lambda_R} + \mathcal{O}(\epsilon^3)\,, \tag{4.43}$$

$$\delta\alpha_1 = \frac{\alpha_R\lambda_R}{32\pi^2\epsilon} - 2\alpha_R + \frac{\alpha_R\lambda_R}{32\pi^2} + \alpha_R\left(1 - \frac{64\pi^2}{\lambda_R}\right)\epsilon + \frac{32\pi^2\alpha_R}{\lambda_R}\left(1 - \frac{64\pi^2}{\lambda_R}\right)\epsilon^2 + \mathcal{O}(\epsilon^3)\,, \tag{4.44}$$

$$\delta\lambda_2 = \frac{\lambda_R^2}{32\pi^2\epsilon} - 2\lambda_R + \frac{\lambda_R^2}{32\pi^2} + \lambda_R\left(1 - \frac{64\pi^2}{\lambda_R}\right)\epsilon + 32\pi^2\left(1 - \frac{64\pi^2}{\lambda_R}\right)\epsilon^2 + \mathcal{O}(\epsilon^3)\,, \tag{4.45}$$

$$\delta m_0^2 = \frac{3\alpha_R^2}{32\pi^2\epsilon} - m_R^2 + \frac{\alpha_R^2}{32\pi^2} + \mathcal{O}(\epsilon)\,. \tag{4.46}$$

We notice that $\delta\lambda_0$ is the same as we had obtained in the Hartree approximation, c.f. (4.9). Furthermore, we observe that $\delta\lambda_2 \neq \delta\lambda_0$ as we had in the on-shell scheme; besides, it is not finite and neither are $\delta\alpha_1$ and δm_0^2. Finally, in the case of $\alpha_R = 0$, we find that δm_0^2 matches its value in the Hartree approximation, (4.11).

We now need the counterterms related to the fields. For this, we need to extract the divergences present in the scalar sunset integral. We approach this by replacing all propagators according to (4.30), and identifying, using power counting arguments, the divergent pieces.

$$
\begin{aligned}
\mathcal{S} &= i\int_q\int_k G_R(q)G_R(k)G_R(k+q) \\
&= i\int_q\int_k G_a(q)G_a(k)G_a(k+q) + 3\int_q \delta G(q)\underbrace{\left[i\int_k G_a(k)G_a(k+q)\right]}_{=\mathcal{I}_a(p^2)\,=\,T_d^{(0)}+\mathcal{I}_{a,\text{fin.}}(p^2)} \\
&\qquad \underbrace{+\,3i\int_q \delta G(q)\int_k \delta G_a(k)G_a(k+q) + i\int_q \delta G(q)\int_k \delta G_a(k)\delta G_a(k+q)}_{\mathcal{S}^{(1)}_{\text{fin.}}} \\
&= \mathcal{S}_a\Big|_{\text{div.}} + \mathcal{S}_{a,\text{fin.}} - 3\left(m^2(\phi)-m_0^2\right)\left(T_d^{(0)}\right)^2 - 3T_d^{(0)}\,i\int_q G_a^2(q)\Pi_2(q^2) \\
&\qquad - 3T_d^{(0)}\int_q G_a^2(q)\left[m^2(\phi)-m_0^2+\Pi_2(q^2)\right]^2 G_R(q) \\
&\qquad \underbrace{-3\int_q G_a^2(q)\left[m^2(\phi)-m_0^2+\Pi_2(q^2)\right]^2 G_R(q)\mathcal{I}_{a,\text{fin.}}(q^2)}_{\mathcal{S}^{(2)}_{\text{fin.}}} \\
&\qquad + \mathcal{S}^{(1)}_{\text{fin.}} - 3\left(m^2(\phi)-m_0^2\right)\,i\int_q G_a^2(q)\,\mathcal{I}_{a,\text{fin.}}(q^2) - 3i\int_q G_a^2(q)\Pi_2(q^2)\,\mathcal{I}_{a,\text{fin.}}(q^2) \\
&= \mathcal{S}_a\Big|_{\text{div.}} + 3\mathcal{T}_{\text{fin.}}\,T_d^{(0)} - 3\left(m^2(\phi)-m_0^2\right)\left[\left(T_d^{(0)}\right)^2 + T_d^{(I,0)}\right] \\
&\qquad + \frac{3(\alpha_R+\lambda_R\phi)^2}{2}\left[T_d^{(0)}\,T_d^{(I,0)} + T_d^{(I,I)}\right] \\
&\qquad - 3(m^2(\phi)-m_0^2)T^{(I,0)}_{\text{fin.}} + 3\frac{(\alpha_R+\lambda_R\phi)^2}{2}T^{(I,I)}_{\text{fin.}} + \mathcal{S}^{(1)}_{\text{fin.}} + \mathcal{S}^{(2)}_{\text{fin.}} \\
&\equiv \mathcal{S}_{\text{div.}} + \mathcal{S}_{\text{fin.}}\,. \qquad (4.47)
\end{aligned}
$$

Note that we continue to carefully tracked the explicitly finite loop integrals and extracted the finite parts of divergent integrals. We have made the replacements $I_{\text{fin.}} \to I_{a,\text{fin.}}$ whenever needed to extract the divergent parts and along the way, have defined the quantity

$$
T_d^{(I,I)} = i\int_q G_a^2(q)\,\mathcal{I}^2_{a,\text{fin.}}(q^2)\Big|_{\text{div.}}\,, \qquad (4.48)
$$

and its finite part is defined accordingly as $T^{(I,I)}_{\text{fin.}}$. Armed with this, we can now examine the minimisation condition

$$\begin{aligned}
&m_R^2 v_R + \frac{\alpha_R}{2} v_R^2 + \frac{\lambda_R}{6} v_R^3 + \frac{\alpha_R}{2}\mathcal{T}_{\text{fin.}} + \frac{\lambda_R}{2} v_R \mathcal{T}_{\text{fin.}} - \frac{\lambda_R(\alpha_R + \lambda_R v_R)}{6}\mathcal{S}_{\text{fin.}} \\
&+ \delta t_1 + \delta m_2^2 v_R + \frac{\delta\alpha_3}{2} v_R^2 + \frac{\delta\lambda_4}{6} v_R^3 + \frac{\alpha_R + \delta\alpha_1}{2}\mathcal{T}_{\text{div.}} + \frac{\lambda_R + \delta\lambda_2}{2} v_R \mathcal{T}_{\text{div.}} \\
&+ \frac{\delta\alpha_1}{2}\mathcal{T}_{\text{fin.}} + \frac{\delta\lambda_2}{2} v_R \mathcal{T}_{\text{fin.}} - \frac{\lambda_R(\alpha_R + \lambda_R v_R)}{6}\mathcal{S}_{\text{div.}} = 0
\end{aligned} \tag{4.49}$$

whereby the last two lines give the necessary cancellation condition to obtain the following equations to determine the remaining counterterms

$$\begin{aligned}
&\delta t_1 + \frac{\alpha_R + \delta\alpha_1}{2}\left[T_d^{(2)} - (m_R^2 - m_0^2)\, T_d^{(0)} + \frac{\alpha_R^2}{2}\, T_d^{(I,0)}\right] \\
&\quad - \frac{\lambda_R \alpha_R}{6}\left\{ S_a\Big|_{\text{div.}} - 3\left(m_R^2 - m_0^2\right)\left[\left(T_d^{(0)}\right)^2 + T_d^{(I,0)}\right] + \frac{3}{2}\alpha_R^2\left[T_d^{(0)}\, T_d^{(I,0)} + T_d^{(I,I)}\right]\right\} = 0\,,
\end{aligned} \tag{4.50}$$

$$\begin{aligned}
&\delta m_2^2 + \frac{\alpha_R + \delta\alpha_1}{2}\left[-\alpha_R\, T_d^{(0)} + \alpha_R\lambda_R\, T_d^{(I,0)}\right] \\
&\quad + \frac{\lambda_R + \delta\lambda_2}{2}\left[T_d^{(2)} - (m_R^2 - m_0^2)\, T_d^{(0)} + \frac{\alpha_R^2}{2}\, T_d^{(I,0)}\right] \\
&\quad - \frac{\alpha_R\lambda_R}{6}\left\{ - 3\alpha_R\left[\left(T_d^{(0)}\right)^2 + T_d^{(I,0)}\right] + 3\alpha_R\lambda_R\left[T_d^{(0)}\, T_d^{(I,0)} + T_d^{(I,I)}\right]\right\} \\
&\quad - \frac{\lambda_R^2}{6}\left\{ S_a\Big|_{\text{div.}} - 3\left(m_R^2 - m_0^2\right)\left[\left(T_d^{(0)}\right)^2 + T_d^{(I,0)}\right] + \frac{3}{2}\alpha_R^2\left[T_d^{(0)}\, T_d^{(I,0)} + T_d^{(I,I)}\right]\right\} = 0\,,
\end{aligned} \tag{4.51}$$

$$\begin{aligned}
&\frac{\delta\alpha_3}{2} + \frac{\alpha_R + \delta\alpha_1}{2}\left[-\frac{\lambda_R}{2}\, T_d^{(0)} + \frac{\lambda_R^2}{2}\, T_d^{(I,0)}\right] + \frac{\lambda_R + \delta\lambda_2}{2}\left[-\alpha_R\, T_d^{(0)} + \alpha_R\lambda_R\, T_d^{(I,0)}\right] \\
&\quad - \frac{\alpha_R\lambda_R}{6}\left\{ - 3\frac{\lambda_R}{2}\left[\left(T_d^{(0)}\right)^2 + T_d^{(I,0)}\right] + 3\frac{\lambda_R}{2}\left[T_d^{(0)}\, T_d^{(I,0)} + T_d^{(I,I)}\right]\right\} \\
&\quad - \frac{\lambda_R^2}{6}\left\{ - 3\alpha_R\left[\left(T_d^{(0)}\right)^2 + T_d^{(I,0)}\right] + 3\alpha_R\lambda_R\left[T_d^{(0)}\, T_d^{(I,0)} + T_d^{(I,I)}\right]\right\} = 0\,,
\end{aligned} \tag{4.52}$$

$$\begin{aligned}
&\frac{\delta\lambda_4}{6} + \frac{\lambda_R + \delta\lambda_2}{2}\left[-\frac{\lambda_R}{2}\, T_d^{(0)} + \frac{\lambda_R^2}{2}\, T_d^{(I,0)}\right] \\
&\quad - \frac{\lambda_R^2}{6}\left\{ - 3\frac{\lambda_R}{2}\left[\left(T_d^{(0)}\right)^2 + T_d^{(I,0)}\right] + 3\frac{\lambda_R^2}{2}\left[T_d^{(0)}\, T_d^{(I,0)} + T_d^{(I,I)}\right]\right\} = 0\,.
\end{aligned} \tag{4.53}$$

We solve these using results of Appendix B to obtain

$$\begin{aligned}\delta t_1 = &\frac{\alpha_R^3\lambda_R}{2(32\pi^2)^3\epsilon^3} - \frac{\alpha_R^3 - 2\alpha_R\lambda_R m_R^2}{2(32\pi^2)^2\epsilon^2} \\ &- \frac{\alpha_R\left(\alpha_R^2\lambda_R^2 - 2(32\pi^2)\lambda_R\left(\alpha_R^2 + \lambda_R m_R^2\right) + 2(32\pi^2)^2\left(\alpha_R^2 + \lambda_R m_R^2\right)\right)}{2\lambda_R(32\pi^2)^3\epsilon} \\ &- \frac{\alpha_R\left(2(32\pi^2) - \lambda_R\right)\left(32\pi^2\left(\alpha_R^2 + 2\lambda_R m_R^2\right) - \alpha_R^2\lambda_R\right)}{2\lambda_R^2(32\pi^2)^2} + \mathcal{O}(\epsilon)\,, \end{aligned} \tag{4.54}$$

$$\begin{aligned}\delta m_2^2 = &\frac{3\alpha_R^2\lambda_R^2}{2(32\pi^2)^3\epsilon^3} + \frac{\lambda_R\left(2\lambda_R m_R^2 - \alpha_R^2\right)}{2(32\pi^2)^2\epsilon^2} \\ &- \frac{3\alpha_R^2\lambda_R^2 + 2(32\pi^2)\lambda_R\left(4\alpha_R^2 + \lambda_R m_R^2\right) + 2(32\pi^2)^2\left(4\alpha_R^2 + \lambda_R m_R^2\right)}{2(32\pi^2)^3\epsilon} \\ &- \frac{\left(2(32\pi^2) - \lambda_R\right)\left(32\pi^2\left(5\alpha_R^2 + 2\lambda_R m_R^2\right) - 3\alpha_R^2\lambda_R\right)}{2\lambda_R(32\pi^2)^2} + \mathcal{O}(\epsilon)\,, \end{aligned} \tag{4.55}$$

$$\delta\alpha_3 = \frac{3\alpha_R\lambda_R^3}{(32\pi^2)^3\epsilon^3} - \frac{3\alpha_R\lambda_R\left(\lambda_R^2 - 3(32\pi^2)\lambda_R + 3(32\pi^2)^2\right)}{(32\pi^2)^3\epsilon} - \frac{3\alpha_R\left(\lambda_R - 2(32\pi^2)\right)^2}{(32\pi^2)^2} + \mathcal{O}(\epsilon)\,, \tag{4.56}$$

$$\delta\lambda_4 = \frac{3\lambda_R^4}{(32\pi^2)^3\epsilon^3} - \frac{3\lambda_R^2\left(\lambda_R^2 - 3(32\pi^2)\lambda_R + 3(32\pi^2)^2\right)}{(32\pi^2)^3\epsilon} - \frac{3\lambda_R\left(\lambda_R - 2(32\pi^2)\right)^2}{(32\pi^2)^2} + \mathcal{O}(\epsilon)\,. \tag{4.57}$$

None of the determined counterterms are finite once the sunset diagram is included, save for $\delta\lambda_0$, which matches its value in the Hartree approximation. Another remark is that $\delta m_2^2 \neq \delta m_0^2$, which is what we noted during the renormalisation in the on-shell scheme. This happens due to the sunset diagram contributing to the minimisation condition.

Effective Potential

Within the scalar sunset approximation, we see that the propagator contains an explicitly momentum-dependent piece, $\Pi_2(p^2)$, due to which we cannot evaluate the loop integrals using the usual results of dimensional regularisation, as in the Hartree approximation. However, having carefully tracked the explicitly finite integrals in (4.36) and (4.47), we may evaluate them (numerically) and add the finite pieces from the divergent loop integrals (see Appendix B) to obtain the full finite parts of the one-point and Sunset integrals.

We have not yet examined the integral $\mathrm{Tr}\left[\log G_R^{-1}\right]$; we proceed by using (4.30)

$$\begin{aligned}&-\frac{i}{2\mathcal{V}}\mathrm{Tr}\left[\log G_R^{-1}\right] \equiv \frac{i}{2}\int_q \log G_R(q) = \frac{i}{2}\int_q \log G_a(q) + \frac{i}{2}\int_q \log\left[1 + G_a^{-1}(q)\,\delta G(q)\right] \\ &= \frac{i}{2}\int_q \log G_a(q) + \frac{i}{2}\int_q \left\{G_a^{-1}(q)\,\delta G(q) - \frac{1}{2}\left[G_a^{-1}(q)\,\delta G(q)\right]^2\right\} + \text{Finite} \\ &= \frac{i}{2}\int_q \log G_a(q)\Big|_{\text{div.}} + \frac{1}{2}\int_q G_a(q)\left[m^2(\phi) - m_0^2 - \frac{(\alpha_R + \lambda_R\phi)^2}{2}\mathcal{I}_{a,\text{fin.}}(q^2)\right]\Big|_{\text{div.}} \end{aligned}$$

$$
\begin{aligned}
&- \frac{i}{4}\int_q G_a^2(q)\left[m^2(\phi)-m_0^2-\frac{(\alpha_R+\lambda_R\phi)^2}{2}\mathcal{I}_{a,\text{fin.}}(q^2)\right]^2\Big|_{\text{div.}} + \left\{-\frac{i}{2}\text{Tr}\left[\log G_R^{-1}\right]\right\}\Big|_{\text{fin.}} \\
&= \frac{i}{2}\int_q \log G_a(q)\Big|_{\text{div.}} + \frac{\left(m^2(\phi)-m_0^2\right)}{2}T_d^{(2)} - \frac{(\alpha_R+\lambda_R\phi)^2}{2}T_d^{(I,2)} - \frac{\left(m^2(\phi)-m_0^2\right)^2}{4}T_d^{(0)} \\
&\quad + \frac{\left(m^2(\phi)-m_0^2\right)(\alpha_R+\lambda_R\phi)^2}{4}T_d^{(I,0)} - \frac{(\alpha_R+\lambda_R\phi)^4}{16}T_d^{(I,I)} + \left\{-\frac{i}{2\mathcal{V}}\text{Tr}\left[\log G_R^{-1}\right]\right\}\Big|_{\text{fin.}}
\end{aligned}
\tag{4.58}
$$

where, in the third line, we have expanded the logarithm and kept the terms that are divergent. The step afterwards, we define the finite part of $\text{Tr}\left[\log G_R^{-1}\right]$ as the parts from the expansion of the logarithm and the finite parts from the marked divergent integrals. Finally, in the last step, we have identified the integrals according to our previous notation and also introduced

$$
T_d^{(I,2)} = \int_q G_a(q)\mathcal{I}_{a,\text{fin.}}(q^2)\Big|_{\text{div.}} . \tag{4.59}
$$

For the various parts of the effective potential (4.17), we have from the following part,

$$
\frac{1}{\mathcal{V}}\Gamma_2 = -\frac{1}{8}\left(\lambda_R+\delta\lambda_0\right)\left[\int_q G_R(q)\right]^2 + \frac{i(\alpha_R+\lambda_R\phi)^2}{12}\int_q\int_k G_R(q)G_R(k)G_R(k+q)\,. \tag{4.60}
$$

We use the same "trick" as in the Hartree approximation for the following part of the effective potential

$$
\begin{aligned}
\frac{i}{2\mathcal{V}}\text{Tr}\left[\tilde{G}_\phi^{-1}G_R\right] &= -\int_p \frac{\delta\Gamma_2}{\delta G_R(p)}G_R(p) + \text{const.} \\
&= \frac{1}{4}\left(\lambda_R+\delta\lambda_0\right)\left[\int_q G_R(q)\right]^2 - \frac{i(\alpha_R+\lambda_R\phi)^2}{4}\int_q\int_k G_R(q)G_R(k)G_R(k+q) + \text{const.}\,,
\end{aligned}
\tag{4.61}
$$

giving us in total

$$
-\frac{i}{2\mathcal{V}}\text{Tr}\left[\tilde{G}_\phi^{-1}\,G_R\right] - \frac{1}{\mathcal{V}}\Gamma_2 = -\frac{(\lambda_R+\delta\lambda_0)}{8}\,\mathcal{T}^2 + \frac{(\alpha_R+\lambda_R\phi)^2}{6}\,\mathcal{S}\,. \tag{4.62}
$$

We already know how to express the divergences and finite pieces of $\mathcal{T}$ and $\mathcal{S}$, c.f.(4.33) and (4.47). We analyse the Hartree part using

$$
\begin{aligned}
&-\frac{(\lambda_R+\delta\lambda_0)}{8}\,\mathcal{T}^2 = \\
&\frac{1}{8}\left(32\pi^2\epsilon + \frac{(32\pi^2\epsilon)^2}{\lambda_R} + \frac{(32\pi^2\epsilon)^3}{\lambda_R^2} + \frac{(32\pi^2\epsilon)^4}{\lambda_R^3}\right)\left[\mathcal{T}_{\text{div.}}^2 + 2\mathcal{T}_{\text{div.}}\mathcal{T}_{\text{fin.}}\right] + \mathcal{O}(\epsilon)\,.
\end{aligned}
\tag{4.63}
$$

We then have the first term of (4.17) as

$$
V_0(\phi) \equiv \delta t_1\phi + \frac{(m_R^2+\delta m_2^2)}{2}\phi^2 + \frac{(\alpha_R+\delta\alpha_3)}{3!}\phi^3 + \frac{(\lambda_R+\delta\lambda_4)}{4!}\phi^4\,, \tag{4.64}
$$

which requires the results from (4.54)-(4.57).

At this point, we are ready to discuss the issue of infinite counterterms in the 2PI formalism. We see divergent pieces littered throughout (4.64), (4.58) and (4.62). However, in what transpires, all divergences cancel when one sums over these pieces to arrive at the 2PI effective potential. This is not so surprising as we had seen a similar occurrence in the Hartree approximation. The scenario is more complicated in the sunset approximation, but once a careful book-keeping of the divergent pieces is done in the manner we have shown, this boils down to an algebraic exercise. One can also think that the result is not unexpected as the counterterms have been determined from various divergent parts of the integrals appearing in the effective potential, so it is indeed likely that the divergences cancel when put back.

We thus write down the finite 2PI effective potential as

$$
\begin{aligned}
V_{\text{2PI}}(\phi) = &\left[-\frac{\alpha_R\left(2(32\pi^2)-\lambda_R\right)\left(32\pi^2\left(\alpha_R^2+2\lambda_R m_R^2\right)-\alpha_R^2\lambda_R\right)}{2\lambda_R^2(32\pi^2)^2}\right]\phi \\
&+\left[m_R^2-\frac{\left(2(32\pi^2)-\lambda_R\right)\left(32\pi^2\left(5\alpha_R^2+2\lambda_R m_R^2\right)-3\alpha_R^2\lambda_R\right)}{2\lambda_R(32\pi^2)^2}\right]\frac{\phi^2}{2!} \\
&+\left[\alpha_R-\frac{3\alpha_R\left(\lambda_R-2(32\pi^2)\right)^2}{(32\pi^2)^2}\right]\frac{\phi^3}{3!}+\left[\lambda_R-\frac{3\lambda_R\left(\lambda_R-2(32\pi^2)\right)^2}{(32\pi^2)^2}\right]\frac{\phi^4}{4!} \\
&+\left\{-\frac{i}{2}\text{Tr}\left[\log G_R^{-1}\right]\right\}\Big|_{\text{fin.}} \\
&+\left[\frac{m^4(\phi)}{2\lambda_R}-\frac{m^2(\phi)\,\mathcal{T}_{\text{fin.}}}{2}-\frac{(\alpha_R+\lambda_R\phi)^2\,\mathcal{T}_{\text{fin.}}}{2\lambda_R}+\frac{(\alpha_R+\lambda_R\phi)^2\,m^2(\phi)}{2\lambda_R^2}+\frac{(\alpha_R+\lambda_R\phi)^4}{8\lambda_R^3}\right. \\
&\left.-\frac{(\alpha_R+\lambda_R\phi)^2\,m^2(\phi)}{64\pi^2}+\frac{(\alpha_R+\lambda_R\phi)^2\,\mathcal{T}_{\text{fin.}}}{128\pi^2}+\frac{(\alpha_R+\lambda_R\phi)^4}{128\pi^2\lambda_R^2}+\frac{(\alpha_R+\lambda_R\phi)^4}{8\lambda_R(32\pi^2)^2}\right] \\
&+\frac{(\alpha_R+\lambda_R\phi)^2}{6}\mathcal{S}_{\text{fin.}}\,. \qquad (4.65)
\end{aligned}
$$

The tree-level potential in this case is

$$
V_{\text{tree}}(\phi)=\frac{m_R^2}{2!}\phi^2+\frac{\alpha_R}{3!}\phi^3+\frac{\lambda_R}{4!}\phi^4\,. \qquad (4.66)
$$

We choose the parameters such that $m_R^2<0$ and $\alpha_R,\lambda_R>0$. Finally, to ensure we are comparing $\overline{\text{MS}}$ quantities, we calculate $\mathcal{T}_{\text{fin.}}$ as follows in the numerics

$$
\begin{aligned}
\mathcal{T}_{\text{fin.}}=\int_q\Big\{&G_R(q)-G_a(q)+iG_a^2(q)\left[m^2(\phi)-m_0^2+\frac{(\alpha_R+\lambda_R\phi_R)^2}{2}\mathcal{I}_{a,\text{fin.}}(q^2)\right]\Big\} \\
&-\frac{m_0^2}{16\pi^2}+\frac{(\alpha_R+\lambda_R\phi_R)^2}{2}T_{\text{fin.}}^{(I,0)}\,, \qquad (4.67)
\end{aligned}
$$

where we introduce the extra finite terms (see Appendix B) to compensate the fact we cannot subtract strictly the divergent pieces when we adopt a numeric implementation. Furthermore, for the numerics, we convert to Euclidean space and calculate all integrals using a cutoff, Λ, as in Chapter 3. We also implement the same iterative approach used in the Hartree approximation and find that the first iteration of the propagator is sufficient,

similar to what we had found in the previous chapter when solving the gap equation in the scalar sunset approximation. In our numerical approach, we first calculate the VEV using the tree-level potential, with a given choice of parameters. From this, we obtain the tree-level mass at this VEV and this sets our m_0. With m_0, we proceed to numerically evaluate various finite quantities in (4.65) and ultimately, the effective potential.

The 2PI improved effective potential within the scalar sunset approximation is shown in Fig. 4.3, and compared to the tree-level and CW potentials for a choice of parameters. We also examine closely the two minima in Fig. 4.4. At the true minimum, $v_R \approx -450\,\text{GeV}$ and at which have performed the renormalisation to define m_0, the 2PI effective potential drives the potential slightly deeper. At the secondary minimum, $\phi \approx 170\,\text{GeV}$, we see that the 2PI effective potential pushes this minimum slightly away from the tree-level minimum and drives the potential deeper here as well.

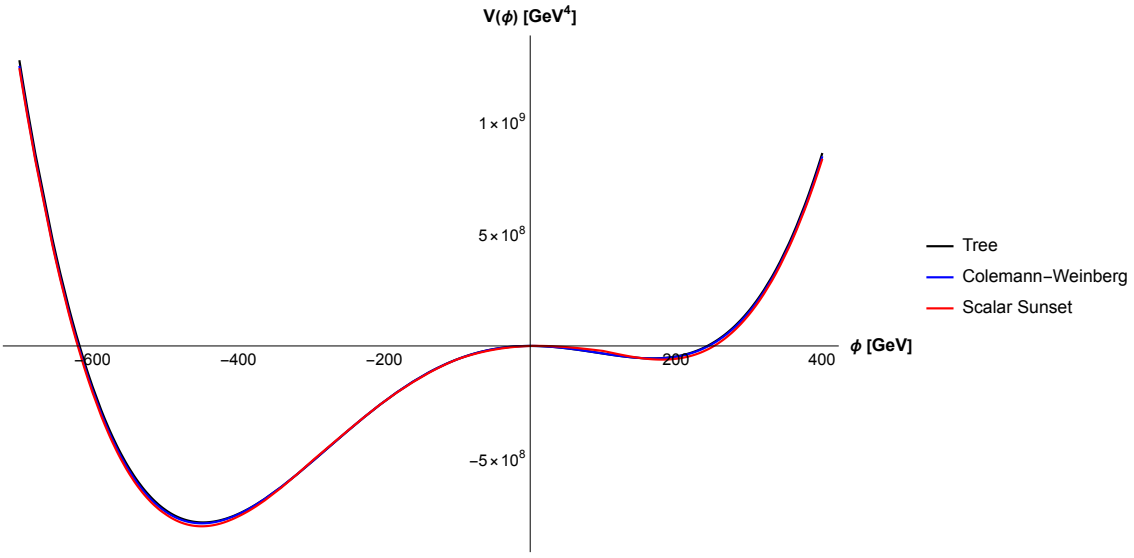

Figure 4.3: The 2PI effective potential in the scalar sunset approximation (red curve) against the field value, with the tree-level potential (4.66) (black curve) and Coleman-Weinberg potential from (4.66) (blue curve) for comparison. The parameters are $\lambda_R = 0.8$, $\alpha_R = 75\,\text{GeV}$ and $|m_R|=$ $100\,\text{GeV}$. We have set the auxiliary mass parameter $m_0 = 271.36\,\text{GeV}$. We find the true minimum of the 2PI effective potential at $v_R \approx -450\,\text{GeV}$. All relevant integrals were calculated with a cutoff of 10^5 GeV.

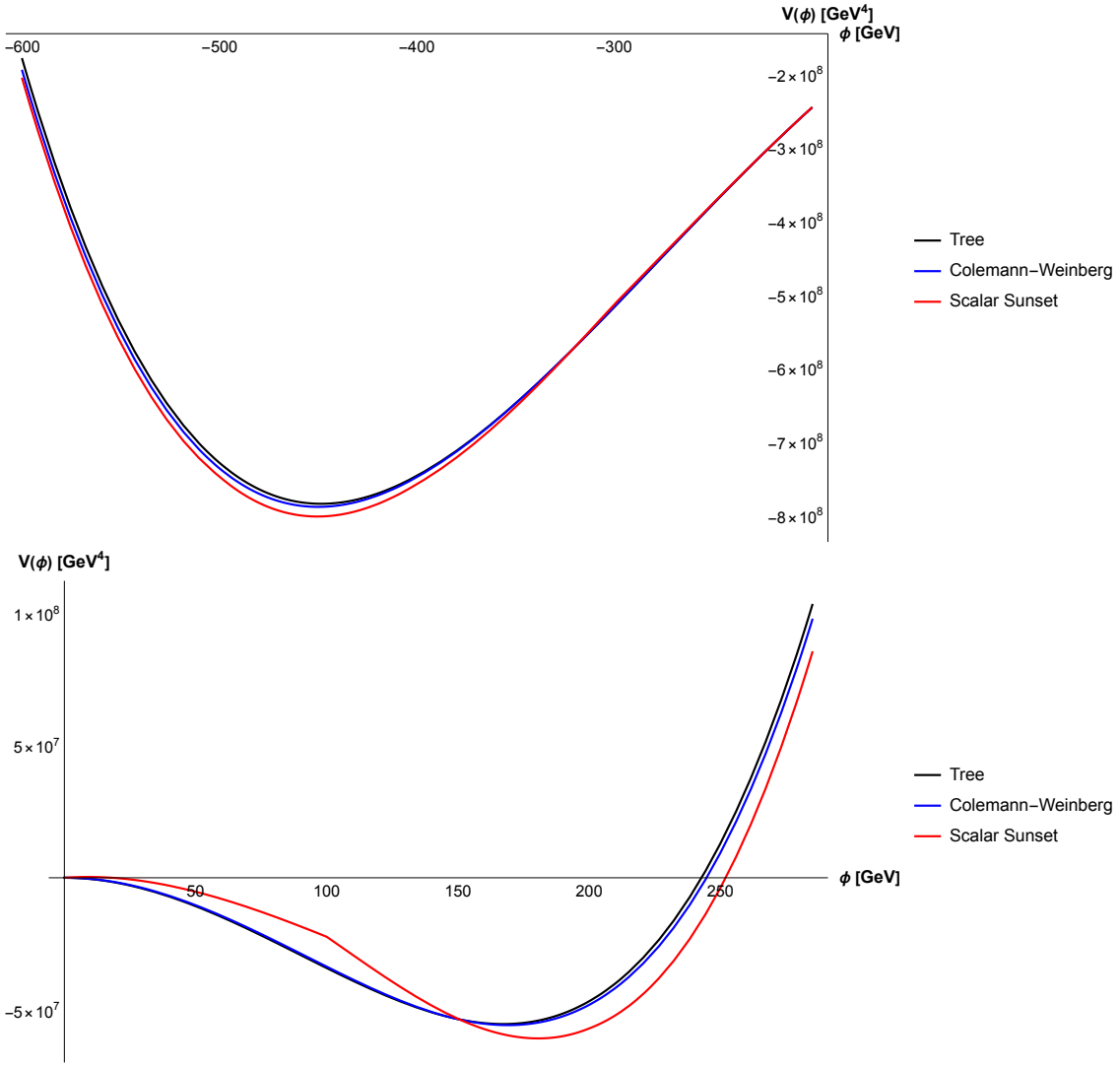

Figure 4.4: Top: A zoomed-in view of Fig. 4.3 at the true minimum $v_R \approx -450\,\text{GeV}$. Bottom: A zoomed-in view of Fig. 4.3 at the secondary minimum $v_R \approx -450\,\text{GeV}$. Curves are coloured as in Fig. 4.3, with the same choice of parameters.

In Fig. 4.5, we set $\alpha_R = 0$, meaning we only retain the scalar sunset diagram in the broken phase, with the effective trilinear coupling $\lambda_R\phi$. We compare this to our result in the Hartree approximation, (4.24) and find that this about only a 10% change. To gain more insight on this, we examine the various contributions to (4.65) in Fig. 4.6. We see that the sunset diagram, by order of magnitude, has the least contribution to the effective potential, and the Hartree diagram has the largest. This appears to be counterintuitive as both are two-loop diagrams; however, the Hartree contribution comes with the coupling $(\lambda_R + \delta\lambda_0) \approx \mathcal{O}(\epsilon)$. The finite pieces eventually obtained in (4.65) had terms free of loop factor suppressions of $16\pi^2$. In contrast, the sunset diagram does not come with such a coupling combination, and therefore feels the suppression of a two-loop diagram by $(16\pi^2)^2$. This reasoning is also somewhat enforced by the fact that the $\text{Tr}\log G_R$, contribution is about an order of magnitude larger, being essentially "one-loop".

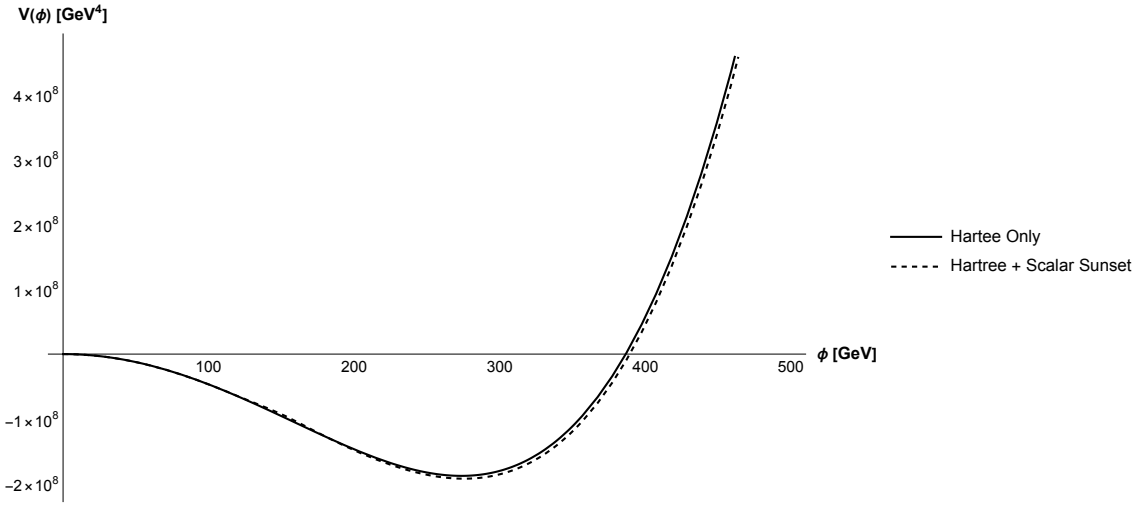

Figure 4.5: Comparisons between 2PI effective potential within the Hartree approximation (solid, black line) and including the sunset diagram (dashed, black line) with coupling $\lambda_R^2\phi^2$. The parameters are $\alpha_R = 0$, $\lambda_R = 0.8$ and $|m_R| = 100\,\text{GeV}$, leading to $v_R \approx 274\,\text{GeV}$. We have accordingly set $m_0 = 200\,\text{GeV}$.

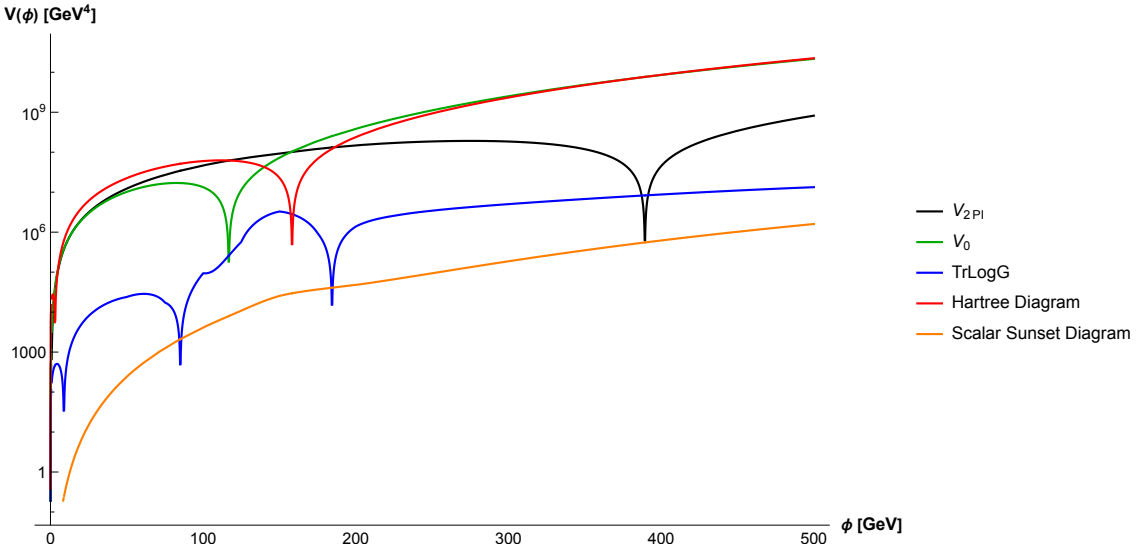

Figure 4.6: The various contributions to the 2PI effective potential within the truncation till sunset diagram with coupling $\lambda_R^2\phi^2$. The parameters are $\lambda_R = 0.8$ and $|m_R| = 100\,\text{GeV}$, leading to $v_R \approx 274\,\text{GeV}$. We have accordingly set $m_0 = 200\,\text{GeV}$. Note that what is shown is the absolute value of the contributions, in this logarithmic plot.

As a final check, we examine the cutoff dependence of the effective potential, arising from our numeric evaluation the various loop integrals. Fig. 4.7 shows that this effect is at most $\mathcal{O}(10^{-5})$ from choosing a cutoff even two orders of magnitude higher. We conclude that the 2PI effective potential is hence cutoff independent, as it should be, in our numeric implementation.

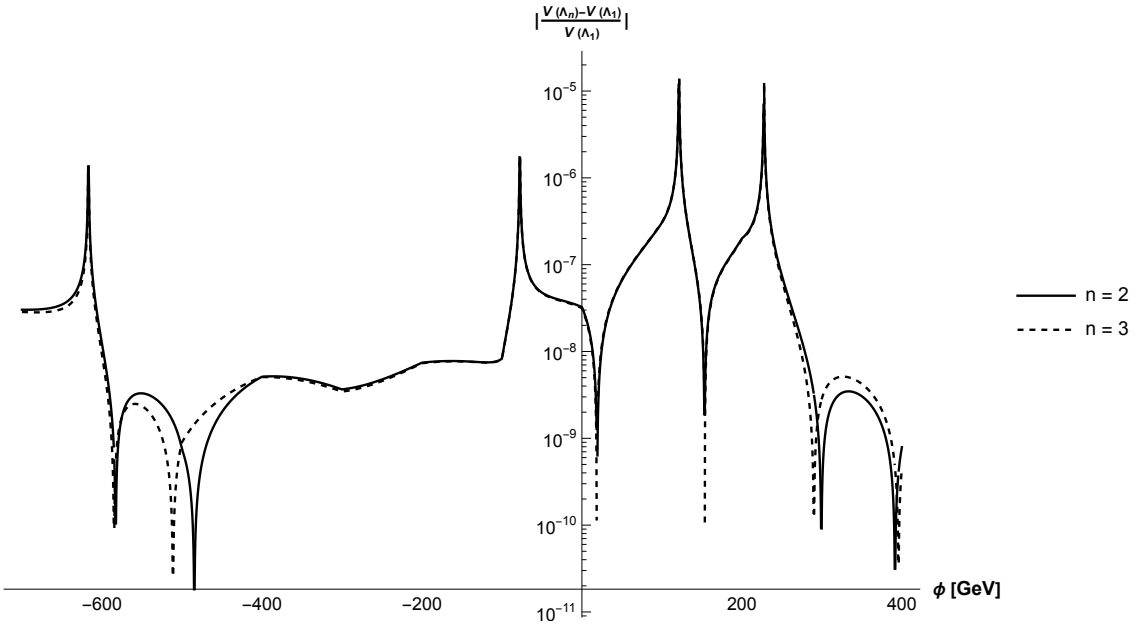

Figure 4.7: The relative difference between the 2PI effective potential evaluated with UV cutoff $\Lambda_1 = 10^5\,\text{GeV}$ and $\Lambda_2 = 10^6\,\text{GeV}$ (solid, black line) and $\Lambda_3 = 10^7\,\text{GeV}$ (dashed, black line). The parameters are $\lambda_R = 0.8$, $\alpha_R = 75\,\text{GeV}$ and $|m_R| = 100\,\text{GeV}$. We have set the auxiliary mass parameter $m_0 = 271.36\,\text{GeV}$.

4.3 Fermionic Sunset Approximation

As seen in the previous chapter, there are now two gap equations, one each for the scalar and fermionic propagators. We set here $M_R = 0$, so that the fermions acquire a mass at non-zero ϕ, via the Yukawa coupling. This is similar to the Standard Model (SM), where the SM fermions acquire masses when the Higgs gains a VEV. This assumption also allows us to set $\alpha_R = 0$, so our theory has three parameters: the quartic coupling λ, the Yukawa coupling g and the scalar mass m. We have thus the following field and momentum dependent masses from (3.121) and (3.122)

$$\begin{aligned} M^2(\phi;p) &= m_R^2 + \delta m_0^2 + \frac{(\lambda_R+\delta\lambda_2)}{2}\phi^2 + \frac{\lambda_R+\delta\lambda_0}{2}\int_q G_R(q) \\ &\quad - \frac{i\lambda_R^2\phi^2}{2}\int_q G_R(p+q)G_R(q) + ig_R^2\int_q \text{tr}\left[D_R(p+q)D_R(q)\right] - p^2\delta Z_{\phi,0} \\ &\equiv m^2(\phi) + \Pi_a(p;\phi) + \Pi_2(p;\phi) \end{aligned} \tag{4.68}$$

$$\begin{aligned} M_\psi(\phi;p) &= \mathbb{I}_4(g_R+\delta g_1)\phi + ig_R^2\int_q D_R(p+q)G_R(q) - \not{p}\delta Z_{\psi,0} \\ &= \mathbb{I}_4 m_\psi(\phi) + \Sigma_a(p;\phi) + \Sigma_2(p;\phi) \end{aligned} \tag{4.69}$$

where we have already set $\delta\lambda_1 = \delta g_0 = 0$, as these are finite renormalisations, as mentioned in Chapter 3. The situation is now complicated by the fact that the wave function renormalisations for both the fermionic and scalar propagators are not finite, as noted in

(3.123) and (3.125), which have led us to the parameterisations for (4.68) and (4.69). The self-energy pieces behave as

$$\lim_{|p|\to\infty} \frac{\Pi_a(p;\phi)}{p^2} \sim \log p, \quad \lim_{|p|\to\infty} \frac{\Pi_2(p;\phi)}{p^2} \longrightarrow 0\,,$$
$$\lim_{|p|\to\infty} \frac{\Sigma_a(p;\phi)}{\not{p}} \sim \log p, \quad \lim_{|p|\to\infty} \frac{\Sigma_2(p;\phi)}{\not{p}} \longrightarrow 0\,,$$

which is a feature we noted in (3.121) and (3.122). This implies that an expansion of the form (4.30) for the scalar propagator (and correspondingly, for the fermionic propagator) is not appropriate as the series would not converge. This can be illustrated as follows: we would obtain using

$$G_a(p) = \frac{i}{p^2 - m_0^2}\,,$$

the following expansion

$$\begin{aligned} G_R(p) &= G_a(p) - iG_a(p)\left[m^2(\phi) - m_0^2 + \Pi_a(p;\phi) + \Pi_2(p;\phi)\right] G_R(p) \\ &= G_a(p) - iG_a(p)\Pi_a(p;\phi)G_R(p) - iG_a(p)\left[m^2(\phi) - m_0^2 + \Pi_2(p;\phi)\right] G_R(p)\,, \end{aligned}$$

and as $\Pi_a(p) \sim p^2 \log\left(p^2\right)$, the second term in the second line is of the same order as the first term in the same line. This would persist (as we iterate G_R further) and hence this is not a convergent expansion. The way out would be to now define the auxiliary propagators in the following form,

$$iG_a^{-1}(p) = p^2 - m_0^2 - \Pi_a(p;\phi)\,, \qquad iD_a^{-1}(p) = \not{p} - M_0 - \Sigma_a(p;\phi)\,, \tag{4.70}$$

where we have introduced a auxiliary mass M_0 for the auxiliary fermionic propagator, $D_a(p)$. We would, in the same vein as for the auxiliary scalar mass m_0, choose it to be the fermionic mass at the VEV. Equation (4.70) ensures now that the expansions of the renormalised propagators about these auxiliary ones would converge, as we would now obtain

$$G_R(p) = G_a(p) - iG_a(p)\left[m^2(\phi) - m_0^2 + \Pi_2(p;\phi)\right] G_R(p)\,, \tag{4.71}$$

$$D_R(p) = D_a(p) - iD_a(p)\left[m_\psi(\phi) - M_0 + \Sigma_2(p;\phi)\right] D_R(p)\,. \tag{4.72}$$

There is a caveat: identification of the divergent parts of the various loop integrals over these auxiliary propagators is no longer straightforward. Essentially, we cannot use the usual results of dimensional regularisation like in the scalar sunset approximation, as the divergences are not simply given in the form of ϵ^{-n} poles. Consequently, we cannot also separate out the finite pieces from these loop integrals and this proves to be a major hurdle in calculating the effective potential. Nevertheless, it is possible indeed to obtain equations similar to (4.39)–(4.42) and (4.50)–(4.53) for the various counterterms, but the technical challenge now lies in obtaining solutions to these. Thus, in the following, we outline the method to extract the divergences from the various loop integrals to obtain the cancellation conditions to determine the counterterms.

Fermionic Propagator

Beginning with the fermionic propagator, we first examine the relevant loop integral

$$\begin{aligned} i\int_q D_R(q+p)G_R(q) &= i\int_q D_a(p+q)G_a(q)\Big|_{\text{div.}} \\ &+ \int_q G_a(q)D_a(p+q)\left[m_\psi(\phi) - M_0 + \Sigma_{2,a}(p+q;\phi)\right]D_a(p+q)\Big|_{\text{div.}} \\ &+ \not{p}X_{\text{fin.}}(p) + \mathbb{I}_4 Y_{\text{fin.}}(p)\,, \end{aligned} \tag{4.73}$$

where we have used (4.71) and (4.72) to identify the various divergent loop integrals. Note that $\Sigma_{2,a}$ refers to the fermionic self-energy Σ_2 but calculated with auxiliary propagators. The wave function renormalisation is determined from the following condition

$$i\frac{\partial D_R^{-1}(p)}{\partial \not{p}}\Big|_{\not{p}=0,\,\phi=v_R} = 1 \quad \Longrightarrow \quad \delta Z_{\psi,0} = ig_R^2\left\{\left[\frac{\partial}{\partial \not{p}}\int_q D_R(q+p)G_R(q)\right]\Big|_{\not{p}=0,\,\phi=v_R}\right\}\Big|_{\text{div.}}, \tag{4.74}$$

and we can use this to remove the momentum dependent divergent part (proportional to $\not{p}$) of this loop integral. We can substitute now

$$\begin{aligned} i\int_q D_R(q+p)G_R(q) - \frac{\not{p}}{g_R^2}\delta Z_{\psi,0} &= i\int_q D_a(q)G_a(q)\Big|_{\text{div.}} \\ &+ \int_q G_a(q)D_a(q)\left[m_\psi(\phi) - M_0 + \Sigma_{2,a}(q;\phi)\right]D_a(q)\Big|_{\text{div.}} + \not{p}X_{\text{fin.}}(p;\phi) + \mathbb{I}_4 Y_{\text{fin.}}(p;\phi)\,, \end{aligned} \tag{4.75}$$

and examine (4.69)

$$\begin{aligned} M_\psi(\phi;p) &= \mathbb{I}_4 g_R\phi + g_R^2\left[\not{p}X_{\text{fin.}}(p) + \mathbb{I}_4 Y_{\text{fin.}}(p)\right] \\ &+ \delta g_1\phi + ig_R^2\int_q D_a(q)G_a(q)\Big|_{\text{div.}} + g_R^2\int_q G_a(q)D_a(q)\left[m_\psi(\phi) - M_0 + \Sigma_2(q;\phi)\right]D_a(q)\Big|_{\text{div.}}. \end{aligned} \tag{4.76}$$

This allows us to identify the following finite quantities,

$$m_\psi(\phi) = g_R\phi\,, \quad \Sigma_a(p;\phi) = g_R^2\not{p}X_{\text{fin.}}(p;\phi)\,, \quad \Sigma_{2,a}(p;\phi) = g_R^2\,\mathbb{I}_4 Y_{\text{fin.}}(p;\phi) \tag{4.77}$$

and gives the last line of (4.76) gives the cancellation condition for the counterterm δg_1. It may appear, *a priori*, that this counterterm would be field dependent, and would depend on the auxiliary parameter M_0, which would make our renormalisation procedure inconsistent, but we will demonstrate later, using the first iteration of the propagators, that this is not the case.

Scalar Propagator

For the scalar propagator, the integrals involving only scalar propagators are resolved in a similar manner as in the scalar sunset approximation. The easiest is the loop integral over two propagators

$$\mathcal{I} = i\int_q G_R(p+q)G_R(q) = i\int_q G_a^2(q)\Big|_{\text{div.}} + \mathcal{I}_{\text{fin.}}(p^2) \tag{4.78}$$

where we mention again, for clarity, the auxiliary propagators defined in (4.70) from now onward, which means we cannot use the results of Appendix B to extract the divergent pieces. The integral over a single scalar propagator has the form

$$\begin{aligned}\mathcal{T} &= \int_q G_R(q) \\ &= \int_q G_a(q)\Big|_{\text{div.}} - \left[m^2(\phi) - m_0^2\right] i\int_q G_a^2(q)\Big|_{\text{div.}} - i\int_q G_a^2(q)\Pi_{2,a}(q^2)\Big|_{\text{div.}} + \mathcal{T}_{\text{fin.}}\,, \end{aligned} \tag{4.79}$$

where $\Pi_{2,a}$ refers to the scalar self-energy Π_2 but calculated with auxiliary propagators. Finally, we have the integral over the trace of two fermionic propagators,

$$\begin{aligned} i\int_q \text{tr}\left[D_R(q+p)D_R(q)\right] &= i\int_q \text{tr}\left[D_a(q+p)D_a(q)\right]\Big|_{\text{div.}} \\ &+ \int_q \text{tr}\left\{D_a(p+q)D_a(q)\left[m_\psi(\phi) - M_0 + \Sigma_{2,a}(q;\phi)\right]D_a(q)\right\}\Big|_{\text{div.}} \\ &- i\int_q \text{tr}\Big\{D_a(p+q)D_a(q)\left[m_\psi(\phi) - M_0 + \Sigma_{2,a}(q;\phi)\right] \\ &\qquad D_a(q)\left[m_\psi(\phi) - M_0 + \Sigma_{2,a}(q;\phi)\right]D_a(q)\Big\}\Big|_{\text{div.}} \\ &+ \int_q \text{tr}\left\{D_a(p+q)\left[m_\psi(\phi) - M_0 + \Sigma_{2,a}(p+q;\phi)\right]D_a(p+q)D_a(q)\right\}\Big|_{\text{div.}} \\ &- i\int_q \text{tr}\{D_a(p+q)\left[m_\psi(\phi) - M_0 + \Sigma_{2,a}(p+q;\phi)\right] \\ &\qquad D_a(p+q)\left[m_\psi(\phi) - M_0 + \Sigma_{2,a}(p+q;\phi)\right]D_a(p+q)D_a(q)\}\Big|_{\text{div.}} \\ &- i\int_q \text{tr}\Big\{D_a(p+q)\left[m_\psi(\phi) - M_0 + \Sigma_{2,a}(p+q;\phi)\right]D_a(p+q) \\ &\qquad D_a(q)\left[m_\psi(\phi) - M_0 + \Sigma_{2,a}(q;\phi)\right]D_a(q)\Big\}\Big|_{\text{div.}} \\ &+ p^2\mathcal{F}_{1,\text{fin.}}(p) + \mathcal{F}_{2,\text{fin.}}(p)\,. \end{aligned} \tag{4.80}$$

We determine the wave function renormalisation for the scalar,

$$\begin{aligned} &i\frac{\partial G_R^{-1}(p)}{\partial p^2}\Big|_{p^2=0,\,\phi=v_R} = 1 \\ &\implies \delta Z_{\phi,0} = ig_R^2\left\{\left[\frac{\partial}{\partial p^2}\int_q \text{tr}\left[D_R(q+p)D_R(q)\right]\right]\Big|_{p^2=0,\,\phi=v_R}\right\}\Big|_{\text{div.}}\,, \end{aligned} \tag{4.81}$$

where we note that this is divergent only due to the fermionic contribution. We use this, like for the fermionic propagator, to eliminate the momentum dependent divergent part (proportional here to p^2) of this loop integral

$$
\begin{aligned}
& i\int_q \mathrm{tr}\left[D_R(q+p)D_R(q)\right] - \frac{p^2}{g_R^2}\delta Z_{\phi,0} = \\
& i\int_q \mathrm{tr}\left[D_a^2(q)\right]\Big|_{\text{div.}} + 2\int_q \mathrm{tr}\left\{D_a^3(q)\left[m_\psi(\phi) - M_0 + \Sigma_{2,a}(q;\phi)\right]\right\}\Big|_{\text{div.}} \\
& \quad - 3i\int_q \mathrm{tr}\left\{D_a^4(q)\left[m_\psi(\phi) - M_0 + \Sigma_{2,a}(q;\phi)\right]^2\right\}\Big|_{\text{div.}} + p^2\mathcal{F}_{1,\text{fin.}}(p^2) + \mathcal{F}_{2,\text{fin.}}(p^2)\,. \quad (4.82)
\end{aligned}
$$

We are now ready to examine (4.68) to identify the finite quantities and obtain the cancellation condition,

$$
\begin{aligned}
& M^2(\phi;p) = m_R^2 + \frac{\lambda_R}{2}\phi^2 + \frac{\lambda_R}{2}\mathcal{T}_{\text{fin.}} - \frac{\lambda_R^2\phi^2}{2}\mathcal{I}_{\text{fin.}}(p^2) + g_R^2\left[p^2\mathcal{F}_{1,\text{fin.}}(p^2) + \mathcal{F}_{2,\text{fin.}}(p^2)\right] \\
& \delta m_0^2 + \frac{\delta\lambda_2}{2}\phi^2 + \frac{\delta\lambda_0}{2}\mathcal{T}_{\text{fin.}} + \frac{\lambda_R+\delta\lambda_0}{2}\Bigg\{\int_q G_a(q)\Big|_{\text{div.}} - \left[m^2(\phi) - m_0^2\right]\, i\int_q G_a^2(q)\Big|_{\text{div.}} \\
& - i\int_q G_a^2(q)\Pi_{2,a}(q^2)\Big|_{\text{div.}}\Bigg\} - \frac{\lambda_R^2\phi^2}{2}\left\{i\int_q G_a^2(q)\right\}\Big|_{\text{div.}} \\
& + g_R^2\Bigg\{i\int_q \mathrm{tr}\left[D_a^2(q)\right]\Big|_{\text{div.}} + 2\int_q \mathrm{tr}\left\{D_a^3(q)\left[m_\psi(\phi) - M_0 + \Sigma_{2,a}(q;\phi)\right]\right\}\Big|_{\text{div.}} \\
& - 3i\int_q \mathrm{tr}\left\{D_a^4(q)\left[m_\psi(\phi) - M_0 + \Sigma_{2,a}(q;\phi)\right]^2\right\}\Big|_{\text{div.}}\Bigg\} \quad (4.83)
\end{aligned}
$$

The first line gives us the following finite quantities

$$
m^2(\phi) = m_R^2 + \frac{\lambda_R}{2}\phi^2 + \frac{\lambda_R}{2}\mathcal{T}_{\text{fin.}} \quad (4.84)
$$

$$
\Pi_a(p;\phi) = g_R^2\, p^2\mathcal{F}_{1,\text{fin.}}(p^2;\phi)\,, \quad \Pi_2(p^2;\phi) = -\frac{\lambda_R^2\phi^2}{2}\mathcal{I}_{\text{fin.}}(p^2) + g_R^2\,\mathcal{F}_{2,\text{fin.}}(p^2;\phi) \quad (4.85)
$$

and the last line of (4.83) gives the cancellation condition for the counterterms when equated to zero.

Minimisation Condition

The minimisation condition with fermions is given by (3.139). With $\alpha_R = 0$ and $M_R = 0$ (implying that $\delta t_1 = 0$), we have

$$
\begin{aligned}
& -(m_R^2 + \delta m_2^2)v_R - \frac{\lambda_R + \delta\lambda_4}{6}v_R^3 \\
& \qquad - \frac{(\lambda_R+\delta\lambda_2)}{2}v_R\,\mathcal{T} + \frac{\lambda_R^2 v_R}{6}\,\mathcal{S} - (g_R + \delta g_1)\int_q \mathrm{tr}\left[D_R(q)\right] \stackrel{!}{=} 0\,, \quad (4.86)
\end{aligned}
$$

where we have the scalar sunset integral $\mathcal{S}$, which we decompose into its divergent and finite parts as in Sec. 4.2

$$
\begin{aligned}
\mathcal{S} &= i\int_q\int_k G_R(q)G_R(k)G_R(k+q) \\
&= \mathcal{S}_a\Big|_{\text{div.}} + 3\mathcal{T}_{\text{fin.}}\left\{i\int_q G_a^2(q)\right\}\Big|_{\text{div.}} \\
&\quad - 3\left(m^2(\phi)-m_0^2\right)\left[\left\{i\int_q G_a^2(q)\Big|_{\text{div.}}\right\}^2 + \left\{i\int_q G_a^2(q)\mathcal{I}_{a,\text{fin.}}(q^2)\right\}\Big|_{\text{div.}}\right] \\
&\quad - 3\Bigg[\left\{i\int_q G_a^2(q)\right\}\Big|_{\text{div.}}\left\{\int_k iG_a^2(k)\Pi_{2,a}(k^2)\right\}\Big|_{\text{div.}} \\
&\qquad + \left\{\int_k iG_a^2(k)\Pi_{2,a}(k^2)\mathcal{I}_{a,\text{fin.}}(k^2)\right\}\Big|_{\text{div.}}\Bigg] + \mathcal{S}_{\text{fin.}} \\
&\equiv \mathcal{S}_{\text{div.}} + \mathcal{S}_{\text{fin.}}\,. \qquad (4.87)
\end{aligned}
$$

We also have to treat the "fermionic tadpole integral"

$$
\begin{aligned}
\int_q \text{tr}\left[D_R(q)\right] &= \int_q \text{tr}\left[D_a(q)\right]\Big|_{\text{div.}} - i\int_q \text{tr}\left\{D_a^2(q)\left[m_\psi(\phi)-M_0+\Sigma_{2,a}(q;\phi)\right]\right\}\Big|_{\text{div.}} \\
&\quad - \int_q \text{tr}\left\{D_a^3(q)\left[m_\psi(\phi)-M_0+\Sigma_{2,a}(q;\phi)\right]^2\right\}\Big|_{\text{div.}} \\
&\quad + \int_q \text{tr}\left\{D_a^4(q)\left[m_\psi(\phi)-M_0+\Sigma_{2,a}(q;\phi)\right]^3\right\}\Big|_{\text{div.}} + \int_q \text{tr}\left[D_R(q)\right]\Big|_{\text{fin.}} \\
&\equiv \int_q \text{tr}\left[D_R(q)\right]\Big|_{\text{div.}} + \int_q \text{tr}\left[D_R(q)\right]\Big|_{\text{fin.}}\,. \qquad (4.88)
\end{aligned}
$$

Substituting this into (4.86), we obtain the following relation linking the various parameters and the VEV

$$
m_R^2 v_R + \frac{\lambda_R}{6}v_R^3 + \frac{\lambda_R}{2}v_R\,\mathcal{T}_{\text{fin.}} + g_R\int_q \text{tr}\left[D_R(q)\right]\Big|_{\text{fin.}} - \frac{\lambda_R^2 v_R}{6}\mathcal{S}_{\text{fin.}} \stackrel{!}{=} 0 \qquad (4.89)
$$

and the following cancellation condition to obtain the remaining counterterms

$$
\begin{aligned}
&-\delta m_2^2 v_R - \frac{\delta\lambda_4}{6}v_R^3 + \frac{\delta\lambda_2}{2}v_R\,\mathcal{T}_{\text{fin.}} - \frac{(\lambda_R+\delta\lambda_2)}{2}v_R\,\mathcal{T}_{\text{div.}} + \frac{\lambda_R^2 v_R}{6}\,\mathcal{S}_{\text{div.}} \\
&\qquad - (g_R+\delta g_1)\int_q \text{tr}\left[D_R(q)\right]\Big|_{\text{div.}} - \delta g_1\int_q \text{tr}\left[D_R(q)\right]\Big|_{\text{fin.}} \stackrel{!}{=} 0 \qquad (4.90)
\end{aligned}
$$

We would now like to understand how various contributions feed into the counterterms. To this end, it is instructive to consider our iterative approach.

Iterating the Gap Equations

Beginning with the free propagators,

$$
G_R^{(0)}(p) = \frac{i}{p^2-m^2(\phi)}\,, \quad G_a^{(0)}(p) = \frac{i}{p^2-m_0^2}\,, \qquad (4.91)
$$

$$D_R^{(0)}(p) = \frac{i}{\not{p} - m_\psi(\phi)}\,, \quad D_a^{(0)}(p) = \frac{i}{\not{p} - M_0}\,, \tag{4.92}$$

we can evaluate the relevant integrals using dim. reg.

$$\begin{aligned} i\int_q D_R^{(0)}(q+p)G_R^{(0)}(q) = \not{p}\left[\frac{B_1(p^2, m_{(0)}^2(\phi), m_\psi^2(\phi)) + B_0(p^2, m_{(0)}^2(\phi), m_\psi^2(\phi))}{16\pi^2}\right] \\ + \mathbb{I}_4 m_\psi(\phi)\left[\frac{B_0(p^2, m_{(0)}^2(\phi), m_\psi^2(\phi))}{16\pi^2}\right] \end{aligned} \tag{4.93}$$

$$\int_q G_R^{(0)}(q) \;=\; \frac{A_0(m_{(0)}^2(\phi))}{16\pi^2} \tag{4.94}$$

$$i\int_q G_R^{(0)}(q+p)G_R^{(0)}(q) \;=\; \frac{B_0(p^2, m_{(0)}^2(\phi), m_{(0)}^2(\phi))}{16\pi^2} \tag{4.95}$$

$$\begin{aligned} i\int_q \mathrm{tr}\left[D_R^{(0)}(q+p)D_R^{(0)}(q)\right] = -2p^2\left[\frac{B_0(p^2, m_\psi^2(\phi), m_\psi^2(\phi))}{16\pi^2}\right] \\ + 4m_\psi^2(\phi)\left[\frac{B_0(p^2, m_\psi^2(\phi), m_\psi^2(\phi))}{16\pi^2}\right] + 4\frac{A_0(m_\psi^2(\phi))}{16\pi^2} \end{aligned} \tag{4.96}$$

which gives us the following wave function counterterms

$$\begin{aligned} \delta Z_{\psi,0}^{(0)} &= g_R^2\left\{\frac{\partial}{\partial\not{p}}\left[i\int_q D_R^{(0)}(q+p)G_R^{(0)}(q)\right]\Big|_{\not{p}=0,\phi=v_R}\right\}\Big|_{\text{div.}} \\ &= \left[\frac{B_1(0, m_0^2, M_0^2) + B_0(0, m_0^2, M_0^2)}{16\pi^2}\right]\Big|_{\text{div.}} = \frac{1}{2}\frac{g_R^2}{16\pi^2\epsilon}\,. \end{aligned} \tag{4.97}$$

$$\begin{aligned} \delta Z_{\phi,0}^{(0)} &= g_R^2\left\{\frac{\partial}{\partial p^2}\left[i\int_q \mathrm{tr}\left[D_R^{(0)}(q+p)G_R^{(0)}(q)\right]\right]\Big|_{\not{p}=0,\phi=v_R}\right\}\Big|_{\text{div.}} \\ &= -2\left[\frac{B_0(0, M_0^2, M_0^2)}{16\pi^2}\right]\Big|_{\text{div.}} = -2\,\frac{g_R^2}{16\pi^2\epsilon}\,. \end{aligned} \tag{4.98}$$

Note that we have used $m^2(v_R) = m_0^2$ and $m_\psi(v_R) = M_0$.

Examining the various cancellation conditions, we see for the counterterm $\delta g_1^{(0)}$ we obtain

$$\begin{aligned} &\delta g_1^{(0)}\phi + ig_R^2\int_q D_a^{(0)}(q)G_a^{(0)}(q)\Big|_{\text{div.}} + g_R^2\,[m_\psi(\phi) - M_0]\int_q G_a^{(0)}(q)(D_a^{(0)}(q))^2\Big|_{\text{div.}} \\ &= \phi\left[\delta g_1^{(0)} + g_R^3\int_q \frac{-i(\not{q} + M_0)^2}{(q^2 - m_0^2)(q^2 - M_0^2)^2}\Big|_{\text{div.}}\right] \end{aligned}$$

$$
\begin{aligned}
&- ig_R^2 \left[\int_q \frac{\not{q} + M_0}{(q^2 - m_0^2)(q^2 - M_0^2)} \bigg|_{\text{div.}} - M_0 \int_q \frac{(\not{q} + M_0)^2}{(q^2 - m_0^2)(q^2 - M_0^2)^2} \bigg|_{\text{div.}} \right] \\
&= \phi \left[\delta g_1^{(0)} - ig_R^3 \int_q \frac{q^2}{(q^2 - m_0^2)(q^2 - M_0^2)^2} \bigg|_{\text{div.}} \right] \\
&\quad - ig_R^2 \left[\int_q \frac{M_0}{(q^2 - m_0^2)(q^2 - M_0^2)} \bigg|_{\text{div.}} - M_0 \int_q \frac{q^2}{(q^2 - m_0^2)(q^2 - M_0^2)^2} \bigg|_{\text{div.}} \right] \\
&= \phi \left[\delta g_1^{(0)} - ig_R^3 \int_q \frac{1}{(q^2 - m_0^2)(q^2 - M_0^2)^2} \bigg|_{\text{div.}} \right] \\
&\quad - ig_R^2 M_0 \left[\cancel{\int_q \frac{1}{(q^2 - m_0^2)(q^2 - M_0^2)} \bigg|_{\text{div.}}} - \cancel{\int_q \frac{1}{(q^2 - m_0^2)(q^2 - M_0^2)} \bigg|_{\text{div.}}} \right] \stackrel{!}{=} 0 \,, \qquad (4.99)
\end{aligned}
$$

where, along the way, we have used

$$(\not{q} + M_0)^2 = \not{q}\not{q} + 2M_0\not{q} + \mathbb{I}_4 M_0^2 = \mathbb{I}_4 q^2 + 2M_0\not{q} + \mathbb{I}_4 M_0^2$$

and the integrals with $\not{q}$ in the numerator vanish as the denominators of (4.99) are symmetric under $q \to -q$. The finite parts of the loop integrals then give the self-energy functions at the first iteration

$$
\begin{aligned}
&\Sigma_a^{(1)}(p) = \\
&\not{p}\, g_R^2 \Bigg\{ \frac{B_1(p^2, m_{(0)}^2(\phi), m_\psi^2(\phi)) - B_1(0, m_0^2, M_0^2)}{16\pi^2} \\
&\qquad + \frac{B_0(p^2, m_{(0)}^2(\phi), m_\psi^2(\phi)) - B_0(0, m_0^2, M_0^2)}{16\pi^2} \Bigg\} \,, \qquad (4.100)
\end{aligned}
$$

$$
\Sigma_2^{(1)}(p) = g_R^2\, m_\psi(\phi) \left\{ \frac{B_0(p^2, m_{(0)}^2(\phi), m_\psi^2(\phi)) - B_0(0, m_0^2, M_0^2)}{16\pi^2} \right\} . \qquad (4.101)
$$

Notice that Σ_2 is proportional to the ($\phi-$dependent) fermion mass, which is as expected from usual QFT [2, 3].

Let us now look at the cancellation conditions arising from the scalar gap equation

$$
\frac{\delta\lambda_0^{(0)}}{2} + \frac{\lambda_R + \delta\lambda_0^{(0)}}{2} \left(-\frac{\lambda_R}{32\pi^2\epsilon} \right) = 0 \,, \qquad (4.102)
$$

$$
\frac{\delta\lambda_2^{(0)}}{2} + \frac{\lambda_R + \delta\lambda_0^{(0)}}{2} \left(-\frac{\lambda_R}{32\pi^2\epsilon} \right) + \frac{\lambda_R^2}{32\pi^2\epsilon} + \frac{12 g_R^4}{16\pi^2\epsilon} = 0 \,, \qquad (4.103)
$$

$$
(\delta m_0^2)^{(0)} + \frac{\lambda_R + \delta\lambda_0^{(0)}}{2} \left(-\frac{m_R^2}{16\pi^2\epsilon} \right) = 0 \,. \qquad (4.104)
$$

Notice how $\delta\lambda_0$ is essentially equivalent to its value in the Hartree approximation, c.f. (4.9). It is $\delta\lambda_2$ that takes on a fermionic contribution which is proportional to g_R^4; this corresponds to the fermion box diagram that contributes to the quartic coupling. From

the finite parts of the loop integral, we obtain the scalar self-energy functions

$$\mathcal{I}^{(1)}_{\text{fin.}}(p^2) = \left\{ \frac{B_0(p^2, m^2_{(0)}(\phi), m^2_{(0)}(\phi)) - B_0(0, m_0^2, m_0^2)}{16\pi^2} \right\}, \tag{4.105}$$

$$\mathcal{F}^{(1)}_{1,\text{fin.}}(p^2;\phi) = -2 \left\{ \frac{B_0(p^2, m^2_{\psi}(\phi), m^2_{\psi}(\phi)) - B_0(0, M_0^2, M_0^2)}{16\pi^2} \right\}, \tag{4.106}$$

$$\begin{aligned}\mathcal{F}^{(1)}_{2,\text{fin.}}(p^2;\phi) = 8m^2_{\psi}(\phi) &\left\{ \frac{B_0(p^2, m^2_{\psi}(\phi), m^2_{\psi}(\phi)) - B_0(0, M_0^2, M_0^2)}{16\pi^2} \right\} \\ &- 4 \left\{ \frac{A_0(m^2_{\psi}(\phi)) - A_0(M_0^2) + \left[m^2_{\psi}(\phi) - M_0^2\right] B_0(0, M_0^2, M_0^2)}{16\pi^2} \right\},\end{aligned} \tag{4.107}$$

where we see the function $\mathcal{F}_2$ is proportional to the (ϕ-dependent) fermionic mass squared.

To properly consider the 2PI formalism, one needs to include the self-energy, which why we skip examination of the minimisation condition with "free" propagators (4.91) and (4.92). Having calculated the self-energy functions, at the first iteration, the propagators are now given by

$$G^{(1)}_R(p) = \frac{i}{p^2 - \left[m^2(\phi) + \Pi^{(1)}_a(p) + \Pi^{(1)}_2(p)\right]}, \quad G^{(0)}_a(p) = \frac{i}{p^2 - m_0^2 - \Pi^{(1)}_a(p)}, \tag{4.108}$$

$$D^{(1)}_R(p) = \frac{i}{\not{p} - \left[m_{\psi}(\phi) + \Sigma^{(1)}_a(p) + \Sigma^{(1)}_2(p)\right]}, \quad D^{(0)}_a(p) = \frac{i}{\not{p} - M_0 - \Sigma^{(1)}_a(p)}. \tag{4.109}$$

which we will use to demonstrate the technical challenges in solving for the counterterms and evaluating the effective potential.

Re-examining the various cancellation conditions, we now have

$$\delta g^{(1)}_1 - g^3_R \left\{ \int_q G^{(1)}_a(q)(D^{(1)}_a(q))^2 \left[1 + \left(\frac{B_0(q^2, m_0^2, M_0^2) - B_0(0, m_0^2, M_0^2)}{16\pi^2} \right)\right]\right\} \Big|_{\text{div.}} = 0 \tag{4.110}$$

$$\frac{\delta\lambda^{(1)}_0}{2} + \frac{\lambda_R + \delta\lambda^{(1)}_0}{2} \left[-\frac{\lambda_R}{2} \int_q i(G^{(1)}_a(q))^2 \right] \Big|_{\text{div.}} = 0, \tag{4.111}$$

$$\begin{aligned}&\frac{\delta\lambda^{(1)}_2}{2} + \frac{\lambda_R + \delta\lambda^{(1)}_0}{2} \Bigg\{ - \left[\frac{\lambda_R}{2} \int_q i(G^{(1)}_a(q))^2 \right] \Big|_{\text{div.}} \\ &+ \int_q i(G^{(1)}_a(q))^2 \left[\frac{\lambda_R^2}{2} \frac{B_0(q^2, m_0^2, m_0^2) - B_0(0, m_0^2, m_0^2)}{16\pi^2} \right. \\ &\left. - 8g^4_R \frac{B_0(q^2, M_0^2, M_0^2) - B_0(0, M_0^2, M_0^2)}{16\pi^2} \right] \Big|_{\text{div.}} \Bigg\} - \frac{\lambda_R^2}{2} \int_q i(G^{(1)}_a(q))^2 \Big|_{\text{div.}}\end{aligned}$$

$$-3g_R^4\int_q \mathrm{tr}\left\{(D_a^{(1)}(q))^4\left[1+g_R^4\left(\frac{B_0(q^2,m_0^2,M_0^2)-B_0(0,m_0^2,M_0^2)}{16\pi^2}\right)^2\right]\right\}\Big|_{\text{div.}}=0\,, \tag{4.112}$$

$$(\delta m_0^2)^{(1)}+\frac{\lambda_R+\delta\lambda_0^{(1)}}{2}\left[\int_q G_a^{(1)}(q)\Big|_{\text{div.}}-(m_R^2-m_0^2)\int_q i(G_a^{(1)}(q))^2\Big|_{\text{div.}}\right]=0\,. \tag{4.113}$$

From the minimisation condition we obtain,

$$\begin{aligned}
&(\delta m_2^2)^{(1)}+\frac{\lambda_R+\delta\lambda_2^{(1)}}{2}\left[\int_q G_a^{(1)}(q)\Big|_{\text{div.}}-(m_R^2-m_0^2)\int_q i(G_a^{(1)}(q))^2\Big|_{\text{div.}}\right]\\
&\quad-\frac{\lambda_R^2}{6}\Bigg\{S_a\Big|_{\text{div.}}-3\left(m_R^2-m_0^2\right)\left[\left(\int_q i(G_a^{(1)}(q))^2\Big|_{\text{div.}}\right)^2\right.\\
&\quad\left.+\int_q i(G_a^{(1)}(q))^2\left(\frac{B_0(q^2,m_0^2,m_0^2)-B_0(0,m_0^2,m_0^2)}{16\pi^2}\right)\Big|_{\text{div.}}\right]\Bigg\}=0\,,
\end{aligned} \tag{4.114}$$

$$\begin{aligned}
&\frac{\delta\lambda_4^{(1)}}{6}+\frac{\lambda_R+\delta\lambda_2^{(1)}}{2}\Bigg\{-\left[\frac{\lambda_R}{2}\int_q i(G_a^{(1)}(q))^2\right]\Big|_{\text{div.}}\\
&+\int_q i(G_a^{(1)}(q))^2\left[\frac{\lambda_R^2}{2}\frac{B_0(q^2,m_0^2,m_0^2)-B_0(0,m_0^2,m_0^2)}{16\pi^2}\right.\\
&\qquad\left.-8g_R^4\frac{B_0(q^2,M_0^2,M_0^2)-B_0(0,M_0^2,M_0^2)}{16\pi^2}\right]\Big|_{\text{div.}}\Bigg\}\\
&-\frac{\lambda_R^2}{6}\Bigg\{-3\frac{\lambda_R}{2}\left[\left(\int_q i(G_a^{(1)}(q))^2\Big|_{\text{div.}}\right)^2\right.\\
&\qquad\left.+\int_q i(G_a^{(1)}(q))^2\left(\frac{B_0(q^2,m_0^2,m_0^2)-B_0(0,m_0^2,m_0^2)}{16\pi^2}\right)\Big|_{\text{div.}}\right]\\
&-3\left[\left(\int_q i(G_a^{(1)}(q))^2\right)^2\left(\frac{B_0(q^2,m_0^2,m_0^2)-B_0(0,m_0^2,m_0^2)}{16\pi^2}\right)\right]\\
&\quad\left[\frac{\lambda_R^2}{2}\frac{B_0(q^2,m_0^2,m_0^2)-B_0(0,m_0^2,m_0^2)}{16\pi^2}\right.\\
&\qquad\left.-8g_R^4\frac{B_0(q^2,M_0^2,M_0^2)-B_0(0,M_0^2,M_0^2)}{16\pi^2}\right]\Bigg\}\Big|_{\text{div.}}=0\,.
\end{aligned} \tag{4.115}$$

The equations that have been obtained for the counterterms are entirely in terms of divergent parts of integrals over the auxiliary propagator, like in the scalar sunset approximation, but the difference lies in the fact that we no longer can evalaute the integrals analytically, making us unable to solve for the counterterms, such as in (4.50)–(4.53). Furthermore, we note that we cannot obtain the 2PI effective potential with the fermionic contribution, as in our approach, we would require also the finite pieces of the aforementioned integrals.

We reiterate that these problems arose due to requiring expansions of the renormalised propagators in the form (4.71) and (4.72), stemming from the fact that the auxiliary propagators need to to be defined as (4.70). We stress that this is because the fermionic sunset diagram in the 2PI effective action modifies the behaviour of the propagators in the UV. In fact, we note that we would have a similar scenario in the case of only scalars, once one includes the so-called basketball diagram [72] and postulate that this is a generic feature in any truncation of the 2PI formalism featuring an infinite wave-function renormalisation.

4.4 Summary

We re-examined the various truncations of the 2PI effective action introduced in the previous chapter by carrying out the renormalisation in the $\overline{\text{MS}}$ scheme. To this end, we presented an alternate method of obtaining the various resummed counterterms, based on [72], which did not rely on the Bethe-Salpeter equations and 2PI kernels introduced in the previous chapter. This was especially powerful when we considered the scalar sunset approximation, where we could circumvent the lengthier diagrammatic analysis and we were able to write down analytic expressions for the counterterms in terms of expansions in powers of ϵ in dim. reg. Consequently, in our analysis, we were able to keep track of finite quantities and eventually assemble the 2PI effective potential for the Hartree approximation and scalar sunset approximation. We emphasise that, to our knowledge, exact expressions for the counterterms and a determination of the 2PI improved effective potential in a transparent way for the scalar sunset approximation has not been reported in the literature. We observed that the 2PI induced corrections were not too large when compared to the tree-level potential; this is expected as we are working with a zero temperature field theory and loop effects have a tendency to dominate at higher temperatures. In fact, it has been reported in [60] that the Hartree approximation has the feature of generating a stronger phase transition in comparison to the Coleman-Weinberg (one-loop) potential. Thus, the next natural step would be to consider finite temperature in our analysis of the scalar sunset approximation. This would serve as an excellent tool to investigate models with additional scalars, useful in examining scenarios such as non-perturbative reheating after inflation and modifications to phase transitions.

We extended our techniques analysis in an analogous manner to examine the fermionic sunset approximation. However, we could only arrive at equations to obtain the counterterms in terms of loop integrals over the appropriately defined auxiliary propagators. The challenge lies in the fact that these integrals cannot be evaluated analytically, making it unable to piece together the effective potential. The determination of fermionic contribution to the 2PI effective potential, at zero temperature, would help us in answering questions such as vacuum stability of the SM [77–81]. Finally, if one extends our analysis to include gauge bosons, then the full 2PI effective potential would provide a framework to study the electroweak phase transition.

PART II

Chapter 5

Leptogenesis

In its simplest form, leptogenesis [82] is similar to baryogenesis in Grand Unified Theories (GUTs) [6]. Analogously, one has **Sakharov's conditions for leptogenesis**, which are realised as follows:

- The deviation of the number density of newly-introduced heavy neutrinos from their equilibrium distributions provides the necessary departure from thermal equilibrium. This out-of-equilibrium process can be studied by the means of Boltzmann equations [83].
- Interactions involving Yukawa couplings of these heavy neutrinos provide the necessary new sources of C and CP violation.
- Lepton number violation is fulfilled via their mass terms.

In this manner, a lepton asymmetry is generated, which is then converted into a baryon asymmetry via the sphaleron process. Finally, successful leptogenesis yields stringent constraints on the masses of the SM and heavy neutrinos.

Since its inception, leptogenesis has been studied with increasing developments throughout the years, such as including flavour effects [84], resonant leptogenesis [85, 86], thermal effects in plasma [87, 88] and so on. In this chapter, we recapitulate some of the essential features in order to study thermal leptogenesis, which we will apply in Chapter 6 to study leptogenesis in a specific model. For comprehensive reviews on leptogenesis, one may refer to [89, 90].

For illustrative purposes, we will often use the Lagrangian of the Type-I Seesaw model throughout various discussions in the following sections. This can be written down as follows

$$\mathcal{L}_N \supset -\frac{1}{2}\sum_i M_i \overline{N_i^c} N_i - \sum_{\alpha,\, i} y_{\alpha i} \bar{L}_\alpha \widetilde{H} N_i + \text{h.c.} \tag{5.1}$$

where N_i refers to the heavy right-handed neutrinos (RHNs), L_α refers to the (left-handed) SM lepton doublets with α referring to the flavour and $\widetilde{H} = i\sigma_2 H^*$ where H is the SM Higgs doublet. We have $N_i^c = C(\overline{N_i})^T$ where C is the charge conjugation matrix. The RHNs are Majorana fermions, with Majorana mass terms M_i and gauge singlets under

the SM gauge group. The $y_{\alpha i}$ refer to the Yukawa couplings of the RHNs with the SM Higgs and SM leptons, some or all of which are complex numbers.

It is often convenient to assign lepton number (L) to the fields in order to identify parameters that break lepton number. The choices are arbitrary but need to be done in a consistent manner. We start with the obvious choice of assigning lepton number $+1$ to L_α. By then requiring that the scalar H does not carry lepton number, we proceed to determine the remaining assignments by demanding the Yukawa terms do not break lepton number. This leads to the RHNs being assigned lepton number $+1$, and we can easily identify that the Majorana mass terms M_i break lepton number by two units. For completeness' sake, we mention that there are no other parameters breaking lepton number, which can be checked by using the assignment we have described.

5.1 CP Violation

The CP violation generated in a lepton flavour α, from the decays of the heavy neutrinos, can be quantified through the CP asymmetry parameter

$$\epsilon_{i\alpha} = \frac{\Gamma\left(N_i \to L_\alpha H\right) - \Gamma\left(N_i \to \bar{L}_\alpha H^\dagger\right)}{\sum_\beta \left[\Gamma\left(N_i \to L_\beta H\right) + \Gamma(N_i \to \bar{L}_\beta H^\dagger)\right]} \tag{5.2}$$

where Γ refers to the partial decay widths of the N_i into the mentioned states. At tree-level, we have

$$\Gamma\left(N_i \to L_\alpha H\right) = |y_{\alpha i}|^2 F_{\text{tree}} = |y^*_{\alpha i}|^2 F_{\text{tree}} = \Gamma\left(N_i \to \overline{L}_\alpha H^\dagger\right) \tag{5.3}$$

where F_{tree} arises from integrating the (squared and summed) kinematic part of the tree-level amplitude over the final state phase space, and hence $\epsilon_{i\alpha} = 0$. Thus, the CP asymmetry arises at lowest order from the interference of tree-level and one-loop amplitudes, the diagrams for which are described in Fig. 5.1.

The width arising from the interference terms, $\Gamma_{\text{int.}}$, are of the form

$$\begin{aligned}
\Gamma_{\text{int.}}\left(N_i \to L_\alpha H\right) &= \sum_{\beta,k} \left[y^*_{\alpha i}\, y_{\alpha k}\, y_{\beta k}\, y^*_{\beta i}\, F_{\text{int.}} + \left(y^*_{\alpha i}\, y_{\alpha k}\, y_{\beta k}\, y^*_{\beta i}\, F_{\text{int.}}\right)^*\right] \\
\Gamma_{\text{int.}}(N_i \to \overline{L}_\alpha H^\dagger) &= \sum_{\beta,k} \left[y_{\alpha i}\, y^*_{\alpha k}\, y^*_{\beta k}\, y_{\beta i}\, F_{\text{int.}} + \left(y_{\alpha i}\, y^*_{\alpha k}\, y^*_{\beta k}\, y_{\beta i}\, F_{\text{int.}}\right)^*\right] ,
\end{aligned}$$

where $F_{\text{int.}}$ refers to the function obtained from integrating the product of the kinematic parts of the tree-level and one-loop level amplitudes over the two-body phase space, i.e.

$$F_{\text{int.}} = \int \mathcal{A}_{\text{tree}}\, \mathcal{A}^\dagger_{\text{loop}} d\Pi_2 \,.$$

Note that, in our convention, the kinematic part of the tree-level amplitude is real and for the the one-loop amplitude can be complex as it would contain the various loop functions (see Appendix A). Now, evaluating the numerator of (5.2), we obtain

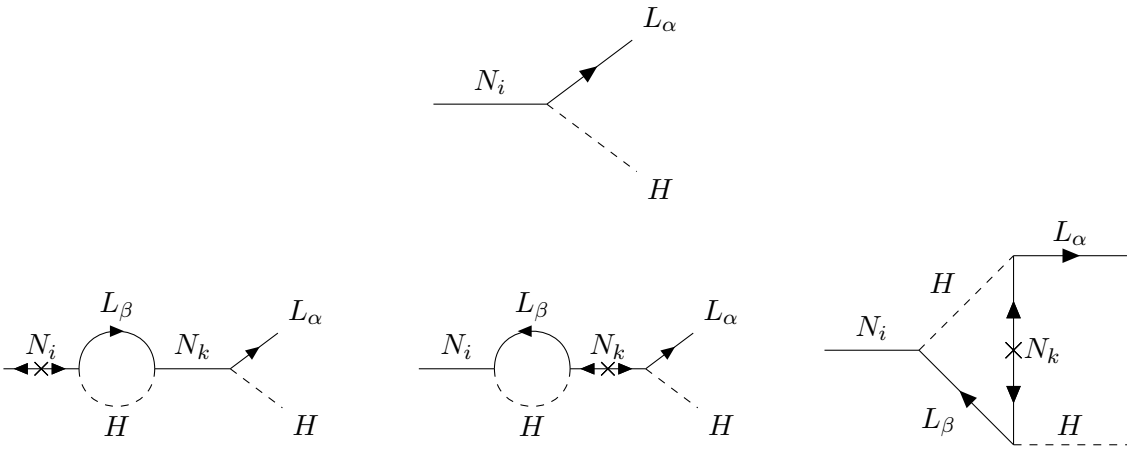

Figure 5.1: First row: the tree-level decay of the N_i into L_α and H. Second row: the corresponding one-loop diagrams for the decay into the same final states. Arrows indicate the flow of lepton number. Crosses on lines indicate mass insertions. The internal lepton flavour β and the internal RHN k are always summed over. Note that the first of the loop diagrams in the second row (one of the "self-energy" diagrams) contributes to a CP asymmetry in the flavour, but not the total asymmetry [91] where as the remaining two loop diagrams (the last of which is often called the "vertex diagram") violate both lepton flavour and lepton number [91–93].

$$\begin{aligned}
&\Gamma\left(N_i \to L_\alpha H\right) - \Gamma(N_i \to \overline{L}_\alpha H^\dagger) \\
&\quad = \sum_{\beta,\,k} \left\{ 2i\, y^*_{\alpha i}\, y_{\alpha k}\, y_{\beta k}\, y^*_{\beta i} \mathrm{Im}\left[F_{\mathrm{int.}}\right] - 2i\, y_{\alpha i}\, y^*_{\alpha k}\, y^*_{\beta k}\, y_{\beta i} \mathrm{Im}\left[F_{\mathrm{int.}}\right] \right\} \\
&\quad = -4 \sum_{\beta,\,k} \mathrm{Im}\left[y^*_{\alpha i}\, y_{\alpha k}\, y_{\beta k}\, y^*_{\beta i} \right] \mathrm{Im}\left[F_{\mathrm{int.}}\right] \,, \qquad (5.4)
\end{aligned}$$

whereby in the first equality, the tree-level parts of the widths cancel. This is then normalised to the total decay width, where it may be assumed that the tree-level partial widths dominate, as the loop-level widths are suppressed by additional couplings and loop factors. Equation (5.4) implies that the CP asymmetry is non-zero only for complex couplings **and** when the loop amplitude acquires an imaginary part, due to intermediate particles going on-shell as dictated by the Cutkosky rules [94]. Finally, if one seeks only the total CP asymmetry (essentially, the "total lepton number violation"), then one performs the sum over the flavours in the final state, i.e.

$$\epsilon_i \equiv \sum_\alpha \epsilon_{i\alpha} = \frac{-2 \sum\limits_{\alpha,\,\beta,\,k} \mathrm{Im}\left[y^*_{\alpha i}\, y_{\alpha k}\, y_{\beta k}\, y^*_{\beta i} \right] \mathrm{Im}\left[F_{\mathrm{int.}}\right]}{\sum\limits_\gamma |y_{\gamma i}|^2\, F_{\mathrm{tree}}} \,. \qquad (5.5)$$

5.2 Boltzmann Equations

The evolution of the number density of the RHNs can be tracked by the Boltzmann equations (BEs), written as

$$\hat{\mathbf{L}}\left[f_{N_i}\right] = \mathbf{C}\left[f_{N_i}\right] , \tag{5.6}$$

where the i index implies an individual equation for the phase space distribution of each RHN. Here, $\mathbf{C}$ is the collision operator, which encodes the particle physics information (in this case the decays of the RHNs), and $\hat{\mathbf{L}}$ is the Liouville operator, which in covariant and relativistic form, can be expressed as

$$\hat{\mathbf{L}} = p^\alpha \frac{\partial}{\partial x^\alpha} - \Gamma^\alpha_{\beta\gamma} p^\beta p^\gamma \frac{\partial}{\partial p^\alpha} , \tag{5.7}$$

where $\Gamma^\alpha_{\beta\gamma}$ are the Christoffel symbols and x^α (p^α) are the coordinate (momentum) four-vectors. The Liouville operator hence describes the effect of the expansion of the universe on the RHNs' phase space distribution. The early universe is usually modelled on the Friedmann-Lemâitre-Robertson-Walker (FLRW) metric which is based on the assumption of homogeneity and isotropy[1], which implies,

$$f_{N_i} \equiv f_{N_i}(E,t) , \qquad \hat{\mathbf{L}}\left[f_{N_i}\right] = E\frac{\partial f_{N_i}}{\partial t} - \frac{\dot{a}}{a}\left|\vec{p}\right|^2 \frac{\partial f_{N_i}}{\partial E} ,$$

where $a \equiv a(t)$ is the scale factor in the FLRW metric and $\dot{a} \equiv da/dt$. At this point, it is convenient to define the **Hubble parameter**

$$H \equiv \frac{\dot{a}}{a} = \sqrt{\frac{8\pi^3 g_*}{90}}\frac{T^2}{M_{\rm Pl}} \tag{5.8}$$

where the equality holds for the radiation-dominated era [6, 95, 96], which is when leptogenesis occurs. The quantity g_* refers to the effective number of relativistic degrees of freedom which in the SM is $g_*^{\rm SM} = 106.75$ [6]. Defining now the number density of the RHNs as

$$n_{N_i}(t) = \frac{g_{N_i}}{(2\pi)^3}\int d^3p\, f_{N_i} ,$$

where g_{N_i} refers to the relativistic degrees of freedom of the N_i ($g_{N_i} = 2$ as they are Majorana fermions), one inserts this into the Boltzmann equation and integrates by parts to arrive at

$$\dot{n} + 3Hn = \frac{g_{N_i}}{(2\pi)^3}\int \mathbf{C}\left[f_{N_i}\right]\frac{d^3p}{E} . \tag{5.9}$$

Now, to treat the collision term, we analyse the decays RHNs, $N_i \to LH\,, \overline{L}H^\dagger$. The squared amplitudes for which can be written in the form

$$\begin{aligned} |\mathcal{M}_{N_i\to LH}|^2 &= |\mathcal{M}_{LH\to N_i}|^2 = \frac{1}{2}(1+\epsilon_i)|\mathcal{M}_0|^2 \\ |\mathcal{M}_{N_i\to \overline{L}H^\dagger}|^2 &= |\mathcal{M}_{\overline{L}H^\dagger\to N_i}|^2 = \frac{1}{2}(1-\epsilon_i)|\mathcal{M}_0|^2 . \end{aligned}$$

where we drop the lepton flavour index, as we will be treating only the total CP asymmetry in what follows. The collision term is hence

[1] For a comprehensive reviews on cosmology, one may refer to [95, 96].

$$
\begin{aligned}
&\frac{g_{N_i}}{(2\pi)^3}\int \mathbf{C}\left[f_{N_i}\right]\frac{d^3p}{E}\\
&=-\int d\Pi_{N_i}\,d\Pi_L\,d\Pi_H\,(2\pi)^4\delta^{(4)}\left(p_{N_i}-p_{L_\alpha}-p_H\right)\Big\{|\mathcal{M}_{N_i\to LH}|^2\,f_{N_i}(1-f_L)(1+f_H)\\
&-|\mathcal{M}_{LH\to N_i}|^2 f_L f_H(1-f_{N_i})+|\mathcal{M}_{N_i\to \overline{L}H^\dagger}|^2\,f_{N_i}(1-f_L)(1+f_H)-|\mathcal{M}_{\overline{L}H^\dagger\to N_i}|^2 f_L f_H(1-f_{N_i})\Big\}\\
&=-2\int d\Pi_{N_i}\,d\Pi_L\,d\Pi_H\,(2\pi)^4\delta^{(4)}\left(p_{N_i}-p_{L_\alpha}-p_H\right)\,|\mathcal{M}_0|^2\left\{f_{N_i}-f_{N_i}^{\text{eq.}}\right\}
\end{aligned}
\tag{5.10}
$$

where $d\Pi$ refers to the phase space of the particle species, but with the degrees of freedom included, i.e.

$$d\Pi_X=\frac{g_X}{(2\pi)^3}\frac{d^3p_X}{2E_X}\,,$$

and the δ-function ensures four-momentum conservation. In the second equality of (5.10), we have used the following simplifications

- The use of Maxwell-Boltzmann statistics in place of Fermi-Dirac/Bose-Einstein statistics, i.e. we ignore Fermi blocking and Bose-Einstein enhancement to write $1\pm f_X\approx 1$ and $f_X=\exp\left(-\frac{E_X}{T}\right)$ where T is the temperature.
- The leptons and Higgs are much lighter than the RHNs and still in equilibrium with the thermal plasma allowing us to use their equilibrium distributions. Energy conservation then ensures $E_L+E_H=E_{N_i}$, which implies

$$f_L f_H=\exp\left(-\frac{(E_L+E_H)}{T}\right)=\exp\left(-\frac{E_{N_i}}{T}\right)=f_{N_i}^{\text{eq.}}\,.$$

Thus, one arrives at the final form for the Boltzmann equations to track the decays of the RHNs

$$\dot{n}_{N_i}+3Hn_{N_i}=-\langle\Gamma_i\rangle\left(n_{N_i}-n_{N_i}^{\text{eq.}}\right)\,. \tag{5.11}$$

Here, $\langle\Gamma_i\rangle$ represents the thermally averaged decay rate over the tree-level decay width $\Gamma_i\equiv\Gamma_{\text{tree}}(N_i\to LH)$, given by [6, 90]

$$
\begin{aligned}
\langle\Gamma_i\rangle&=-2\int d\Pi_{N_i}\,d\Pi_L\,d\Pi_H\,(2\pi)^4\delta^{(4)}\left(p_{N_i}-p_{L_\alpha}-p_H\right)\,|\mathcal{M}_0|^2\exp\left(-\frac{E_{N_i}}{T}\right)\\
&=\frac{g_{N_i}}{2\pi^2}\frac{M_i^2}{T}\,\mathcal{K}_1\left(\frac{M_i}{T}\right)\Gamma_i
\end{aligned}
\tag{5.12}
$$

where $\mathcal{K}_n$ refer to the modified Bessel functions of the second kind. We also have their equilibrium number density, given by

$$n_{N_i}^{\text{eq.}}\;=\;\frac{g_{N_i}M_i\,T}{2\pi^2}\mathcal{K}_2\left(\frac{M_i}{T}\right)\,.$$

The decays of the heavy RHNs produce a lepton asymmetry as discussed earlier, and therefore in $B-L$ where B is the baryon number. Again, for simplicity, we will consider

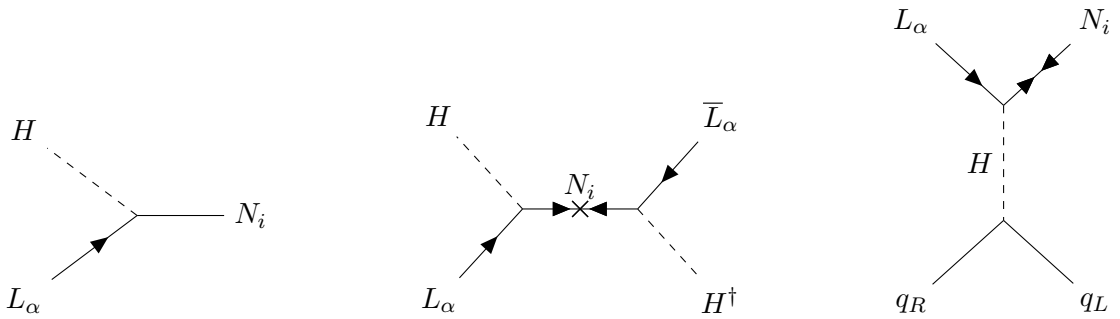

Figure 5.2: Examples of washout processes, with arrows representing the flow of lepton number. From the left to right, we have the inverse decay, an example of a $\Delta L = 2$ process and finally, an example of a $\Delta L = 1$ process, where $q_{L,R}$ represents the left (right)-handed quarks. The dominant contribution to the $\Delta L = 1$ process would come in the case of a top-quark, due to the relevant Yukawa coupling. Note that in the $\Delta L = 2$ process, the intermediate N_i can go on-shell, and thus one needs to subtract the relevant contribution from the cross-section; otherwise, one double counts the decays of the N_i in the BEs.

only the total lepton asymmetry and hence will sum over the flavours. To track the asymmetry in $B - L$, we can write down the following BE

$$\dot{n}_{B-L} + 3Hn_{B-L} = -\sum_i \epsilon_i \langle \Gamma_i \rangle \left(n_{N_i} - n_{N_i}^{\text{eq.}} \right) - \left[\sum_i \frac{n_{N_i}^{\text{eq.}}}{n_L^{\text{eq.}}} + 2\langle \sigma\, v \rangle_{\Delta L \neq 0} \right] n_{B-L} \,, \quad (5.13)$$

where the terms proportional to n_{B-L} are the **washout** terms, which reduce the final asymmetry. The contributions to these come from the inverse decays (production of the N_i) and the scattering terms (quantified by the thermally averaged cross-section $\langle \sigma\, v \rangle_{\Delta L \neq 0}$) that violate lepton number [6, 97]. Examples of various washout processes are described in Fig. 5.2. Note that one needs to retain only the non-resonant part of the scattering processes, such as an s-channel process with the N_i as propagator. This is because the on-shell decays of the RHNs have already be considered in the BEs and hence one would "double count" the decays. Finally, from (5.13), we can deduce that $n_{B-L} \neq 0$ only if $\epsilon_i \neq 0$ and $n_{N_i} \neq n_{N_i}^{\text{eq.}}$, which is essentially a quantitive formulation of Sakharov's conditions.

To scale out the expansion of the universe, one defines co-moving number densities

$$N_{N_i} \;=\; n_{N_i}\, a^3 \,, \qquad N_{B-L} \;=\; n_{B-L}\, a^3 \,,$$

and for convenience one defines dimensionless variables $z_i = M_i/T$. Note that the variables can be related to each other by $z_i = M_i/M_1\, z_1$, where M_1 is the mass of the lightest RHN, so one typically chooses z_1 to solve the resulting equations. This also allows one to recast the Hubble parameter as

$$H(z_i) \;=\; \frac{H(T = M_i)}{z_i^2} \,. \quad (5.14)$$

With these transformations, one arrives at the following differential equations for leptogenesis [98, 99]

$$\frac{dN_{N_i}}{dz_1} \;=\; -\, D_i(z_i) \left(N_{N_i} - N_{N_i}^{\text{eq.}} \right) \,, \quad (5.15)$$

$$\frac{dN_{B-L}}{dz_1} \;=\; -\sum_i \epsilon_i\, D_i(z_i) \frac{M_i}{M_1}\, K_i \left(N_{N_i} - N_{N_i}^{\text{eq.}} \right) - \sum_i \left(W_{\text{ID}}^{(i)} + W_{\text{S}}^{(i)} \right) N_{B-L} \,, \quad (5.16)$$

where we have defined the following rescaled interaction rates for the decays, inverse decays and scatterings

$$D_i(z_i) = \boldsymbol{K}_i \, \frac{M_i}{M_1} \, \frac{z_i \, \mathcal{K}_1(z_i)}{\mathcal{K}_2(z_i)} \,, \qquad W_{\rm ID}^{(i)} = \frac{1}{4} \, \frac{M_i}{M_1} \, \boldsymbol{K}_i \, z_i^3 \, \mathcal{K}_2(z_i) \,, \quad W_{\rm S}^{(i)} = \frac{M_i}{M_1} \frac{2 \langle \sigma \, v \rangle_{\Delta L \neq 0}}{H(z_i) \, z_i} \,, \tag{5.17}$$

where we stress again that the equations are solved in terms of z_1, with replacements of $z_i = M_i/M_1 \, z_1$ in order to be consistent.

In order to have successful leptogenesis, the decays of the RHNs must go out out of equilibirum and at the same time, washout processes must "freeze out". A naïve estimate for this is

$$D_i(z_i = 1) < 1 \,, \qquad (W_{\rm ID}^{(i)} + W_{\rm S}^{(i)}) \Big|_{z_i = 1} < 1 \,.$$

However, a convenient tool to answer the question regarding the washout of the generated asymmetry are the **decay parameters**

$$K_i \equiv \frac{\Gamma_i}{H(T = M_i)} \,, \tag{5.18}$$

which we have marked in bold in (5.17). Based on the values of the decay parameter, one classifies various regimes that determine the effectiveness of the washout terms [89, 90]. For $K_i \lesssim 1$, one realises the **weak washout regime**, where the inverse decays freeze out first, and the asymmetry generated in the decays of the N_i is reduced by the $\Delta L \neq 0$ scatterings. One is then left with a $B-L$ asymmetry after the scatterings have frozen out. There is then an intermediate regime, until one reaches $K_i \gtrsim 3$, which is classified as the **strong washout regime**. Here, scatterings freeze-out before when the RHNs remain in equilibrium, and the inverse decays freeze out last, and one can thus neglect the effects of the former in the BE. The final $B-L$ asymmetry is generated after the inverse decays are no longer effective. Thus, the N_i "decouple" from the thermal plasma and their remaining number density decays to source N_{B-L}. Thus, in the strong washout regime, leptogenesis is essentially described by competition between decays and inverse decays of the RHNs [89].

One (numerically) solves the set of equations (5.15) and (5.16) together with a set of initial conditions[2] typically chosen as

$$N_{N_i}(z_1 \ll 1) = N_{N_i}^{\rm eq.} \,, \qquad N_{B-L}(z_1 \ll 1) = 0 \,, \tag{5.19}$$

and tracks these number densities down to low temperatures, i.e. $z_1 \gg 1$, until one obtains[3] the final (or present-day) value $N_{B-L}^{\rm fin.}$.

[2] In [97, 99], it has been shown that, deep in equilibrium, one could even start with an initial condition of $N_{N_i}(z_1 \ll 1) = 0$, and this has no impact on the asymmetry. This is because processes in equilibrium are so rapidly occurring that the N_i are quickly driven to their equilibrium number distributions.

[3] For example, for the initial condition, one could choose $z_1 = 10^{-4}$ and solve the set of equations till $z_1 = 10^3$.

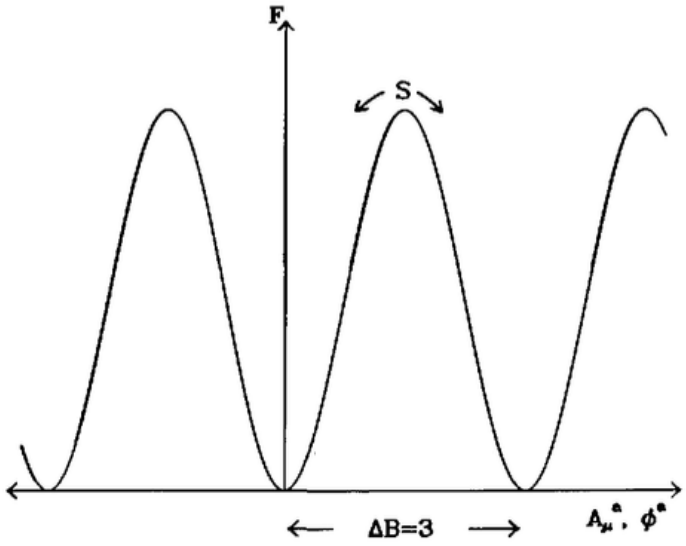

Figure 5.3: Depiction of the EW vacuum, from [6], with the various vacua. The free energy, F, is plotted against the gauge-field and Higgs-field configurations. Between adjacent vacua, B and L change by N_f units (here, it is 3 as in the SM). The sphalerons (S) are represented by the path which moves over the barrier, from one vacuum to another.

5.3 Sphalerons: Converting Leptons to Baryons

To compare to observations, one needs to convert the obtained value of the $B-L$ asymmetry, from the Boltzmann equations, into the baryon asymmetry. This is facilitated by the sphaleron process that exists in the SM.

Baryon and lepton numbers are accidental symmetries in the SM, meaning that, although they are preserved at the classical level, quantum effects may break these symmetries leaving them anomalous [2, 3]. In the electroweak theory, the anomalous current is given by [3, 6]

$$\partial_\mu J^\mu_{B,L} \;=\; N_f \,\frac{g_2^2}{32\pi^2}\, W^a_{\mu\nu}\widetilde{W}^{a\,\mu\nu}\,, \tag{5.20}$$

where $W_{\mu\nu}$ ($\widetilde{W}^a_{\mu\nu}$) is the SU(2)$_L$ (dual) field strength tensor, g_2 is the corresponding gauge coupling and N_f is the number of generations of the fermions (3 in the SM). This current leaves $B-L$ conserved, but breaks B, L and $B+L$. By integrating the anomalous current, one can obtain the change in B and L as [100]

$$\Delta B = \Delta L = \int d^4x\, \partial_\mu J^\mu_{B,L} \equiv N_f\, \Delta N_{\rm CS}\,. \tag{5.21}$$

Here, $\Delta N_{\rm CS} = \pm 1, \pm 2\,, \ldots$ denotes the change of the Chern-Simons number, which arises from a transition from one electroweak vacuum to another, which mediated by the sphalerons [15] (see Fig. 5.3). At low temperatures, this is exponentially suppressed due to energy barriers between vacuum states. However, at temperatures $T \gtrsim 100\,\text{GeV}$, the transition becomes very efficient and results in a violation of B and L in multiples of N_f units, while conserving $B-L$. Hence, the sphalerons allow conversion of lepton number into baryon number, with a conversion factor estimated via [101]

$$C_{\rm sphal.} \;=\; \frac{8N_f + 4N_D}{22N_f + 13N_D} \tag{5.22}$$

where N_D is the number of scalar $SU(2)_L$ doublets in the model. Thus, to obtain the final baryon asymmetry from the $B-L$ asymmetry we get from the Boltzmann equations, we may use

$$\eta_B \equiv \frac{n_B}{n_\gamma} \approx \frac{3}{4} C_{\text{sphal.}} \frac{g_*^0}{g_*} |N_{B-L}^{\text{fin.}}| \tag{5.23}$$

where $g_*^0 = 43/11$ is the present value of the number relativistic degrees of freedom.

Chapter 6

Phenomenology of a Scotogenic Model

In this chapter, we extend the Standard Model (SM) through the framework of a scotogenic model. Such models generate masses for the SM neutrinos radiatively, through newly introduced particles running in the loops. The SM neutrino masses are hence additionally suppressed by loop factors and couplings to this newly introduced sector. At the same time, if the new particles are electrically neutral and stable, they can serve as good dark matter (DM) candidates.

After the first works on a minimal scotogenic realisation [102–106], more complex models have emerged in recent years, studied mainly at the level of dark matter phenomenology and lepton flavour violating (LFV) observables, such as [103, 107–111]. A general classification of viable scotogenic frameworks can be found in [112]. We note for completeness that the model we consider in this chapter is the "T1-2-A" model [112, 113] with an extra fermionic singlet. Although the T1-2-A model features a very predictive dark matter phenomenology and can explain the SM neutrino masses, it cannot account for the recent measurements of the anomalous magnetic moment of the muon without being in tension with constrains on LFV decays. Furthermore, leptogenesis cannot be achieved in this setup, as the single fermionic singlet in this model never goes out of equilibrium with the thermal plasma.

We will show that the T1-2-A model with the extra fermionic singlet, introduces enough degrees of freedom to allow for generation of neutrino masses compatible with neutrino oscillation data, while being consistent with the bounds on lepton flavour violating decays. Furthermore, certain couplings can be chosen such that the deviation related to the anomalous magnetic moment of the muon can be accommodated. Finally, we study leptogenesis within this model, to account for the baryon asymmetry of the Universe. This chapter is based on the results of [1].

6.1 Model

The SM is extended with two Weyl fermion $\mathrm{SU}(2)_L$ doublets, Ψ_1 and Ψ_2, two Majorana fermion singlets, F_1 and F_2, a scalar $\mathrm{SU}(2)_L$ doublet, η, and a real scalar singlet, S.

	Ψ_1	Ψ_2	F_1	F_2	η	S
$\mathrm{SU}(2)_L$	**2**	**2**	**1**	**1**	**2**	**1**
$\mathrm{U}(1)_Y$	-1	1	0	0	1	0

Table 6.1: BSM field content of the scotogenic model under consideration and their representations/charges.

However, these additional fields are singlets with respect to $\mathrm{SU}(3)_C$. In addition, we assume a $\mathbb{Z}_2$-symmetry under which the SM fields are even and the newly introduced ones are odd, as per the scotogenic framework. This ensures neutrino mass generation at loop level and stability of potential DM candidates. The new field content, with their respective representations under $\mathrm{SU}(2)_L \times \mathrm{U}(1)_Y$, is summarised in Table 6.1. We will now describe the various sectors, with their corresponding Lagrangians and set the notation.

6.1.1 Scalar Sector

The scalar sector of the model consists of the SM Higgs doublet H, an additional real singlet S, and a $\mathrm{SU}(2)_L$ doublet η. Upon electroweak symmetry breaking (EWSB), the doublets are conveniently expanded into components according to

$$H \;=\; \begin{pmatrix} G^+ \\ \frac{1}{\sqrt{2}}[v + h^0 + iG^0] \end{pmatrix}, \qquad \eta \;=\; \begin{pmatrix} \eta^+ \\ \frac{1}{\sqrt{2}}[\eta^0 + iA^0] \end{pmatrix}. \tag{6.1}$$

Here, h^0 is the physical SM Higgs boson, G^0 and G^+ are the would-be Goldstone bosons, and $v = \sqrt{2}\langle H \rangle \approx 246$ GeV denotes the vacuum expectation value (VEV) acquired by the Higgs. η^0 and A^0 are CP-even and CP-odd neutral scalars, and η^+ is a charged scalar. The assumed $\mathbb{Z}_2$-symmetry forbids η and S from acquiring a VEV. The scalar potential of the model is hence given by

$$\begin{aligned} V_{\text{scalar}} \;&= M_H^2|H|^2 + \lambda_H|H|^4 + \frac{1}{2}M_S^2 S^2 + \frac{1}{2}\lambda_{4S}S^4 + M_\eta^2|\eta|^2 + \lambda_{4\eta}|\eta|^4 \\ &+ \frac{1}{2}\lambda_S S^2|H|^2 + \frac{1}{2}\lambda_{S\eta}S^2|\eta|^2 + \lambda_\eta|\eta|^2|H|^2 + \lambda'_\eta|H\eta^\dagger|^2 \\ &+ \frac{1}{2}\lambda''_\eta\Big[(H\eta^\dagger)^2 + \text{h.c.}\Big] + \alpha\Big[SH\eta^\dagger + \text{h.c.}\Big] \end{aligned} \tag{6.2}$$

The first two terms form the usual SM Higgs potential. We assume here for simplicity that λ''_η and α are real. During EWSB, the neutral CP-even component of the Higgs doublet acquires a VEV, leading to the usual minimisation relation,

$$m_{h^0}^2 \;=\; -2M_H^2 \;=\; 2\lambda_H v^2\,, \tag{6.3}$$

allowing one to eliminate the mass parameter M_H^2 in favour of the Higgs self-coupling λ_H. Imposing $m_{h^0} \approx 125$ GeV leads to a tree-level value of $\lambda_H \approx 0.13$. Further, after EWSB, the neutral components of η and S can mix according to the mass matrix

$$\mathcal{M}_\phi^2 \;=\; \begin{pmatrix} M_S^2 + \frac{1}{2}v^2\lambda_S & v\alpha & 0 \\ v\alpha & M_\eta^2 + \frac{1}{2}v^2\lambda_L & 0 \\ 0 & 0 & M_\eta^2 + \frac{1}{2}v^2\lambda_A \end{pmatrix}, \tag{6.4}$$

where we work in the basis $\{S, \eta^0, A^0\}$. Here, we have defined $\lambda_{L,A} = \lambda_\eta + \lambda'_\eta \pm \lambda''_\eta$. The mass eigenstates are ordered according to

$$(\phi_1^0, \phi_2^0, A^0)^T = U_\phi \, (S, \eta^0, A^0)^T \, . \tag{6.5}$$

where U_ϕ is an orthogonal matrix. The corresponding squared masses at tree-level read as

$$m^2_{\phi^0_{1,2}} = \frac{1}{2}\left\{ M_S^2 + M_\eta^2 + \frac{1}{2}v^2\,(\lambda_S + \lambda_L) \mp \sqrt{\left[M_S^2 - M_\eta^2 + \frac{1}{2}v^2\,(\lambda_S - \lambda_L)\right]^2 + 4v^2\alpha^2} \right\},$$

$$m^2_{A^0} = M_\eta^2 + \frac{1}{2}v^2\lambda_A \, , \tag{6.6}$$

where $m_{\phi_1^0} < m_{\phi_2^0}$. The tree-level mass of the charged scalars is given by

$$m^2_{\eta^\pm} = M_\eta^2 + \frac{1}{2}v^2\lambda_\eta \, . \tag{6.7}$$

6.1.2 Fermionic Sector

The Lagrangian for the BSM fermions in Table 6.1 can be written down in two-component form as

$$\begin{aligned}\mathcal{L}_{\text{fermion}} &= i\Big(\overline{\Psi}_j \sigma^\mu D_\mu \Psi_j + \frac{1}{2}\overline{F}_j \sigma^\mu \partial_\mu F_j\Big) - \frac{1}{2}M_i F_i F_i - M_\Psi \Psi_1 \Psi_2 \\ &\quad - y_{1i}\Psi_1 H F_i - y_{2i}\Psi_2 \tilde{H} F_i - g^k_\Psi \Psi_2 L_k S - g^k_{F_j}\eta L_k F_j - g^k_R \, e^c_k \, \tilde{\eta}\, \Psi_1 + \text{h.c.}\end{aligned} \tag{6.8}$$

with $i, j = 1, 2$ and $k = 1, 2, 3$. L_k and e^c_k denote the left-handed and right-handed leptons and $\tilde{\phi} = i\sigma_2\phi^*$ for $\phi = H, \eta$. For the singlet fermions, we have chosen a basis such that their mass matrix is diagonal, with $|M_1| \leq |M_2|$. Finally, we take the phase-convention $\Psi_1 = (\Psi_1^0, \Psi_1^-)$ and $\Psi_2 = (\Psi_2^+, -\Psi_2^0)$ for the $SU(2)_L$ doublets.

After EWSB, we have a charged heavy Dirac state Ψ^+ with mass M_Ψ and four neutral Majorana fermions. Their mass matrix, in the basis $\{F_1, F_2, \Psi_1^0, \Psi_2^0\}$, is given as

$$\mathcal{M}_{\chi^0} = \begin{pmatrix} M_1 & 0 & \frac{v}{\sqrt{2}}\,y_{11} & \frac{v}{\sqrt{2}}\,y_{21} \\ 0 & M_2 & \frac{v}{\sqrt{2}}\,y_{12} & \frac{v}{\sqrt{2}}\,y_{22} \\ \frac{v}{\sqrt{2}}y_{11} & \frac{v}{\sqrt{2}}\,y_{12} & 0 & M_\Psi \\ \frac{v}{\sqrt{2}}y_{21} & \frac{v}{\sqrt{2}}y_{22} & M_\Psi & 0 \end{pmatrix} . \tag{6.9}$$

This matrix is diagonalised by a unitary matrix U_χ according to

$$\text{diag}(m_{\chi_1^0}, m_{\chi_2^0}, m_{\chi_3^0}, m_{\chi_4^0}) = U_\chi \mathcal{M}_{\chi^0} U_\chi^{-1} \, , \tag{6.10}$$

with the convention $m_{\chi_i^0} \leq m_{\chi_j^0}$ for $i < j$.

6.2 SM Neutrino Mass Generation

Majorana mass terms are generated at one-loop level for the SM neutrinos, after EWSB, through diagrams of the following form

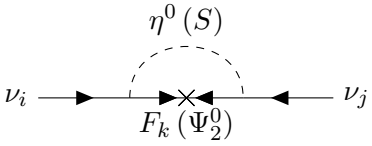

$$\equiv \quad (\nu_j)^T \, (\mathcal{M}_\nu)_{ji} \, \nu_i \, , \tag{6.11}$$

where the particles in the loop are in the gauge eigenstate bases. The SM neutrino mass matrix $(\mathcal{M}_\nu)_{ji}$ can be expressed in the following form

$$\mathcal{M}_\nu \;=\; \mathcal{G}^T\, M_L\, \mathcal{G}\,, \tag{6.12}$$

where $\mathcal{G}$ is the "coupling matrix" according to (6.8), ordered as

$$\mathcal{G} \;=\; \begin{pmatrix} g^1_\Psi & g^2_\Psi & g^3_\Psi \\ g^1_{F_1} & g^2_{F_1} & g^3_{F_1} \\ g^1_{F_2} & g^2_{F_2} & g^3_{F_2} \end{pmatrix}. \tag{6.13}$$

Note that the masses for the SM neutrinos are generated after EWSB, so it is more convenient to work in the mass eigenstate basis in what follows; the mixings in the neutral scalar and fermion sectors are defined in (6.5) and (6.10). Now, M_L is a 3×3 symmetric matrix containing the loop functions, evaluated using dimensional regularisation, whose components are given explicitly as

$$\begin{aligned}
(M_L)_{11} &= \sum_{k,n} b_{kn} (U^\dagger_\chi)^2_{4k} (U^T_\phi)^2_{1n}\,, \\
(M_L)_{22} &= \frac{1}{2} \sum_{k,n} b_{kn} (U^\dagger_\chi)^2_{1k} \left[(U^T_\phi)^2_{2n} - (U^T_\phi)^2_{3n}\right]\,, \\
(M_L)_{33} &= \frac{1}{2} \sum_{k,n} b_{kn} (U^\dagger_\chi)^2_{2k} \left[(U^T_\phi)^2_{2n} - (U^T_\phi)^2_{3n}\right]\,, \\
(M_L)_{12} = (M_L)_{21} &= \frac{1}{\sqrt{2}} \sum_{k,n} b_{kn} (U^\dagger_\chi)_{1k} (U^\dagger_\chi)_{4k} (U^T_\phi)_{1n} (U^T_\phi)_{2n}\,, \\
(M_L)_{13} = (M_L)_{31} &= \frac{1}{\sqrt{2}} \sum_{k,n} b_{kn} (U^\dagger_\chi)_{2k} (U^\dagger_\chi)_{4k} (U^T_\phi)_{1n} (U^T_\phi)_{2n}\,, \\
(M_L)_{23} = (M_L)_{32} &= \frac{1}{2} \sum_{k,n} b_{kn} (U^\dagger_\chi)_{2k} (U^\dagger_\chi)_{1k} \left[(U^T_\phi)^2_{2n} - (U^T_\phi)^2_{3n}\right]\,,
\end{aligned}$$

where $k = 1,2,3,4$ and $n = 1,2,3$, and the coefficients b_{kn} are given by

$$b_{kn} \;=\; \frac{1}{16\pi^2} \frac{m_{\chi^0_k}}{m^2_{\phi^0_n} - m^2_{\chi^0_k}} \left[m^2_{\chi^0_k} \log\left(\frac{m^2_{\chi^0_k}}{Q^2}\right) - m^2_{\phi^0_n} \log\left(\frac{m^2_{\phi^0_n}}{Q^2}\right)\right]\,,$$

where Q is the renormalisation scale. However, one can exploit the unitarity and orthogonality of the U_χ and U_ϕ to show that this drops out in the end.

Next, we make use of the Casas-Ibarra parametrisation [114, 115] to express the couplings in (6.13) in terms of neutrino oscillation data [38, 39], according to

$$\mathcal{G} \;=\; U_L\, D_L^{-1/2}\, R\, D_\nu^{1/2}\, U^*_{\rm PMNS}\,, \tag{6.14}$$

where D_L is a diagonal matrix defined as

$$D_L \;=\; U_L^T\, M_L\, U_L\,, \tag{6.15}$$

and D_ν is the diagonal matrix containing the neutrino mass eigenvalues. Finally, U_{PMNS} is the usual Pontecorvo-Maki-Nakagawa-Sakata (PMNS) unitary matrix relating neutrino flavours to their mass eigenstates, assuming that the charged leptons are already in their mass eigenbasis, i.e.

$$\begin{pmatrix} \nu_e \\ \nu_\mu \\ \nu_\tau \end{pmatrix} = \underbrace{\begin{pmatrix} U_{e1} & U_{e2} & U_{e3} \\ U_{\mu 1} & U_{\mu 2} & U_{\mu 3} \\ U_{\tau 1} & U_{\tau 2} & U_{\tau 3} \end{pmatrix}}_{U_{\text{PMNS}}} \begin{pmatrix} \nu_1 \\ \nu_2 \\ \nu_3 \end{pmatrix} . \tag{6.16}$$

Here, the column vector on the left of the equality represents the SM neutrinos in their flavour eigenstate basis and the column vector on the right of the equality represents the SM neutrinos in their mass eigenstate basis.

As $\mathcal{G}$ is not uniquely defined from all parameters and observables in M_L and $\mathcal{M}_\nu$, the extra degrees of freedom have been encoded in a complex, orthogonal 3×3 matrix R, parameterised as

$$R = \begin{pmatrix} c_2 c_3 & -c_1 s_3 - s_1 s_2 c_3 & s_1 s_3 - c_1 s_2 c_3 \\ c_2 s_3 & c_1 c_3 - s_1 s_2 s_3 & -s_1 c_3 - c_1 s_2 s_3 \\ s_2 & s_1 c_2 & c_1 c_2 \end{pmatrix} , \tag{6.17}$$

which depends on three complex angles θ_i with $s_i = \sin\theta_i$ and $c_i = \sqrt{1 - s_i^2}$.

6.3 Anomalous Magnetic Moment of the Muon

The SM is challenged by precision measurements of the anomalous magnetic moment of the muon [116, 117]. This deviation persists between the SM prediction and the experimental value of the anomalous magnetic moment of the muon, defined as $a_\mu = (g-2)_\mu/2$. The discrepancy amounts to a significance of 4.2σ, and leads to the following range for the new physics contribution to a_μ [117, 118],[1]

$$a_\mu^{\text{BSM}} = a_\mu^{\text{exp}} - a_\mu^{\text{SM}} = (251 \pm 59) \times 10^{-11} . \tag{6.18}$$

In general, every scotogenic-like model will contribute to the anomalous magnetic moment of leptons at one-loop level. These contributions can be encoded in the effective electromagnetic (EM) dipole moment operator $c_R^{ij}\, \bar{\ell}_i \sigma_{\mu\nu} P_R \ell_j F^{\mu\nu}$ [125] where the contribution to $(g-2)$ and the electric dipole momentum of a lepton is given through c_R^{ii}, where as c_R^{ij}, $(i \neq j)$ gives information about charged lepton flavour violating (cLFV) processes [125, 126].

The contribution to $(g-2)_\mu$ is generally suppressed by the muon mass. As the EM dipole operator connects the left- and right-handed parts of the leptons, while neutrino mass models contain typically couplings of BSM fields to only left-handed parts, this leads to this operator being chirally suppressed. This pushes new physics explanations of $(g-2)_\mu$ to low mass scales and large, non-perturbative couplings. One way to avoid this, is to introduce extra fields outside the neutrino mass mechanism, coupling to μ_R, in order to enhance the contribution to $(g-2)_\mu$ and simultaneously fit to the anomaly within

[1] We note here that the SM calculation is currently under discussion due to recent lattice results that weaken the anomaly [119–121]. However, these results are still in tension with $e^+e^- \to$ hadrons cross-section data and EW precision observables [122–124].

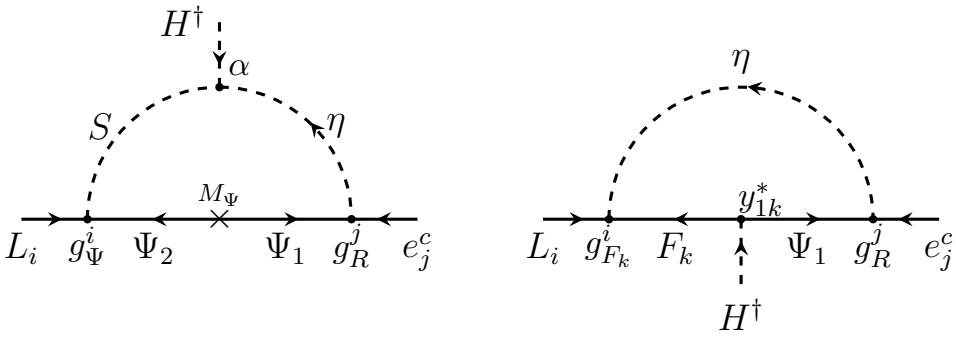

Figure 6.1: Dominant one-loop contributions to $(g-2)$ and charged LFV processes before EWSB. Arrows indicate the flow of quantum numbers and couplings are specified for clarity. A photon should be attached to the respective charged components.

a phenomenologically reasonable parameter space [127]. This solution is realised in this model, through the coupling g_R of the lepton singlets to η and Ψ_1, c.f. (6.8). The latter two fields also participate in the generation of SM neutrino masses, and thus, no extra fields are needed besides those involved in the neutrino mass mechanism to have a chirally enhanced contribution to $(g-2)_\mu$, the new leading contributions to which are shown in Fig. 6.1.

Charged lepton flavour violating decays rank among the most stringent constraints for neutrino mass models, as fitting the neutrino mixing angles, in general, requires non-diagonal Yukawa matrices that connect also to the charged leptons and allow for transitions between different lepton flavours. While the limits to the branching ratios of these processes are already remarkable, especially for the limit on the decay $\mu \to e\gamma$ from the MEG collaboration [128], there is a renovate interest with new experiments expected to take place in the near future, such as MEGII [129], Mu3e [130], or COMET [131], with an expected improvement on the sensitivity of even four orders of magnitude for certain processes like $\mu \to 3e$, or Belle and Belle II for the tau decays [132–134].

Both diagrams depicted in Fig. 6.1 generate sizeable contributions to strongly constrained cLFV processes, in particular $\mu \to e\gamma$, which has an upper limit of 4.2×10^{-13} on its branching ratio [128]. Although these large contributions seem unavoidable, one can somewhat circumvent this problem by realising that the off-diagonal part of the Yukawa matrix $\mathcal{G}$ is connected to neutrino mixing, see (6.14). This means we can assume certain flavour structures for the Yukawa couplings which suppress the off-diagonal components in favour of the diagonal ones [135], thus enhancing contributions to $(g-2)_\mu$ while keeping contributions to cLFV processes under control.

With this in mind, we focus on a region of the parameter space where the left diagram in Fig. 6.1 dominates, as the flavour structure of the diagram is simpler, with just two three-component Yukawa vectors involved. To do so, we consider $y_{1,2}$ to be small and push the trilinear coupling α to larger values. This also indirectly suppresses g_F and enhances g_Ψ through the neutrino fit, c.f. (6.14). However, the components of g_R are free, which allows us to fit the value of $(g-2)_\mu$ while keeping the contributions to the cLFV decays, $\mu \to e\gamma$ and $\tau \to \mu\gamma$, under control.

For completeness, we note that we focus on a particular region of parameter space. However, given the complexity of the system, we were not able to find a more general approach that could deliver results within reasonable computing time. This region of parameter space has interesting consequences for leptogenesis (see later in Sec. 6.5).

6.4 Markov chain Monte Carlo Scan

6.4.1 Constraints and Observables

Similar to the analysis in [113], a Markov chain Monte Carlo (MCMC) scan [136] was implemented, based on the Metropolis-Hastings algorithm [137, 138] to efficiently scrutinise the parameter space of this scotogenic model in view of the numerous constraints discussed earlier. Essentially, this technique explores the parameter space iteratively, with restrictions imposed by a set of constraints, through the computation of the likelihood. For further details on the implementation of the MCMC, see [1, 113].

In addition to the implicit constraints from neutrino masses and the anomalous magnetic moment of the muon, we explicitly impose constraints coming from the following sectors: DM observables, cLFV processes and the mass of the Higgs boson. These are summarised in Table 6.2, along with their associated experimental limits and uncertainties[2]. We also ensure that the lightest $\mathbb{Z}_2$-odd particle is electrically neutral in order to have a stable neutral DM candidate and avoid stable charged relics [8, 144–146].

Observable	Constraint	Observable	Constraint
m_H	125.25 ± 1.0 GeV	BR($\tau^- \to e^-\pi$)	$< 8.0 \times 10^{-8}$
$\Omega_{\text{CDM}}h^2$	0.120 ± 0.012	BR($\tau^- \to e^-\eta$)	$< 9.2 \times 10^{-8}$
BR($\mu^- \to e^-\gamma$)	$< 4.2 \times 10^{-13}$	BR($\tau^- \to e^-\eta'$)	$< 1.6 \times 10^{-7}$
BR($\tau^- \to e^-\gamma$)	$< 3.3 \times 10^{-8}$	BR($\tau^- \to \mu^-\pi$)	$< 1.1 \times 10^{-7}$
BR($\tau^- \to \mu^-\gamma$)	$< 4.2 \times 10^{-8}$	BR($\tau^- \to \mu^-\eta$)	$< 6.5 \times 10^{-8}$
BR($\mu^- \to e^-e^+e^-$)	$< 1.0 \times 10^{-12}$	BR($\tau^- \to \mu^-\eta'$)	$< 1.3 \times 10^{-7}$
BR($\tau^- \to e^-e^+e^-$)	$< 2.7 \times 10^{-8}$	$\text{CR}_{\mu\to e}$(Ti)	$< 4.3 \times 10^{-12}$
BR($\tau^- \to \mu^-\mu^+\mu^-$)	$< 2.1 \times 10^{-8}$	$\text{CR}_{\mu\to e}$(Pb)	$< 4.3 \times 10^{-11}$
BR($\tau^- \to e^-\mu^+\mu^-$)	$< 2.7 \times 10^{-8}$	$\text{CR}_{\mu\to e}$(Au)	$< 7.0 \times 10^{-13}$
BR($\tau^- \to \mu^-e^+e^-$)	$< 1.8 \times 10^{-8}$	BR($Z^0 \to e^\pm\mu^\mp$)	$< 7.5 \times 10^{-7}$
BR($\tau^- \to \mu^-e^+\mu^-$)	$< 1.7 \times 10^{-8}$	BR($Z^0 \to e^\pm\tau^\mp$)	$< 5.0 \times 10^{-6}$
BR($\tau^- \to \mu^+e^-e^-$)	$< 1.5 \times 10^{-8}$	BR($Z^0 \to \mu^\pm\tau^\mp$)	$< 6.5 \times 10^{-6}$

Table 6.2: Constraints considered in the MCMC analysis: Higgs mass and charged LFV observables [8] and the DM relic density [11]. The limits from XENON1T [147] to the direct detection cross-section are also taken into account.

Parameter	Interval	Parameter	Interval
λ_H	[0.1; 0.4]	M_S^2, M_η^2	$[5 \times 10^5; 5 \times 10^6]$
λ_{4S}, $\lambda_{4\eta}$	$[10^{-7}; 1]$	M_1, M_2	$[100; 2 \times 10^4]$
$\lambda_{S\eta}$, λ_S	[-1; 1]	M_Ψ	[700; 2000]
λ_η, λ'_η, λ''_η	[-1; 1]	y_{11}, y_{12}, y_{21}, y_{22}	$[-10^{-4}; 10^{-4}]$
α	$[-10^4; 10^4]$	m_{ν_1}	$[10^{-32}; 10^{-10}]$

Table 6.3: Input parameters for the MCMC scan, with dimensionful quantities given in GeV.

In total, the MCMC scan runs over 20 free parameters: 8 couplings in the scalar potential, 6 Yukawa couplings, 5 masses, the lightest SM neutrino mass and the unconstrained

[2]Note that for the Higgs mass, m_H, and the DM relic density, $\Omega_{\text{CDM}}h^2$, we apply the theory uncertainties [139–143] as these are larger than the experimental ones. We estimate those on m_H to be of similar size as those in supersymmetric models due to electroweak corrections.

angle of the rotation matrix R, which is assumed to be real. The ranges of the scalar and fermion mass parameters are chosen allowing them to (in principle) be in the reach of the high luminosity LHC. For the singlet fermions, we allow for a larger range, in view of leptogenesis. The sign of the quartic couplings λ_H, λ_{4S} and $\lambda_{4\eta}$ is fixed from the requirement that the scalar potential is bounded from below. The input parameters are summarised in Table 6.3, and the details on the setup and implementation of the scan are described in [1]. For completeness, we mention that the model was implemented in `SARAH-4.14.` [148] and generate code for `SPheno-4.0.4` [149], `FlavorKit` [150] and `micrOMEGAS-5.2.7` [151]. The former two compute the mass spectrum and low energy observables, while the latter evaluates the DM relic density and the direct detection (DD) cross-sections. In the end, about 12000 points in parameter space were generated.

6.4.2 Results of the Scan

Couplings

Firstly, we examine the Yukawa couplings connecting the SM particles to the BSM fields, i.e. $g^i_{F_1}$, $g^i_{F_2}$, g^i_Ψ, and g^i_R, as these turn out to be relevant for leptogenesis. These are all three-component vectors and relevant for neutrino masses, the $(g-2)_\mu$ and LFV decays. Fig. 6.2 shows the correlations among the different components for each coupling vector, whereas Fig. 6.3 shows the correlation between selected components and the trilinear coupling α.

We clearly see that all components of $g_{F_{1,2}}$ behave in a similar manner, with an approximate upper limit of $|g^i_{F_{1,2}}| \lesssim 10^{-3}$ for $i = 1, 2, 3$. As already explained in Sec. 6.3, this upper limit is a result of our requirement to fit neutrino masses along with $(g-2)_\mu$, and adhering to constraints from $\mu \to e$ transitions. At the same time, the overall scaling behaviour of all the components of g_{F_1} is caused by the trilinear coupling α, which can be discerned from the left plot of Fig. 6.3. We find an analogous behaviour for g_{F_2}. Larger values of α imply larger scalar mixing, which then suppresses the scale of $g_{F_{1,2}}$ via the neutrino mass fit.

As already described in Sec. 6.3, g_Ψ requires a specific hierarchy among its components is realised to fit $(g-2)_\mu$, while being below the limits of cLFV searches. This hierarchy is reflected in g_R, as both these couplings contribute to these processes. This results in g^2_Ψ and g^2_R being large to fit $(g-2)_\mu$, where as $g^{1,3}_\Psi$ and $g^{1,3}_R$ need to remain small to not exceed the current limit on branching ratios of $\mu \to e\gamma$ and $\tau \to \mu\gamma$. Furthermore, fitting $(g-2)_\mu$ links g^2_R and g^2_Ψ with the trilinear coupling α, as shown in the plot of Fig. 6.3. As discussed in Sec. 6.3, the dominant contribution to $(g-2)_\mu$ and cLFV decays comes from the left diagram in Fig. 6.1, which is proportional to α. This implies that smaller values of α require larger values of g^2_Ψ and g^2_R to fit $(g-2)_\mu$. The perturbativity requirement for both these Yukawa couplings and α requires[3] 30 GeV $\lesssim \alpha \lesssim 4\, m_{\phi^0_1}$.

DM Observables

The $\mathbb{Z}_2$-odd parity of the BSM particles allows for three viable DM candidates: the lightest neutral fermion χ^0_1, the lightest scalar ϕ^0_1, and the pseudo-scalar A^0, depending on the mass hierarchies in a given parameter configuration.

[3] Note, that the upper bound is actually given for α/M_ϕ where M_ϕ is the average masses of the scalars involved in this coupling.

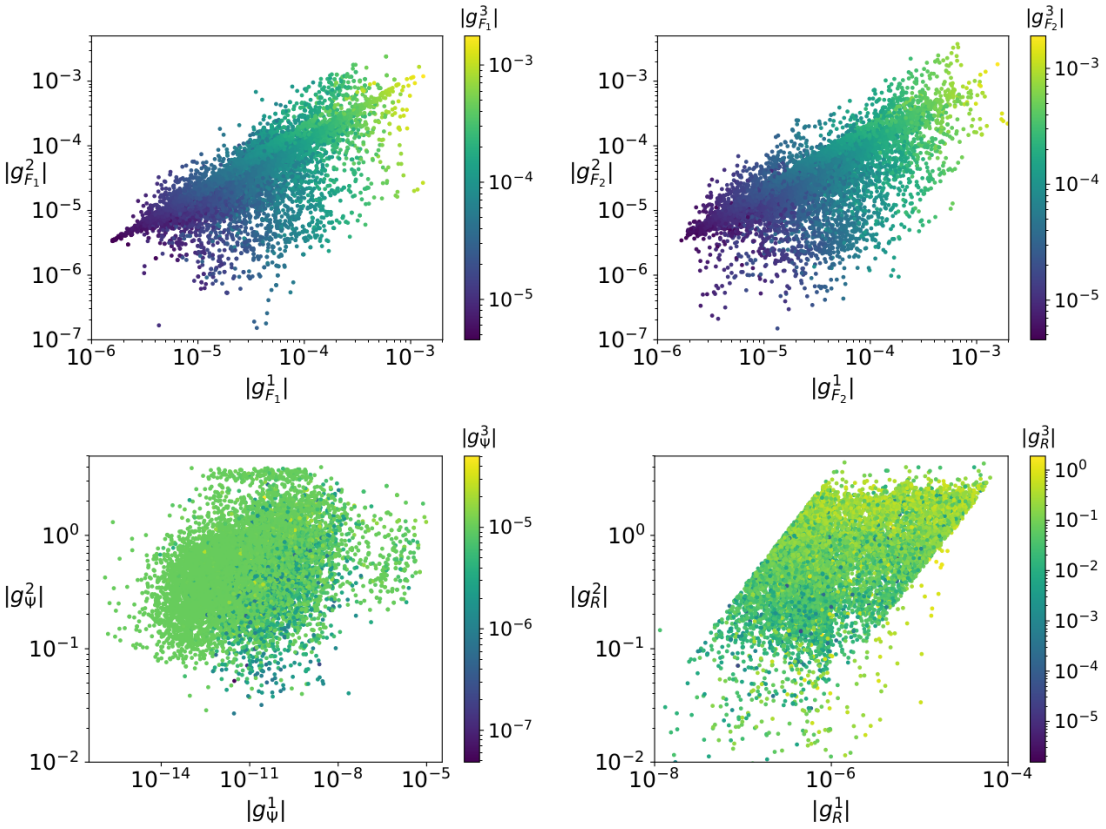

Figure 6.2: Distributions of the absolute values of the components of the Yukawa couplings g_{F_1} (upper left), g_{F_2} (upper right), g_Ψ (lower left) and g_R (lower right) obtained from the MCMC scan. The plots corroborate the hierarchy among the components, as enforced by the neutrino mass fit, accommodating $(g-2)_\mu$, and the constraints coming from cLFV processes.

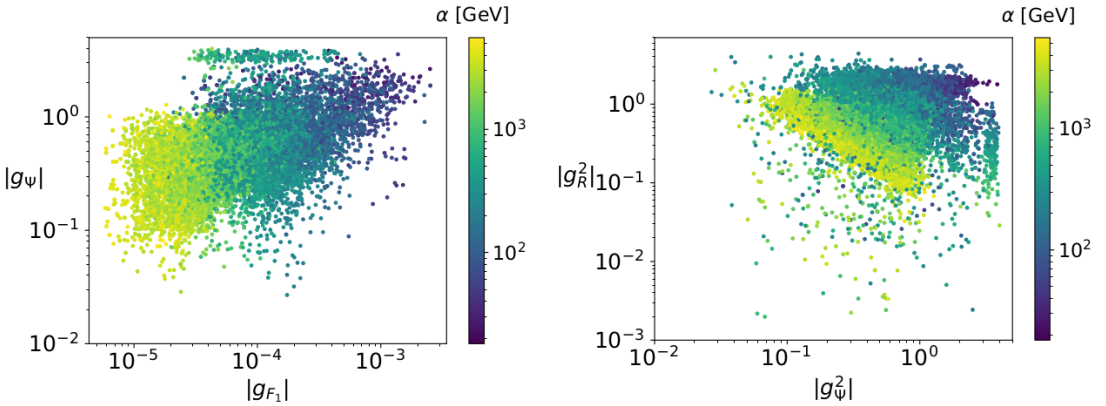

Figure 6.3: Correlation of selected Yukawa couplings with the trilinear coupling α. The couplings g_Ψ and g_{F_1} are connected to the trilinear couplings α through the fit of the neutrino masses, while the connection of g^2_Ψ and g^2_R with α stems from the fit of the anomalous magnetic moment $(g-2)_\mu$.

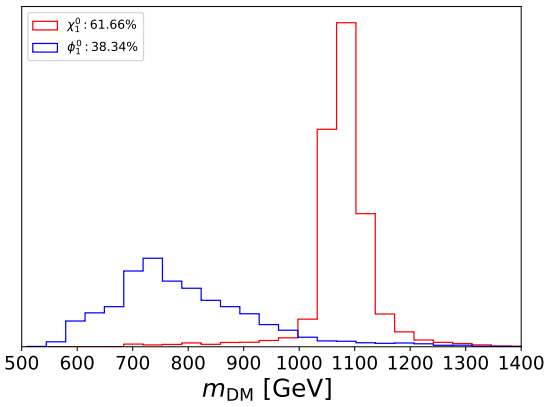

Figure 6.4: Histograms of the mass and nature of the DM candidate. The separation into fermionic and scalar DM clearly exhibits a preference for fermionic DM with a mass around 1100 GeV.

Fig. 6.4 shows the obtained distribution for the DM mass, separating fermionic (χ_1^0) and scalar (ϕ_1^0) DM, which is similar to the behaviour found in [113] for the T1-2-A scotogenic model. We observe that fermionic DM dominates the model parameter space, with a preferred mass of around 1100 GeV. Scalar DM accounts for about 38% of the viable parameter points, with preferred masses of about 600 to 1000 GeV.

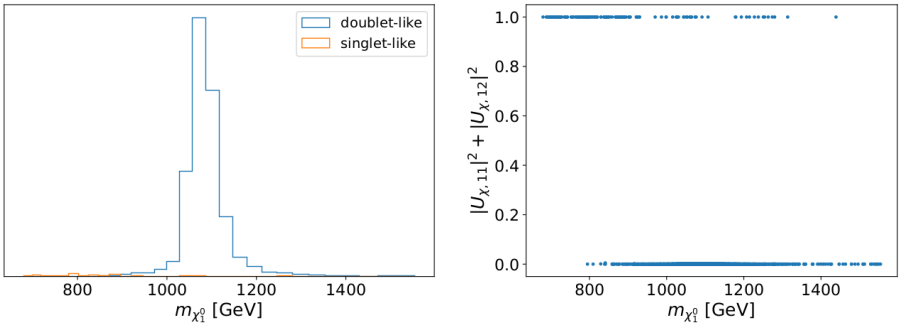

Figure 6.5: Left: Distribution of the masses in case of fermionic DM candidates, separating the scenarios where the DM candidate is doublet-dominated (blue line) from those where it is singlet-dominated (orange line). Right: singlet content of the DM candidate as a function of the DM mass.

Fig. 6.5 shows the that DM is essentially doublet-dominated, which can be traced to necessary co-annihilations [152] occurring naturally between the doublet-dominated state χ_1^0 and $\chi^\pm$ and χ_2^0, due to the very small mass splitting between these states. As already mentioned, sizeable Yukawa couplings to the muons are necessary to explain the potential deviation of its anomalous magnetic moment. This gives additional annihilation channels into muons via scalars, stemming from the doublet η in the t-channel. In case χ_1^0 is singlet-dominated, it is harder to satisfy the DM relic density [104]. While singlet fermions F_i are produced thermally, they can annihilate only via the Yukawa g_{F_i} or through the mixing with $\Psi_{1,2}$. Both these couplings are small because of cLFV constraints and accommodating $(g-2)_\mu$. In the case of scalar DM, the doublet-like states also dominate the phenomenologically viable parameter regions for similar reasons. Finally, we note that we do not find any pseudo-scalar DM in this model. The reason for this can be discerned by

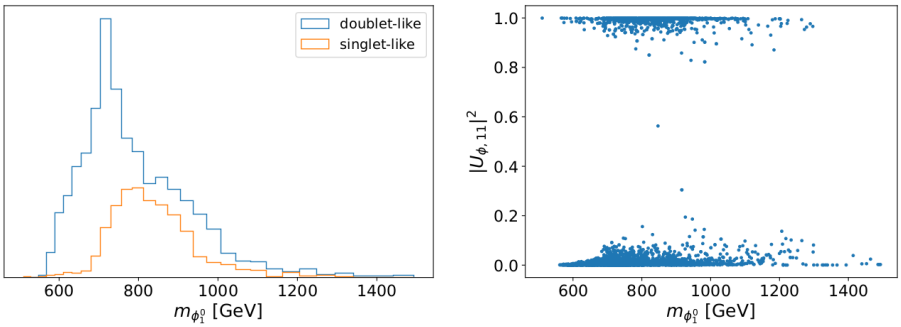

Figure 6.6: Left: Distribution of the masses in case of scalar DM candidates, separating the scenarios where the DM candidate is doublet-dominated (blue line) from those where it is singlet-dominated (orange line). Right: singlet content of the DM as a function of the DM mass.

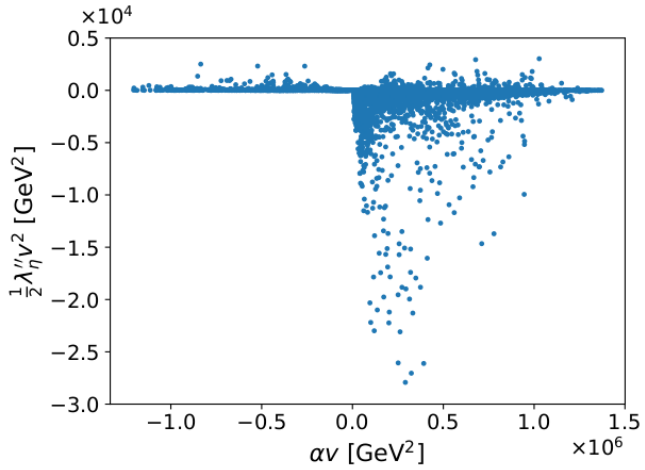

Figure 6.7: Contributions to the scalar mass matrix in equation (6.4).

inspecting the mass matrix given in (6.4). The mass splitting between the scalar doublet component and the pseudo-scalar is given by $\frac{1}{2}\lambda''_\eta v^2$ and the mixing between the doublet scalar and the singlet is given by $|\alpha v|$. For pseudo-scalar DM, one needs the doublet to be lighter than the singlet, which is not the case as can be seen in Fig. 6.7, implying that the scalar will always be lighter than the pseudo-scalar.

In Fig. 6.8, we show the results for the spin-independent DD cross-section for the scalar DM case. As mentioned earlier, the XENON1T [147] limit is taken as a constraint, such that points not satisfying the current limits are excluded. Most of the remaining viable points can be tested by future experiments like DARWIN [154].

In both cases, the direct detection cross-section is mainly dominated by Higgs exchange, since we actually have an inelastic dark matter candidate. Inelastic dark matter refers to DM candidates with a mass splitting between the CP-even and CP-odd components of a neutral state. As the Z-boson couples between the CP-even and CP-odd components, for the part of the parameter space where the mass splitting between these two states is larger than the kinetic energy of the DM, the contribution from Z channel to the DD cross-section is kinematically forbidden. Since the coupling of DM to the Z-boson is proportional to the gauge coupling, if it is active, then it will be excluded by direct detection. We note here that this contribution had to be calculated separately, as outlined in Appendix D,

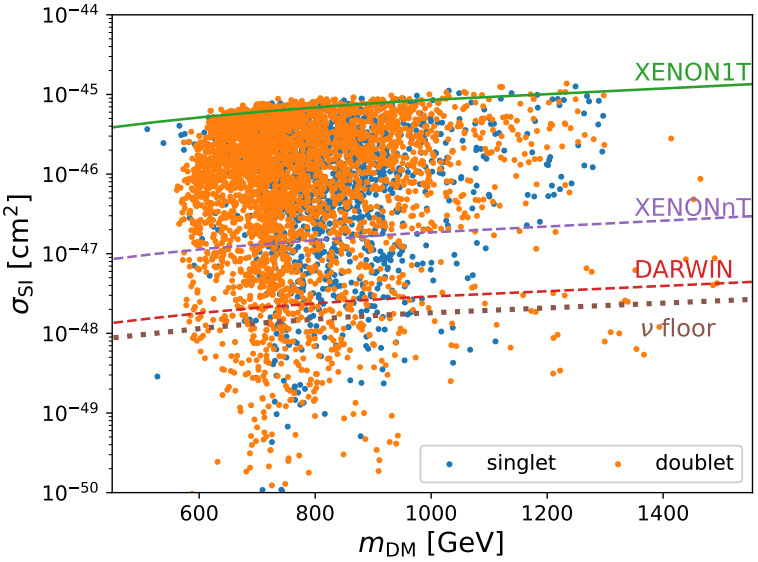

Figure 6.8: Spin-independent DD cross-section versus the mass of the DM in the scalar case, differentiating between singlet (blue) and double-like (orange). The current limit from XENON1T [147], as well as the future limits from XENONnT [153] and DARWIN [154] are given, as well as the corresponding line for the neutrino floor [155]. The fermionic DM case is not shown as the DD cross-section lays below the neutrino floor, around 10^{-60} cm^2.

as `micrOMEGAS` does not include inelastic channels. Nevertheless, this excluded very few points, as in practice given the typical DM average relative velocity, the mass splitting needs to be only larger than $\mathcal{O}(100)$ keV to kinematically close the Z-channel [156].

As the dominant channel for scattering is via Higgs exchange, we hence do not find any constraints in the case of fermionic DM. The reason for this is that our scan requires the modulus of the relevant Yukawa couplings, $|y_{ij}|$, to be smaller than 10^{-4}. The spin-independent cross section is hence suppressed and pushed well below the neutrino floor.

6.5 Leptogenesis

In order to study leptogenesis, we first identify sources of lepton number violation in this model. To this end, we assign lepton number to fields in this model, in a manner similar to the Type-I Seesaw model in Chap. 5. We start with the obvious choice of assigning lepton numbers $+1$ and -1 to the L_i and e_i^c. Requiring that the scalars H, η and S are not assigned lepton number, we proceed to determine the rest of the assignments by demanding the Yukawa terms, as far as possible, do not break lepton number. Looking at (6.8), this leads to assignments of -1 to the F_i and $+1$ to $\Psi_{1,2}$. As a consequence, this means that the parameters that break lepton number are the Majorana mass terms $M_{1,2}$, the Dirac mass term M_Ψ and the Yukawa coupling g_Ψ. Lepton number violation can hence essentially be switched off by setting all these parameters to 0. Our chosen lepton number assignments are summarised in Table 6.4.

Due to the large number of free parameters in this model, we will not attempt a scan of the parameter space. Instead, we focus on the region of parameter space outlined at the end of Sec. 6.3. Based on this, we note that we are in the region of parameter space where the couplings y_{ij}, which determine the mixing between the SU(2)$_L$ doublet and

	L_i	e_i^c	H	Ψ_1	Ψ_2	F_i	η	S
Lepton No.	1	-1	0	1	1	-1	0	0

Table 6.4: Summary of lepton number assignments to the fields in the model.

singlet fermions in (6.9), are small. Thus, in practice, only the singlet-like fermions will contribute to a possible lepton asymmetry. Further, we observed that there appears to be a preference for doublet-like DM (recall that this would be mixtures of neutral parts of $\Psi_{1,2}$) in this model, which provides more reason to focus on this region of parameter space, where (at least one of) the F_i can decay on-shell via its dominant decay modes $F_i \to L\eta\,(\overline{L}\eta^\dagger)$ and $F_i \to \Psi H\,(\overline{\Psi}H^\dagger)$ and produce a leptonic asymmetry.

As leptogenesis occurs above EWSB, it is more convenient to work in the gauge eigenstate basis. The tree-level decay widths for the aforementioned modes are given by

$$\Gamma_{\text{tree}}(F_i \to L\,\eta) = \Gamma_{\text{tree}}(F_i \to \overline{L}\,\eta^\dagger) \;=\; \sum_j \frac{|g^j_{F_i}|^2}{32\pi} M_i \left(1 - \frac{M_\eta^2}{M_i^2}\right)^2 \tag{6.19}$$

$$\Gamma_{\text{tree}}(F_i \to \Psi\,H) = \Gamma_{\text{tree}}(F_i \to \overline{\Psi}\,H^\dagger) \;= \\ \frac{M_i}{32\pi}\left\{(|y_{1i}|^2+|y_{2i}|^2)\left[1-\left(\frac{M_\Psi^2}{M_i^2}\right)^2\right] - 4\,\text{Re}[(y_{1i})^* y_{2i}]\,\frac{M_\Psi}{M_i}\left(1-\frac{M_\Psi^2}{M_i^2}\right)\right\}, \tag{6.20}$$

where we have neglected the masses of the SM leptons and Higgs boson. Note the mass insertion of the M_i in the decay width; as mentioned earlier, this is a parameter breaking lepton number, so it is natural for it to appear in these expressions. For later convenience, we define at this point

$$\Gamma^i_{\text{tot.}} = \Gamma_{\text{tree}}(F_i \to L\,\eta) + \Gamma_{\text{tree}}(F_i \to \overline{L}\,\eta^\dagger) + \Gamma_{\text{tree}}(F_i \to \Psi\,H) + \Gamma_{\text{tree}}(F_i \to \overline{\Psi}\,H^\dagger)\,. \tag{6.21}$$

6.5.1 CP Violation

The contributing diagrams to CP violation necessary for leptogenesis are displayed in Fig. 6.9. Similar to the Type-I seesaw model [89, 91], we have the typical wave-function and vertex diagrams depicted in the upper row involving the other singlet fermion in the loop. However there are additional possible vertex diagrams, which are depicted in the lower row, featuring the couplings g_R (left diagram) and g_Ψ and the trilinear coupling α (right diagram). Recall that these couplings played an important role in contributions to $(g-2)_\mu$, as discussed in Sec. 6.3.

The CP asymmetry parameter in this model is given by

$$\begin{aligned}\epsilon_i &= \frac{\Gamma(F_i \to L\,\eta) + \Gamma(F_i \to \psi\,H) - \Gamma(F_i \to \bar{L}\,\eta^\dagger) - \Gamma(F_i \to \bar{\psi}\,H^\dagger)}{\Gamma(F_i \to L\,\eta) + \Gamma(F_i \to \psi\,H) + \Gamma(F_i \to \bar{L}\,\eta^\dagger) + \Gamma(F_i \to \bar{\psi}\,H^\dagger)} \\ &\approx \frac{\Gamma(F_i \to L\,\eta) + \Gamma(F_i \to \psi\,H) - \Gamma(F_i \to \bar{L}\,\eta^\dagger) - \Gamma(F_i \to \bar{\psi}\,H^\dagger)}{\Gamma_{\text{tot.}}}\,,\end{aligned} \tag{6.22}$$

where in the second step, we neglect the loop-level decay widths in the denominator. Note that we have summed over the flavours of the final state leptons, and hence focus on the

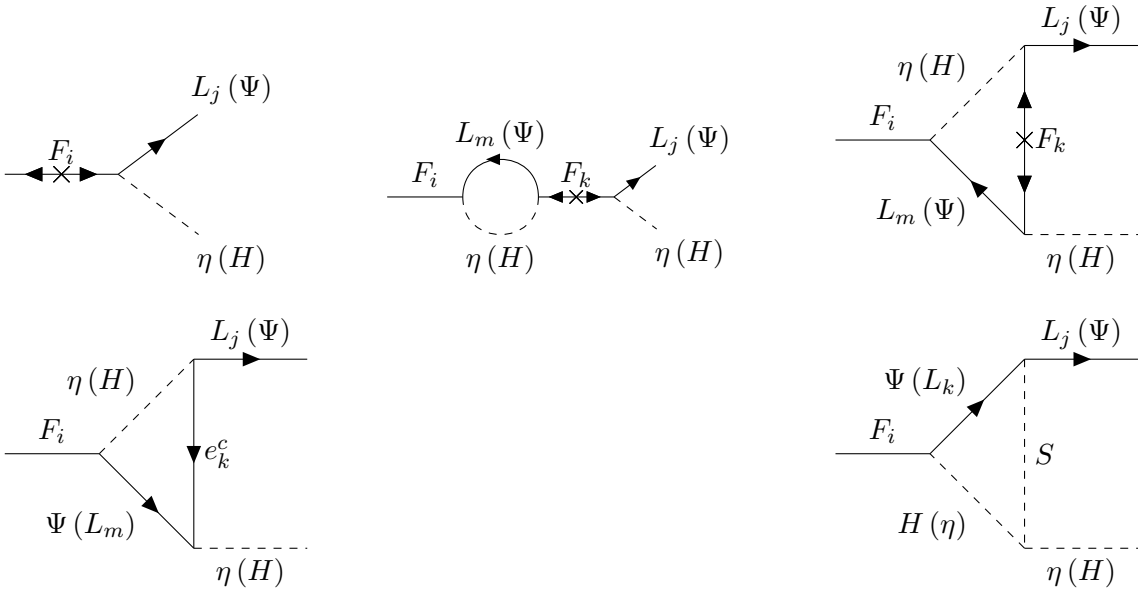

Figure 6.9: Diagrams contributing to the CP asymmetry generated in the decays of F_i $(i = 1, 2)$. Upper row: diagrams that are similar to the ones obtained in the type-I seesaw model. The arrows indicate the flow of lepton number. Note that another self-energy diagram exists with the mass insertion of F_i instead, by reversing the arrow of $L_m\,(\Psi)$. Lower row: Additional vertex diagrams contributing to the CP asymmetry generated in the decays of the singlet fermions F_i.

"total lepton number violation". Obtaining the different contributions to the ϵ_i leads to rather cumbersome expressions and thus, these are delegated to Appendix E, where an outline of the calculation and a compilation of these expressions can be found.

6.5.2 Washout

Having determined the asymmetry, we now need to determine to what extent it survives till present date, for which we examine the decay parameters of the F_i. Using (5.18), we have for this model,

$$K_i \equiv \frac{\Gamma^i_{\text{tot.}}}{H(T = M_i)} \simeq 7 \times 10^6 \left(\frac{\max\{|g_{F_i}|\}}{10^{-3}}\right)^2 \left(\frac{\text{TeV}}{M_i}\right) , \tag{6.23}$$

where in the second part of the above equation, we refer to the discussion in the beginning of Sec. 6.4.2, where the MCMC yielded that in general, either $\max(|g^k_{F_i}|) \gg \max(|y_{ij}|)$ or they are of equal size. Thus, we may take the decay $F_i \to L_j\eta$, via the g_{F_i} coupling, to be the dominant decay mode for the F_i. Furthermore, based on the parameter space discussed in Sec. 6.4.2, we are always in the strong washout regime (see Sec. 5.2), evident from the second part of (6.23). As an example, we display K_1 in (6.10). For completeness, we note that, although we based our estimations on g_{F_i}, all parameters were properly taken into account in the numerics. These large values of the decay parameter allow us to neglect washout through scattering processes, as the inverse decays are the main sources of the washout.

6.5.3 Results

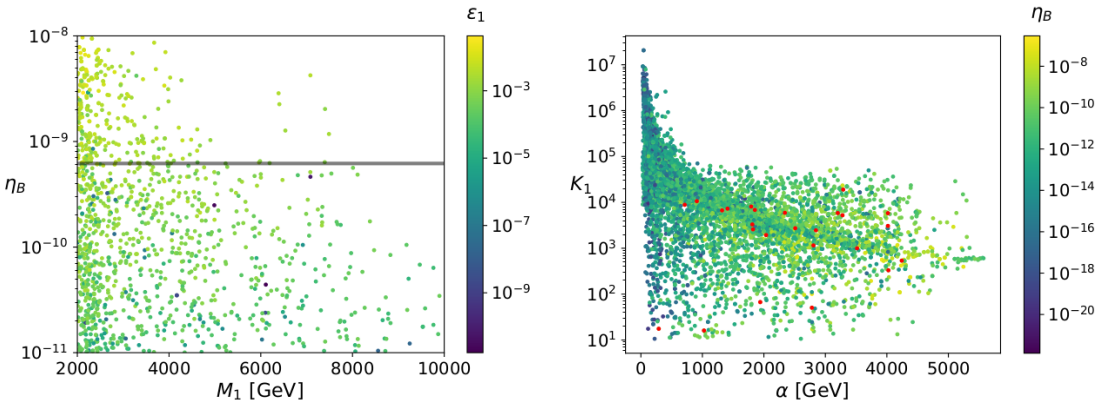

Figure 6.10: Left: resulting baryon-to-photon ratio η_B plotted against the mass of the lighter singlet fermion driving leptogenesis. The solid grey line denotes the observed value of η_B from Planck. The CP asymmetry generated in the decays of the singlet fermion is indicated by the hue. Right: Decay parameter K_1 of the lighter singlet fermion versus the absolute value of the trilinear coupling α. The value of η_B is indicated by the hue. The points in red are within the grey band on the plot to the right.

We solve numerically the corresponding Boltzmann equations given in Sec. 5.2 with the following initial conditions at $T = 10^4 M_2$ implying $z_1 \ll 1$

$$N_{F_1} = N_{F_1}^{\text{eq.}}, \qquad N_{F_2} = N_{F_2}^{\text{eq.}}, \qquad N_{B-L} = 0, \tag{6.24}$$

and track these number densities down to lower temperatures, $z_1 = 200$. Unlike usual thermal leptogenesis implemented in Seesaw models, we do not assume a large hierarchy between the masses of F_1 and F_2, meaning we account for the decays of both in our Boltzmann equations [99].

As mentioned in Sec. 5.3, we need the inverse decays of the singlet fermions to freeze-out at a temperature before the sphalerons fall out of equilibrium ($T \sim 100$ GeV); otherwise, the leptonic asymmetry generated in their decays is not converted into a baryonic asymmetry. As we are in the strong washout regime, we can estimate the freeze-out temperature for the inverse decays as [157],

$$T_{\text{F.O.}}^{\text{ID}} \approx \frac{M_i}{5\sqrt{\log(K_i)}}. \tag{6.25}$$

This gives an approximate lower bound on the mass of the lightest decaying singlet $M_i \gtrsim 2\,\text{TeV}$ for which the sphalerons remain active.

At lower temperatures, $T \ll \min\{M_1, M_2\}$, we obtain the final $B-L$ number density $N_{B-L}^{\text{fin.}}$, which is converted to the baryon-to-photon ratio, η_B, via the sphaleron process

$$\eta_B \approx \frac{3}{4}\left(\frac{8}{23}\right)\frac{43/11}{122.25}\,|N_{B-L}^{\text{fin.}}| \simeq 8\times 10^{-3}\,|N_{B-L}^{\text{fin.}}|, \tag{6.26}$$

where the sphaleron conversion factor, c.f. (5.23), was calculated with $N_f = 3$ and $N_D = 2$ and $g_* = 122.25$ due to the additional particle content of the model.

Fig. 6.10 depicts the final baryon-to-photon ratio obtained from solving the Boltzmann equations, using the sets of parameters mentioned before, against the mass of the singlet

fermion driving leptogenesis. We observe that in contrast to the typical case of strong washout in the Type-I Seesaw model and the "classic" scotogenic model [158], the final value of η_B has a tendency to decrease with increasing M_1. Besides, we also find that the CP asymmetries generated in the decays of lighter F_1 are much larger. We note large contributions to ϵ_i come from the loop diagrams in the lower row of Fig. 6.9.

In the minimal scotogenic model, it is possible to express the decay parameter (5.18) as a function of the lightest neutrino mass and the λ''_η parameter [158]. In our model, the link is not so direct due to the additional couplings and particle states present. Moreover, the requirement to explain the potential deviation of the $(g-2)$ of the muon while being consistent with the bounds on the LFV decays requires, for example, larger values of the trilinear coupling α. As can be seen from the left plot in Fig. 6.10, the decay parameter decreases with increasing $|\alpha|$. While this coupling does not appear directly in the calculation of the decay parameter (6.23), it reduces the value of the coupling g_{F_i} through the neutrino fit, which in turn decreases the tree-level decay width and, hence, lowers the value of K_i.

From the right plot in Fig. 6.10, there are 25 points able to explain the observed baryon asymmetry, within the observed limit [11]. We also observe that all these points feature doublet-dominated χ_1^0 as a DM candidate, except for one which has singlet dominated ϕ_1^0 as a DM candidate.

6.6 Summary and Outlook

In this chapter, we studied a scotogenic model with a very rich phenomenology. We presented a numerical analysis of the associated parameter space, taking into account constraints from SM neutrino masses sector, LFV processes, the muon anomalous magnetic moment and DM observables.

Neutrino data governed the couplings of the new particles to the left-handed leptons and the requirement of explaining the observed deviation of the anomalous magnetic moment of the muon $(g-2)_\mu$ required sizeable couplings to muons. Imposing the constraint of the dark matter relic density led to a preference of fermionic dark matter, which is doublet-like in the mass range 1 to 1.2 TeV, and whose cross-sections were well below the neutrino floor. However, scenarios featuring scalar dark matter can be tested by future direct detection experiments like XENONnT or DARWIN.

Finally, requiring successful leptogenesis in addition resulted in the available parameter space being severely constrained. Almost all the viable points in the parameter space featured a fermionic dark matter candidate. This specific region of parameter space may be scrutinised further, and improvements may be made along the lines of tracking the asymmetry along leptonic flavours, as our requirements of fitting $(g-2)_\mu$ resulted in larger couplings to muons. Thus, this may have an impact in the production of an asymmetry in the muon flavour, and ultimately the baryon asymmetry.

Chapter 7

Conclusion and Outlook

Based on observations, we are convinced that the observable Universe presently consists primarily of matter, with little to no anti-matter. To resolve this mystery of "missing" anti-matter, we require an asymmetry between the baryons and anti-baryons before the onset of proton formation. Within the Standard Model (SM) of particle physics there exists no feasible mechanism to dynamically generate this baryon asymmetry, and hence demands new physics. In this thesis, we considered two approaches aimed at addressing this long standing issue in particle physics.

The first approach was presented in Part I, where we introduced the two-particle irreducible (2PI) formalism in Chapter 2, as a means to study non-equilibrium phenomena. After motivating and establishing the framework, we arrived at the 2PI effective action and the corresponding equations of motion (EOMs) to describe the evolution of the one-point function and the propagators. In order to obtain self-consistent results, these must be renormalised.

With this task in mind, we began Chapter 3 by describing the complexities of renormalisation arising due to the resummed nature of the propagator in the 2PI formalism. We proceeded to write down the renormalised 2PI effective action and outlined the tools required to obtain the counterterms in an on-shell scheme. As an application of our methods, we considered three separate truncations, up to two-loop order, namely the Hartree approximation, the scalar sunset approximation and the fermionic sunset approximation. We focused on obtaining the counterterms and renormalised quantities in the broken phase. For the Hartree approximation, we found that the renormalised propagator was identical to the bare one and all counterterms were finite. In the scalar sunset approximation, we found that the inclusion of the scalar sunset diagram led to many of the counterterms no longer being finite. Moreover, the propagator could only be determined through a numerical solution to the gap equation, for which we used an iterative scheme. We demonstrated that even for the choice of large couplings, our iterative scheme converges rapidly and one could, for practical purposes, use the solution obtained at the first iteration. Finally, we extended our toolkit to include fermions in the 2PI formalism, when considering the fermionic sunset approximation. To our knowledge, renormalisation of the 2PI effective with fermions has not been treated extensively in the literature, and our techniques are im-

mediately applicable to higher-loop truncations involving fermions. Using our techniques, we found that none of the counterterms were finite. Moreover, we obtained a coupled system of gap equations to determine the form of the fermionic and scalar propagators, for which we again applied our iterative approach. For a large Yukawa coupling, we still observed convergence for successive iterations.

The application of our methods would be to obtain the counterterms for the renormalised EOMs, which can be used to study bubble evolution during a phase transition. Furthermore, the techniques for renormalisation in the 2PI formalism involving fermions that we have outlined allow one to consistently include their effects in the renormalised EOMs. The renormalised EOMs with fermions provide an excellent starting point to study electroweak baryogenesis, as they feature in the transport equations. Furthermore, we propose that our analysis can be analogously performed to extend the renormalisation toolkit to consider gauge bosons, through careful tracking of Lorentz indices. With this, we would have the full setup to investigate the electroweak phase transition (EWPT).

In Chapter 4, we presented an alternative method to renormalise the 2PI effective action in an $\overline{\text{MS}}$ scheme, which is more suitable to calculate the 2PI effective potential. This method was based on identifying manifestly finite quantities in the gap equation and obtaining the counterterms from cancellation conditions derived from equations involving divergent parts of various loop integrals. We considered the same truncations that we had in the previous chapter. For the Hartree approximation, the procedure was simplified due to the fact that the propagator was identically the bare one. The counterterms obtained also matched the ones determined from our on-shell scheme. Subsequently, we obtained the effective potential in the Hartree approximation and compared it to the Coleman-Weinberg (CW) effective potential and tree-level potential. We observed that the CW potential offers a very small correction to the tree-level potential, whereas the 2PI effective potential provides a more pronounced correction. The vacuum expectation value (VEV) for all three potentials occurred at nearly the same field value. We next considered the scalar sunset approximation, which was more involved due to the fact established in Chapter 3, that the propagator needs to be determined through a numerical solution to the gap equation. To this end, we used an auxiliary Pauli-Villars propagator to extract divergences from the various loop integrals. This allowed us to obtain the required cancellation conditions to determine the counterterms in terms of divergent parts of loop integrals over the auxiliary propagator. As these loop integrals involving the auxiliary propagator could be evaluated analytically using dimensional regularisation, we were able write down explicit expressions for the counterterms. Having carefully tracked and pieced together the finite contributions, we were subsequently able to evaluate the 2PI effective potential in the scalar sunset approximation in a transparent manner, which, as far as we know, has not been reported in the literature and constitutes a novel result. Finally, we attempted a similar analysis for the fermionic sunset approximation, where complications arose due to the presence of infinite wave-function renormalisations, which led to modifications in the UV behaviour of both the scalar and fermionic propagators. We attempted a similar analysis using appropriately defined auxiliary propagators, which allowed us to obtain the cancellation conditions. Although the divergent structures of these integrals are known, they cannot be evaluated analytically like in the scalar sunset approximation, owing to which we could not give explicit expressions for the counterterms. Consequently, we could not calculate the effective potential, because the finite parts required from the very same integrals could not be extracted.

The 2PI effective potential with fermionic contributions would allow one to address

issues such as vacuum stability of the SM. Also, we have noted that in the Hartree and the scalar sunset approximations that the corrections to the tree-level potential appear to be small. This is because we have restrained ourselves to the zero temperature field theory; the next natural step would be to include finite temperature effects, where we would expect the loop-level effects to be more prominent. With this, one could immediately study phase transitions in models with additional scalars and other non-equilibrium phenomena, such as reheating after inflation. Finally, having worked out the fermionic contribution, the full temperature corrected 2PI effective potential would provide an insight in the case of very strong transitions, and in particular when there are strongly interacting relatively heavy states contributing to dynamics. This is relevant in the SM, where we know the top quark is much more massive than the SM Higgs. This would thus offer a a self-consistent tool to investigate the electroweak phase transition.

Progressing to Part II, we presented in Chapter 5 our second approach through leptogenesis. We described the essential features of leptogenesis, using the Type-I Seesaw Lagrangian as a pedagogical example. We showed that lepton number violation, CP violation and out-of-equilibrium decays of newly introduced heavy neutrinos, tracked by Boltzmann equations, lead to a lepton asymmetry. This lepton asymmetry is then converted into the required baryon asymmetry through the sphaleron process in the SM.

In Chapter 6, we extended the Standard Model through the framework of a scotogenic model, characterised by radiative generation of SM neutrino masses along with a suitable dark matter (DM) candidate due to an imposed $\mathbb{Z}_2$ symmetry on the new fields. After describing the full model in detail, we considered various constraints on the couplings coming from neutrino oscillation data, limits on branching ratios of charged lepton flavour violating processes, electroweak and dark matter (DM) observables. Using the the results of a Markov Chain Monte Carlo scan to obtain the parameter space consistent with these constraints and adhering to the observed value of the anomalous magnetic moment of the muon, $(g-2)_\mu$, we examined the various couplings relevant for leptogenesis. For DM phenomenology, we observed the parameter space favoured primarily fermionic doublet-like DM. This ascertained parameter space was used to examine the impact on leptogenesis in this model. The heavy Majorana fermionic singlets, decaying out-of-equilibrium, sourced the required lepton asymmetry, for which we numerically solved a set of Boltzmann equations. This was converted appropriately into the baryon asymmetry and compared with the observed limit from Planck. We found that very few points in the parameter space could explain the baryon asymmetry of Universe. This specific region of parameter space may be scrutinised further, and improvements may be made along the lines of tracking the asymmetry along leptonic flavours, as our requirements of fitting the observed value of $(g-2)_\mu$ resulted in larger couplings to muons. Further, we observed a correlation between couplings required to explain $(g-2)_\mu$ value and the decay parameter, which governed the efficiency of out-of-equilibrium decays of the fermionic singlets.

To summarise, this thesis offered insights into avenues through which the problem of the matter asymmetry of the Universe can be addressed. This was through two different approaches: *(i)* using 2PI methods to ultimately study the electroweak phase transition and electroweak baryogenesis in a consistent manner and *(ii)* through the viewpoint of model building, describing the interplay between leptogenesis and various other unresolved phenomena in the Standard Model of particle physics.

APPENDICES

Appendix A

Loop Integrals 101

In this appendix, we will go through the methods required to resolve the various loop integrals that appear throughout this thesis. We first outline the procedure to handle loop integrals in the framework of dimensional regularisation (dim. reg.) and discuss various examples of Passarino-Veltman functions that appear throughout this thesis. Finally, we describe the numerical implementation of these integrals in four dimensional Euclidean space.

A.1 Dimensional Regularisation

Note that we will work primarily in four-dimensional Minkowski space-time for this section, with the metric signature. Quantities in Euclidean coordinates will be explicitly specified with a subscript E. We will also typically use the shorthand notation $\int_l = \int \frac{d^d l}{(2\pi)^d}$.

The following tools are useful in dimensional regularisation

- **Feynman Parameters:** Typically, to combine multiple propagator denominators appearing in the loop integrals, one makes use of Feynman parameters.

$$\frac{1}{A_1^{a_1} A_2^{a_2} \dots A_n^{a_n}} = \tag{A.1}$$

$$\frac{\Gamma(a_1 + a_2 + \dots + a_n)}{\Gamma(a_1)\Gamma(a_2)\dots\Gamma(a_n)} \int_0^1 dx_1 dx_2 \dots dx_n \frac{\delta(1 - x_1 - x_2 - \dots - x_n)\, x_1^{a_1-1} x_2^{a_2-1} \dots x_n^{a_n-1}}{[A_1 x_1 + A_2 x_2 + \dots + A_n x_n]^{(a_1+a_2+\dots+a_n)}} . \tag{A.2}$$

  Note the $\delta-$function which results in the variables not being linearly independent of each other. Specifically, for two denominators, with $a_1 = a_2 = 1$ we end up with

$$\frac{1}{A_1\, A_2} = \int_0^1 dx \frac{1}{[A_1 x + A_2(1-x)]^2} \tag{A.3}$$

- **Gamma Function Expansions:** The following expansion of the Gamma function, $\Gamma(n)$, about its poles are useful in extracting divergent parts:

$$\Gamma(x - n) = \frac{(-1)^n}{n!} \left(\frac{1}{x} + \psi(n+1) + \mathcal{O}(x) \right) , \qquad \text{for} \qquad n \geq 0 \tag{A.4}$$

where $\psi(z)$ is the **Euler digamma function**, with the following properties

$$\psi(n+1) = \frac{1}{n} + \psi(n)\,, \qquad \psi(1) = -\gamma_{\mathrm{E}}\,.$$

Here, γ_{E} is the Euler-Mascheroni constant.

A.1.1 Scalar Integrals

Using the Feynman parameters, we obtain a structure of the form $(l^2-\kappa)^{-n}$, after appropriately completing the square and shifting variables to l for the loop momentum. To progress, we perform a Wick rotation $l^0 = il_E^0$, such that $l^2 = -l_E^2$. After these transformations, the resulting integral may be evaluated by converting to n-dimensional spherical polar coordinates, where we may make use of the following results:

- the angular integration over the solid angle of a d-dimensional unit sphere

$$\int d\Omega_d = \frac{2\pi^{\frac{d}{2}}}{\Gamma\left(\frac{d}{2}\right)} \tag{A.5}$$

- to resolve the radial integral, we make use of the following special integral

$$\int_0^\infty dz\, \frac{z^a}{(z^2+1)^b} = \frac{\Gamma\left(\frac{a+1}{2}\right)\,\Gamma\left(b-\frac{(a+1)}{2}\right)}{2\,\Gamma\left(b\right)} \tag{A.6}$$

We now apply all of this to the following scalar integral

$$\begin{aligned}
\int_l \frac{1}{(l^2-\kappa)^n} &= i\int \frac{d^dl_E}{(2\pi)^d}\frac{1}{(-l_E^2-\kappa)^n} = \frac{(-1)^n i}{(2\pi)^d}\int_0^\infty dl_E \frac{l_E^{d-1}}{(l_E^2+\kappa)^n}\int d\Omega_d \\
&= \frac{(-1)^n i}{(2\pi)^d}\left[\int_0^\infty dz \frac{z^{d-1}}{(z^2+1)^n}\right]\left[\int d\Omega_d\right]\left(\frac{1}{\kappa}\right)^{n-\frac{d}{2}}, \quad \text{where} \quad z^2 = \frac{l_E^2}{\kappa} \\
&= \frac{(-1)^n i}{(2\pi)^d}\left[\frac{\Gamma\left(\frac{d}{2}\right)\,\Gamma\left(n-\frac{d}{2}\right)}{2\,\Gamma\left(n\right)}\right]\left[\frac{2\pi^{\frac{d}{2}}}{\Gamma\left(\frac{d}{2}\right)}\right]\left(\frac{1}{\kappa}\right)^{n-\frac{d}{2}} \\
&= \frac{(-1)^n i}{(4\pi)^{\frac{d}{2}}}\frac{\Gamma(n-\frac{d}{2})}{\Gamma(n)}\left(\frac{1}{\kappa}\right)^{n-\frac{d}{2}}\,.
\end{aligned} \tag{A.7}$$

To regulate UV divergences, one sets $d = 4-2\epsilon$, where $\epsilon > 0$. In the limit of $\epsilon \to 0$, one recovers four spacetime dimensions, and hence the UV divergences are captured in poles of the form ϵ^{-n}.

Consider now the scalar one-point integral, denoted as $A_0(m^2)$ in the notation of Passarino and Veltman,

$$\begin{aligned}
A_0(m^2) &\equiv \frac{(2\pi Q)^{4-d}}{i\pi^2}\int d^dq \frac{1}{(q^2-m^2)} = \frac{(2\pi Q)^{4-d}}{i\pi^2}(2\pi)^d\left[-\frac{i}{(4\pi)^{\frac{d}{2}}}\frac{\Gamma(1-\frac{d}{2})}{\Gamma(1)}\left(\frac{1}{m^2}\right)^{1-\frac{d}{2}}\right] \\
&= m^2\left[-(4\pi Q^2)^\epsilon\,\Gamma(\epsilon-1)\,(m^2)^{-\epsilon}\right]
\end{aligned}$$

$$= m^2 \left[\frac{1}{\epsilon} + 1 - \gamma_{\mathrm{E}} + \mathcal{O}(\epsilon)\right] \left[1 + \log\left(\frac{4\pi Q^2}{m^2}\right) + \mathcal{O}(\epsilon)\right]$$
$$= m^2 \left[\frac{1}{\epsilon} - \gamma_{\mathrm{E}} + 1 + \log\left(\frac{4\pi Q^2}{m^2}\right) + \mathcal{O}(\epsilon)\right] \equiv m^2 \left[\frac{1}{\epsilon} + 1 + \log\left(\frac{\overline{Q}^2}{m^2}\right) + \mathcal{O}(\epsilon)\right] \tag{A.8}$$

where we have used (A.4) and $a^x = 1 + x\log(a) + \mathcal{O}(x^2)$ in the third step. Here, Q^2 is a factor that arises typically from ensuring the various couplings remain dimensionless when one goes to d dimensions [2, 3]; it is typically related to a renormalisation scale. We have additionally defined the quantity $\overline{Q}^2 = 4\pi e^{-\gamma_{\mathrm{E}}} Q^2$ in the last step.

Next, we take a look at the two-point function B_0,

$$B_0(p^2, m_1^2, m_2^2) \equiv \frac{(2\pi Q)^{4-d}}{i\pi^2} \int d^d q \frac{1}{(q^2 - m_1^2)[(q+p)^2 - m_2^2]}$$
$$= \frac{(2\pi Q)^{4-d}}{i\pi^2} (2\pi)^d \int_0^1 dx \int_l \frac{1}{(l^2 - \kappa(x))^2}, \quad \text{where} \quad l = q + px$$
$$= \int_0^1 dx \left[\Gamma(\epsilon)\left(\frac{4\pi Q^2}{\kappa(x)}\right)^{\epsilon}\right] = \frac{1}{\epsilon} + \int_0^1 dx \log\left(\frac{\overline{Q}^2}{\kappa(x)}\right) + \mathcal{O}(\epsilon) \tag{A.9}$$

where we have made use of the Feynman parameter x to combine the denominators as in (A.3). Note that p is the external momentum and hence, a constant with respect to the q integration. This allows us to perform the described linear shift to l in the second step. On appropriately completing the square, one obtains the following quantity

$$\kappa(x) = m_1^2\, x + m_2^2\,(1-x) - p^2 x(1-x)\,. \tag{A.10}$$

We also define the scalar three-point function C_0,

$$C_0(p_1^2, p_2^2, p_1\cdot p_2; m_1^2, m_2^2, m_3^2) = \frac{(2\pi Q)^{4-d}}{i\pi^2} \int d^d q \frac{1}{(q^2 - m_1^2)[(q+p_1)^2 - m_2^2][(q+p_2)^2 - m_3^2]}$$
$$= \frac{(2\pi Q)^{4-d}}{i\pi^2} (2\pi)^d\, 2 \int_0^1 \int_0^{1-x} dy \int_l \frac{1}{(l^2 - \alpha(x,y))^3} \quad \text{where} \quad l = q + p_1 x + p_2 y$$
$$= 2\int_0^1 dx \int_0^{1-x} dy \left[\frac{\Gamma(\epsilon+1)}{\Gamma(3)} \left(\frac{4\pi Q^2}{\alpha(x,y)}\right)^{\epsilon} \frac{1}{\alpha(x,y)}\right] \tag{A.11}$$

where x and y are the two Feynman parameters required to combine the denominators, and $\alpha(x,y)$ is the quantity

$$\alpha(x,y) = m_1^2\,(1-x-y) + m_2^2\, x + m_3^2\, y - p_1^2 x(1-x) - p_2^2 y(1-y) + 2p_1\cdot p_2 xy\,. \tag{A.12}$$

Note that the C_0 function does not diverge for $\epsilon \to 0$, so we may take this limit safely. This gives us the following UV finite expression

$$C_0(p_1^2, p_2^2, p_1\cdot p_2; m_1^2, m_2^2, m_3^2)$$
$$= \int_0^1 \int_0^{1-x} \frac{dx\, dy}{m_1^2\,(1-x-y) + m_2^2\, x + m_3^2\, y - p_1^2 x(1-x) - p_2^2 y(1-y) + 2p_1\cdot p_2 xy}\,. \tag{A.13}$$

One can similarly define the scalar D_0 function, involving four propagators, which is also UV finite. For completeness' sake, we note that there may be infrared (IR) divergences in the C_0 and D_0 functions, in various kinematic limits.

The last scalar integral we discuss is rather important in the context of the effective potential

$$\begin{aligned}\frac{(2\pi Q)^{4-d}}{i\pi^2}\int d^dq\log G^{-1} &= \frac{(2\pi Q)^{4-d}}{i\pi^2}\int d^dq\log\left(q^2-m^2\right)\\ &= \frac{(2\pi Q)^{4-d}}{i\pi^2}\int d^dq\left[-\int dm^2\frac{1}{q^2-m^2}\right]\\ &= -\int dm^2A_0(m^2) = -\frac{m^4}{2}\left[\frac{1}{\epsilon}+\frac{3}{2}+\log\left(\frac{\overline{Q}^2}{m^2}\right)+\mathcal{O}(\epsilon)\right]+\text{const.}\end{aligned} \tag{A.14}$$

A.1.2 Tensor Integrals and Passarino-Veltman Reduction

By using Lorentz covariance in d dimensions, it is possible to reduce tensor integrals in terms of scalar integrals [159]. The simplest example, which has been used in this thesis, in the context of loop integrals involving fermionic propagators, is given by

$$B^\mu(p^2,m_1^2,m_2^2) = \frac{(2\pi Q)^{4-d}}{i\pi^2}\int d^dq\,\frac{q^\mu}{(q^2-m_1^2)[(q+p)^2-m_2^2]}\,. \tag{A.15}$$

We can then use Lorentz covariance to write

$$B^\mu(p^2,m_1^2,m_2^2) = p^\mu\,B_1(p^2,m_1^2,m_2^2) \tag{A.16}$$

and then contract both sides with p_μ to yield

$$p^2B_1(p^2,m_1^2,m_2^2) = p_\mu B^\mu(p^2,m_1^2,m_2^2) = \frac{(2\pi Q)^{4-d}}{i\pi^2}\int d^dq\,\frac{p\cdot q}{(q^2-m_1^2)[(q+p)^2-m_2^2]}\,. \tag{A.17}$$

We can then use the identity

$$p\cdot q = \frac{(p+q)^2-p^2-q^2}{2} = \frac{\left[(p+q)^2-m_2^2\right]-(q^2-m_1^2)-p^2+m_2^2-m_1^2}{2}$$

to separate out the various integrals. Dividing out both sides of (A.17) by p^2 gives us

$$\begin{aligned}B_1(p^2,m_1^2,m_2^2) = \frac{1}{2p^2}\Bigg[&\frac{(2\pi Q)^{4-d}}{i\pi^2}\int d^dq\,\frac{1}{(q^2-m_1^2)} - \frac{(2\pi Q)^{4-d}}{i\pi^2}\int d^dq\,\frac{1}{(p+q)^2-m_2^2)}\\ &-\left[p^2-m_2^2+m_1^2\right]\frac{(2\pi Q)^{4-d}}{i\pi^2}\int d^dq\,\frac{1}{(q^2-m_1^2)[(p+q)^2-m_2^2)]}\Bigg]\\ =\ &\frac{A_0(m_1^2)-A_0(m_2^2)+(m_2^2-m_1^2)B_0(p^2,m_1^2,m_2^2)}{2p^2} - \frac{B_0(p^2,m_1^2,m_2^2)}{2}\,.\end{aligned} \tag{A.18}$$

We use the fact that the difference of two A_0 functions can actually be written as a B_0 at zero external momentum

$$A_0(m_1^2) - A_0(m_2^2) = \frac{(2\pi Q)^{4-d}}{i\pi^2} \int d^d q \, \frac{(-m_2^2 + m_1^2)}{(q^2 - m_1^2)(q^2 - m_2^2)} = -(m_2^2 - m_1^2) B_0(0, m_1^2, m_2^2) \,, \tag{A.19}$$

so the B_1 can be re-expressed as

$$B_1(p^2, m_1^2, m_2^2) = \frac{(m_2^2 - m_1^2)}{2p^2} \left[B_0(p^2, m_1^2, m_2^2) - B_0(0, m_1^2, m_2^2) \right] - \frac{B_0(p^2, m_1^2, m_2^2)}{2} \,. \tag{A.20}$$

Similar techniques can be used to re-express three-point tensor integrals. For example, one can express

$$\begin{aligned} C^\mu(p_1^2, p_2^2, p_1 \cdot p_2; m_1^2, m_2^2, m_3^2) &= \frac{(2\pi Q)^{4-d}}{i\pi^2} \int d^d q \, \frac{q^\mu}{(q^2 - m_1^2)[(q+p_1)^2 - m_2^2][(q+p_2)^2 - m_3^2]} \\ &= p_1^\mu \, C_1(p_1^2, p_2^2, p_1 \cdot p_2; m_1^2, m_2^2, m_3^2) + p_2^\mu \, C_2(p_1^2, p_2^2, p_1 \cdot p_2; m_1^2, m_2^2, m_3^2) \end{aligned} \tag{A.21}$$

This can then be reduced to scalar integrals by appropriate contractions of the external momenta p_1 and p_2 to find the coefficient functions C_1 and C_2.

A.2 Numerical Evaluation in Euclidean Space

In this section, we directly evaluate the loop integrals for one- and two-points in four space-time dimensions after converting to Euclidean space through an appropriate Wick rotation. These methods were made use of extensively in Chapter 3 to iteratively solve the gap equation, where we do not work with the free propagator. We will make use of the fact that the propagator is a function of the Euclidean norm of the (Euclidean) four-momentum, i.e. $G(p_E) \equiv G(|p_E|)$.

The integration element over the Euclidean momentum is given by

$$\int \frac{d^4 k_E}{(2\pi)^4} = \frac{1}{(2\pi)^4} \int_0^\Lambda dk_E \, k_E^3 \int d\Omega_4 = \frac{1}{(2\pi)^4} \int_0^\Lambda dk_E \, k_E^3 \int_0^\pi d\theta \sin^2\theta \int_0^\pi d\psi \sin\psi \int_0^{2\pi} d\phi \,. \tag{A.22}$$

To evaluate the radial integral, we have defined an appropriate cutoff, denoted as Λ. The UV divergences are captured in the limit $\Lambda \to \infty$. Thus, Λ should be chosen to be significantly larger than all the mass scales in the system. Finally, when considering the differences of these loop integrals, the cutoff dependence should vanish.

A.2.1 One-Point Scalar Integral

Converting to Euclidean momentum, we have

$$\int \frac{d^4 q_E}{(2\pi)^4} \, G(|q_E|) = \frac{1}{(2\pi)^4} \int_0^\Lambda dq_E \, q_E^3 \, G(|q_E|) \int d\Omega_4 = \frac{1}{8\pi^2} \int_0^\Lambda dq_E \, q_E^3 \, G(|q_E|) \tag{A.23}$$

where we have used the fact that the integrand has no angular dependence, so we can directly integrate over the solid angle. Explicitly for the free propagator, we have

$$\frac{1}{8\pi^2} \int_0^\Lambda dq_E \frac{q_E^3}{q_E^2 + m^2} = \frac{1}{16\pi^2} \left[\Lambda^2 - m^2 \log\left(1 + \frac{\Lambda^2}{m^2}\right) \right] \,. \tag{A.24}$$

The result is quadratically divergent as $\Lambda \to \infty$ as expected from power counting arguments.

A.2.2 Two-Point Scalar Integral

In this case, there is an external momentum involved, so the evaluation of the angular integration is not straightforward as an angular dependence arises due to the angles between the external and integrating momenta. With this in mind, we have

$$\int \frac{dq_E^4}{(2\pi)^4} G(|q_E|)G(|q_E+p_E|) = \frac{1}{(2\pi)^4}\int_0^\Lambda dq_E\, q_E^3\, G(|q_E|)\int_0^\pi d\theta\, \sin^2\theta\, G(|q_E+p_E|)\int_0^\pi d\psi \sin\psi \int_0^{2\pi} d\phi \tag{A.25}$$

and now define

$$u^2 \equiv |q_E+p_E|^2 = q_E^2 + p_E^2 + 2q_E\, p_E\, \cos\theta\,, \tag{A.26}$$

where we have chosen the coordinate system such that the dot product between the vectors q_E and p_E depends only on the angle θ. This variable transformation gives

$$\sin\theta = \frac{\sqrt{4q_E^2\, p_E^2 - (u^2 - q_E^2 - p_E^2)^2}}{2q_E\, p_E}\,, \quad d\theta \sin\theta = -\frac{u\, du}{q_E\, p_E\, \sin\theta}\,. \tag{A.27}$$

Substituting this in (A.25), and integrating over the remaining angles, we obtain

$$\begin{aligned}\int \frac{dq_E^4}{(2\pi)^4} G(|q_E|)G(|q_E+p_E|) &= \frac{1}{8\pi^3\, p_E^2}\int_0^\Lambda dq_E\, q_E\, G(|q_E|)\int_{|q_E-p_E|}^{|q_E+p_E|} du\, u\, \sqrt{4q_E^2\, p_E^2 - (u^2-q_E^2-p_E^2)^2}\, G(|u|)\\ &\equiv \frac{1}{8\pi^3\, p_E^2}\int_0^\Lambda dq_E\, q_E\, G(|q_E|)\int_{|q_E-p_E|}^{|q_E+p_E|} du\, u\, \sqrt{-\lambda(u^2,q_E^2,p_E^2)}\, G(|u|)\,,\end{aligned} \tag{A.28}$$

where $\lambda(x,y,z) = x^2+y^2+z^2-2xy-2yz-2zx$ is the Källén function.

Note that for the case of $p_E^2 \to 0$, it is easier to directly perform the integration, like for the scalar one-point function, as there is no angular dependence in the integrand, i.e.

$$\int \frac{d^4q_E}{(2\pi)^4}\, G^2(|q_E|) = \frac{1}{8\pi^2}\int_0^\Lambda dq_E\, q_E^3\, G^2(|q_E|)\,. \tag{A.29}$$

For free propagators, one obtains the following result

$$\frac{1}{8\pi^2}\int_0^\Lambda dq_E \frac{q_E^3}{(q_E^2+m^2)^2} = \frac{1}{16\pi^2}\left[\log\left(1+\frac{\Lambda^2}{m^2}\right) - \frac{\Lambda^2}{m^2+\Lambda^2}\right]\,, \tag{A.30}$$

which is logarithmically divergent as $\Lambda \to \infty$.

Appendix B

Integrals for the Scalar Sunset Approximation

In this appendix, we calculate and give explicit expressions for the divergent and finite parts of various loop integrals encountered in Chapter 4, when one includes the sunset diagrams in the computation of the 2PI effective potential. Recall that the relevant loop integrals involved the auxiliary propagator $iG_a^{-1}(q) = q^2 - m_0^2$, so we can make use of the results of dimensional regularisation. We work in $d = 4 - 2\epsilon$, and as such, the divergences are expressed in terms of poles of the form ϵ^{-n} with $n > 0$.

We begin with the easier one-loop integrals, the first of which is

$$T^{(2)} = \int_q G_a(q) = \underbrace{-\frac{m_0^2}{16\pi^2\epsilon}}_{T_d^{(2)}} + \frac{m_0^2}{16\pi^2}\left[\overline{\log}(m_0^2) - 1\right] + \mathcal{O}(\epsilon) \tag{B.1}$$

where we have identified the divergent piece and use the notation $\overline{\log}(x) = \log\left(\frac{x}{\overline{Q}^2}\right)$ where $\overline{Q}$ is defined as in Appendix A. We eventually set $\overline{Q}^2 = m_0^2$, essentially carrying out the renormalisation at the VEV, so we will use this throughout, as this leads to easier to handle expressions for the counterterms and finite parts. We thus have,

$$T^{(2)} = T_d^{(2)} - \frac{m_0^2}{16\pi^2} + \mathcal{O}(\epsilon)\,. \tag{B.2}$$

The finite piece here is precisely one of those added back to the integral $\mathcal{T}_{\text{fin.}}$ in (4.67), when defining the $\overline{\text{MS}}$ renormalised one-point integral. For the integral over two propagators, we have

$$T^{(0)} = \int_q G_a^2(q) = \frac{1}{16\pi^2\epsilon} - \overline{\log}(m_0^2) + \mathcal{O}(\epsilon) \overset{\overline{Q}^2 = m_0^2}{=} T_d^{(0)} + \mathcal{O}(\epsilon)\,. \tag{B.3}$$

Now, we will tackle the two-loop integrals. We introduce some notation, similar to [160], for definite integrals that appear in the determination of finite parts,

$$\text{Ls}_2 \equiv -\int_0^{\frac{2\pi}{3}} dx \log\left[\sin\left(\frac{x}{2}\right)\right], \quad \text{Ls}_3 \equiv -\int_0^{\frac{2\pi}{3}} dx \log^2\left[\sin\left(\frac{x}{2}\right)\right]. \tag{B.4}$$

Let us now look at

$$T^{(I,2)} \equiv \int_q G_a(q)\,\mathcal{I}_{a,\text{fin.}}(q^2) = \int_q G_a(q) \int_k i\left[G_a(k+q)G_a(k) - G^2(k)\right]$$
$$= \underbrace{\int_q G_a(q)\, i \int_k G_a(k+q)G_a(k)}_{\mathcal{S}_a} - \int_q G_a(q)\, i \int_k G_a^2(k)\,. \tag{B.5}$$

We evaluate each two-loop integral separately; the second one is easier as it "factorises" into two separate integrals. This gives

$$\int_q G_a(q)\, i \int_k G_a^2(k)$$
$$= \frac{m_0^2}{(16\pi^2)^2}\left[-\frac{1}{\epsilon^2} - \frac{\left(1 - 2\overline{\log}(m_0^2)\right)}{\epsilon} + \left(-1 - \zeta(2) + 2\overline{\log}(m_0^2) - 2\overline{\log}^2(m_0^2)\right)\right] + \mathcal{O}(\epsilon)\,,$$

where ζ is the Riemann-zeta function, with $\zeta(2) = \pi^2/6$. The sunset integral with auxiliary propagators, $\mathcal{S}_a$, has the following result [160]

$$S_a = \frac{3m_0^2}{(16\pi^2)^2}\left\{ -\frac{1}{2\epsilon^2} + \frac{1}{\epsilon}\left[-\frac{1}{2} + \left(\overline{\log}(m_0^2) - 1\right)\right]\right.$$
$$\left. - \frac{1}{2}\left[7 - 8\sqrt{3}\mathrm{Ls}_2 + \frac{\pi^2}{6} - 6\overline{\log}(m_0^2) + 2\overline{\log}^2(m_0^2)\right]\right\} + \mathcal{O}(\epsilon)\,. \tag{B.6}$$

Putting these together yields the result

$$T^{(I,2)} \overset{\overline{Q}^2 = m_0^2}{=} \frac{m_0^2}{(16\pi^2)^2}\left\{ -\frac{1}{2\epsilon^2} - \frac{7}{2\epsilon} - \left[\frac{19}{2} - 12\sqrt{3}\mathrm{Ls}_2 + \frac{\pi^2}{12}\right]\right\} + \mathcal{O}(\epsilon) \equiv T_d^{(I,2)} + T_{\text{fin.}}^{(I,2)}\,. \tag{B.7}$$

The integral $T^{(I,0)}$ is then closely related as

$$T^{(I,0)} \equiv \int_q G_a^2(q)\,\mathcal{I}_{a,\text{fin.}}(q^2) = \int_q G_a^2(q) \int_k i\left[G_a(k+q)G_a(k) - G^2(k)\right]$$
$$= -\frac{1}{3}\frac{\partial S_a}{\partial m_0^2}\bigg|_{\overline{Q}^2=m_0^2} - \frac{1}{(16\pi^2)^2}\left[\frac{1}{\epsilon^2} - \frac{2\overline{\log}(m_0^2)}{\epsilon} + \frac{\pi^2}{6} + 2\overline{\log}^2(m_0^2) + \mathcal{O}(\epsilon)\right]\bigg|_{\overline{Q}^2=m_0^2}$$
$$= \frac{1}{(16\pi^2)^2}\left\{-\frac{1}{2\epsilon^2} + \frac{1}{2\epsilon} + \left[\frac{1}{2} - \frac{\pi^2}{12} - 4\sqrt{3}\mathrm{Ls}_2\right]\right\} + \mathcal{O}(\epsilon) \equiv T_d^{(I,0)} + T_{\text{fin.}}^{(I,0)}\,. \tag{B.8}$$

$T_{\text{fin.}}^{(I,0)}$ is the other finite part added to (4.67), to render it $\overline{\text{MS}}$ renormalised.

The only three-loop integrals encountered are in $T^{(I,I)}$,

$$T^{(I,I)} \equiv i\int_q G_a^2(q)\,\mathcal{I}_{a,\text{fin.}}^2(q^2) = i\int_q G_a^2(q) \int_k \left\{i\left[G_a(k+q)G_a(k) - G^2(k)\right]\right\}^2$$
$$= i\int_q G_a^2(q)\, i\int_k G_a(k+q)G_a(k)\, i\int_r G_a(r+q)G_a(r)$$

$$- 2i \int_q G_a^2(q)\, i \int_k G_a(k+q) G_a(k)\, i \int_r G_a^2(r) + i \int_q G_a^2(q)\, i \int_k G_a^2(k)\, i \int_r G_a^2(r) \tag{B.9}$$

The integrals in the last line are easier to treat; the results for these are

$$i \int_q G_a^2(q)\, i \int_k G_a^2(k)\, i \int_r G_a^2(r) \overset{\overline{Q}^2 = m_0^2}{=} \frac{1}{(16\pi^2)^3} \left[\frac{1}{\epsilon^3} + \frac{\pi^2}{4\epsilon} - \zeta(3) \right] + \mathcal{O}(\epsilon)$$

$$i \int_q G_a^2(q)\, i \int_k G_a(k+q) G_a(k)\, i \int_r G_a^2(r) \overset{\overline{Q}^2 = m_0^2}{=}$$
$$\frac{1}{(16\pi^2)^3} \left[\frac{1}{2\epsilon^3} + \frac{1}{2\epsilon^2} + \frac{1}{\epsilon} \left(\frac{1}{2} - 4\sqrt{3}\mathrm{Ls}_2 + + \frac{\pi^2}{8} \right) \right.$$
$$\left. + \left(\frac{\sqrt{3}}{2} \mathrm{Ls}_2(\log 9 - 2) - \frac{1}{2} \left(2\sqrt{3}\mathrm{Ls}_3 + \zeta(3) - 1 \right) - \frac{\sqrt{3}\pi^3}{18} + \frac{\pi^2}{8} \right) \right] + \mathcal{O}(\epsilon)$$

To treat the first integral, we Wick rotate

$$i \int_q G_a^2(q)\, i \int_k G_a(k+q) G_a(k)\, i \int_k G_a(r+q) G_a(r)$$
$$= \int_{q_E} \int_{k_E} \int_{r_E} \frac{1}{(q_E^2 + m_0^2)^2 \left[(k_E + q_E)^2 + m_0^2 \right] (k_E^2 + m_0^2) \left[(r_E + q_E)^2 + m_0^2 \right] (r_E^2 + m_0^2)}$$
$$= \frac{1}{(16\pi^2)^3} \mathbf{T}^{(2,1,1,1,1,0)}(m_0^2, m_0^2, m_0^2, m_0^2, m_0^2, m_0^2)\,,$$

whereby, in the last line, we adopt the notation in [160]. We then perform a reduction to so-called "master integrals" via integration-by-parts (IBP) identities (see, for e.g.,[161]) using the program `FIRE6` [162]. This yields

$$\frac{\mathbf{T}^{(2,1,1,1,1,0)}(m_0^2, m_0^2, m_0^2, m_0^2, m_0^2, m_0^2)}{(16\pi^2)^3} = -\frac{(3d-8)}{6m_0^4} \left[\frac{\mathbf{E}(m_0^2, m_0^2, m_0^2, m_0^2)}{(16\pi^2)^3} \right]$$
$$+ \frac{2(d-2)}{3m_0^4} \left[\frac{\mathbf{A}(m_0^2)}{16\pi^2} \right] \left[\frac{\mathbf{I}(m_0^2, m_0^2, m_0^2)}{(16\pi^2)^2} \right] - \frac{(d-6)}{6m_0^2} \left[\frac{\mathbf{G}(m_0^2, m_0^2, m_0^2, m_0^2, m_0^2)}{(16\pi^2)^3} \right], \tag{B.10}$$

where we continue with the notation for the integrals as in [160]. Gathering all the various pieces, we obtain

$$\left. \frac{\mathbf{T}^{(2,1,1,1,1,0)}(m_0^2, m_0^2, m_0^2, m_0^2, m_0^2, m_0^2)}{(16\pi^2)^3} \right|_{\overline{Q}^2 = m_0^2} =$$
$$\frac{1}{(16\pi^2)^3} \left[\frac{1}{3\epsilon^3} + \frac{2}{3\epsilon^2} + \frac{1}{\epsilon} \left(1 - 4\sqrt{3}\mathrm{Ls}_2 \right) \right.$$
$$\left. + \left(\frac{1}{3} \left(6\sqrt{3}\mathrm{Ls}_2 \log(3) + 5\zeta(3) - 2 \right) - 2\sqrt{3}\mathrm{Ls}_3 + \frac{\pi^2}{18} \left(3 - 2\sqrt{3} \right) \right) \right] + \mathcal{O}(\epsilon) \tag{B.11}$$

Putting together everything, we finally arrive at

$$T^{(I,I)} = \frac{1}{(16\pi^2)^3}\left[\frac{1}{3\epsilon^3} - \frac{1}{3\epsilon^2} + \left(2\sqrt{3}\mathrm{Ls}_2 + \frac{5}{3}(\zeta(3)-1) + \frac{\pi^3}{9}\sqrt{3} - \frac{\pi^2}{36}\left(4\sqrt{3}+3\right)\right)\right] + \mathcal{O}(\epsilon)$$
$$= T_d^{(I,I)} + T_{\text{fin.}}^{(I,I)}\,. \tag{B.12}$$

Appendix C

$\overline{\text{MS}}$ Renormalisation with 2PI Kernels

In Chapter 4, we obtained counterterms for the various coupling constants in the Hartree and scalar sunset approximations in the $\overline{\text{MS}}$ scheme, by extracting divergent parts from the various loop integrals and identifying parts of these as contributions to renormalised quantities. This led to cancellation conditions (see (4.8) and (4.15) for the Hartree approximation and (4.34) and (4.49) for the scalar sunset approximation) to determine these counterterms. In this appendix, we would like to reconcile this with the approach of using Bethe-Salpeter equations (BSEs) introduced and used in Chapter 3 to determine the very same coupling constant counterterms.

C.1 Hartree Approximation

Our starting point is (3.36), which gives

$$\overline{V}^{(4)}(p) = -(\lambda_R + \delta\lambda_0) \; - \; \frac{1}{2}(\lambda_R + \delta\lambda_0)\, \overline{V}^{(4)}(p) \left[\mathcal{I}(p^2)\right] \tag{C.1}$$

where in the Hartree approximation, we have

$$iG_R^{-1} = p^2 - m^2(\phi)\,.$$

Therefore, we can evaluate the loop integral in dim. reg.

$$\begin{aligned}\mathcal{I}(p^2) = i\int_q G_R(p+q)G_R(q) &\equiv \frac{B_0(p^2, m^2(\phi), m^2(\phi))}{16\pi^2} \\ &= \frac{1}{16\pi^2\epsilon} \underbrace{-\frac{1}{16\pi^2}\int_0^1 dx\, \overline{\log}\left[m^2(\phi) - p^2x(1-x)\right]}_{\mathcal{I}_{\text{fin.}}(p^2)} + \mathcal{O}(\epsilon)\,.\end{aligned} \tag{C.2}$$

Substituting this into (C.1), we get

$$\overline{V}^{(4)}(p) = -\lambda_R - \frac{\lambda_R}{2}\,\overline{V}^{(4)}(p)\,\mathcal{I}_{\text{fin.}}(p^2) - \delta\lambda_0 - \frac{(\lambda_R + \delta\lambda_0)}{32\pi^2\epsilon}\,\overline{V}^{(4)}(p) - \frac{\delta\lambda_0}{2}\overline{V}^{(4)}(p)\,\mathcal{I}_{\text{fin.}}(p^2) \tag{C.3}$$

Using now the same idea as in (4.7), we define the vertex function from the first explicitly finite terms

$$\overline{V}^{(4)}(p) = -\lambda_R - \frac{\lambda_R}{2}\,\overline{V}^{(4)}(p)\,\mathcal{I}_{\text{fin.}}(p^2) \quad \Longrightarrow \quad \overline{V}^{(4)}(p) = -\frac{\lambda_R}{1+\frac{\lambda_R}{2}\mathcal{I}_{\text{fin.}}(p^2)}\,. \tag{C.4}$$

This can be compared to (3.53) if we set $p_*^2 = 0$. Now, we also have a cancellation condition from the remaining terms of (C.3),

$$\delta\lambda_0 + \left[\frac{(\lambda_R+\delta\lambda_0)}{32\pi^2} + \frac{\delta\lambda_0\,\mathcal{I}_{\text{fin.}}(p^2)}{2}\right]\overline{V}^{(4)}(p) = 0 \tag{C.5}$$

Substituting (C.4), and solving for $\delta\lambda_0$, we end up with the following result

$$\delta\lambda_0 = \frac{\lambda_R^2}{32\pi^2\epsilon}\,\frac{1}{\left(1-\frac{\lambda_R}{32\pi^2\epsilon}\right)}\,, \tag{C.6}$$

which is exactly the same result as (4.9).

Now, for the counterterm $\delta\lambda_2$, we use the auxiliary kernel and BSE

$$\begin{aligned} V^{(4)}(p) &= -(\lambda_R+\delta\lambda_2) - \frac{1}{2}(\lambda_R+\delta\lambda_2)\,\overline{V}^{(4)}(p)\,\big[\mathcal{I}(p^2)\big] \\ &= -\lambda_R - \frac{\lambda_R}{2}\,\overline{V}^{(4)}(p)\,\mathcal{I}_{\text{fin.}}(p^2) - \left\{\delta\lambda_2 + \left[\frac{(\lambda_R+\delta\lambda_2)}{32\pi^2} + \frac{\delta\lambda_2\,\mathcal{I}_{\text{fin.}}(p^2)}{2}\right]\overline{V}^{(4)}(p)\right\}. \end{aligned} \tag{C.7}$$

In an analogous manner, we obtain

$$V^{(4)}(p) = -\lambda_R - \frac{\lambda_R}{2}\,\overline{V}^{(4)}(p)\,\mathcal{I}_{\text{fin.}}(p^2) = -\frac{\lambda_R}{1+\frac{\lambda_R}{2}\mathcal{I}_{\text{fin.}}(p^2)} = \overline{V}^{(4)}(p) \tag{C.8}$$

and the counterterm

$$\delta\lambda_2 = \frac{\lambda_R^2}{32\pi^2\epsilon}\,\frac{1}{\left(1-\frac{\lambda_R}{32\pi^2\epsilon}\right)} = \delta\lambda_0\,, \tag{C.9}$$

which, again, matches the result (4.10).

C.2 Scalar Sunset Approximation

We begin with (3.70),

$$\begin{aligned} \overline{V}^{(4)}(p_1,p_2,p_3,p_4) &= -(\lambda_R+\delta\lambda_0) + 2i(\alpha_R+\lambda_R\phi)^2 G_R(p_3-p_1) \\ &\quad - \frac{i}{2}(\lambda_R+\delta\lambda_0)\int_q G_R(p+q)G_R(q)\,\overline{V}^{(4)}(p+q,-q,p_3,p_4) \\ &\quad - (\alpha_R+\lambda_R\phi)^2\int_q G_R(p+q)G_R(q)G_R(p_1+q)\overline{V}^{(4)}(p+q,-q,p_3,p_4)\,. \end{aligned} \tag{C.10}$$

Here, the analysis is not so straightforward as the propagator is now of the form (see (4.29)),

$$iG_R^{-1} = p^2 - M^2(\phi;p^2)\,, \tag{C.11}$$

so we cannot evaluate the integrals in dim. reg. Furthermore, the vertex function, $\overline{V}^{(4)}$, also has a momentum dependence so it cannot be "pulled" out of the integrals like in the Hartree approximation. However, we can still use power counting arguments to identify divergent quantities. The propagator is of course finite and so is $\overline{V}^{(4)}$, which imply that the loop integral in the second line of (C.10) is divergent and the one in the last line is not. This means that we can express the divergent loop integral as

$$I_1(p,p_3,p_4) \equiv i\int_q G_R(p+q)G_R(q)\,\overline{V}^{(4)}(p+q,-q,p_3,p_4) = I_{1,\text{div.}} + I_{1,\text{fin.}}(p,p_3,p_4)\,, \quad \text{(C.12)}$$

where we have used the fact that $\overline{V}^{(4)}$ is dimensionless, and there are two propagators involved in the loop integral. This allows us to identify the divergent piece when the momenta are 0. With this, we can re-write (C.10) as

$$\begin{aligned}
&\overline{V}^{(4)}(p_1,p_2,p_3,p_4) = \\
&-\lambda_R + 2i(\alpha_R+\lambda_R\phi)^2 G_R(p_3-p_1) - \frac{\lambda_R}{2} I_{1,\text{fin.}}(p,p_3,p_4) - (\alpha_R+\lambda_R\phi)^2 I_2(p,p_3,p_4) \\
&-\delta\lambda_0 - \frac{(\lambda_R+\delta\lambda_0)}{2} I_{1,\text{div.}} - \frac{\delta\lambda_0}{2} I_{1,\text{fin.}}(p,p_3,p_4)\,. \qquad \text{(C.13)}
\end{aligned}$$

where we adhere to the notation in (3.73) and (3.74). The first term defines the finite vertex function via an implicit, integral equation

$$\begin{aligned}
&\overline{V}^{(4)}(p_1,p_2,p_3,p_4) = \\
&-\lambda_R - \frac{\lambda_R}{2} I_{1,\text{fin.}}(p,p_3,p_4) + 2i(\alpha_R+\lambda_R\phi)^2 G_R(p_3-p_1) - (\alpha_R+\lambda_R\phi)^2 I_2(p,p_2,p_3,p_4) \qquad \text{(C.14)}
\end{aligned}$$

On comparison with (C.4), we can see that the first two terms of (C.14) are essentially the Hartree contribution and the other two terms are the pieces we get due to the inclusion of the scalar sunset diagram in the 2PI effective action.

We now examine the cancellation condition

$$\delta\lambda_0 + \frac{(\lambda_R+\delta\lambda_0)}{2} I_{1,\text{div.}} + \frac{\delta\lambda_0}{2} I_{1,\text{fin.}}(p=0,p_3=0,p_4=0) = 0\,, \qquad \text{(C.15)}$$

where this is at zero momentum as this is where the effective potential is evaluated. This is similar to (C.5), except now we need to analyse the divergences in the integral I_1 carefully,

$$\begin{aligned}
I_{1,\text{div.}} &= i\int_q G_R^2(q)\overline{V}^{(4)}(q,-q,0,0)\Big|_{\text{div.}} \\
&= i\int_q G_R^2(q)\Big[-\lambda_R - \frac{\lambda_R}{2} I_{1,\text{fin.}}(0,0,0) + 2i(\alpha_R+\lambda_R\phi)^2 G_R(q) \\
&\qquad - (\alpha_R+\lambda_R\phi)^2 I_2(0,-q,0,0)\Big]\Big|_{\text{div.}} \\
&= -\frac{\lambda_R}{16\pi^2\epsilon}\left[1 + \frac{I_{1,\text{fin.}}(0,0,0)}{2}\right]. \qquad \text{(C.16)}
\end{aligned}$$

Substituting this into (C.15), we obtain

$$\left[\delta\lambda_0 - \frac{\lambda_R\left(\lambda_R + \delta\lambda_0\right)}{32\pi^2\epsilon}\right]\left[1 + \frac{I_{1,\text{fin.}}(0,0)}{2}\right] = 0\,. \tag{C.17}$$

This is only possible if

$$\delta\lambda_0 = \frac{\lambda_R\left(\lambda_R + \delta\lambda_0\right)}{32\pi^2\epsilon} \quad \Longrightarrow \; \delta\lambda_0 = \frac{\lambda_R^2}{32\pi^2\epsilon}\,\frac{1}{\left(1 - \frac{\lambda_R}{32\pi^2\epsilon}\right)} \tag{C.18}$$

which is the result found in (4.43). Note that this counterterm matches its value in the Hartree approximation, c.f. (4.9) and also the previous section in this appendix.

Next, we seek the counterterms $\delta\lambda_2$ and $\delta\alpha_1$. Starting with the auxiliary four-point vertex function (3.76), we have

$$\begin{aligned}
V^{(4)}(p) &= -(\lambda_R + \delta\lambda_2) + \lambda_R^2\mathcal{I}(p^2) \\
&\quad + \frac{i}{2}\left[-(\lambda_R + \delta\lambda_2) + \lambda_R^2\mathcal{I}(p^2)\right]\int_q G_R(q)G_R(q+p)\overline{V}^{(4)}(q+p,-q,p_3,p_4) \\
&= -\lambda_R - \frac{\lambda_R}{2}I_1(p,p_3) + \lambda_R^2\mathcal{I}_{\text{fin.}}(p^2) + \frac{\lambda_R^2}{2}\mathcal{I}_{\text{fin.}}(p^2)I_{1,\text{fin.}}(p,p_3,p_4) \\
&\quad - \delta\lambda_2 + \lambda_R^2 T_d^{(0)} - \frac{(\lambda_R + \delta\lambda_2)}{2}I_{1,\text{div.}} + \frac{\lambda_R^2}{2}T_d^{(0)}I_{1,\text{div.}} + \frac{\lambda_R^2}{2}\mathcal{I}_{\text{fin.}}(p^2)I_{1,\text{div.}} \\
&\quad - \frac{\delta\lambda_2}{2}I_{1,\text{fin.}}(p,p_3,p_4) + \frac{\lambda_R^2}{2}T_d^{(0)}I_{1,\text{fin.}}(p,p_3,p_4)\,,
\end{aligned} \tag{C.19}$$

where the last two lines of the second equality gives the cancellation condition required when setting the momenta to zero,

$$\begin{aligned}
-\delta\lambda_2 + \lambda_R^2 T_d^{(0)} - \frac{(\lambda_R + \delta\lambda_2)}{2}I_{1,\text{div.}} + \frac{\lambda_R^2}{2}T_d^{(0)}I_{1,\text{div.}} + \frac{\lambda_R^2}{2}\mathcal{I}_{\text{fin.}}(0)I_{1,\text{div.}} \\
- \frac{\delta\lambda_2}{2}I_{1,\text{fin.}}(0,0,0) + \frac{\lambda_R^2}{2}T_d^{(0)}I_{1,\text{fin.}}(0,0,0) = 0\,,
\end{aligned} \tag{C.20}$$

where $T_d^{(0)} = 1/16\pi^2\epsilon$, as determined in Appendix B. This then gives us

$$\begin{aligned}
\delta\lambda_2 &= \left[\frac{3\lambda_R}{32\pi^2\epsilon} - \frac{\lambda_R^2}{(32\pi^2\epsilon)^2}\right]\left[1 - \frac{\lambda_R}{32\pi^2\epsilon}\right]^{-1} \\
&= \frac{\lambda_R^2}{32\pi^2\epsilon} - 2\lambda_R + \frac{\lambda_R^2}{32\pi^2} + \lambda_R\left(1 - \frac{64\pi^2}{\lambda_R}\right)\epsilon + 32\pi^2\left(1 - \frac{64\pi^2}{\lambda_R}\right)\epsilon^2 + \mathcal{O}(\epsilon^3)
\end{aligned} \tag{C.21}$$

which reproduces the result (4.45) after the expansion in ϵ in the second step.

Finally, the counterterm $\delta\alpha_1$ is obtained similarly, as the structure of the 3-point vertex function (3.69) is similar to the auxiliary four-point vertex. The result is

$$\begin{aligned}\delta\alpha_1 &= \left[\frac{3\alpha_R}{32\pi^2\epsilon} - \frac{\alpha_R\lambda_R}{(32\pi^2\epsilon)^2}\right]\left[1 - \frac{\lambda_R}{32\pi^2\epsilon}\right]^{-1} \\ &= \frac{\alpha_R\lambda_R}{32\pi^2\epsilon} - 2\alpha_R + \frac{\alpha_R\lambda_R}{32\pi^2} + \alpha_R\left(1 - \frac{64\pi^2}{\lambda_R}\right)\epsilon + \frac{32\pi^2\alpha_R}{\lambda_R}\left(1 - \frac{64\pi^2}{\lambda_R}\right)\epsilon^2 + \mathcal{O}(\epsilon^3)\end{aligned} \tag{C.22}$$

which matches (4.44) after expanding in powers of ϵ.

Appendix D

Dark Matter Inelastic Scattering

We present here a calculation of the spin-independent cross-section for inelastic nucleon-dark matter scattering. This is relevant when considering DM-nucleon interactions via Z-boson exchange, which couples between CP-even and CP-odd states. In the context of the scotogenic model considered in Chapter 6, for which the calculation in this appendix is done, this could be between one of the scalars ϕ_n^0 and the pseudo-scalar A^0, or between two Majorana fermions χ_m and χ_n. For completeness, we note that this channel is active only when the CP-odd state is produced on-shell, which is when the DM candidate acquires enough kinetic energy. As the mass difference between the two states is typically small, our calculation will proceed along the lines of the usual DM-nucleon elastic scattering for direct detection [33, 163–167].

D.1 Fermionic Dark Matter

Here ,we consider χ_1^0 to be the DM candidate and χ_m^0 to be the other state. As the mass splitting is very small, we may take $m_{\chi_1^0} \approx m_{\chi_n^0}$. Our starting point is the matrix element for the process given in Fig. D.1

$$
\begin{aligned}
i\mathcal{M}_{\text{ferm.}} = \bar{u}(p_3)\left[-\frac{i\,g_2\,\gamma_\mu(a_{1m}-b_{1m}\gamma^5)}{\cos\theta_W}\right]u(p_1)\left[-\frac{i}{q^2-M_Z^2}\left(\eta^{\mu\nu}+\frac{q^\mu q^\nu}{M_Z^2}\right)\right] \\
\bar{u}(p_4)\left[-\frac{i\,g_2}{\cos\theta_W}\gamma_\nu(c_V^q-c_A^q\gamma^5)\right]u(p_2) \\
= i\left(-\frac{g_2^2}{M_Z^2\cos\theta_W}\right)\bar{u}(p_3)\left[\gamma_\mu(a_{1m}-b_{1m}\gamma^5)\right]u(p_1)\,\bar{u}(p_4)\left[\gamma^\mu(c_V^q-c_A^q\gamma^5)\right]u(p_2)\,,
\end{aligned}
$$

where we have used the couplings from the SM of the quarks to the Z-boson and work in unitarity gauge to write down the propagator for the Z-boson [168]. The coefficients a_{1m} and b_{1m} contain components of the unitary matrix U_χ (c.f. (6.10)). In going from the first to the second step, we have used that the momentum transfer $-q^2 \approx |\vec{q}|^2 \ll M_Z^2$. We now map the above matrix element, as outlined in [165, 166], onto the following Wilson

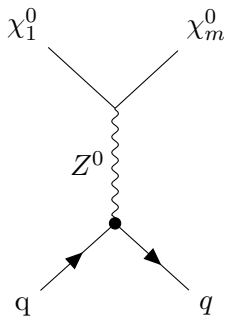

Figure D.1: Inelastic scattering between two Majorana fermions, the DM candidate χ_1^0, and a heavier state χ_m^0, via Z-boson exchange. q refers to up and down quarks in a nucleon.

coefficients times effective operators describing DM-quark interactions

$$\sum_{q=u,\,d}\Big[c_5^q\left(\overline{\chi_1}\gamma^\mu\chi_m\right)\left(\overline{q}\gamma^\mu q\right)+c_6^q\left(\overline{\chi_1}\gamma^\mu\gamma^5\chi_m\right)\left(\overline{q}\gamma^\mu q\right)$$
$$+\,c_7^q\left(\overline{\chi_1}\gamma^\mu\gamma^5\chi_m\right)\left(\overline{q}\gamma^\mu q\right)+c_8^q\left(\overline{\chi_1}\gamma^\mu\gamma^5\chi_m\right)\left(\overline{q}\gamma^\mu\gamma^5 q\right)+\text{h.c.}\Big]$$

where, for this model, the couplings are given as

$$c_5^q=-\frac{g_2^2\,a_{1m}\,c_V^q}{M_Z^2\,\cos\theta_W}\,,\qquad c_6^q=\frac{g_2^2\,b_{1m}\,c_V^q}{M_Z^2\,\cos\theta_W}\,,$$
$$c_7^q=\frac{g_2^2\,a_{1m}\,c_A^q}{M_Z^2\,\cos\theta_W}\,,\qquad c_8^q=-\frac{g_2^2\,b_{1m}\,c_A^q}{M_Z^2\,\cos\theta_W}\,.$$

This induces the following effective Lagrangian at the nucleon level

$$\mathcal{L}_{\text{eff.}}=\sum_{N=p,\,n}\sum_{i=5}^{8}c_i^N\,\mathcal{O}_i^N \tag{D.1}$$

where we defined the following operators

$$\mathcal{O}_5^N=\left(\overline{\chi_1}\gamma^\mu\chi_m\right)\left(\overline{N}\gamma^\mu N\right)\,,\qquad \mathcal{O}_6^N=\left(\overline{\chi_1}\gamma^\mu\gamma^5\chi_m\right)\left(\overline{N}\gamma^\mu N\right)\,,$$
$$\mathcal{O}_7^N=\left(\overline{\chi_1}\gamma^\mu\gamma^5\chi_m\right)\left(\overline{N}\gamma^\mu N\right)\,,\qquad \mathcal{O}_8^N=\left(\overline{\chi_1}\gamma^\mu\gamma^5\chi_m\right)\left(\overline{N}\gamma^\mu\gamma^5 N\right)\,,$$

and the nucleon-DM couplings are

$$c_{5,6}^p=2c_3^u+c_3^d\,,\quad c_{5,6}^n=c_3^u+2c_3^d\,,\quad c_{7,8}^N=\sum_{q=u,d}c_{7,8}^q\Delta_q^{(N)}\,,$$

where $\Delta_q^{(N)}$ is associated to the quark spin content of the nucleon, and hence the contributions from these operators eventually go to spin-dependent cross-section. For the remaining operators, we evaluate the nucleon-DM matrix element by expanding out the spinors in the non-relativistic limit [166]. We find that the operator $\mathcal{O}_6^N$ is velocity-suppressed, and hence the dominant contribution comes from the $\mathcal{O}_5^N$. We thus obtain the final cross-section as

$$\sigma_{\text{fermion}}^{\text{inelastic S.I.}}=\frac{1}{\pi}\left(\frac{M_N\,m_{\chi_1^0}}{M_N+m_{\chi_1^0}}\right)^2|c_5^N|^2\,. \tag{D.2}$$

Not that for $m = 1$, i.e. when the final state is the same as the initial one, the operator vanishes as Majorana fermions cannot carry a vector current; this is easily verified by explicitly writing down a_{1m}

$$a_{1m} = (U_\chi)^*_{m2}\,(U_\chi)_{12} - (U_\chi)^*_{m3}\,(U_\chi)^*_{13} - (U_\chi)^*_{12}\,(U_\chi)_{m2} + (U_\chi)^*_{13}\,(U_\chi)_{m3}\ .$$

D.2 Scalar Dark Matter

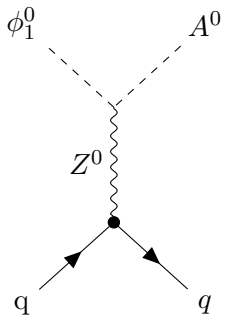

Figure D.2: Inelastic scattering between the scalar DM candidate, ϕ_1^0, and the pseudo-scalar A^0 via Z-boson exchange.

In this case, we take $m^2_{\phi_1^0} \approx m^2_{A^0}$ and our analysis proceeds along similar lines to fermionic DM. The matrix element for the process given in Fig. D.2 is

$$\begin{aligned} i\mathcal{M}_{\text{scalar}} &= \left[-\frac{g_2\,U\,(p_1+p_3)_\mu}{2\cos\theta_W}\right]\left[\frac{-i}{q^2-M_Z^2}\left(\eta^{\mu\nu}+\frac{q^\mu q^\nu}{M_Z^2}\right)\right]\bar{u}(p_4)\left[\frac{-i\,g_2}{\cos\theta_W}\gamma_\nu(c_V^q-c_A^q\gamma^5)\right]u(p_2) \\ &= \left[-\frac{g_2^2}{2\cos\theta_W\,M_Z^2}\right](p_1+p_3)_\mu\,\bar{u}(p_4)\left[\gamma^\mu(c_V^q-c_A^q\gamma^5)\right]u(p_2)\,. \end{aligned}$$

This translates to the following effective Wilson coefficients times quark-DM operators

$$\sum_{q=u,\,d}\left[c_3^q\left(i\phi^*\overset{\leftrightarrow}{\partial_\mu}A^0\right)\,\bar{q}\gamma^\mu q + c_4^q\left(i\phi^*\overset{\leftrightarrow}{\partial_\mu}A^0\right)\,\bar{q}\gamma^\mu\gamma^5 q\right]$$

where $X\overset{\leftrightarrow}{\partial_\mu}Y = X\partial_\mu Y - Y\partial_\mu X$. The couplings are now given as

$$c_3^q = -\frac{g_2^2\,(U_\phi)_{12}\,c_V^q}{2\cos\theta_W\,M_Z^2}\,,\qquad c_4^q = -\frac{g_2^2\,(U_\phi)_{12}\,c_A^q}{2\cos\theta_W\,M_Z^2}\,.$$

The effective Lagrangian induced at nucleon level is then given by

$$\mathcal{L}_{\text{eff.}} = \sum_{N=p,\,n}\left[c_3^N\left(i\phi^*\overset{\leftrightarrow}{\partial_\mu}A^0\right)\,\overline{N}\gamma^\mu N + c_4^N\left(i\phi^*\overset{\leftrightarrow}{\partial_\mu}A^0\right)\,\overline{N}\gamma^\mu\gamma^5 N\right]$$

where the couplings at this level are given by

$$c_3^p = 2c_3^u + c_3^d\,,\quad c_3^n = c_3^u + 2c_3^d\,,\quad c_4^N = \sum_{q=u,d} c_4^q\Delta_q^{(N)}\,. \tag{D.3}$$

Thus, $\mathcal{O}_4^N$ would contribute to the spin-dependent cross section, so we use $\mathcal{O}_3^N$ to obtain the final spin-independent cross-section as

$$\sigma_{\text{scalar}}^{\text{inelastic S.I.}} = \frac{1}{\pi}\left(\frac{M_N\, M_\phi}{M_N + M_\phi}\right)^2 |c_3^N|^2 \,. \tag{D.4}$$

Appendix E

Calculation of the CP Asymmetry Parameters

In this appendix, we outline the calculations and collect the expressions for the various diagrams that contribute to the CP asymmetry parameter ϵ_i in the model described in Chapter 6. The basis of the calculation is the following formula obtained in Chapter 5

$$\epsilon_i = \sum_\alpha \epsilon_{i\alpha} = \frac{-2 \sum\limits_{\alpha,\beta,k} \mathrm{Im}\left[y^*_{\alpha i}\, y_{\alpha k}\, y_{\beta k}\, y^*_{\beta i}\right]\, \mathrm{Im}\left[F_{\text{int.}}\right]}{\sum\limits_\gamma |y_{\gamma i}|^2\, F_{\text{tree}}} \,. \tag{E.1}$$

The total CP asymmetry generated in the decay of one of the Majorana fermions F_i is the sum of all possible Wave Function (WF) and Vertex (V) diagrams

$$\epsilon_i \;=\; \sum_j \mathrm{WF}^{(i)}_j + \sum_j \mathrm{V}^{(i)}_j \,. \tag{E.2}$$

To deal with the loop integrals, we work in dimensional regularisation, and make use of the Passarino-Veltman functions discussed in Appendix A. Along the way, we would require the evaluation of Dirac traces, as well as reduction of tensor integrals, both of which were carried out conveniently using FeynCalc [169–171]. Further, we would require the imaginary parts of the various loop functions. For the B_0 function, this is given by

$$\mathrm{Im}\left[B_0(p^2, m_1^2, m_2^2)\right] \;=\; \pi \frac{\lambda^{\frac{1}{2}}\left(p^2, m_1^2, m_2^2\right)}{p^2} \Theta\left(p^2 - (m_1 + m_2)^2\right) \,, \tag{E.3}$$

where $\lambda(x, y, z)$ is the Källén function and $\Theta(x)$ is the Heaviside-step function, which enforces the fact that the imaginary part exists only when particles in the loop can go on-shell. The imaginary part of the C_0 function was calculated numerically using PackageX [172], as analytic expressions exist only for particular cases.

Finally, as it is customary to normalise the asymmetry to the total decay width into leptonic and anti-leptonic state, we define

$$\Gamma^i_{\text{tot.}} = \Gamma(F_i \to L\,\eta) + \Gamma(F_i \to \psi\, H) + \Gamma(F_i \to \bar{L}\,\eta^\dagger) + \Gamma(F_i \to \bar{\psi}\, H^\dagger) \tag{E.4}$$

where the decay widths of the F_i are defined in (6.19).

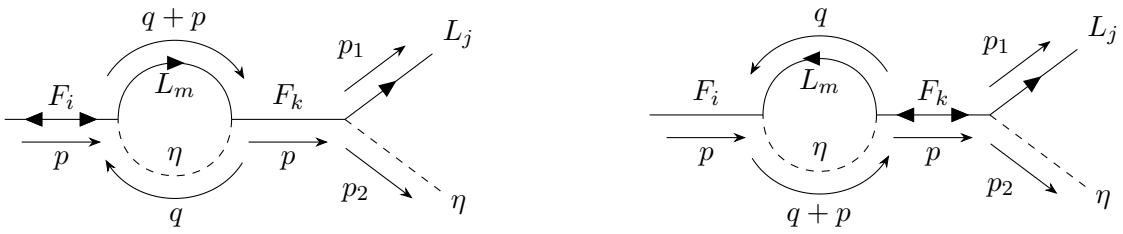

Figure E.1: Examples of one-loop wave function diagrams for the decays of F_i. Note the flow of lepton number, and the 'clash' on the line of the F, indicating the mass insertion.

E.1 Wave Function Diagrams

For the wave-function diagrams, one should carefully take into account the flow of lepton number and observe the various mass insertions. To this end, we use the prescription outlined in [173] for the Feynman rules when writing down the amplitude. Thus, we will explicitly calculate the diagrams in Fig. E.1 to demonstrate the procedure of obtaining the expression for the CP asymmetry.

For the left diagram, we obtain as matrix element

$$\begin{aligned} i\mathcal{M}_1 = &\sum_{k\neq i}\sum_{m=1}^{3} \bar{u}(p_1)\left[-i(g^j_{F_k})^*\frac{(1+\gamma^5)}{2}\right]\frac{i(\not{p}+M_k)}{p^2-M_k^2}\left[-ig^m_{F_k}\frac{(1-\gamma^5)}{2}\right] \\ &\left\{\int_q \frac{i(\not{q}+\not{p})}{(q+p)^2}\left[-i(g^m_{F_i})^*\frac{(1+\gamma^5)}{2}\right]\frac{i}{q^2-M_\eta^2}\right\}u(p) \\ = &\sum_{k\neq i}\sum_{m=1}^{3}\frac{(g^j_{F_k})^*\,g^m_{F_k}\,(g^m_{F_i})^*}{4}\bar{u}(p_1)(1+\gamma^5)\frac{\not{p}}{p^2-M_k^2} \\ &\left\{\frac{i\left[B_1(p^2,M_\eta^2,0)+B_0(p^2,M_\eta^2,0)\right]\not{p}}{16\pi^2}\right\}(1+\gamma^5)u(p) \\ = &\sum_{k\neq i}\sum_{m=1}^{3}\frac{i\,M_i^2}{M_i^2-M_k^2}\frac{(g^j_{F_k})^*\,g^m_{F_k}\,(g^m_{F_i})^*}{32\pi^2} \\ &\left[B_1(M_i^2,M_\eta^2,0)+B_0(M_i^2,M_\eta^2,0)\right]\left[\bar{u}(p_1)(1+\gamma^5)u(p)\right]\,. \end{aligned} \tag{E.5}$$

where in the last step we used the fact that the spinors are on-shell so

$$\not{p}u(p) = M_i u(p)\,, \quad \text{and} \quad p^2 = M_i^2\,.$$

For the right diagram, where the lepton flow in the loop is reversed, we have

$$\begin{aligned} i\mathcal{M}_2 = &\sum_{k\neq i}\sum_{m=1}^{3} \bar{u}(p_1)\left[-i(g^j_{F_k})^*\frac{(1+\gamma^5)}{2}\right]\frac{i(\not{p}+M_k)}{p^2-M_k^2}\left[-i(g^m_{F_k})^*\frac{(1+\gamma^5)}{2}\right] \\ &\left\{\int_q \frac{-i\not{q}}{q^2}\left[-ig^m_{F_i}\frac{(1-\gamma^5)}{2}\right]\frac{i}{(q+p)^2-M_\eta^2}\right\}u(p) \end{aligned}$$

$$= -\sum_{k\neq i}\sum_{m=1}^{3}\frac{(g^j_{F_k})^*\,(g^m_{F_k})^*\,g^m_{F_i}}{4}\bar{u}(p_1)(1+\gamma^5)\frac{M_k}{p^2-M_k^2}\int_q\frac{\not{q}}{q^2\left[(q+p)^2-M_\eta^2\right]}(1-\gamma^5)u(p)$$

$$= -\sum_{k\neq i}\sum_{m=1}^{3}\frac{i\,M_i\,M_k}{M_i^2-M_k^2}\frac{(g^j_{F_k})^*\,(g^m_{F_k})^*\,g^m_{F_i}}{32\pi^2}\left[B_1(M_i^2,0,M_\eta^2)\right]\left[\bar{u}(p_1)(1+\gamma^5)u(p)\right]\,. \tag{E.6}$$

We then take the sum of both loop-level amplitudes to get the total CP asymmetry for this process. Taking the interference of the sum with the tree-level amplitude and mapping this to (E.1), we obtain the following expression

$$\frac{2}{32\pi^2}\sum_{k\neq i}\sum_{m=1}^{3}\frac{M_i}{M_i^2-M_k^2}\Big\{M_i\,\mathrm{Im}\left[(g^j_{F_k})^*\,g^m_{F_k}\,(g^m_{F_i})^*\,g^j_{F_i}\right]\mathrm{Im}\left[B_1(M_i^2,M_\eta^2,0)+B_0(M_i^2,M_\eta^2,0)\right]$$

$$-M_k\,\mathrm{Im}\left[(g^j_{F_k})^*\,(g^m_{F_k})^*\,g^m_{F_i}\,g^j_{F_i}\right]\mathrm{Im}\left[B_1(M_i^2,0,M_\eta^2)\right]\Big\}\,\mathrm{tr}\left[\not{p}_1(1+\gamma^5)(\not{p}+M_i)(1-\gamma^5)\right]$$

$$=\frac{1}{16\pi}\sum_{k\neq i}\frac{M_i}{M_i^2-M_k^2}\left(1-\frac{M_\eta^2}{M_i^2}\right)^2\Theta\left(M_i^2-M_\eta^2\right)$$

$$\left\{M_i\,\mathrm{Im}\left[(g^j_{F_k})^*\,g^m_{F_k}\,(g^m_{F_i})^*\,g^j_{F_i}\right]+M_k\,\mathrm{Im}\left[(g^j_{F_k})^*\,(g^m_{F_k})^*\,g^m_{F_i}\,g^j_{F_i}\right]\right\}(8p_1\cdot p)\,, \tag{E.7}$$

where the factor 2 in the first line accounts for all possible $\mathrm{SU}(2)_L$ doublet combinations in the loop. Note for $k=i$, where the internal F is degenerate with the decaying one, the asymmetry vanishes as one obtains the following combination

$$(g^j_{F_i})^*\,(g^m_{F_i})^*\,g^m_{F_i}\,g^j_{F_i}=|g^m_{F_i}|^2\,|g^j_{F_i}|^2$$

which is real. Secondly, we sum over the final leptonic states and thus, the term proportional to M_i vanishes as the combination of couplings is again purely real. This may contribute to a CP asymmetry in a particular lepton flavour, however [84, 90, 91] Finally, we perform the phase space integral, and normalise this to the total decay width to obtain the final result

$$\mathrm{WF}_1^{(i)} \;=\; \frac{1}{128\pi^2}\frac{M_i}{\Gamma^i_{\mathrm{tot.}}}\left(1-\frac{M_\eta^2}{M_i^2}\right)^4\Theta\left(M_i^2-M_\eta^2\right)\sum_{k\neq i}\mathrm{Im}\left[\left(\sum_{j=1}^{3}g^j_{F_i}(g^j_{F_k})^*\right)^2\right]\frac{M_iM_k}{M_i^2-M_k^2}\,. \tag{E.8}$$

Similarly, one may treat the other possible particles in the loop and final states. We enlist the expressions as below.

$$\mathrm{WF}_2^{(i)} \;=\; \frac{1}{128\pi^2}\frac{M_i\left(1-\frac{M_\eta^2}{M_i^2}\right)^2}{\Gamma^i_{\mathrm{tot.}}}\left(1-\frac{M_\Psi^2}{M_i^2}\right)\Theta\left(M_i^2-M_\Psi^2\right)$$

$$\sum_{k\neq i}\sum_{j=1}^{3}\frac{1}{M_i^2-M_k^2}\Big\{M_i^2\left[\mathrm{Im}\left[g^j_{F_i}\,(g^j_{F_k})^*\,y_{1k}\,y_{1i}^*\right]\left(1+\frac{M_\Psi^2}{M_i^2}\right)+\mathrm{Im}\left[g^j_{F_i}\,(g^j_{F_k})^*\,y_{1k}\,y_{2i}^*\right]\frac{M_\Psi}{M_i}\right]$$

$$
\begin{aligned}
&+ M_i\, M_k \left[\mathrm{Im}\left[g^j_{F_i}\, (g^j_{F_k})^*\, y_{2k}\, y^*_{2i} \right] \left(1 + \frac{M^2_\Psi}{M^2_i} \right) + \mathrm{Im}\left[g^j_{F_i}\, (g^j_{F_k})^*\, y_{2k}\, y^*_{1i} \right] \frac{M_\Psi}{M_i} \right] \\
&+ M^2_i \left[\mathrm{Im}\left[g^j_{F_i}\, (g^j_{F_k})^*\, y_{2k}\, y^*_{2i} \right] \left(1 + \frac{M^2_\Psi}{M^2_i} \right) + \mathrm{Im}\left[g^j_{F_i}\, (g^j_{F_k})^*\, y_{1k}\, y^*_{2i} \right] \frac{M_\Psi}{M_i} \right] \\
&+ M_i\, M_k \left[\mathrm{Im}\left[g^j_{F_i}\, (g^j_{F_k})^*\, y_{1k}\, y^*_{1i} \right] \left(1 + \frac{M^2_\Psi}{M^2_i} \right) + \mathrm{Im}\left[g^j_{F_i}\, (g^j_{F_k})^*\, y_{2k}\, y^*_{1i} \right] \frac{M_\Psi}{M_i} \right] \Bigg\}
\end{aligned}
\tag{E.9}
$$

$$
\begin{aligned}
\mathrm{WF}^{(i)}_3 \;=\; & \frac{1}{128\pi^2} \frac{M_i}{\Gamma^i_{\mathrm{tot.}}} \left(1 - \frac{M^2_\Psi}{M^2_i} \right)^2 \Theta\left(M^2_i - M^2_\Psi \right) \\
& \sum_{k \neq i} \frac{1}{M^2_i - M^2_k} \Bigg\{ M^2_i \left[\mathrm{Im}\left[y_{1i}\, y_{2i}\, y^*_{1k}\, y^*_{2k} \right] \left(1 + \frac{M^2_\Psi}{M^2_i} \right) - 2\,\mathrm{Im}\left[(y^2_{1i} + y^2_{2i})\, y^*_{1k}\, y^*_{2k} \right] \frac{M_\Psi}{M_i} \right] \\
& + M_\Psi\, M_i \left[\mathrm{Im}\left[(y^2_{1i} + y^2_{2i})\, y^*_{1k}\, y^*_{2k} \right] \left(1 + \frac{M^2_\Psi}{M^2_i} \right) - 2\,\mathrm{Im}\left[y_{1i}\, y_{2i}\, y^*_{1k}\, y^*_{2k} \right] \frac{M_\Psi}{M_i} \right] \\
& + M_k\, M_i \left[\mathrm{Im}\left[y^2_{1i}\, (y^*_{1k})^2 + y^2_{1i}\, (y^*_{2k})^2 \right] \left(1 + \frac{M^2_\Psi}{M^2_i} \right) - 2\,\mathrm{Im}\left[[(y^*_{1k})^2 + (y^*_{2k})^2]\, y^i_1\, y^i_2 \right] \frac{M_\Psi}{M_i} \right] \\
& + M_k\, M_\Psi \left[\mathrm{Im}\left[[(y^*_{1k})^2 + (y^*_{2k})^2]\, y_{1i}\, y_{2i} \right] \left(1 + \frac{M^2_\Psi}{M^2_i} \right) - 2\,\mathrm{Im}\left[y^2_{1i}\, (y^*_{1k})^2 + y^2_{1i}\, (y^*_{2k})^2 \right] \frac{M_\Psi}{M_i} \right] \Bigg\}
\end{aligned}
\tag{E.10}
$$

$$
\begin{aligned}
\mathrm{WF}^{(i)}_4 \;=\; & \frac{1}{128\pi^2} \frac{M_i \left(1 - \frac{M^2_\Psi}{M^2_i} \right)}{\Gamma^i_{\mathrm{tot.}}} \left(1 - \frac{M^2_\eta}{M^2_i} \right)^2 \Theta\left(M^2_i - M^2_\eta \right) \\
& \sum_{k \neq i} \sum_{j=1}^{3} \frac{1}{M^2_i - M^2_k} \Bigg\{ M^2_i \left[\mathrm{Im}\left[g^j_{F_k}\, (g^j_{F_i})^*\, y_{1i}\, y^*_{1k} \right] \left(1 + \frac{M^2_\Psi}{M^2_i} \right) - 2\,\mathrm{Im}\left[g^j_{F_k}\, (g^j_{F_i})^*\, y_{2i}\, y^*_{1k} \right] \frac{M_\Psi}{M_i} \right] \\
& + M_i\, M_k \left[\mathrm{Im}\left[g^j_{F_k}\, (g^j_{F_i})^*\, y_{2i}\, y^*_{2k} \right] \left(1 + \frac{M^2_\Psi}{M^2_i} \right) - 2\,\mathrm{Im}\left[g^j_{F_k}\, (g^j_{F_i})^*\, y_{1i}\, y^*_{2k} \right] \frac{M_\Psi}{M_i} \right] \\
& + M^2_i \left[\mathrm{Im}\left[g^j_{F_i}\, (g^j_{F_k})^*\, y_{1i}\, y^*_{1k} \right] \left(1 + \frac{M^2_\Psi}{M^2_i} \right) - 2\,\mathrm{Im}\left[g^j_{F_i}\, (g^j_{F_k})^*\, y_{2i}\, y^*_{1k} \right] \frac{M_\Psi}{M_i} \right] \\
& + M_i\, M_k \left[\mathrm{Im}\left[g^j_{F_i}\, (g^j_{F_k})^*\, y_{2i}\, y^*_{2k} \right] \left(1 + \frac{M^2_\Psi}{M^2_i} \right) - 2\,\mathrm{Im}\left[g^j_{F_i}\, (g^j_{F_k})^*\, y_{1i}\, y^*_{2k} \right] \frac{M_\Psi}{M_i} \right] \Bigg\}
\end{aligned}
\tag{E.11}
$$

E.2 Vertex Diagrams

An example of such a process is given in Fig. E.2, which we will calculate for demonstrative purposes. Note that, unlike the self-energy diagram, there is no second diagram involved,

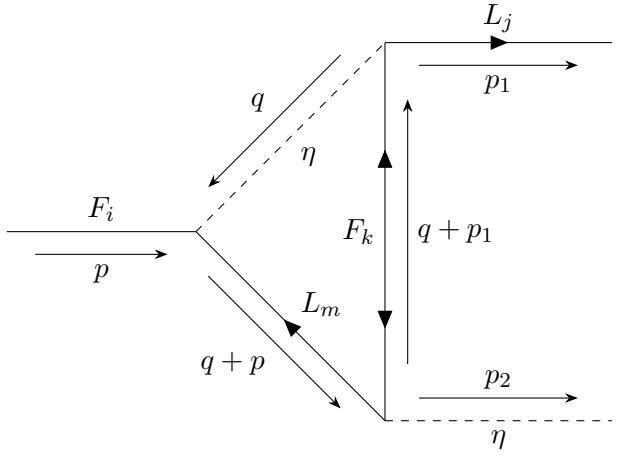

Figure E.2: Example of a one-loop vertex diagram for the decays of F_i.

in which the internal lepton line is reversed. The matrix element is given by

$$
\begin{aligned}
i\mathcal{M} = \bar{u}(p_1)\left[-i(g^j_{F_k})^*\frac{(1+\gamma^5)}{2}\right]\Bigg\{\int_q \frac{i(\not{q}+\not{p}_1+M^k_N)}{(q+p_1)^2-M^2_k}\left[-i(g^{km}_F)^*\frac{(1+\gamma^5)}{2}\right]\frac{i(\not{q}+\not{p})}{(q+p)^2} \\
\left[-ig^m_{F_i}\frac{(1-\gamma^5)}{2}\right]\frac{i}{q^2-M^2_\eta}\Bigg\}u(p) \\
= \frac{(g^j_{F_k})^*(g^{km}_F)^*g^m_{F_i}}{2}\,M^k_N\,\bar{u}(p_1)\left\{\int_q \frac{\not{q}+\not{p}}{(q-M^2_\eta)\left[(q+p_1)^2-(M^k_N)^2\right)(q+p)^2}\right\}(1-\gamma^5)u(p) \\
= \frac{(g^j_{F_k})^*(g^{km}_F)^*g^m_{F_i}}{2}\,M^k_N\,\bar{u}(p_1)\Bigg\{\frac{i\left[\not{p}_1\,C_1(p_1,p_2,M^2_\eta,(M^k_N)^2,0)+\not{p}_2\,C_2(p_1,p_2,M^2_\eta,(M^k_N)^2,0)\right]}{16\pi^2} \\
+\frac{i\not{p}\,C_0(p_1,p_2,M^2_\eta,(M^k_N)^2,0)}{16\pi^2}\Bigg\}(1-\gamma^5)u(p) \\
= \frac{i(g^j_{F_k})^*(g^{km}_F)^*g^m_{F_i}}{32\pi^2}M_iM_k\left[C_0(p_1,p_2,M^2_\eta,(M^k_N)^2,0)+C_2(p_1,p_2,M^2_\eta,(M^k_N)^2,0)\right] \\
\left[\bar{u}(p_1)(1+\gamma^5)u(p)\right] \qquad \text{(E.12)}
\end{aligned}
$$

where the C_1 function does not contribute as the SM fermions are massless above EWSB. We now calculate the relevant interference term, while summing over the leptons in the loop and final state, to obtain

$$
\begin{aligned}
\frac{1}{16\pi^2}\sum_{k\neq i}\mathrm{Im}\left[\left(\sum_{j=1}^{3}g^j_{F_i}(g^j_{F_k})^*\right)^2\right]M_kM_i\,\mathrm{Im}\left\{\left[C_0(p_1,p_2,M^2_k,M^2_\eta,0)+C_2(p_1,p_2,M^2_k,M^2_\eta,0)\right]\right\} \\
\mathrm{tr}\left[\not{p}_1(1+\gamma^5)(\not{p}+m_F)(1-\gamma^5)\right]
\end{aligned}
$$

$$= \frac{1}{16\pi}\sum_{k\neq i}\mathrm{Im}\left[\left(\sum_{j=1}^{3} g^j_{F_i}(g^j_{F_k})^*\right)^2\right] M_k M_i \left\{\frac{\Theta\left(M_i^2-M_\eta^2\right)}{M_i^2} - \frac{M_\eta^2-M_k^2}{M_i^2-M_\eta^2}\,\Theta\left(M_\eta^2-M_k^2\right)\right.$$
$$\left. + \left[1+\frac{M_k^2-M_\eta^2}{M_i^2-M_\eta^2}\right]\mathrm{Im}\left\{\frac{1}{\pi}C_0(p_1,p_2,M_k^2,M_\eta^2,0)\right\}\right\}(8p_1\cdot p) \tag{E.13}$$

As before, states degenerate with the initial state in the loop, do not contribute to the CP asymmetry. Again, we perform the phase space integral, and after normalising to the total decay width, we obtain the final expression as

$$\mathrm{V}_1^{(i)} = \frac{1}{128\pi^2}\frac{M_i\left(1-\frac{M_\eta^2}{M_i^2}\right)^2}{\Gamma^i_{\mathrm{tot.}}}$$
$$\sum_{k\neq i}\mathrm{Im}\left[\left(\sum_{j=1}^{3} g^j_{F_i}(g^j_{F_k})^*\right)^2\right] M_k\, M_i \left\{\frac{\Theta\left(M_i^2-M_\eta^2\right)}{M_i^2} - \frac{M_\eta^2-M_k^2}{M_i^2-M_\eta^2}\,\frac{\Theta\left(M_\eta^2-M_k^2\right)}{M_\eta^2}\right.$$
$$\left. + 2\left(1-\frac{M_\eta^2-M_k^2}{M_i^2-M_\eta^2}\right)\mathrm{Im}\left[\frac{C_0(0,M_\eta^2,M_i^2,M_\eta^2,M_k^2,0)}{\pi}\right]\right\}. \tag{E.14}$$

The result for the other diagram involving the other state F is given by

$$\mathrm{V}_2^{(i)} = \frac{1}{128\pi^2}\frac{M_i\left(1-\frac{M_\Psi^2}{M_i^2}\right)}{\Gamma^i_{\mathrm{tot.}}}\sum_{k\neq i}\frac{1}{(M_i^2-M_\Psi^2)^2}\left\{\left(1+\frac{M_\Psi^2}{M_i^2}\right)(\mathcal{F}_{1a}+\mathcal{F}_{1b}) + 2\frac{M_\Psi}{M_i}(\mathcal{F}_{2a}+\mathcal{F}_{2b})\right\} \tag{E.15}$$

where

$$\mathcal{F}_{1a} =$$
$$-\left(1-\frac{M_\Psi^2}{M_i^2}\right)\Theta\left(M_i^2-M_\Psi^2\right)\left\{-2M_k^2M_iM_\Psi\,\mathrm{Im}\left[y_{1i}\,y_{2i}\,(y^*_{2k})^2\right] - M_kM_i\left(M_i^2+M_\Psi^2\right)\mathrm{Im}\left[y_{1i}^2\,(y^*_{1k})^2\right]\right.$$
$$-M_i^4\,\mathrm{Im}\left[(y_{1i}\,y_{2i}\,y^*_{1k}\,y^*_{2k})\right] - M_i^3M_\Psi\,\mathrm{Im}\left[y_{1i}^2\,y^*_{1k}\,y^*_{2k}\right] + 3M_i^2M_\Psi^2\,\mathrm{Im}\left[y_{1i}\,y_{2i}\,y^*_{1k}\,y^*_{2k}\right]$$
$$\left.+2M_iM_\Psi^3\,\mathrm{Im}\left[y_{1i}^2\,y^*_{1k}\,y^*_{2k}\right]\right\}$$
$$+\left(1-\frac{M_k^2}{M_\Psi^2}\right)\Theta\left(M_\Psi^2-M_k^2\right)\left\{-M_k\,M_\Psi\left(M_i^2+M_\Psi^2\right)\mathrm{Im}\left[y_{1i}\,y_{2i}\,y^*_{2k}\,y^*_{2k}\right] - 2M_kM_iM_\Psi^2\,\mathrm{Im}\left[y_{1i}^2\,(y^*_{1k})^2\right]\right.$$
$$\left.-M_i^3\,M_\Psi\,\mathrm{Im}\left[y_{1i}^2\,y^*_{1k}y^*_{2k}\right] + 3M_iM_\Psi^3\,\mathrm{Im}\left[y_{1i}^2\,y^*_{1k}\,y^*_{2k}\right] + 2M_\Psi^4\,\mathrm{Im}\left[y_{1i}\,y_{2i}\,y^*_{1k}\,y^*_{2k}\right]\right\}$$
$$+\,\mathrm{Im}\left[\frac{C_0(M_\Psi^2,0,M_i^2,0,M_k^2,M_\Psi^2)}{\pi}\right]\left\{-M_k\,M_\Psi\left(-2\left(M_k^2-M_\Psi^2\right)-M_i^4+M_\Psi^4\right)\mathrm{Im}\left[y_{1i}\,y_{2i}\,(y^*_{2k})^2\right]\right.$$

$$
\begin{aligned}
&+ M_k^2 M_i^4 \,\mathrm{Im}\left[y_{1i}\, y_{2i}\, y_{1k}^*\, y_{2k}^*\right] - M_k^2 M_i^3 M_\Psi \,\mathrm{Im}\left[y_{1i}^2\, y_{1k}^*\, y_{2k}^*\right] + M_k^2 M_i^3 M_\Psi \,\mathrm{Im}\left[y_{1i}^2\, y_{1k}^*\, y_{2k}^*\right] \\
&- 2M_k^2 M_i^2 M_\Psi^2 \,\mathrm{Im}\left[y_{1i}\, y_{2i}\, y_{1k}^*\, y_{2k}^*\right] + M_k^2 M_i^2 M_\Psi^2 \,\mathrm{Im}\left[y_{1i}\, y_{2i}\, y_{1k}^*\, y_{2k}^*\right] \\
&- M_k\, M_i \left(M_i^2 + M_\Psi^2\right)\left(-M_k^2 - M_i^2 + 2M_\Psi^2\right) \mathrm{Im}\left[y_{1i}^2\, \left(y_{1k}^*\right)^2\right] + 2M_\Psi^2 \left(M_\Psi^4 - M_k^2 M_i^2\right) \mathrm{Im}\left[y_{1i}\, y_{2i}\, y_{1k}^*\, y_{2k}^*\right] \\
&- 2M_k^2 M_i\, M_\Psi^3 \,\mathrm{Im}\left[y_{1i}^2\, y_{1k}^*\, y_{2k}^*\right] + M_k\, M_\Psi \left(M_i^2 - M_\Psi^2\right)^2 \mathrm{Im}\left[y_{1i}\, y_{2i}\, \left(y_{1k}^*\right)^2\right] - M_i^4 M_\Psi^2 \,\mathrm{Im}\left[y_{1i}\, y_{2i}\, y_{1k}^*\, y_{2k}^*\right] \\
&+ M_i^4 M_\Psi^2 \mathrm{Im}\left[y_{1i}\, y_{2i}\, y_{1k}^*\, y_{2k}^*\right] - 2M_i^3 M_\Psi^3 \mathrm{Im}\left[y_{1i}^2\, y_{1k}^*\, y_{2k}^*\right] - M_i^2 M_\Psi^4 \mathrm{Im}\left[y_{1i}\, y_{2i}\, y_{1k}^*\, y_{2k}^*\right] \\
&+ 4M_i\, M_\Psi^5 \mathrm{Im}\left[y_{1i}^2\, y_{1k}^*\, y_{2k}^*\right] + M_\Psi^6 \,\mathrm{Im}\left[y_{1i}\, y_{2i}\, y_{1k}^*\, y_{2k}^*\right] \Bigg\}
\end{aligned}
$$

$$
\begin{aligned}
\mathcal{F}_{1b} \;=\; &\left(1 - \frac{M_\Psi^2}{M_i^2}\right) \Theta\left(M_i^2 - M_\Psi^2\right) \Bigg\{ M_k\, M_i \left(M_i^2 + M_\Psi^2\right) \mathrm{Im}\left[y_{2i}^2\, \left(y_{2k}^*\right)^2\right] + 2M_k\, M_i^2 M_\Psi \,\mathrm{Im}\left[\left(y_{1k}^*\right)^2 y_{1i}\, y_{2i}\right] \\
&+ M_i^4 \mathrm{Im}\left[y_{1i}\, y_{2i}\, y_{1k}^*\, y_{2k}^*\right] + M_i^3 M_\Psi \,\mathrm{Im}\left[y_{2i}^2\, y_{1k}^*\, y_{2k}^*\right] - 3M_i^2 M_\Psi^2 \,\mathrm{Im}\left[y_{1i}\, y_{2i}\, y_{1k}^*\, y_{2k}^*\right] \\
&- 2M_i\, M_\Psi^3 \mathrm{Im}\left[y_{2i}^2\, y_{1k}^*\, y_{2k}^*\right] \Bigg\} \\
&- \left(1 - \frac{M_k^2}{M_\Psi^2}\right) \Theta\left(M_\Psi^2 - M_k^2\right) \Bigg\{ M_k\, M_\Psi \left(M_i^2 + M_\Psi^2\right) \mathrm{Im}\left[\left(y_{1k}^*\right)^2 y_{1i}\, y_{2i}\right] + 2M_k\, M_i\, M_\Psi^2 \,\mathrm{Im}\left[y_{2i}^2\, y_{2k}^*\, y_{2k}^*\right] \\
&+ M_i^3 M_\Psi \,\mathrm{Im}\left[y_{2i}^2\, y_{1k}^*\, y_{2k}^*\right] - 3M_i\, M_\Psi^3 \,\mathrm{Im}\left[y_{2i}^2\, y_{1k}^*\, y_{2k}^*\right] - 2M_\Psi^4 \,\mathrm{Im}\left[y_{1i}\, y_{2i}\, y_{1k}^*\, y_{2k}^*\right] \Bigg\} \\
&- \mathrm{Im}\left[\frac{C_0(M_\Psi^2, 0, M_i^2, 0, M_k^2, M_\Psi^2)}{\pi}\right] \Bigg\{ - M_k\, M_\Psi \left(-2\left(M_k^2 - M_\Psi^2\right) - M_i^4 + M_\Psi^4\right) \mathrm{Im}\left[y_{2i}^2\, \left(y_{2k}^*\right)^2\right] \\
&+ M_k^2\, M_i^4 \,\mathrm{Im}\left[y_{2i}^2\, y_{1k}^*\, y_{2k}^*\right] - M_k^2\, M_i^3\, M_\Psi \,\mathrm{Im}\left[y_{1i}\, y_{2i}\, y_{1k}^*\, y_{2k}^*\right] + M_k^2\, M_i^3\, M_\Psi \,\mathrm{Im}\left[y_{1i}\, y_{2i}\, y_{1k}^*\, y_{2k}^*\right] \\
&- 2M_k^2\, M_i^2\, M_\Psi^2 \,\mathrm{Im}\left[y_{2i}^2\, y_{1k}^*\, y_{2k}^*\right] + M_k^2\, M_i^2\, M_\Psi^2 \,\mathrm{Im}\left[y_{2i}^2\, y_{1k}^*\, y_{2k}^*\right] \\
&- M_k\, M_i \left(M_i^2 + M_\Psi^2\right)\left(-M_k^2 - M_i^2 + 2M_\Psi^2\right) \mathrm{Im}\left[y_{1i}\, y_{2i}\, \left(y_{1k}^*\right)^2\right] + 2M_\Psi^2 \left(M_\Psi^4 - M_k^2 M_i^2\right) \mathrm{Im}\left[y_{2i}^2\, y_{1k}^*\, y_{2k}^*\right] \\
&- 2M_k^2\, M_i\, M_\Psi^3 \,\mathrm{Im}\left[y_{1i}\, y_{2i}\, y_{1k}^*\, y_{2k}^*\right] - M_k\, M_\Psi \left(M_i^2 - M_\Psi^2\right)^2 \mathrm{Im}\left[y_{2i}^2\, \left(y_{1k}^*\right)^2\right] - M_i^4\, M_\Psi^2 \,\mathrm{Im}\left[y_{2i}^2\, y_{1k}^*\, y_{2k}^*\right] \\
&+ M_i^4\, M_\Psi^2 \,\mathrm{Im}\left[y_{2i}^2\, y_{1k}^*\, y_{2k}^*\right] - 2M_i^3\, M_\Psi^3 \,\mathrm{Im}\left[y_{1i}\, y_{2i}\, y_{1k}^*\, y_{2k}^*\right] - M_i^2 M_\Psi^4 \,\mathrm{Im}\left[y_{2i}^2\, y_{1k}^*\, y_{2k}^*\right] \\
&+ 4M_i\, M_\Psi^5 \,\mathrm{Im}\left[y_{1i}\, y_{2i}\, y_{1k}^*\, y_{2k}^*\right] + M_\Psi^6 \,\mathrm{Im}\left[y_{2i}^2\, y_{1k}^* y_{2k}^*\right] \Bigg\}
\end{aligned}
$$

$$
\begin{aligned}
&\mathcal{F}_{2a} \;=\\
&-\left(1-\frac{M_\Psi^2}{M_i^2}\right)\Theta\left(M_i^2-M_\Psi^2\right)\Bigg\{M_k\,M_i\left(M_i^2+M_\Psi^2\right)\mathrm{Im}\left[y_{1i}\,y_{2i}\;(y_{2k}^*)^2\right]+2M_k\,M_i^2\,M_\Psi\,\mathrm{Im}\left[y_{1i}^2\,(y_{1k}^*)^2\right]\\
&+M_i^4\,\mathrm{Im}\left[(y_{1i}^2\,y_{1k}^*\,y_{2k}^*\right]+M_i^3\,M_\Psi\,\mathrm{Im}\left[y_{1i}\,y_{2i}\,y_{1k}^*\,y_{2k}^*\right]-3M_i^2\,M_\Psi^2\,\mathrm{Im}\left[y_{1i}^2\,y_{1k}^*\,y_{2k}^*\right]\\
&-2M_i\,M_\Psi^3\,\mathrm{Im}\left[y_{1i}\,y_{2i}\,y_{1k}^*\,y_{2k}^*\right]\Bigg\}\\
&+\left(1-\frac{M_k^2}{M_\Psi^2}\right)\Theta\left(M_\Psi^2-M_k^2\right)\Bigg\{M_k\,M_\Psi\left(M_i^2+M_\Psi^2\right)\mathrm{Im}\left[y_{1i}^2\;(y_{1k}^*)^2\right]+2M_k\,M_i\,M_\Psi^2\mathrm{Im}\left[y_{1i}\,y_{2i}\,y_{2k}^*\,y_{2k}^*\right]\\
&+M_i^3\,M_\Psi\,\mathrm{Im}\left[y_{1i}\,y_{2i}\,y_{1k}^*\,y_{2k}^*\right]-3M_i\,M_\Psi^3\,\mathrm{Im}\left[y_{1i}\,y_{2i}\,y_{1k}^*\,y_{2k}^*\right]-2M_\Psi^4\,\mathrm{Im}\left[y_{1i}^2\,y_{1k}^*\,y_{2k}^*\right]\Bigg\}\\
&+\mathrm{Im}\left[\frac{C_0(M_\Psi^2,0,M_i^2,0,M_k^2,M_\Psi^2)}{\pi}\right]\Bigg\{-M_k^2M_i^4\mathrm{Im}\left[y_{1i}^2\,y_{1k}^*\,y_{2k}^*\right]-M_k^2\,M_i^3\,M_\Psi\,\mathrm{Im}\left[y_{1i}y_{2i}y_{1k}^*y_{2k}^*\right]\\
&+M_k^2\,M_i^3\,M_\Psi\,\mathrm{Im}\left[y_{1i}\,y_{2i}\,y_{1k}^*\,y_{2k}^*\right]-M_k^2\,M_i^2\,M_\Psi^2\,\mathrm{Im}\left[y_{1i}^2\,y_{1k}^*\,y_{2k}^*\right]+2M_k^2\,M_i^2\,M_\Psi^2\,\mathrm{Im}\left[y_{1i}^2\,y_{1k}^*\,y_{2k}^*\right]\\
&+M_k\,M_i\,\left(M_i^2+M_\Psi^2\right)\left(-M_k^2-M_i^2-2M_\Psi^2\right)\mathrm{Im}\left[y_{1i}\,y_{2i}\,y_{2k}^*\,y_{2k}^*\right]-2M_\Psi^2\left(M_\Psi^4-M_k^2M_i^2\right)\mathrm{Im}\left[y_{1i}^2\,y_{1k}^*\,y_{2k}^*\right]\\
&+M_k\,M_\Psi\left(-2M_i^2\left(M_k^2-M_\Psi^2\right)-M_i^4+M_\Psi^4\right)\mathrm{Im}\left[y_{1i}^2\,(y_{1k}^*)^2\right]+2M_k^2\,M_i\,M_\Psi^3\,\mathrm{Im}\left[y_{1i}\,y_{2i}\,y_{1k}^*\,y_{2k}^*\right]\\
&+M_k\,M_\Psi\left(M_i^2-M_\Psi^2\right)^2\mathrm{Im}\left[y_{1i}^2\,(y_{2k}^*)^2\right]+2M_i^3\,M_\Psi^3\,\mathrm{Im}\left[y_{1i}\,y_{2i}\,y_{1k}^*\,y_{2k}^*\right]+M_i^2\,M_\Psi^4\,\mathrm{Im}\left[y_{1i}^2\,y_{1k}^*\,y_{2k}^*\right]\\
&-4M_i\,M_\Psi^5\,\mathrm{Im}\left[y_{1i}\,y_{2i}\,y_{1k}^*\,y_{2k}^*\right]-M_\Psi^6\mathrm{Im}\left[y_{1i}^2\,y_{1k}^*\,y_{2k}^*\right]\Bigg\}
\end{aligned}
$$

$$
\begin{aligned}
&\mathcal{F}_{2b} \;=\\
&\left(1-\frac{M_\Psi^2}{M_i^2}\right)\Theta\left(M_i^2-M_\Psi^2\right)\Bigg\{-2M_k^2\,M_i\,M_\Psi\,\mathrm{Im}\left[y_{2i}^2\;(y_{2k}^*)^2\right]+M_k\,M_i\left(M_i^2+M_\Psi^2\right)\;\mathrm{Im}\left[(y_{1k}^*)^2\,y_{1i}\,y_{2i}\right]\\
&-M_i^4\,\mathrm{Im}\left[y_{2i}^2\,y_{1k}^*\,y_{2k}^*\right]-M_i^3\,M_\Psi\,\mathrm{Im}\left[y_{1i}\,y_{2i}\,y_{1k}^*\,y_{2k}^*\right]+3M_i^2\,M_\Psi^2\,\mathrm{Im}\left[y_{2i}^2\,y_{1k}^*\,y_{2k}^*\right]\\
&+2M_i\,M_\Psi^3\,\mathrm{Im}\left[y_{1i}\,y_{2i}\,y_{1k}^*\,y_{2k}^*\right]\Bigg\}\\
&-\left(1-\frac{M_k^2}{M_\Psi^2}\right)\Theta\left(M_\Psi^2-M_k^2\right)\Bigg\{-M_k\,M_\Psi\left(M_i^2+M_\Psi^2\right)\mathrm{Im}\left[y_{2i}^2\,y_{2k}^*\,y_{2k}^*\right]-2M_k\,M_i\,M_\Psi^2\,\mathrm{Im}\left[(y_{1k}^*)^2\;y_{1i}\,y_{2i}\right]
\end{aligned}
$$

$$- M_i^3\, M_\Psi\, \mathrm{Im}\left[y_{1i}\, y_{2i}\, y_{1k}^*\, y_{2k}^*\right] + 3M_i\, M_\Psi^3\, \mathrm{Im}\left[y_{1i}\, y_{2i}\, y_{1k}^*\, y_{2k}^*\right] + 2M_\Psi^4\, \mathrm{Im}\left[y_{2i}^2\, y_{1k}^*\, y_{2k}^*\right] \Bigg\}$$

$$- \mathrm{Im}\left[\frac{C_0(M_\Psi^2, 0, M_i^2, 0, M_k^2, M_\Psi^2)}{\pi}\right] \Bigg\{ - M_k M_\Psi \left(-2\left(M_k^2 - M_\Psi^2\right) - M_i^4 + M_\Psi^4\right) \mathrm{Im}\left[y_{2i}^2\, (y_{2k}^*)^2\right]$$

$$+ M_k^2\, M_i^4\, \mathrm{Im}\left[y_{2i}^2\, y_{1k}^*\, y_{2k}^*\right] - M_k^2\, M_i^2\, M_\Psi^2\, \mathrm{Im}\left[y_{2i}^2\, y_{1k}^*\, y_{2k}^*\right]$$

$$- M_k\, M_i \left(M_i^2 + M_\Psi^2\right) \left(-M_k^2 - M_i^2 + 2M_\Psi^2\right)\, \mathrm{Im}\left[y_{1i}\, y_{2i}\, (y_{1k}^*)^2\right] + 2M_\Psi^2\, \left(M_\Psi^4 - M_k^2 M_i^2\right) \mathrm{Im}\left[y_{2i}^2\, y_{1k}^*\, y_{2k}^*\right]$$

$$- 2M_k^2\, M_i\, M_\Psi^3\, \mathrm{Im}\left[y_{1i}\, y_{2i}\, y_{1k}^*\, y_{2k}^*\right] - M_k\, M_\Psi \left(M_i^2 - M_\Psi^2\right)^2 \mathrm{Im}\left[y_{2i}^2\, (y_{1k}^*)^2\right] - M_i^4\, M_\Psi^2\, \mathrm{Im}\left[y_{2i}^2\, y_{1k}^*\, y_{2k}^*\right]$$

$$+ M_i^4\, M_\Psi^2\, \mathrm{Im}\left[y_{2i}^2\, y_{1k}^*\, y_{2k}^*\right] - 2M_i^3\, M_\Psi^3\, \mathrm{Im}\left[y_{1i}\, y_{2i}\, y_{1k}^*\, y_{2k}^*\right] - M_i^2\, M_\Psi^4\, \mathrm{Im}\left[y_{2i}^2\, y_{1k}^*\, y_{2k}^*\right]$$

$$+ 4M_i\, M_\Psi^5\, \mathrm{Im}\left[y_{1i}\, y_{2i}\, y_{1k}^*\, y_{2k}^*\right] + M_\Psi^6\, \mathrm{Im}\left[y_{2i}^2\, y_{1k}^*\, y_{2k}^*\right] \Bigg\}$$

Next, there are set of vertex diagrams with the SM lepton-Higgs yukawa couplings, y^{SM}, which do not involve the other F state. The final expressions for these, which are calculated in a similar manner, are given by

$$\begin{aligned}
\mathrm{V}_3^{(i)} \;=\; & \frac{1}{128\pi^2} \frac{M_i \left(1 - \frac{M_\eta^2}{M_i^2}\right)^2}{\Gamma_{\mathrm{tot.}}^i} \sum_{j,k=1}^{3} \mathrm{Im}\left[g_{F_i}^j\, y_{jk}^{\mathrm{SM}}\, g_R^k\, y_{1i}^*\right] \Bigg\{ \left(1 - \frac{M_\Psi^2}{M_\eta^2}\right) \Theta\left(M_\eta^2 - M_\Psi^2\right) \\
& + \frac{M_i^2}{M_i^2 - M_\eta^2} \left[\left(1 - \frac{M_\Psi^2}{M_i^2}\right) \Theta\left(M_i^2 - M_\Psi^2\right) - \left(1 - \frac{M_\Psi^2}{M_\eta^2}\right) \Theta\left(M_\eta^2 - M_\Psi^2\right) \right] \Bigg\} \\
& - \frac{1}{128\pi^2} \frac{M_i \left(1 - \frac{M_\eta^2}{M_i^2}\right)^2}{\Gamma_{\mathrm{tot.}}^i} \sum_{j,k=1}^{3} \mathrm{Im}\left[g_{F_i}^j\, y_{jk}^{\mathrm{SM}}\, g_R^k\, y_{2i}^*\right] \frac{M_i\, M_\Psi}{M_i^2 - M_\eta^2} \Bigg\{ \left(1 - \frac{M_\Psi^2}{M_i^2}\right) \Theta\left(M_i^2 - M_\Psi^2\right) \\
& - \left(1 - \frac{M_\Psi^2}{M_\eta^2}\right) \Theta\left(M_\eta^2 - M_\Psi^2\right) \Bigg\}, \qquad \text{(E.16)}
\end{aligned}$$

$$\begin{aligned}
\mathrm{V}_4^{(i)} \;=\; & - \frac{1}{128\pi^2} \frac{M_i \left(1 - \frac{M_\Psi^2}{M_i^2}\right)}{\Gamma_{\mathrm{tot.}}^i} \sum_{j,k=1}^{3} \mathrm{Im}\left[(g_{F_i}^j)^*\, (y_{jk}^{\mathrm{SM}})^*\, (g_R^k)^*\, y_{1i}\right] \Bigg\{ \left(1 + \frac{M_\Psi^2}{M_i^2}\right) \mathcal{F}_3\left(M_i^2, M_\Psi^2, M_\eta^2\right) \\
& - 2\frac{M_\Psi}{M_i} \mathcal{F}_4\left(M_i^2, M_\Psi^2, M_\eta^2\right) \Bigg\} \\
& - \frac{1}{128\pi^2} \frac{M_i \left(1 - \frac{M_\Psi^2}{M_i^2}\right)}{\Gamma_{\mathrm{tot.}}^i} \sum_{j,k=1}^{3} \mathrm{Im}\left[(g_{F_i}^j)^*\, (y_{jk}^{\mathrm{SM}})^*\, (g_R^k)^*\, y_{2i}\right] \Bigg\{ \left(1 + \frac{M_\Psi^2}{M_i^2}\right) \mathcal{F}_4\left(M_i^2, M_\Psi^2, M_\eta^2\right) \\
& - 2\frac{M_\Psi}{M_i} \mathcal{F}_3\left(M_i^2, M_\Psi^2, M_\eta^2\right) \Bigg\}, \qquad \text{(E.17)}
\end{aligned}$$

where

$$\mathcal{F}_3\left(M_i^2, M_\Psi^2, M_\eta^2\right) = \frac{1}{M_i^2 - M_\Psi^2}\left[M_\Psi^2\left(1-\frac{M_\eta^2}{M_\Psi^2}\right)\Theta(M_\Psi^2 - M_\eta^2) - M_i^2\left(1-\frac{M_\eta^2}{M_i^2}\right)\Theta(M_i^2 - M_\eta^2)\right.$$
$$\left. - 2M_i^2\left(M_\Psi^2 - M_\eta^2\right)\mathrm{Im}\left[\frac{C_0(M_\psi^2, 0, M_i^2, M_\eta^2, 0, 0)}{\pi}\right]\right]$$

$$\mathcal{F}_4\left(M_i^2, M_\Psi^2, M_\eta^2\right) = \frac{M_i\, M_\Psi}{M_i^2 - M_\Psi^2}\left[\left(1-\frac{M_\eta^2}{M_\Psi^2}\right)\Theta(M_\Psi^2 - M_\eta^2) - \left(1-\frac{M_\eta^2}{M_i^2}\right)\Theta(M_i^2 - M_\eta^2)\right].$$

Finally, there are vertex diagrams featuring the scalar trilinear coupling α,

$$\mathrm{V}_5^{(i)} = \frac{1}{128\pi^2}\frac{M_i\left(1-\frac{M_\eta^2}{M_i^2}\right)^2}{\Gamma^i_{\text{tot.}}}\sum_{j=1}^{3}\mathrm{Im}\left[\alpha\, g^j_{F_i}\left(g^j_\Psi\right)^* y^*_{1i}\right] M_\Psi\,\mathrm{Im}\left[\frac{C_0(0, M_\eta^2, M_i^2, M_\Psi^2, M_S^2, 0)}{\pi}\right]$$
$$- \frac{1}{128\pi^2}\frac{M_i\left(1-\frac{M_\eta^2}{M_i^2}\right)^2}{\Gamma^i_{\text{tot.}}}\sum_{j=1}^{3}\mathrm{Im}\left[\alpha\, g^j_{F_i}\left(g^j_\Psi\right)^* y^*_{2i}\right] M_i\left\{\frac{1}{M_i^2 - M_\eta^2}\left(1-\frac{M_S^2}{M_\eta^2}\right)\Theta\left(M_\eta^2 - M_S^2\right)\right.$$
$$\left. - \frac{1}{M_i^2 - M_\eta^2}\left(1-\frac{M_\Psi^2}{M_i^2}\right)\Theta\left(M_i^2 - M_\Psi^2\right) + \frac{M_\Psi^2 - M_S^2}{M_i^2 - M_\eta^2}\,\mathrm{Im}\left[\frac{C_0(0, M_\eta^2, M_i^2, M_\Psi^2, M_S^2, 0)}{\pi}\right]\right\}, \tag{E.18}$$

$$\mathrm{V}_6^{(i)} = -\frac{1}{128\pi^2}\frac{M_i\left(1-\frac{M_\Psi^2}{M_i^2}\right)}{\Gamma^i_{\text{tot.}}}\sum_{j=1}^{3}\mathrm{Im}\left[\alpha^*\left(g^j_{F_i}\right)^* g^j_\Psi\, y_{1i}\right]\left\{\left(1+\frac{M_\Psi^2}{M_i^2}\right)\mathcal{F}_5\left(M_i, M_\Psi, M_\eta, M_S\right)\right.$$
$$\left. - 2\frac{M_\Psi}{M_i}\mathcal{F}_6\left(M_i, M_\Psi, M_\eta, M_S\right)\right\}$$
$$- \frac{1}{128\pi^2}\frac{M_i\left(1-\frac{M_\Psi^2}{M_i^2}\right)}{\Gamma^i_{\text{tot.}}}\sum_{j=1}^{3}\mathrm{Im}\left[\alpha^*\left(g^j_{F_i}\right)^* g^j_\Psi\, y_{2i}\right]\left\{\left(1+\frac{M_\Psi^2}{M_i^2}\right)\mathcal{F}_6\left(M_i^2, M_\Psi^2, M_\eta^2, M_S^2\right)\right.$$
$$\left. - 2\frac{M_\Psi}{M_i}\mathcal{F}_5\left(M_i^2, M_\Psi^2, M_\eta^2, M_S^2\right)\right\}, \tag{E.19}$$

where

$$\mathcal{F}_5\left(M_i, M_\Psi, M_\eta, M_S\right) =$$
$$\frac{M_\Psi}{(M_i^2 - M_\Psi^2)^2}\left[(M_i^2 + M_\Psi^2)\left(1-\frac{M_S^2}{M_\Psi^2}\right)\Theta(M_\Psi^2 - M_S^2) - 2M_i^2\left(1-\frac{M_\eta^2}{M_i^2}\right)\Theta(M_i^2 - M_\eta^2)\right.$$

$$+ (M_i^4 - M_i^2(M_\Psi^2 + M_\eta^2 - 2M_S^2) - M_\Psi^2 M_\eta^2)\,\mathrm{Im}\left[\frac{C_0(M_\psi^2, 0, M_i^2, 0, M_S^2, M_\eta^2)}{\pi}\right]\Bigg],$$

$$\mathcal{F}_6\,(M_i, M_\Psi, M_\eta, M_S) \;=$$

$$\frac{M_i}{(M_i^2 - M_\Psi^2)^2}\Bigg[2M_\Psi^2\left(1 - \frac{M_S^2}{M_\Psi^2}\right)\Theta(M_\Psi^2 - M_S^2) - (M_i^2 + M_\Psi^2)\left(1 - \frac{M_\eta^2}{M_i^2}\right)\Theta(M_i^2 - M_\eta^2)$$

$$+ (M_\Psi^4 - M_\Psi^2(M_i^2 + M_S^2 - 2M_\eta^2) - M_i^2 M_S^2)\,\mathrm{Im}\left[\frac{C_0(M_\psi^2, 0, M_i^2, 0, M_S^2, M_\eta^2)}{\pi}\right]\Bigg].$$

As a final note, we have checked that the expressions $\mathrm{WF}_1^{(i)}$ and $\mathrm{V}_1^{(i)}$ reproduce the known results [91] in the limiting case of $M_\eta \to 0$.

Bibliography

[1] A. Alvarez et al. *Accommodating muon* $(g-2)$ *and leptogenesis in a scotogenic model*. JHEP **06** (2023) 163. DOI: 10.1007/JHEP06(2023)163. arXiv: 2301.08485 [hep-ph].

[2] M. Peskin and D. V. Schroeder. *An Introduction to Quantum Field Theory*. Reading, USA: Addison-Wesley, 1995. ISBN: 978-0-201-50397-5.

[3] M. Schwartz. *Quantum Field Theory and the Standard Model*. Cambridge University Press, 2014. ISBN: 978-1-107-03473-0.

[4] **[Pierre Auger Collab.]**, A. Aab, et al. *Combined fit of spectrum and composition data as measured by the Pierre Auger Observatory*. JCAP **04** (2017). [Erratum: JCAP 03, E02 (2018)] 038. DOI: 10.1088/1475-7516/2017/04/038. arXiv: 1612.07155 [astro-ph.HE].

[5] G. Steigman. *Observational tests of antimatter cosmologies*. Ann. Rev. Astron. Astrophys. **14** (1976) 339–372. DOI: 10.1146/annurev.aa.14.090176.002011.

[6] E. W. Kolb and M. S. Turner. *The Early Universe*. Vol. 69. 1990. ISBN: 978-0-201-62674-2. DOI: 10.1201/9780429492860.

[7] B. D. Fields, K. A. Olive, T.-H. Yeh, and C. Young. *Big-Bang Nucleosynthesis after Planck*. JCAP **03** (2020). [Erratum: JCAP 11, E02 (2020)] 010. DOI: 10.1088/1475-7516/2020/03/010. arXiv: 1912.01132 [astro-ph.CO].

[8] **[Particle Data Group Collab.]**, R. L. Workman, et al. *Review of Particle Physics*. PTEP **2022** (2022) 083C01. DOI: 10.1093/ptep/ptac097.

[9] **[WMAP Collab.]**, C. L. Bennett, et al. *Nine-Year Wilkinson Microwave Anisotropy Probe (WMAP) Observations: Final Maps and Results*. Astrophys. J. Suppl. **208** (2013) 20. DOI: 10.1088/0067-0049/208/2/20. arXiv: 1212.5225 [astro-ph.CO].

[10] **[Planck Collab.]**, P. A. R. Ade, et al. *Planck 2015 results. XIII. Cosmological parameters*. Astron. Astrophys. **594** (2016) A13. DOI: 10.1051/0004-6361/201525830. arXiv: 1502.01589 [astro-ph.CO].

[11] **[Planck Collab.]**, N. Aghanim, et al. *Planck 2018 results. VI. Cosmological parameters*. Astron. Astrophys. **641** (2020). [Erratum: Astron.Astrophys. 652, C4 (2021)] A6. DOI: 10.1051/0004-6361/201833910. arXiv: 1807.06209 [astro-ph.CO].

[12] D. Baumann. *Inflation*. Theoretical Advanced Study Institute in Elementary Particle Physics: Physics of the Large and the Small. 2011 523–686. DOI: 10.1142/9789814327183_0010. arXiv: 0907.5424 [hep-th].

[13] **[BICEP2 Collab]** and **CERN** and **NASA**. https://home.cern/news/series/lhc-physics-ten/recreating-big-bang-matter-earth.

[14] A. D. Sakharov. *Violation of CP Invariance, C asymmetry, and baryon asymmetry of the universe*. Pisma Zh. Eksp. Teor. Fiz. **5** (1967) 32–35. DOI: 10.1070/PU1991v034n05ABEH002497.

[15] V. A. Kuzmin, V. A. Rubakov, and M. E. Shaposhnikov. *On the Anomalous Electroweak Baryon Number Nonconservation in the Early Universe*. Phys. Lett. B **155** (1985) 36. DOI: 10.1016/0370-2693(85)91028-7.

[16] G. 't Hooft. *Symmetry Breaking Through Bell-Jackiw Anomalies*. Phys. Rev. Lett. **37** (1976). Ed. by M. A. Shifman 8–11. DOI: 10.1103/PhysRevLett.37.8.

[17] M. Kobayashi and T. Maskawa. *CP Violation in the Renormalizable Theory of Weak Interaction*. Prog. Theor. Phys. **49** (1973) 652–657. DOI: 10.1143/PTP.49.652.

[18] C. Jarlskog. *Commutator of the Quark Mass Matrices in the Standard Electroweak Model and a Measure of Maximal CP Nonconservation*. Phys. Rev. Lett. **55** (1985) 1039. DOI: 10.1103/PhysRevLett.55.1039.

[19] M. B. Gavela, M. Lozano, J. Orloff, and O. Pene. *Standard model CP violation and baryon asymmetry. Part 1: Zero temperature*. Nucl. Phys. B **430** (1994) 345–381. DOI: 10.1016/0550-3213(94)00409-9. arXiv: hep-ph/9406288.

[20] M. B. Gavela et al. *Standard model CP violation and baryon asymmetry. Part 2: Finite temperature*. Nucl. Phys. B **430** (1994) 382–426. DOI: 10.1016/0550-3213(94)00410-2. arXiv: hep-ph/9406289.

[21] V. A. Rubakov and M. E. Shaposhnikov. *Electroweak baryon number nonconservation in the early universe and in high-energy collisions*. Usp. Fiz. Nauk **166** (1996) 493–537. DOI: 10.1070/PU1996v039n05ABEH000145. arXiv: hep-ph/9603208.

[22] M. Trodden. *Electroweak baryogenesis*. Rev. Mod. Phys. **71** (1999) 1463–1500. DOI: 10.1103/RevModPhys.71.1463. arXiv: hep-ph/9803479.

[23] K. Kajantie, M. Laine, K. Rummukainen, and M. E. Shaposhnikov. *Is there a hot electroweak phase transition at $m_H \gtrsim m_W$?* Phys. Rev. Lett. **77** (1996) 2887–2890. DOI: 10.1103/PhysRevLett.77.2887. arXiv: hep-ph/9605288.

[24] K. Kajantie, M. Laine, K. Rummukainen, and M. E. Shaposhnikov. *A Nonperturbative analysis of the finite T phase transition in SU(2) x U(1) electroweak theory*. Nucl. Phys. B **493** (1997) 413–438. DOI: 10.1016/S0550-3213(97)00164-8. arXiv: hep-lat/9612006.

[25] F. Csikor, Z. Fodor, and J. Heitger. *Endpoint of the hot electroweak phase transition*. Phys. Rev. Lett. **82** (1999) 21–24. DOI: 10.1103/PhysRevLett.82.21. arXiv: hep-ph/9809291.

[26] T. S. van Albada, J. N. Bahcall, K. Begeman, and R. Sancisi. *Distribution of dark matter in the spiral galaxy NGC 3198*. Astrophysical J., Pt. 1 **295** (1985) 305–313. DOI: 10.1086/163375.

[27] C. J. Peterson, V. C. Rubin, W. K. Ford, and M. S. Roberts. *Extended rotation curves of high-luminosity spiral galaxies. III - The spiral galaxy NGC 7217*. Astrophysical J., Pt. 1 **226** (1978) 770–776. DOI: 10.1086/156658.

[28] V. C. Rubin, W. K. Ford, and N. Thonnard. *Extended rotation curves of high-luminosity spiral galaxies. IV - Systematic dynamical properties, SA through SC.* Astrophysical J., Pt. 2 - Lett. to Ed. **225** (1978) L107–L111. DOI: 10.1086/182804.

[29] K. G. Begeman, A. H. Broeils, and R. H. Sanders. *Extended rotation curves of spiral galaxies: Dark haloes and modified dynamics.* Mon. Not. Roy. Astron. Soc. **249** (1991) 523.

[30] D. Clowe, A. H. Gonzalez, and M. Markevitch. *Weak-Lensing Mass Reconstruction of the Interacting Cluster 1E 0657-558: Direct Evidence for the Existence of Dark Matter.* The Astrophysical J. **604**.2 (2004) 596–603. DOI: 10.1086/381970.

[31] D. Clowe, M. Bradač, A. H. Gonzalez, M. Markevitch, et al. *A Direct Empirical Proof of the Existence of Dark Matter.* The Astrophysical J. **648**.2 (2006) L109–L113. DOI: 10.1086/508162.

[32] R. Massey, T. Kitching, and J. Richard. *The dark matter of gravitational lensing.* Rept. Prog. Phys. **73** (2010) 086901. DOI: 10.1088/0034-4885/73/8/086901. arXiv: 1001.1739 [astro-ph.CO].

[33] G. Jungman, M. Kamionkowski, and K. Griest. *Supersymmetric dark matter.* Phys. Rept. **267** (1996) 195–373. DOI: 10.1016/0370-1573(95)00058-5. arXiv: hep-ph/9506380.

[34] G. Bertone, D. Hooper, and J. Silk. *Particle dark matter: Evidence, candidates and constraints.* Phys. Rept. **405** (2005) 279–390. DOI: 10.1016/j.physrep.2004.08.031. arXiv: hep-ph/0404175.

[35] J. L. Feng. *Dark Matter Candidates from Particle Physics and Methods of Detection.* Ann. Rev. Astron. Astrophys. **48** (2010) 495–545. DOI: 10.1146/annurev-astro-082708-101659. arXiv: 1003.0904 [astro-ph.CO].

[36] G. Bertone and D. Hooper. *History of dark matter.* Rev. Mod. Phys. **90**.4 (2018) 045002. DOI: 10.1103/RevModPhys.90.045002. arXiv: 1605.04909 [astro-ph.CO].

[37] M. Drees. *Dark Matter Theory.* PoS **ICHEP2018** (2019) 730. DOI: 10.22323/1.340.0730. arXiv: 1811.06406 [hep-ph].

[38] P. F. de Salas et al. *2020 global reassessment of the neutrino oscillation picture.* JHEP **02** (2021) 071. DOI: 10.1007/JHEP02(2021)071. arXiv: 2006.11237 [hep-ph].

[39] M. C. Gonzalez-Garcia, M. Maltoni, and T. Schwetz. *NuFIT: Three-Flavour Global Analyses of Neutrino Oscillation Experiments.* Universe **7**.12 (2021) 459. DOI: 10.3390/universe7120459. arXiv: 2111.03086 [hep-ph].

[40] J. M. Cornwall, R. Jackiw, and E. Tomboulis. *Effective Action for Composite Operators.* Phys. Rev. D **10** (1974) 2428–2445. DOI: 10.1103/PhysRevD.10.2428.

[41] E. Braaten and R. D. Pisarski. *Soft Amplitudes in Hot Gauge Theories: A General Analysis.* Nucl. Phys. B **337** (1990) 569–634. DOI: 10.1016/0550-3213(90)90508-B.

[42] J. P. Blaizot, E. Iancu, and A. Rebhan. *Selfconsistent hard thermal loop thermodynamics for the quark gluon plasma.* Phys. Lett. B **470** (1999) 181–188. DOI: 10.1016/S0370-2693(99)01306-4. arXiv: hep-ph/9910309.

[43] J.-P. Blaizot, E. Iancu, and A. Rebhan. *Thermodynamics of the high temperature quark gluon plasma*. Mar. 2003 60–122. DOI: 10.1142/9789812795533_0002. arXiv: hep-ph/0303185.

[44] J. P. Blaizot, E. Iancu, and A. Rebhan. *Approximately selfconsistent resummations for the thermodynamics of the quark gluon plasma. 1. Entropy and density*. Phys. Rev. D **63** (2001) 065003. DOI: 10.1103/PhysRevD.63.065003. arXiv: hep-ph/0005003.

[45] J. O. Andersen and M. Strickland. *Three-loop Phi-derivable approximation in QED*. Phys. Rev. D **71** (2005) 025011. DOI: 10.1103/PhysRevD.71.025011. arXiv: hep-ph/0406163.

[46] J. Berges, S. Borsanyi, U. Reinosa, and J. Serreau. *Renormalized thermodynamics from the 2PI effective action*. Phys. Rev. D **71** (2005) 105004. DOI: 10.1103/PhysRevD.71.105004. arXiv: hep-ph/0409123.

[47] E. Calzetta and B. L. Hu. *Nonequilibrium quantum fields: Closed-time-path effective action, Wigner function, and Boltzmann equation*. Phys. Rev. D **37** (10 1988) 2878–2900. DOI: 10.1103/PhysRevD.37.2878.

[48] Y. B. Ivanov, J. Knoll, and D. N. Voskresensky. *Selfconsistent approximations to nonequilibrium many body theory*. Nucl. Phys. A **657** (1999) 413–445. DOI: 10.1016/S0375-9474(99)00313-9. arXiv: hep-ph/9807351.

[49] J. Berges. *Introduction to nonequilibrium quantum field theory*. AIP Conf. Proc. **739**.1 (2004). Ed. by M. Bracco, M. Chiapparini, E. Ferreira, and T. Kodama 3–62. DOI: 10.1063/1.1843591. arXiv: hep-ph/0409233.

[50] J. Berges. *Nonequilibrium Quantum Fields: From Cold Atoms to Cosmology* (Mar. 2015). arXiv: 1503.02907 [hep-ph].

[51] J. Berges. *N-particle irreducible effective action techniques for gauge theories*. Phys. Rev. D **70** (2004) 105010. DOI: 10.1103/PhysRevD.70.105010. arXiv: hep-ph/0401172.

[52] J. Berges. *Controlled nonperturbative dynamics of quantum fields out-of-equilibrium*. Nucl. Phys. A **699** (2002) 847–886. DOI: 10.1016/S0375-9474(01)01295-7. arXiv: hep-ph/0105311.

[53] G. Aarts et al. *Far from equilibrium dynamics with broken symmetries from the 2PI - 1/N expansion*. Phys. Rev. D **66** (2002) 045008. DOI: 10.1103/PhysRevD.66.045008. arXiv: hep-ph/0201308.

[54] A. Arrizabalaga, J. Smit, and A. Tranberg. *Equilibration in phi**4 theory in 3+1 dimensions*. Phys. Rev. D **72** (2005) 025014. DOI: 10.1103/PhysRevD.72.025014. arXiv: hep-ph/0503287.

[55] J. Berges and S. Roth. *Topological defect formation from 2PI effective action techniques*. Nucl. Phys. B **847** (2011) 197–219. DOI: 10.1016/j.nuclphysb.2011.01.024. arXiv: 1012.1212 [hep-ph].

[56] U. Reinosa and J. Serreau. *2PI effective action for gauge theories: Renormalization*. JHEP **07** (2006) 028. DOI: 10.1088/1126-6708/2006/07/028. arXiv: hep-th/0605023.

[57] U. Reinosa and J. Serreau. *Ward Identities for the 2PI effective action in QED*. JHEP **11** (2007) 097. DOI: 10.1088/1126-6708/2007/11/097. arXiv: 0708.0971 [hep-th].

[58] U. Reinosa and J. Serreau. *2PI functional techniques for gauge theories: QED*. Annals Phys. **325** (2010) 969–1017. DOI: 10.1016/j.aop.2009.11.005. arXiv: 0906.2881 [hep-ph].

[59] O. Oliveira and R. C. Terin. *The Dyson-Schwinger equations and the non-perturbative solution of QED: exploring the two-photon-two-fermion irreducible vertex* (Apr. 2022). arXiv: 2204.04197 [hep-ph].

[60] K. Kainulainen and O. Koskivaara. *Non-equilibrium dynamics of a scalar field with quantum backreaction*. JHEP **12** (2021) 190. DOI: 10.1007/JHEP12(2021)190. arXiv: 2105.09598 [hep-ph].

[61] M. Laine. *Effective theories of MSSM at high temperature*. Nucl. Phys. B **481** (1996). [Erratum: Nucl.Phys.B 548, 637–638 (1999)] 43–84. DOI: 10.1016/S0550-3213(96)90121-2. arXiv: hep-ph/9605283.

[62] K. Kainulainen et al. *On the validity of perturbative studies of the electroweak phase transition in the Two Higgs Doublet model*. JHEP **06** (2019) 075. DOI: 10.1007/JHEP06(2019)075. arXiv: 1904.01329 [hep-ph].

[63] L. V. Keldysh. *Diagram technique for nonequilibrium processes*. Zh. Eksp. Teor. Fiz. **47** (1964) 1515–1527.

[64] R. Jackiw. *Functional evaluation of the effective potential*. Phys. Rev. D **9** (1974) 1686. DOI: 10.1103/PhysRevD.9.1686.

[65] J. Berges, S. Borsanyi, U. Reinosa, and J. Serreau. *Nonperturbative renormalization for 2PI effective action techniques*. Annals Phys. **320** (2005) 344–398. DOI: 10.1016/j.aop.2005.06.001. arXiv: hep-ph/0503240.

[66] U. Reinosa. *Nonperturbative renormalization of phi-derivable approximations in theories with fermions*. Nucl. Phys. A **772** (2006) 138–166. DOI: 10.1016/j.nuclphysa.2006.03.014. arXiv: hep-ph/0510119.

[67] A. Banik, H. Hinrichsen, K. Kainulainen, and W. Porod. *Aspects of renormalisation in the 2PI formalism* (2023). arXiv: 23XX.XXXXX.

[68] J.-P. Blaizot, E. Iancu, and U. Reinosa. *Renormalizability of Phi derivable approximations in scalar phi**4 theory*. Phys. Lett. B **568** (2003) 160–166. DOI: 10.1016/j.physletb.2003.06.008. arXiv: hep-ph/0301201.

[69] J.-P. Blaizot, E. Iancu, and U. Reinosa. *Renormalization of Phi derivable approximations in scalar field theories*. Nucl. Phys. A **736** (2004) 149–200. DOI: 10.1016/j.nuclphysa.2004.02.019. arXiv: hep-ph/0312085.

[70] A. Pilaftsis and D. Teresi. *Exact RG Invariance and Symmetry Improved 2PI Effective Potential*. Nucl. Phys. B **920** (2017) 298–318. DOI: 10.1016/j.nuclphysb.2017.04.015. arXiv: 1703.02079 [hep-ph].

[71] A. Pilaftsis and D. Teresi. *Symmetry Improved CJT Effective Action*. Nucl. Phys. B **874**.2 (2013) 594–619. DOI: 10.1016/j.nuclphysb.2013.06.004. arXiv: 1305.3221 [hep-ph].

[72] A. Patkos and Z. Szep. *Counterterm resummation for 2PI-approximation in constant background*. Nucl. Phys. A **811** (2008) 329–352. DOI: 10.1016/j.nuclphysa.2008.08.001. arXiv: 0806.2554 [hep-ph].

[73] A. Pilaftsis and D. Teresi. *Symmetry Improved 2PI Effective Action and the Infrared Divergences of the Standard Model*. J. Phys. Conf. Ser. **631**.1 (2015). Ed. by N. E. Mavromatos, V. A. Mitsou, D. Skliros, and A. Di Domenico 012008. DOI: 10.1088/1742-6596/631/1/012008. arXiv: 1502.07986 [hep-ph].

[74] H. Jukkala, K. Kainulainen, and P. M. Rahkila. *Flavour mixing transport theory and resonant leptogenesis*. JHEP **09** (2021) 119. DOI: 10.1007/JHEP09(2021)119. arXiv: 2104.03998 [hep-ph].

[75] K. Kainulainen. *CP-violating transport theory for electroweak baryogenesis with thermal corrections*. JCAP **11**.11 (2021) 042. DOI: 10.1088/1475-7516/2021/11/042. arXiv: 2108.08336 [hep-ph].

[76] G. Amelino-Camelia and S.-Y. Pi. *Selfconsistent improvement of the finite temperature effective potential*. Phys. Rev. D **47** (1993) 2356–2362. DOI: 10.1103/PhysRevD.47.2356. arXiv: hep-ph/9211211.

[77] P. Q. Hung. *Vacuum Instability and New Constraints on Fermion Masses*. Phys. Rev. Lett. **42** (1979) 873. DOI: 10.1103/PhysRevLett.42.873.

[78] M. Sher. *Electroweak Higgs Potentials and Vacuum Stability*. Phys. Rept. **179** (1989) 273–418. DOI: 10.1016/0370-1573(89)90061-6.

[79] J. A. Casas, J. R. Espinosa, and M. Quiros. *Improved Higgs mass stability bound in the standard model and implications for supersymmetry*. Phys. Lett. B **342** (1995) 171–179. DOI: 10.1016/0370-2693(94)01404-Z. arXiv: hep-ph/9409458.

[80] G. Isidori, G. Ridolfi, and A. Strumia. *On the metastability of the standard model vacuum*. Nucl. Phys. B **609** (2001) 387–409. DOI: 10.1016/S0550-3213(01)00302-9. arXiv: hep-ph/0104016.

[81] G. Degrassi et al. *Higgs mass and vacuum stability in the Standard Model at NNLO*. JHEP **08** (2012) 098. DOI: 10.1007/JHEP08(2012)098. arXiv: 1205.6497 [hep-ph].

[82] M. Fukugita and T. Yanagida. *Baryogenesis Without Grand Unification*. Phys. Lett. B **174** (1986) 45–47. DOI: 10.1016/0370-2693(86)91126-3.

[83] E. W. Kolb and S. Wolfram. *Baryon Number Generation in the Early Universe*. Nucl. Phys. B **172** (1980). [Erratum: Nucl.Phys.B 195, 542 (1982)] 224. DOI: 10.1016/0550-3213(82)90012-8.

[84] S. Davidson. *Flavoured Leptogenesis*. 12th International Workshop on Neutrinos Telescopes: Twenty Years after the Supernova 1987A Neutrino Bursts Discovery. May 2007 531–545. arXiv: 0705.1590 [hep-ph].

[85] A. Pilaftsis and T. E. J. Underwood. *Resonant leptogenesis*. Nucl. Phys. B **692** (2004) 303–345. DOI: 10.1016/j.nuclphysb.2004.05.029. arXiv: hep-ph/0309342.

[86] P. C. da Silva, D. Karamitros, T. McKelvey, and A. Pilaftsis. *Tri-resonant leptogenesis in a seesaw extension of the Standard Model*. JHEP **11** (2022) 065. DOI: 10.1007/JHEP11(2022)065. arXiv: 2206.08352 [hep-ph].

[87] T. Hambye. *Leptogenesis: beyond the minimal type I seesaw scenario*. New J. Phys. **14** (2012) 125014. DOI: 10.1088/1367-2630/14/12/125014. arXiv: 1212.2888 [hep-ph].

[88] T. Hambye and D. Teresi. *Higgs doublet decay as the origin of the baryon asymmetry*. Phys. Rev. Lett. **117**.9 (2016) 091801. DOI: 10.1103/PhysRevLett.117.091801. arXiv: 1606.00017 [hep-ph].

[89] W. Buchmüller, P. Di Bari, and M. Plümacher. *Leptogenesis for pedestrians*. Annals Phys. **315** (2005) 305–351. DOI: 10.1016/j.aop.2004.02.003. arXiv: hep-ph/0401240.

[90] S. Davidson, E. Nardi, and Y. Nir. *Leptogenesis*. Phys. Rept. **466** (2008) 105–177. DOI: 10.1016/j.physrep.2008.06.002. arXiv: 0802.2962 [hep-ph].

[91] L. Covi, E. Roulet, and F. Vissani. *CP violating decays in leptogenesis scenarios*. Phys. Lett. B **384** (1996) 169–174. DOI: 10.1016/0370-2693(96)00817-9. arXiv: hep-ph/9605319.

[92] J. Liu and G. Segre. *Reexamination of generation of baryon and lepton number asymmetries by heavy particle decay*. Phys. Rev. D **48** (1993) 4609–4612. DOI: 10.1103/PhysRevD.48.4609. arXiv: hep-ph/9304241.

[93] J. Liu and G. Segre. *Unstable particle mixing and CP violation in weak decays*. Phys. Rev. D **49** (1994) 1342–1349. DOI: 10.1103/PhysRevD.49.1342. arXiv: hep-ph/9310248.

[94] R. E. Cutkosky. *Singularities and discontinuities of Feynman amplitudes*. J. Math. Phys. **1** (1960) 429–433. DOI: 10.1063/1.1703676.

[95] S. Dodelson. *Modern Cosmology*. Amsterdam: Academic Press, 2003. ISBN: 978-0-12-219141-1.

[96] D. Baumann. *Cosmology*. Cambridge University Press, July 2022. ISBN: 978-1-108-93709-2. DOI: 10.1017/9781108937092.

[97] W. Buchmuller, P. Di Bari, and M. Plumacher. *Cosmic microwave background, matter - antimatter asymmetry and neutrino masses*. Nucl. Phys. B **643** (2002). [Erratum: Nucl.Phys.B 793, 362 (2008)] 367–390. DOI: 10.1016/S0550-3213(02)00737-X. arXiv: hep-ph/0205349.

[98] M. A. Luty. *Baryogenesis via leptogenesis*. Phys. Rev. D **45** (1992) 455–465. DOI: 10.1103/PhysRevD.45.455.

[99] M. Plümacher. *Baryogenesis and lepton number violation*. Z. Phys. C **74** (1997) 549–559. DOI: 10.1007/s002880050418. arXiv: hep-ph/9604229.

[100] V. A. Rubakov and D. S. Gorbunov. *Introduction to the Theory of the Early Universe: Hot big bang theory*. Singapore: World Scientific, 2017. ISBN: 978-981-320-987-9. DOI: 10.1142/10447.

[101] J. A. Harvey and M. S. Turner. *Cosmological baryon and lepton number in the presence of electroweak fermion number violation*. Phys. Rev. D **42** (1990) 3344–3349. DOI: 10.1103/PhysRevD.42.3344.

[102] E. Ma. *Verifiable radiative seesaw mechanism of neutrino mass and dark matter*. Phys. Rev. D **73** (2006) 077301. DOI: 10.1103/PhysRevD.73.077301. arXiv: hep-ph/0601225.

[103] T. Toma and A. Vicente. *Lepton Flavor Violation in the Scotogenic Model*. JHEP **01** (2014) 160. DOI: 10.1007/JHEP01(2014)160. arXiv: 1312.2840 [hep-ph].

[104] A. Vicente and C. E. Yaguna. *Probing the scotogenic model with lepton flavor violating processes*. JHEP **02** (2015) 144. DOI: 10.1007/JHEP02(2015)144. arXiv: 1412.2545 [hep-ph].

[105] S. Fraser, E. Ma, and O. Popov. *Scotogenic Inverse Seesaw Model of Neutrino Mass*. Phys. Lett. B **737** (2014) 280–282. DOI: 10.1016/j.physletb.2014.08.069. arXiv: 1408.4785 [hep-ph].

[106] S. Baumholzer, V. Brdar, P. Schwaller, and A. Segner. *Shining Light on the Scotogenic Model: Interplay of Colliders and Cosmology*. JHEP **09** (2020) 136. DOI: 10.1007/JHEP09(2020)136. arXiv: 1912.08215 [hep-ph].

[107] P. Rocha-Moran and A. Vicente. *Lepton Flavor Violation in the singlet-triplet scotogenic model*. JHEP **07** (2016) 078. DOI: 10.1007/JHEP07(2016)078. arXiv: 1605.01915 [hep-ph].

[108] I. M. Ávila, V. De Romeri, L. Duarte, and J. W. F. Valle. *Phenomenology of scotogenic scalar dark matter*. Eur. Phys. J. C **80**.10 (2020) 908. DOI: 10.1140/epjc/s10052-020-08480-z. arXiv: 1910.08422 [hep-ph].

[109] A. Ahriche, A. Jueid, and S. Nasri. *A natural scotogenic model for neutrino mass & dark matter*. Phys. Lett. B **814** (2021) 136077. DOI: 10.1016/j.physletb.2021.136077. arXiv: 2007.05845 [hep-ph].

[110] V. De Romeri, M. Puerta, and A. Vicente. *Dark matter in a charged variant of the Scotogenic model* (June 2021). arXiv: 2106.00481 [hep-ph].

[111] B. B. Boruah, L. Sarma, and M. K. Das. *Lepton flavor violation and leptogenesis in discrete flavor symmetric scotogenic model*. Nucl. Phys. B **969** (2021) 115472. DOI: 10.1016/j.nuclphysb.2021.115472.

[112] D. Restrepo, O. Zapata, and C. E. Yaguna. *Models with radiative neutrino masses and viable dark matter candidates*. JHEP **11** (2013) 011. DOI: 10.1007/JHEP11(2013)011. arXiv: 1308.3655 [hep-ph].

[113] M. Sarazin, J. Bernigaud, and B. Herrmann. *Dark matter and lepton flavour phenomenology in a singlet-doublet scotogenic model*. JHEP **12** (2021) 116. DOI: 10.1007/JHEP12(2021)116. arXiv: 2107.04613 [hep-ph].

[114] J. A. Casas and A. Ibarra. *Oscillating neutrinos and $\mu \to e, \gamma$*. Nucl. Phys. B **618** (2001) 171–204. DOI: 10.1016/S0550-3213(01)00475-8. arXiv: hep-ph/0103065.

[115] L. Basso et al. *Proposal for generalised Supersymmetry Les Houches Accord for see-saw models and PDG numbering scheme*. Comput. Phys. Commun. **184** (2013) 698–719. DOI: 10.1016/j.cpc.2012.11.004. arXiv: 1206.4563 [hep-ph].

[116] **[Muon g-2 Collab.]**, G. W. Bennett, et al. *Final Report of the Muon E821 Anomalous Magnetic Moment Measurement at BNL*. Phys. Rev. D **73** (2006) 072003. DOI: 10.1103/PhysRevD.73.072003. arXiv: hep-ex/0602035.

[117] **[Muon g-2 Collab.]**, B. Abi, et al. *Measurement of the Positive Muon Anomalous Magnetic Moment to 0.46 ppm*. Phys. Rev. Lett. **126**.14 (2021) 141801. DOI: 10.1103/PhysRevLett.126.141801. arXiv: 2104.03281 [hep-ex].

[118] T. Aoyama et al. *The anomalous magnetic moment of the muon in the Standard Model*. Phys. Rept. **887** (2020) 1–166. DOI: 10.1016/j.physrep.2020.07.006. arXiv: 2006.04822 [hep-ph].

[119] S. Borsanyi et al. *Leading hadronic contribution to the muon magnetic moment from lattice QCD*. Nature **593**.7857 (2021) 51–55. DOI: 10.1038/s41586-021-03418-1. arXiv: 2002.12347 [hep-lat].

[120] M. Cè et al. *Window observable for the hadronic vacuum polarization contribution to the muon g-2 from lattice QCD*. Phys. Rev. D **106**.11 (2022) 114502. DOI: 10.1103/PhysRevD.106.114502. arXiv: 2206.06582 [hep-lat].

[121] C. Alexandrou et al. *Lattice calculation of the short and intermediate time-distance hadronic vacuum polarization contributions to the muon magnetic moment using twisted-mass fermions* (June 2022). arXiv: 2206.15084 [hep-lat].

[122] A. Keshavarzi, W. J. Marciano, M. Passera, and A. Sirlin. *Muon $g-2$ and $\Delta\alpha$ connection*. Phys. Rev. D **102**.3 (2020) 033002. DOI: 10.1103/PhysRevD.102.033002. arXiv: 2006.12666 [hep-ph].

[123] A. Crivellin, M. Hoferichter, C. A. Manzari, and M. Montull. *Hadronic Vacuum Polarization: $(g-2)_\mu$ versus Global Electroweak Fits*. Phys. Rev. Lett. **125**.9 (2020) 091801. DOI: 10.1103/PhysRevLett.125.091801. arXiv: 2003.04886 [hep-ph].

[124] G. Colangelo et al. *Data-driven evaluations of Euclidean windows to scrutinize hadronic vacuum polarization*. Phys. Lett. B **833** (2022) 137313. DOI: 10.1016/j.physletb.2022.137313. arXiv: 2205.12963 [hep-ph].

[125] B. Grzadkowski, M. Iskrzynski, M. Misiak, and J. Rosiek. *Dimension-Six Terms in the Standard Model Lagrangian*. JHEP **10** (2010) 085. DOI: 10.1007/JHEP10(2010)085. arXiv: 1008.4884 [hep-ph].

[126] A. Crivellin, M. Hoferichter, and P. Schmidt-Wellenburg. *Combined explanations of $(g-2)_{\mu,e}$ and implications for a large muon EDM*. Phys. Rev. D **98**.11 (2018) 113002. DOI: 10.1103/PhysRevD.98.113002. arXiv: 1807.11484 [hep-ph].

[127] C. Arbeláez, R. Cepedello, R. M. Fonseca, and M. Hirsch. *$(g-2)$ anomalies and neutrino mass*. Phys. Rev. D **102**.7 (2020) 075005. DOI: 10.1103/PhysRevD.102.075005. arXiv: 2007.11007 [hep-ph].

[128] **[MEG Collab.]**, A. M. Baldini, et al. *Search for the lepton flavour violating decay $\mu^+ \to e^+\gamma$ with the full dataset of the MEG experiment*. Eur. Phys. J. C **76**.8 (2016) 434. DOI: 10.1140/epjc/s10052-016-4271-x. arXiv: 1605.05081 [hep-ex].

[129] **[MEG II Collab.]** *MEG II experiment status and prospect*. PoS **NuFact2021** (2022) 120. DOI: 10.22323/1.402.0120. arXiv: 2201.08200 [hep-ex].

[130] A. Blondel et al. *Research Proposal for an Experiment to Search for the Decay $\mu \to eee$* (Jan. 2013). arXiv: 1301.6113 [physics.ins-det].

[131] **[COMET Collab.]**, R. Abramishvili, et al. *COMET Phase-I Technical Design Report*. PTEP **2020**.3 (2020) 033C01. DOI: 10.1093/ptep/ptz125. arXiv: 1812.09018 [physics.ins-det].

[132] K. Hayasaka et al. *Search for Lepton Flavor Violating Tau Decays into Three Leptons with 719 Million Produced Tau+Tau- Pairs*. Phys. Lett. B **687** (2010) 139–143. DOI: 10.1016/j.physletb.2010.03.037. arXiv: 1001.3221 [hep-ex].

[133] **[Belle Collab.]**, A. Abdesselam, et al. *Search for lepton-flavor-violating tau-lepton decays to $\ell\gamma$ at Belle*. JHEP **10** (2021) 19. DOI: 10.1007/JHEP10(2021)019. arXiv: 2103.12994 [hep-ex].

[134] S. Banerjee. *Searches for Lepton Flavor Violation in Tau Decays at Belle II*. Universe **8**.9 (2022) 480. DOI: 10.3390/universe8090480. arXiv: 2209.11639 [hep-ex].

[135] M. Cannoni, J. Ellis, M. E. Gomez, and S. Lola. *Neutrino textures and charged lepton flavour violation in light of θ_{13}, MEG and LHC data*. Phys. Rev. D **88**.7 (2013) 075005. DOI: 10.1103/PhysRevD.88.075005. arXiv: 1301.6002 [hep-ph].

[136] A. A. Markov. *Extension of the limit theorems of probability theory to a sum of variables connected in a chain*. reprinted in Appendix B of: R. Howard, *Dynamic Probabilistic Systems, volume 1: Markov Chains*, John Wiley and Sons, 1971.

[137] N. Metropolis et al. *Equation of state calculations by fast computing machines*. J. Chem. Phys. **21** (1953) 1087–1092. DOI: 10.1063/1.1699114.

[138] W. K. Hastings. *Monte Carlo Sampling Methods Using Markov Chains and Their Applications*. Biometrika **57** (1970) 97–109. DOI: 10.1093/biomet/57.1.97.

[139] B. C. Allanach et al. *Precise determination of the neutral Higgs boson masses in the MSSM*. JHEP **09** (2004) 044. DOI: 10.1088/1126-6708/2004/09/044. arXiv: hep-ph/0406166.

[140] P. Slavich et al. *Higgs-mass predictions in the MSSM and beyond*. Eur. Phys. J. C **81**.5 (2021). Ed. by P. Slavich and S. Heinemeyer 450. DOI: 10.1140/epjc/s10052-021-09198-2. arXiv: 2012.15629 [hep-ph].

[141] F. Boudjema, G. Drieu La Rochelle, and S. Kulkarni. *One-loop corrections, uncertainties and approximations in neutralino annihilations: Examples*. Phys. Rev. D **84** (2011) 116001. DOI: 10.1103/PhysRevD.84.116001. arXiv: 1108.4291 [hep-ph].

[142] F. Boudjema, G. Drieu La Rochelle, and A. Mariano. *Relic density calculations beyond tree-level, exact calculations versus effective couplings: the ZZ final state*. Phys. Rev. D **89**.11 (2014) 115020. DOI: 10.1103/PhysRevD.89.115020. arXiv: 1403.7459 [hep-ph].

[143] J. Harz et al. *Theoretical uncertainty of the supersymmetric dark matter relic density from scheme and scale variations*. Phys. Rev. D **93**.11 (2016) 114023. DOI: 10.1103/PhysRevD.93.114023. arXiv: 1602.08103 [hep-ph].

[144] T. K. Hemmick et al. *A Search for Anomalously Heavy Isotopes of Low Z Nuclei*. Phys. Rev. D **41** (1990) 2074–2080. DOI: 10.1103/PhysRevD.41.2074.

[145] A. Kudo and M. Yamaguchi. *Inflation with low reheat temperature and cosmological constraint on stable charged massive particles*. Phys. Lett. B **516** (2001) 151–155. DOI: 10.1016/S0370-2693(01)00938-8. arXiv: hep-ph/0103272.

[146] M. Taoso, G. Bertone, and A. Masiero. *Dark Matter Candidates: A Ten-Point Test*. JCAP **03** (2008) 022. DOI: 10.1088/1475-7516/2008/03/022. arXiv: 0711.4996 [astro-ph].

[147] **[XENON Collab.]**, E. Aprile, et al. *Dark Matter Search Results from a One Ton-Year Exposure of XENON1T*. Phys. Rev. Lett. **121**.11 (2018) 111302. DOI: 10.1103/PhysRevLett.121.111302. arXiv: 1805.12562 [astro-ph.CO].

[148] F. Staub. *SARAH 4: A tool for (not only SUSY) model builders*. Comput. Phys. Commun. **185** (2014) 1773–1790. DOI: 10.1016/j.cpc.2014.02.018. arXiv: 1309.7223 [hep-ph].

[149] W. Porod and F. Staub. *SPheno 3.1: Extensions including flavour, CP-phases and models beyond the MSSM*. Comput. Phys. Commun. **183** (2012) 2458–2469. DOI: 10.1016/j.cpc.2012.05.021. arXiv: 1104.1573 [hep-ph].

[150] W. Porod, F. Staub, and A. Vicente. *A Flavor Kit for BSM models*. Eur. Phys. J. C **74**.8 (2014) 2992. DOI: 10.1140/epjc/s10052-014-2992-2. arXiv: 1405.1434 [hep-ph].

[151] G. Bélanger et al. *micrOMEGAs5.0 : Freeze-in*. Comput. Phys. Commun. **231** (2018) 173–186. DOI: 10.1016/j.cpc.2018.04.027. arXiv: 1801.03509 [hep-ph].

[152] K. Griest and D. Seckel. *Three exceptions in the calculation of relic abundances*. Phys. Rev. D **43** (1991) 3191–3203. DOI: 10.1103/PhysRevD.43.3191.

[153] [**XENON Collab.**], E. Aprile, et al. *Projected WIMP sensitivity of the XENONnT dark matter experiment*. JCAP **11** (2020) 031. DOI: 10.1088/1475-7516/2020/11/031. arXiv: 2007.08796 [physics.ins-det].

[154] [**DARWIN Collab.**], J. Aalbers, et al. *DARWIN: towards the ultimate dark matter detector*. JCAP **11** (2016) 017. DOI: 10.1088/1475-7516/2016/11/017. arXiv: 1606.07001 [astro-ph.IM].

[155] C. A. J. O'Hare. *New Definition of the Neutrino Floor for Direct Dark Matter Searches*. Phys. Rev. Lett. **127**.25 (2021) 251802. DOI: 10.1103/PhysRevLett.127.251802. arXiv: 2109.03116 [hep-ph].

[156] S. Bottaro et al. *The last complex WIMPs standing*. Eur. Phys. J. C **82**.11 (2022) 992. DOI: 10.1140/epjc/s10052-022-10918-5. arXiv: 2205.04486 [hep-ph].

[157] G. F. Giudice et al. *Towards a complete theory of thermal leptogenesis in the SM and MSSM*. Nucl. Phys. B **685** (2004) 89–149. DOI: 10.1016/j.nuclphysb.2004.02.019. arXiv: hep-ph/0310123.

[158] T. Hugle, M. Platscher, and K. Schmitz. *Low-Scale Leptogenesis in the Scotogenic Neutrino Mass Model*. Phys. Rev. D **98**.2 (2018) 023020. DOI: 10.1103/PhysRevD.98.023020. arXiv: 1804.09660 [hep-ph].

[159] D. Ross. *Veltman Passarino Reduction*. https://www.southampton.ac.uk/~doug/mhv/vp.pdf. 2007.

[160] S. P. Martin and D. G. Robertson. *Evaluation of the general 3-loop vacuum Feynman integral*. Phys. Rev. D **95**.1 (2017) 016008. DOI: 10.1103/PhysRevD.95.016008. arXiv: 1610.07720 [hep-ph].

[161] S. Weinzierl. *Feynman Integrals*. Jan. 2022. DOI: 10.1007/978-3-030-99558-4. arXiv: 2201.03593 [hep-th].

[162] A. V. Smirnov and F. S. Chuharev. *FIRE6: Feynman Integral REduction with Modular Arithmetic*. Comput. Phys. Commun. **247** (2020) 106877. DOI: 10.1016/j.cpc.2019.106877. arXiv: 1901.07808 [hep-ph].

[163] M. Drees and M. Nojiri. *Neutralino - nucleon scattering revisited*. Phys. Rev. D **48** (1993) 3483–3501. DOI: 10.1103/PhysRevD.48.3483. arXiv: hep-ph/9307208.

[164] J. R. Ellis, A. Ferstl, and K. A. Olive. *Reevaluation of the elastic scattering of supersymmetric dark matter*. Phys. Lett. B **481** (2000) 304–314. DOI: 10.1016/S0370-2693(00)00459-7. arXiv: hep-ph/0001005.

[165] A. L. Fitzpatrick et al. *The Effective Field Theory of Dark Matter Direct Detection*. JCAP **02** (2013) 004. DOI: 10.1088/1475-7516/2013/02/004. arXiv: 1203.3542 [hep-ph].

[166] M. Cirelli, E. Del Nobile, and P. Panci. *Tools for model-independent bounds in direct dark matter searches*. JCAP **10** (2013) 019. DOI: 10.1088/1475-7516/2013/10/019. arXiv: 1307.5955 [hep-ph].

[167] F. Bishara, J. Brod, B. Grinstein, and J. Zupan. *From quarks to nucleons in dark matter direct detection*. JHEP **11** (2017) 059. DOI: 10.1007/JHEP11(2017)059. arXiv: 1707.06998 [hep-ph].

[168] J. C. Romao and J. P. Silva. *A resource for signs and Feynman diagrams of the Standard Model*. Int. J. Mod. Phys. A **27** (2012) 1230025. DOI: 10.1142/S0217751X12300256. arXiv: 1209.6213 [hep-ph].

[169] R. Mertig, M. Bohm, and A. Denner. *FEYN CALC: Computer algebraic calculation of Feynman amplitudes*. Comput. Phys. Commun. **64** (1991) 345–359. DOI: 10.1016/0010-4655(91)90130-D.

[170] V. Shtabovenko, R. Mertig, and F. Orellana. *New Developments in FeynCalc 9.0*. Comput. Phys. Commun. **207** (2016) 432–444. DOI: 10.1016/j.cpc.2016.06.008. arXiv: 1601.01167 [hep-ph].

[171] V. Shtabovenko, R. Mertig, and F. Orellana. *FeynCalc 9.3: New features and improvements*. Comput. Phys. Commun. **256** (2020) 107478. DOI: 10.1016/j.cpc.2020.107478. arXiv: 2001.04407 [hep-ph].

[172] H. H. Patel. *Package-X 2.0: A Mathematica package for the analytic calculation of one-loop integrals*. Comput. Phys. Commun. **218** (2017) 66–70. DOI: 10.1016/j.cpc.2017.04.015. arXiv: 1612.00009 [hep-ph].

[173] A. Denner, H. Eck, O. Hahn, and J. Kublbeck. *Feynman rules for fermion number violating interactions*. Nucl. Phys. B **387** (1992) 467–481. DOI: 10.1016/0550-3213(92)90169-C.

List of Figures

List of Tables

Acknowledgements

Now comes possibly the hardest part: thanking everyone over the last 3 years without missing out. I shall try to mention as many as I can for who I am grateful, but if I leave someone out, I do apologise and hope that I can make amends.

I'd firstly like to thank Prof. Haye Hinrichsen and Prof. Werner Porod. I am very grateful for the mentorship provided throughout this PhD. Their doors were always open, whether it be for physics discussions, general guidance about my career or just to alleviate my worries about the future. Next, I would like to thank Prof. Kimmo Kainulainen for his wisdom and insight that steered me towards a better understanding of my work. I look forward to continue working with all of you. Last but not least, I would like to thank Prof. Raimund Ströhmer for immediately agreeing to join my doctoral committee.

The members (old and current) at TP2 all deserve a shout-out for the discussions (physics and otherwise) that made coming to the office hardly a routine. Especially thanks to Alex, Benjamin, Ricardo, and Yang for all the fun times we had. I would like to thank Karina and Nelly for helping me avoid the troubles of bureaucracy, especially with my broken German. I'd also like to thank Björn and Maud for the interesting physics discussions during my visits in Annecy.

From back home, Arnav, Sidhant and Vivasvaan, I am very grateful for the regular video calls on the weekend, and the memories of "heavy driving" whenever I was in Delhi. My friends from back in Bonn (even though some are no longer in Bonn): Srijan, Aishwarya, Yong, Lina and Janak, thank you for the occasional check-ins. To Saniya, I am very grateful for taking the time out to bear my ranting and being there to cheer me up during my lows. I would like to mention Deeksha; we haven't known each other long but thank you for all the care and support over the last couple of months.

Finally, I'd like to close by thanking my wonderful parents; Mum and Dad, I would not have realised this journey without your love and support.